The University Of Sheffield.

Development of a Tissue-Engineered Oral Mucosa Model to Investigate the Role of Tumour-Associated Macrophages in Oral Cancer Progression

Lucie Hadley

A thesis submitted in partial fulfilment of the requirements for the degree of Doctor of Philosophy

The University of Sheffield
Faculty of Medicine, Dentistry and Health
School of Clinical Dentistry

February 2017

Abstract

Tumour-associated macrophages (TAM) represent a prominent component of the leukocytic infiltrate of human tumours and their accumulation in oral squamous cell carcinoma (OSCC) has been shown to be a predictor of poor prognosis. Evidence suggests that the tumour microenvironment drives TAM into a pro-tumour phenotype which exacerbates tumour growth. Three-dimensional (3D) models are gaining in popularity as they can replicate complex *in vivo* environments without the regulatory or financial barriers presented by *in vivo* experiments, whilst improving clinical relevance.

The research described in this thesis addresses a lack of oral mucosa models containing human macrophages or tools with which to analyse cells cultured within 3D models by developing (i) a 3D model of the oral mucosa containing primary human macrophages, and (ii) an optimised multi-colour flow cytometry panel to quantitatively measure the expression of CD14, CD36, CD45, CD80, CD86, CD163 and CD206 on macrophages cultured within the tissue-engineered oral mucosa.

An oral mucosa model containing FNB6 epithelial cells and monocyte-derived macrophages (MDM) was developed and characterised using immunohistochemistry; E-cadherin, AE1/3 and Ki67 were visualised in the epithelium and CD68 staining was visualised in the connective tissue. The expression of vimentin and collagen IV was also analysed. In addition, flow cytometry confirmed the viability of MDM cultured within this model, and ELISA detected a significant increase in IL-6 release following LPS challenge.

The use of 8-colour flow cytometry and rheometry provided preliminary results to demonstrate that models containing the OSCC cell line, H357, contained an increased number of CD163+ MDM and a stiffer extracellular matrix compared to those models cultured with normal oral keratinocytes or immortalised keratinocyte cell line, FNB6. These results demonstrate that the macrophage-containing oral mucosa model and molecular tools presented in this thesis will be useful in improving understanding of the role macrophages play in oral cancer progression.

Acknowledgements

I would like to firstly thank The University of Sheffield scholarship which has funded this research and Dr Craig Murdoch and Dr Helen Colley for their supervision and support, as well as giving me the opportunity to take part in international conferences and in an industrial placement. Additional thanks for this must go to the Higher Education Funding Council for England (HEFCE) and DermTreat for providing the funding and the opportunity to contribute to developing a medical device for drug delivery in the treatment of oral diseases. In addition, I would like to thank Professor Paul Hatton, Professor Martin Thornhill and Dr Jens Hansen for supporting my part in this project.

I would also like to thank David Thompson, Hayley Stanhope, Michelle Gaunt, Rikki Risorto, Brenka McCabe, Jason Heath, Sue Clark, Julie Swales, Dr Rob Moorehead and Dr Matt Worsley for offering excellent technical expertise, and always with a smile. To Dr Dan Lambert, Dr Lynne Bingle, Dr Vanessa Hearnden, Dr Toby Holmes and Dr Chris Hollands I thank you for being excellent mentors and offering so much of your time to teach me skills essential to my PhD and guidance for my future career. Thank you to Ione Smallwood for working with me on some aspects of this work and TA:SURE for funding our work.

I would like to thank all my friends and colleagues for contributing to a pleasant work environment and active social life, but in particular I would like to thank Amy Izzard, Priyanka Prajapati, Milena von und zur Mühlen, Dr Martin Eduardo Santocildes Romero and Charlie Brittain for joining me on well-earned escapes in nature and abroad, and Diana Tavares Ferreira, Dr Hanan Niaz, Sofía Granados Aparici and Dr Silvia Caddeo for providing the support of a family both in and out of the lab.

I am eternally grateful to James Legg, Pascale Hadley, Colin Hadley, Julien Hadley and Chloe Underhill for their unwavering support and guidance in all my pursuits and aspirations, and to Bessie Hadley for bestowing on me the Rawlings spirit needed to complete this research.

"Above all, don't fear the difficult moment. The best comes from them."

- Rita Levi Montalcini

Publications

Santocildes-Romero, M.E., Hadley, L., Clitherow, K.H., Hansen, J., Murdoch, C., Colley, H.E., Thornhill, M.H., Hatton, P.V. (2017). **Fabrication of electrospun mucoadhesive membranes for therapeutic applications in oral medicine**. ACS Applied Materials & Interfaces *9*, 11557-11567.

Published Abstracts

Hadley, L., Santocildes-Romero, M.E., Thornhill, M.H., Hansen, J., Colley, H.E., Hatton, P.V., Murdoch, C. (2016). **Pre-clinical evaluation of novel electrospun patches for intra-oral drug delivery.** Oral Diseases *22* (suppl. 2), 10-13.

Hadley, L., Colley, H.E., Murdoch, C. (2016). **Development of macrophage-containing *in vitro* 3D models of oral cancer.** Oral Diseases *22* (suppl. 2), 10-13.

Santocildes-Romero, M.E., Hadley, L., Clitherow K.H., Hansen, J., Murdoch, C., Colley, H.E., Thornhill, M.H., Hatton, P.V. (2016). **Novel electrospun bioadhesive oral patches for mucosal drug delivery.** Oral Diseases *22* (suppl. 2), 10-13.

Oral Presentations

Use of 3D organotypic models of oral squamous cell carcinoma to examine the role of tumour-associated macrophages in tumour progression. Yorkshire Immunology Group symposium, British Society for Immunology. Leeds, UK, November 2014.

What is genomics? Patient representative group meeting, Cancer Research UK. Sheffield, UK, February 2015.

A new dimension to cancer research. Medicine, Dentistry and Health post-graduate research forum. Sheffield, UK, September 2015.

Development of tissue-engineered oral mucosa to examine the role of macrophages in oral cancer progression. 17th Annual Meeting of the Biomaterial and Tissue Engineering group. York, UK, December 2015.

Investigating the role of macrophages in oral cancer progression using 3D *in vitro* models of oral mucosa. Sheffield Cancer Research Day 2016. Sheffield, UK, January 2016.

Investigating the role of tumour-associated macrophages in oral cancer progression using an *in vitro* 3D model of oral squamous cell carcinoma. Tumour Microenvironment and Signalling, EMBL. Heidlberg, Germany, April 2016.

Poster Presentations

Hadley, L., Jennings, L., Murdoch, C., Colley, H.E. **Use of 3D organotypic models of oral squamous cell carcinoma to examine the role of tumour-associated macrophages in tumour progression.** European Association for Cancer Research, Goodbye flat biology: 3D models & the tumour microenvironment conference. Berlin, Germany, November 2014.

Hadley, L., Jennings, L., Murdoch, C., Colley, H.E. **Use of 3D organotypic models of oral squamous cell carcinoma to examine the role of tumour-associated macrophages in tumour progression.** NC3Rs understanding target-to-function biology in non-clinical oncology research. London, UK, February 2015.

Hadley, L., Colley, H.E., Murdoch, C. **Use of 3D organotypic models of oral squamous cell carcinoma to examine the role of tumour-associated macrophages in tumour progression.** British Society for Oral and Dental Research Annual Meeting. Cardiff, UK, September 2015.

Hadley, L., Colley, H.E., Murdoch, C. **Investigating the role of macrophages in oral cancer progression using 3D *in vitro* models of oral mucosa.** Sheffield Cancer Research Day. Sheffield, UK, January 2016.

Hadley, L., Colley, H.E., Murdoch, C. **Development of an immunocompetent tissue engineered mucosa model to study oral disease.** Tissue Engineering and Regenerative Medicine International Society meeting. Uppsala, Sweden, June 2016.

Hadley, L., Santocildes-Romero, M.E., Thornhill, M., Hansen, J., Colley, H.E., Hatton, P.V., Murdoch, C. **Pre-clinical evaluation of novel electropsun patches for intra-oral drug**

delivery. The 13th biennial congress of the European Association for Oral Medicine. Turin, Italy, September 2016.

Hadley, L., Colley, H.E., Murdoch, C. **Development of macrophage-containing *in vitro* 3D model of oral cancer.** The 13th biennial congress of the European Association of Oral Medicine. Turin, Italy, September 2016.

Table of Contents

List of Figures

List of Tables

List of Equations

Abbreviations

2D	Two-dimensional
3D	Three-dimensional
ALI	Air-liquid interface
AML	Acute myeloid leukaemia
ANOVA	Analysis of variance
APC	Allophycocyanin
CBA	Cytometric bead array
CCL	Chemokine ligand
CCR	Chemokine receptor
cDNA	Complementary deoxyribonucleic acid
Ctrl	Control
CPM	Carboxypeptidase M
CT	Cycle threshold
CTLA	Cytotoxic T-lymphocyte-associated
DED	De-epidermized dermis
DMEM	Dulbecco's modified Eagle's medium
DMSO	Dimethyl sulfoxide
DNA	Deoxyribonucleic acid
DPX	Dibutyl phthalate, polystyrene, xylene
ECM	Extracellular matrix
EDTA	Ethylenediaminetetraacetic acid
EGF	Epidermal growth factor
EGFR	Epidermal growth factor receptor
ELISA	Enzyme-linked immunosorbent assay
EMT	Epithelial-mesenchymal transition
FBS	Foetal bovine serum
FcγR	Fcγ receptor
FITC	Fluorescein-isothiocyanate
FFPE	Formalin-fixed paraffin-embedded

FSC	Forward scatter
FGF	Fibroblast growth factor
FMO	Fluorescence-minus-one
GAG	Glycosaminoglycans
G-CSF	Granulocyte colony-stimulating factor
GM-CSF	Granulocyte-macrophage colony-stimulating factor
GM-CSFR	Granulocyte-macrophage colony-stimulating factor receptor
H&E	Haematoxylin and eosin
HBSS	Hank's balanced salt solution
HEPES	4-(2-hydroxyethyl)-1-piperazinethanesulfonic acid
HGF	Hepatocyte growth factor
HNSCC	Head and neck squamous cell carcinoma
HPV	Human papilloma virus
HSC	Haematopoietic stem cell
IACR	International Agency for Cancer Research
IDA	Industrial denatured alcohol
IDO	Indoleamine 2,3-dioxygenase
IF	Immunofluorescence
IFN	Interferon
IFNGR1	Interferon γ receptor 1
IHC	Immunohistochemistry
IL	Interleukin
IMDM	Iscove's modified Dulbecco's medium
INT	Iodonitrotetrazolium chloride
Ig	Immunoglobulin
iNOS	Inducible Nitric Oxide Synthase
KGF	Keratinocyte growth factor
LDL	Low-density lipoprotein
LDH	Lactate dehydrogenase
LOT	Liquid overlay technique

LPS	Lipopolysaccharide
MALT	Mucosa-associated lymphoma tissue
MARCO	Macrophage receptor with collagenase structure
MCP	Monocyte chemoattractant protein
MDSC	Myeloid-derived suppressor cell
M-CSF	Macrophage colony-stimulating factor
MDM	Monocyte-derived macrophage
MFI	Median fluorescence intensity
MHC	Major histocompatibility complex
MIF	Migration inhibitory factor
MM6	Mono Mac 6
MMP	Matrix metalloproteinase
MTT	3-4,5-dimethylthiazol-2-yl)-2,5-diphenyltetrazolium bromide) tetrazolium
NaOH	Sodium hydroxide
NEAA	Non-essential amino acids
nMFI	Normalised median fluorescence index
NO	Nitric oxide
NOF	Normal oral fibroblast
NOK	Normal oral keratinocyte
OSMF	Oral sub-mucous fibrosis
OSCC	Oral squamous cell carcinoma
PAMP	Pathogen-associated molecular pattern
PBM	Peripheral blood monocyte
PBMC	Peripheral blood mononuclear cell
PBS	Phosphate-buffered solution
PDGF	Platelet-derived growth factor
PE	Phycoerythrin
PGA	Polyglycolic acid
PI	Propium iodide
PKC	Protein kinase C

PLLA	Poly-(L)-lactic acid
PMA	Phorbol 12-myristate 13-acetate
PRR	Pattern recognition receptor
PVL	Proliferative verrucous leukoplakia
qPCR	Quantitative polymerase chain reaction
qRT-PCR	Quantitative real-time polymerase chain reaction
RNA	Ribonucleic acid
rpm	Revolutions per minute
ROS	Reactive oxygen species
RNS	Reactive nitrogen species
RPMI	Roswell Park Memorial Institute
RTK	Receptor tyrosine kinase
SOCS	Suppressor of cytokine signalling
SSC	Side scatter
TAM	Tumour-associated macrophage
TEER	Transepithelial electrical resistance
TGFβ	Tumour growth factor β
TNF	Tumour necrosis factor
TNM	Tumour-Node-Metastasis
UICC	Union Internationale Contre le Cancer
UV	Ultraviolet
VEGF	Vascular endothelial growth factor
WHO	World Health Organisation

Chapter Summaries

Chapter 1

The literature review presented in this chapter provides an overview of oral cancer, including its clinical and molecular pathogenesis. In addition, it details the known roles that macrophages play in health and disease, with a particular focus on their involvement in oral cancer. Finally, the range of pre-clinical models currently available for research is described. This review leads into the problems this thesis aims to address.

Chapter 2

In this chapter, a comprehensive description of the materials and methods used for this research is provided.

Chapter 3

Firstly, this chapter explores and optimises the isolation and 2D culture of primary and cell line monocytes and macrophages, including the stimulation of monocyte to macrophage differentiation. This leads into a preliminary comparison between primary and cell line monocytes and macrophages using single-colour flow cytometry.

Chapter 4

At first, this chapter develops methods for the 3D culture of monocytes and macrophages, and analysis of cell viability using flow cytometry using THP-1 monocytes. Optimised methods are then applied to primary and alternative cell line monocytes and macrophages. Consequently, monocyte-derived macrophages (MDM) are selected for incorporation within the tissue-engineered model of oral mucosa presented in chapter 5. This chapter ends with data showing that 3D-cultured MDM are viable and respond to stimulation with LPS by releasing inflammatory cytokine, IL-6.

Chapter 5

The results presented in chapter 5 describe the development of an oral mucosa model containing an immune component. At first, THP-1 monocytes are used to optimise methods

which are later applied to generate an optimised 3D *in vitro* model of the oral mucosa containing MDM. In this chapter, MDM are shown to be viable and responsive to LPS when cultured within this 3D co-culture model. This chapter concludes with the optimisation of rheometry to analyse the stiffness of the engineered oral mucosa.

Chapter 6

Chapter 6 describes the development of a fully optimised multi-colour flow cytometry panel (OMIP) to analyse the expression of key macrophage polarization markers, CD36, CD80, CD86, CD163 and CD206. The results in this chapter detail the selection of reagents used in the panel, stimulation of macrophages to express selected polarisation markers and the optimisation of controls required.

Chapter 7

This chapter begins by optimising the multi-colour flow cytometry panel, described in chapter 6, for use on macrophages cultured within a tissue-engineered oral mucosa model. In addition, tissue-engineered models containing MDM in the presence of normal oral keratinocytes (NOK), immortalised 'normal' (FNB6) and OSCC cell line (H357), or polarised MDM in the presence of FNB6 cells, begin to be explored using histology, rheometry, the OMIP and contraction assays.

Chapter 8

The conclusion of this thesis, and proposed future work are presented in this chapter.

1 Chapter 1: Literature Review

1.1 Oral Cancer

1.1.1 An overview of oral cancer

Seventy five per cent of oral cancers are preventable by simple lifestyle changes, such as tobacco smoking cessation and reduced alcohol consumption (Warnakulasuriya, 2009). Head and neck cancer is defined as cancer arising in the head and neck, including the nasal cavity, sinuses, lips, mouth, salivary glands, throat and larynx. Oral cancer however is limited to those cancers found in the oral cavity and oropharynx (National Cancer Institute, UK). Globally, lip and oral cavity cancers account for 2.7 % of cancers, excluding non-melanoma skin cancer, and are most commonly found in North America, Europe and Australasia. These cancers amounted to 2.1 % of mortalities due to cancer in 2012 (Ferlay *et al.,* 2013). Around 90 % of oral cancers are classified as oral squamous cell carcinoma (OSCC, Chen *et al.,* 1999) which tend to primarily affect the tongue (British Association of Otorhinolaryngology of Head and Neck Surgery (ENT.UK), 2011). Oral cancer arises from a series of genetic mutations in response to various mutagens, that lead to excessive proliferation of oral keratinocytes. These typically progress through stages of dysplastic epithelial lesions leading to malignant cancers which characteristically penetrate the epithelial basement membrane (Scully and Bagan, 2009a).

Oral cancer incidence and epidemiology

Whilst oral cancer is relatively rare compared to other cancers, its incidence is increasing particularly in young people (less than 45 years old) and this trend has previously been reviewed in detail (Majchrzak *et al.,* 2014). Data published in January 2014 shows oral cancer to be the 11th most common cancer in the UK, with nearly 6000 people diagnosed in 2011 alone (**Figure 1.1**). Oral cancer has a 27 % mortality rate, with more than double the number of men affected than women (Cancer Research UK, 2014). In the rest of the world, Papua New Guinea shows the highest incidence of lip and oral cavity cancers globally with 24.95 people per 100 000 of the population affected, and Nicaragua the lowest with 0.55 cases per 100 000 (**Figure 1.2**) and this is reflected in mortality statistics where Papua New

Guinea also shows the highest mortality rates due to lip and oral cavity cancers, and Nicaragua the lowest with 0.26 cases per 100 000 of the population (Ferlay *et al.,* 2013, **Figure 1.2**).

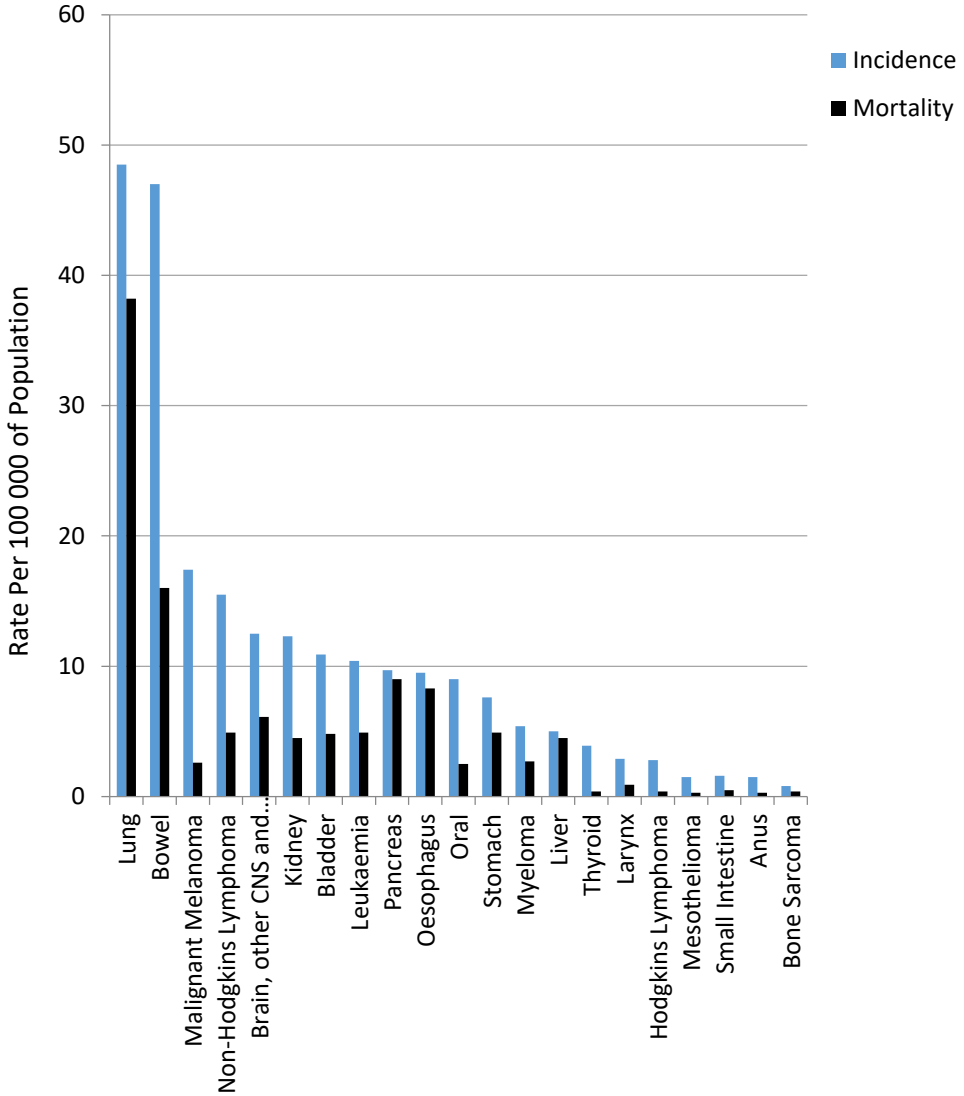

Figure 1.1. Incidence and mortality rates for cancers in the UK in 2011. Age-standardised incidence (blue) and mortality (black) rates for cancers in the UK in 2011. Data from Cancer Research UK.

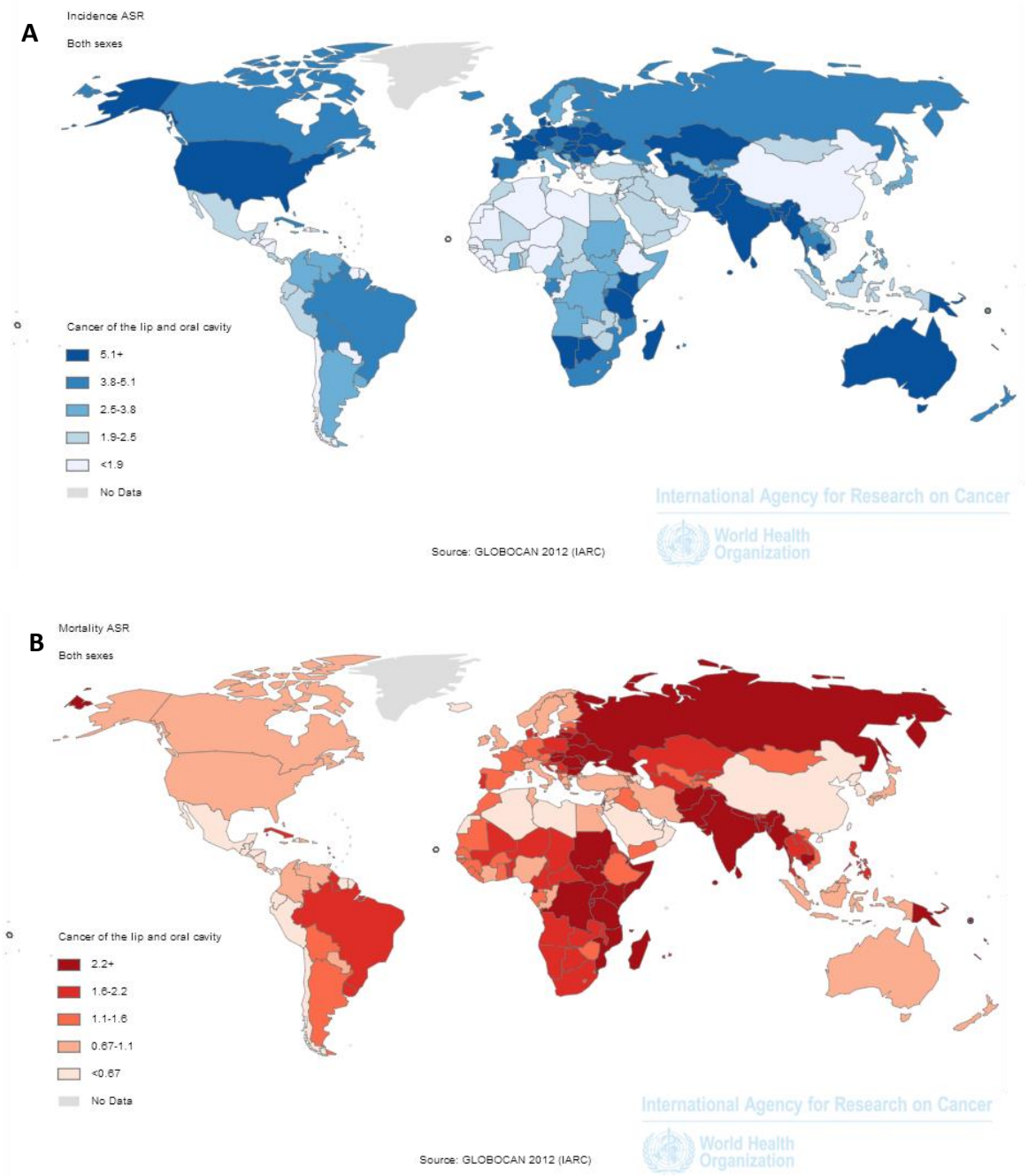

Figure 1.2. Incidence and mortality rates for cancers of the lip and oral cavity globally in 2012. Age-standardised incidence (**A**) and mortality (**B**) rates of lip and oral cavity cancers in 2012. Data is shown as rates per 100,000 of the global population for both males and females. Modified from Ferlay J, Globocan 2012 (IACR).

In England, the 27 % mortality and 56 % five-year survival rate (Oxford Cancer Intelligence Unit) of oral cancer can be largely attributed to late diagnosis by which time the cancer is

so advanced, that prognosis is poor (Sargeran *et al.,* 2008). Oral cancer caught in the early stages has survival rates as high as 90 %, so development of methods for early diagnosis are key. However, early cancer is often over-looked as the disease is often asymptomatic until the cancer has progressed to advanced stages (Bagan *et al.,* 2010) and diagnostic delays of even just one month have a huge impact on prognosis (Allison *et al.,* 1998). In addition, patients generally wait more than three months from the onset of potential oral cancer symptoms before seeking professional advice (Scott *et al.,* 2006). With the number of oral cancer cases set to rise to between 30-40 % by 2020 (Moller *et al.,* 2007) new methods must be developed to understand, then prevent and treat oral cancer. The World Health Organisation (WHO) aims to 'ensure that prevention of oral cancer is an integral part of national cancer-control programmes' but for this to be successful, risk factors need to be determined (Petersen, 2008).

Oral cancer risk factors

Many studies have investigated the risk factors for the continuing rise in the incidence of oral cancer (Saman, 2012). Currently, known risk factors include tobacco and alcohol which have been strongly implicated in more than 75 % of oral and pharyngeal cancer cases with a synergistic effect observed (Blot *et al.,* 1988).

Tobacco releases tobacco-specific nitrosamines and free radicals which have been implicated in carcinogenesis in both smoked and chewed tobacco (Scully and Bagan, 2009b). Alcohol dehydrogenases convert ethanol to acetaldehyde which promotes DNA damage leading to carcinogenesis and an increase in the risk of oral cancer by five-fold (Scully and Bagan, 2009b). Many studies have also sought to determine whether alcohol in mouthwashes make a contribution to oral cancer risk, however evidence is conflicting as the effects of mouthwash use cannot be segregated from other independent risk factors (Ahrens *et al.,* 2014).

Betel quid is a preparation of tobacco, areca nut and betel leaf which is regularly chewed by around 10 % of the world's population and is the leading risk factor for oral cancer in

developing countries (Joshi *et al.,* 2014). Areca nut is the main ingredient of betel quid which contains arecoline, a known carcinogen. Arecoline blocks tumour suppressor genes, including p53, to repress DNA repair responses (Scully and Bagan, 2009a). The areca nut is also linked with oral sub-mucous fibrosis (OSMF), a pre-malignant condition which causes trismus (Gupta *et al.,* 1998).

Unbalanced diets are found in both developed and undeveloped countries, with both showing a shift to high fat and sugar diets (Petti, 2009) which have many health implications, including an increased risk of oral cancer. A study has shown that high meat intake and low fruit and vegetable consumption may account for between 49-65 % of oral and pharyngeal cancers (Levi *et al.,* 1998). The protective effect of fruits and vegetables could be at least a 25 % reduction in oral cancer risk (Warnakulasuriya, 2010). The WHO have made recommendations for the global population to achieve a balanced diet and lifestyle which they believe is 'most likely to protect against cancer' (Wiseman, 2008).

Other risk factors for oral cancer include human papilloma virus (HPV) infection which was found in almost 4 % of oral cavity cancers. Nearly 95 % of these cases were due to HPV16 which also causes cervical cancer (Herrero *et al.,* 2003). Infection of the oral mucosa from oral pathogens such as *Porphyromonas gingivalis* disrupts the immune system, creating a pro-inflammatory environment which dysregulates proliferation of oral epithelial cells, contributing to oral cancer development (Whitmore and Lamont, 2014). Sun exposure has also been linked to oral cancer, in particular to lip cancer, due to ultra-violet (UV) radiation damage to DNA (Scully and Bagan, 2009b). These risk factors have been further reviewed in detail previously (Radoi and Luce, 2013).

1.1.2 **Clinical pathogenesis of oral cancer**

Pre-malignant lesions

The first sign of a potential malignancy is the appearance of leukoplakia or erythroplakia, which are white and red patches respectively which cannot be 'characterised clinically or pathologically as any other disease' (WHO). Whilst erythroplakia is well demarcated, often

asymptomatic and less common than leukoplakia, it is more likely to show signs of dysplasia or carcinoma (Shafer and Waldron, 1975). Another form of leukoplakia, known as proliferative verrucous leukoplakia (PVL) is rare, but occurs at multiple sites on the oral mucosa and has a high recurrence rate, with a 70 % risk of progressing into an aggressive OSCC (Silverman and Gorsky, 1997).

Early malignant leukoplakia or erythroplakia may then progress into a non-healing ulcer followed by bleeding, tooth loosening and dysphagia. However by this time, 65 % of oral carcinomas have progressed to stage 3 or 4 (Brandizzi *et al.,* 2008). Delays in diagnosis make a large contribution to the overall low (50-55 %) five-year survival rates of OSCC which have not improved in 30 years (Neville and Day, 2002).

Histologically, dysplasia can range from mild to severe and is described as a disruption of the stratification of the oral mucosa. Dysplasia is characterised by drop-shaped rete ridges, cellular and nuclear pleomorphisms with an increase in nuclear to cytoplasmic ratio of epithelial cells and loss of keratinocyte differentiation compared to normal epithelium (WHO, **Figure 1.3**). With progression of lesions from dysplasia to carcinoma *in situ* comes an increased risk of invasive carcinoma development (Bradley *et al.,* 2010).

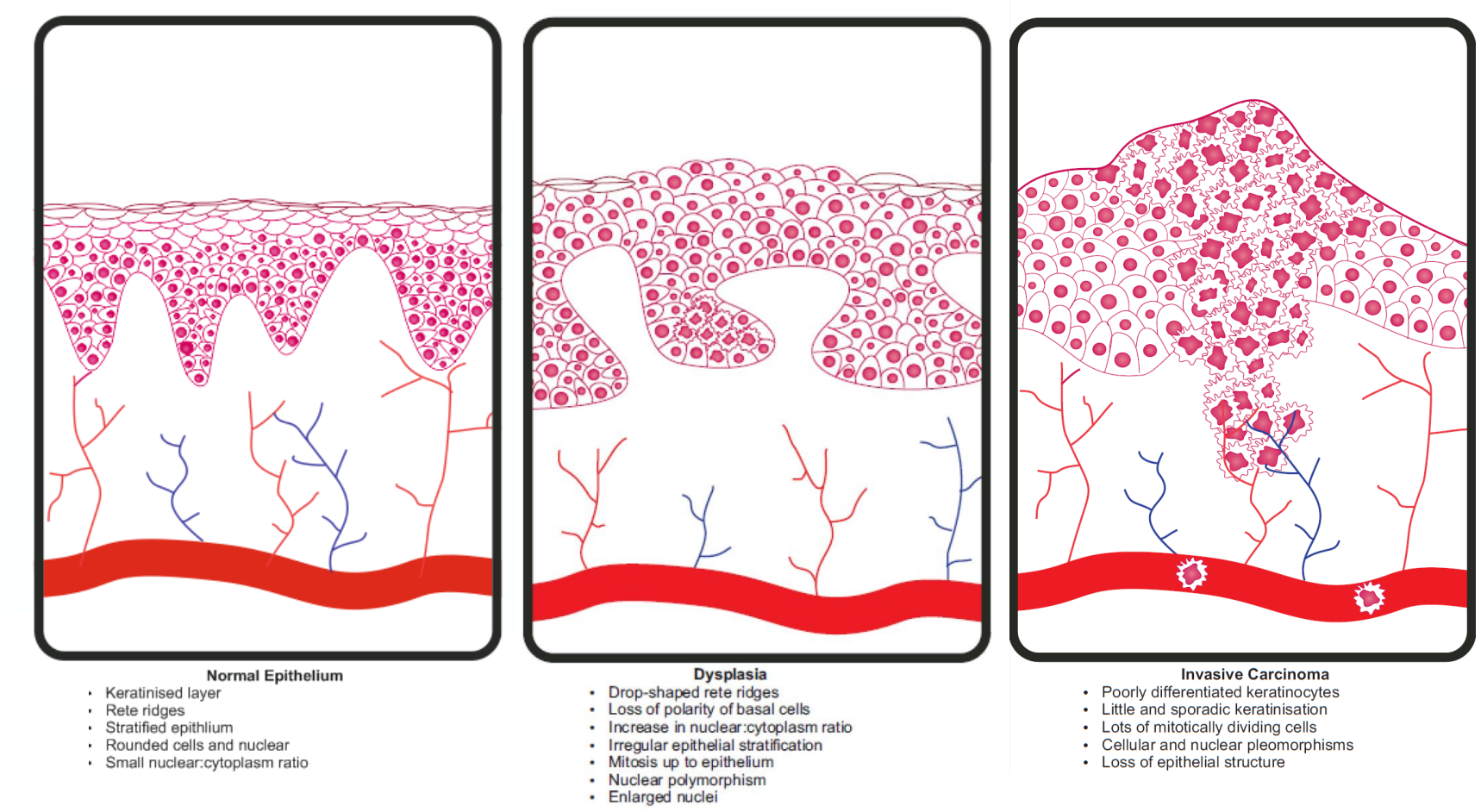

Figure 1.3. Changes in the structure of the oral mucosa during oral cancer development. Differences in the epithelium are diagrammatically represented for normal oral mucosa, dysplasia and invasive carcinoma.

Carcinoma *in situ*

Carcinoma *in situ*, as first described by Ackerman and McGavran (Ackerman and McGavran, 1958), is considered to be an extreme form of dysplasia and only differs from invasive carcinoma by a lack of stromal invasion (WHO). There is extensive epithelial disruption which is full thickness and many nuclear and cellular pleomorphisms can be observed. With current treatments, head and neck carcinoma *in situ* has a 98 % five-year survival rate with a 20 % recurrence rate (Christensen *et al.,* 2013). As with invasive oral carcinoma, the number of diagnoses of oral carcinoma *in situ* are also increasing, and when left untreated, carcinoma *in situ* has a high transition rate to invasive carcinoma (Reid *et al.,* 2000).

Invasive carcinoma

By the time an oral lesion is described as invasive carcinoma, the epithelial structure has been completely lost; there is little keratinocyte differentiation and hence little keratinisation, destruction of the basement membrane, rapid proliferation of cells and therefore many multi-nucleated cells which can be observed histologically (**Figure 1.3**). This is due to many abnormal mitoses resulting in most cells containing either cellular or nuclear pleomorphisms or both. The first malignancy to be classified was squamous cell carcinoma, which can be graded from grade 1 to 3 using Broders' method for histological grading (Broders, 1927). Alternatively, Anneroth's malignancy grading can be used (Anneroth *et al.,* 1987) however the tumour-node-metastasis (TNM) staging is now the most commonly used tumour classification system and can be applied universally to a range of malignancies. This was originally developed by Professor Pierre Denoix between 1943 and 1952, but has since been revised several times by the Union Internationale Contre le Cancer (IUCC). TNM staging takes into account tumour (extent of primary tumour), node (presence or absence of lymph node metastasis) and metastasis (distant to the primary tumour). Grading is used to predict aggressiveness of the cancer, patient prognosis and to determine treatment strategy.

Oral squamous cell carcinoma

OSCC arises from a malignancy in the basal cells of a stratified squamous epithelium. These cells are highly proliferative in order to maintain the structure and integrity of the oral mucosa. Invasive carcinomas include basaloid squamous cell carcinoma, spindle cell carcinoma and verrucous carcinoma, however OSCC is the most common, accounting for 90 % of all oral cancer cases (Bagan *et al.,* 2010).

Current treatments for OSCC primarily involve surgery and radiotherapy, but these have debilitating side effects which have a huge detrimental impact on the quality of life of patients (Funk *et al.,* 2002). Radiotherapy has a 90 % success rate with stage 1 oral cancers, however oral cancers are rarely diagnosed before stage 3 or 4, by which time surgery is usually required to remove the malignancy (Sargeran *et al.,* 2008). Side effects of radiotherapy include oral mucositis which is severe in 50 % of patients, xerostomia which is moderate to severe in 60 % of patients, and also dysphagia, dermatitis, thyroid dysfunction, trismus and osteoradionecrosis (Argiris *et al.,* 2008). Radiotherapy side effects can be either temporary or permanent (Foulkes, 2013). Adverse side effects of surgery include loss of oral function and devastating disfigurement. Often, treatment of OSCC becomes palliative to restore some oral function and ease discomfort.

1.1.3 Molecular pathogenesis of oral cancer

In the development of oral cancer, there are a number of specific cellular changes at the molecular level which are propagated into the development of disease. Carcinogens or mutagens, such as tobacco, alcohol and poor diet can damage DNA in oral keratinocytes on the surface of the oral mucosa which, if left un-repaired, may lead to uncontrolled cell proliferation and become the starting point for OSCC (Blot *et al.,* 1988; Levi *et al.,* 1998; Petti, 2009; Scully and Bagan, 2009b). Increased exposure to mutagens leads to accumulation of genetic changes which develop into premalignant lesions. Often in oral cancer there is loss of heterozygosity of the 17p chromosome region, the CDKN2A locus is missing, there is increased expression of epidermal growth factor receptor (EGFR) and C-

met receptor tyrosine kinase (RTK) is overexpressed or mutated. This is discussed in further detail below.

P53 tumour suppressor gene

The 17p chromosome region encodes many genes, including *p53* tumour suppressor gene which encodes a protein with a critical role in cell cycle regulation and apoptosis (Zilfou and Lowe, 2009). *P53* is the most commonly mutated gene in cancer, often due to tobacco and alcohol consumption in the case of oral cancer, and is implicated in around 50 % of oral cancer cases (Baral *et al.,* 1998; Boyle *et al.,* 1993; Caamano *et al.,* 1993). Presence of mutated *p53* is associated with the transition from dysplasia to invasive carcinoma (Choi and Myers, 2008) and poor prognosis, due to a reduced sensitivity of the tumour to chemotherapy (Cabelguenne *et al.,* 2000).

CDKN2A locus

CDKN2A locus contains CDKN2A/ARF, two tumour suppressor genes which encode INK4A and ARF cell cycle regulatory proteins (Berggren *et al.,* 2003). This locus is found in the 9p21 chromosomal region which is missing in 71 % of dysplastic lesions in head and neck cancer (Vanderriet *et al.,* 1994). Typically, tumour suppressor genes have a role in containing cell proliferation, but with these missing or mutated, there is uncontrolled cell proliferation, leading to tumour formation.

Epidermal growth factor receptor

EGFR binds a total of seven ligands to promote cell proliferation as well as migration, DNA synthesis and adhesion (Schneider and Wolf, 2009). Mutations in EGFR, such as EGFRvIII variant in 42 % of oral cancer, contribute to tumour formation (Pidone Ribeiro *et al.,* 2014). EGFR is overexpressed in 72 % of OSCC and thus is an attractive therapeutic target (Forastiere *et al.,* 2006) which has been explored through anti-EGFR antibodies which have so far produced mixed results (Thomas *et al.,* 2012).

C-met receptor tyrosine kinase

Hepatocyte growth factor (HGF) ligand binds c-met RTK encoded by *c-met* proto-oncogene (Bottaro *et al.,* 1991). The receptor is often overexpressed or mutated in cancer, leading to an increase in matrix metalloproteinase expression (Hasina *et al.,* 1999). These enzymes have a role in degradation of connective tissue and the basement membrane, and are thought to enable cancer epithelial invasion of the basement membrane for increased metastasis by malignant keratinocytes. The potential therapeutic benefits of using c-met RTK have been reviewed (Ma *et al.,* 2003).

Despite what is currently known about oral cancer, therapeutics have not changed in a long time, and there is a real need for further understanding how this disease progresses. Therefore, improved pre-clinical models are required.

1.2 Macrophages in Health and Disease

Macrophages are a highly specialised leukocyte, with roles in development and disease. Their primary role in the innate immune system is in the identification and elimination of invading micro-organisms, using highly sensitive receptors on their cell surface, and phagocytosis. In addition, release of a large variety of cytokines during pathogen elimination results in macrophages tuning the adaptive immune response. Whilst the inflammatory response of macrophages to invading pathogens is key for host survival of an immune challenge, the same arsenal has been shown to play a role in the initiation of cancer.

1.2.1 The role of macrophages in the immune system

Origin and development of macrophages

Monocytes are macrophage pre-cursors which originate from hematopoietic stem cells (HSCs) in the bone marrow and spleen. During development to mature monocytes, HSCs proceed through several stages (including a common myeloid progenitor, a myeloblast,

monoblast and finally, a pro-monocyte) before finally maturing into a monocyte. Monocytes are small, spherical cells with a reniform nucleus and very few granules (Auffray *et al.,* 2009; Geissmann, 2010; Ginhoux and Jung, 2014; Terry and Miller, 2014).

During the acute inflammatory response, neutrophils are the first to be recruited to a site of injury or infection and through a cytokine signalling cascade which ends with epithelial and stromal cell secretion of MCP-1, monocytes are recruited. Here, they extravasate from the blood stream into tissues and quickly differentiate into macrophages, promoted by the presence of GM-CSF and M-CSF, among other cytokines (Sheel and Engwerda, 2012; Shi and Pamer, 2011; Wrigley *et al.,* 2011; Yang *et al.,* 2014b). Monocyte to macrophage differentiation is characterised by a morphological change as cells increase in size, cytoplasmic to nuclear ratio and number of cytoplasmic granules to increase production of hydrolytic enzymes (Chang *et al.,* 2012).

Macrophages in innate immunity

Macrophages possess a large array of pattern recognition receptors (PRRs) including scavenger receptors, integrins and toll-like receptors which readily bind pathogen-associated molecular patterns (PAMPs) such as lipopolysaccharide (LPS) on gram-negative bacteria. Binding of PAMPs to these receptors results in the initiation of inflammation characterised by redness, swelling, heat and pain as macrophages become activated (Sheel and Engwerda, 2012; Shi and Pamer, 2011; Wrigley *et al.,* 2011; Yang *et al.,* 2014b).

Activated macrophages become the main secretors of growth factors, chemokines and cytokines to create an inflammatory environment; increased integrin expression on endothelial cells enables additional monocytes and neutrophils to extravasate into the affected tissue; CXCL1, 2 and 5 attract additional neutrophils; and TNF induces vasodilation to increase the permeability of blood vessels for increased flow of lymph containing antigen-presenting cells (APCs) into tissues (Porcheray *et al.,* 2005). Additionally, macrophages can engage with the adaptive immune system through release of IL-6 resulting in differentiation of B cells into plasma cells for antibody production, and antigen

presentation of PAMPs, following phagocytosis, activates T lymphocytes. An anti-microbial environment is further promoted by the production of reactive oxygen and nitrogen species (ROS and RNS) to fight infection (Coussens and Werb, 2002).

1.2.2 From inflammation to cancer initiation

The same mechanisms that enable macrophages to defend the host against invading pathogens are increasingly shown to have major roles in the initiation of cancer. The chronic inflammation caused by infection is thought to lead to 15 % of all tumours (Kuper *et al.,* 2000). Inflammation due to oral lichen planus and gingivitis is associated with OSCC; sialadentitis has been linked to salivary gland carcinoma; Sjögren's syndrome is associated with mucosa-associated lymphoma tissue (MALT) lymphoma which commonly affects the oral cavity; and inflammation due to oral HPV infection is strongly associated with carcinomas of the oral cavity and oropharynx (Balkwill *et al.,* 2005; Coussens and Werb, 2002). Macrophage migration inhibitory factor (MIF) is thought to provide the link between chronic inflammation and cancer due to its role in leukocyte accumulation which is one of the hallmarks of cancer-associated inflammation (Mitchell, 2004; Pollard, 2004). Macrophages release many pro-inflammatory cytokines, including tumour necrosis factor (TNF), interleukin-1 (IL-1), IL-6 and IL-8 during inflammation. In acute inflammation, secretion of anti-inflammatory cytokines closely follows the secretion of pro-inflammatory cytokines, however in chronic inflammation leading to cancer, pro-inflammatory cytokines persist long term, in the absence of anti-inflammatory signals. Under the influence of persistent pro-inflammatory signals, macrophages can switch from an M1 to an M2 phenotype (Shapiro *et al.,* 2011).

DNA damage

At sites of inflammation, macrophage inducible nitric oxide synthase (iNOS) enzymes produce reactive nitrogen and oxygen species free radicals to fight infection which react together to form peroxynitrite which is highly reactive with DNA. Whilst the inflammatory

response is short-lived, ROS and RNS cause DNA damage in proliferating cells, thus accelerating mutagenesis (Maeda and Akaike, 1998).

In addition to DNA damage, nitric oxide (NO) released by iNOS enables more efficient supply of nutrients to tumour tissues, through vasodilation, to facilitate tumour growth (Maeda and Akaike, 1998). Through this process, chronic inflammation can lead to cancer by enabling cells to undergo malignant transformation, or 'cancer initiation', and continue to proliferate in the growth-supportive inflammatory environment. High expression of iNOS is often observed in oral cancer and pre-malignant lesions (Choudhari *et al.,* 2014).

Faulty DNA repair mechanisms

During pathogen challenge, MIF is released by leukocytes, such as macrophages and neutrophils, to further attract leukocytes to the site of inflammation. MIF has a variety of roles in both the innate and adaptive immune systems, including regulation of cytokine secretion through extracellular signalling, or inhibition of p53 through intracellular signalling (Bach *et al.,* 2008).

Tumour suppressor protein, p53, plays a key role in cell cycle regulation. MIF has been shown to suppress the transcriptional activity of *TP53* gene in proliferating cells, leading to a lack of DNA damage response and repair mechanisms. This results in an accumulation of mutations and chromosome abnormalities (Hudson *et al.,* 1999). Several studies have shown a strong positive correlation between an increase in the expression of MIF and increased tumour growth, cell survival, metastasis and angiogenesis in oral carcinomas, especially those of the lip which have a high infiltration of CD68+ cells (Franca *et al.,* 2013). This is in direct contrast with gastric carcinomas where a high level of MIF is associated with a more favourable prognosis; here, patients whose tumours do not express MIF had a worse prognosis than patients with tumours that did express MIF (Xia *et al.,* 2009).

1.2.3 **Tissue-resident macrophages**

Whilst the majority of macrophages residing within the oral mucosa originate from blood monocytes recruited following inflammation, other tissues have been shown to be

populated with tissue-resident macrophages during foetal development, which persist throughout life and are independent of recruited monocyte-derived macrophages (Davies *et al*., 2013). Tissue-resident macrophages such as, peritoneal, alveolar and cardiac macrophages as well as microglia and Langerhans cells play a role in homeostasis (such as immune surveillance, clearing of cellular debris and iron processing) in addition to supplementing the numbers of macrophages during inflammation (Davies *et al*., 2015). As with monocyte-derived macrophages recruited during inflammation, tissue-resident macrophages are highly plastic and alter their phenotype in response to environmental stimuli and can be associated with M1 or M2 phenotypes (Lavin *et al*., 2014). However, in contrast with recruited monocyte-derived macrophages which are typically considered terminally differentiated, tissue-resident macrophages have been observed to proliferate to maintain cell numbers (Chorro *et al*., 2009). Monocyte-derived macrophages recruited during inflammation can persist in tissues for up to 60 days following resolution of inflammation, therefore it can be challenging to distinguish between these and tissue-resident macrophages. Specific markers have been sought to distinguish between the two, with CD64 identified as a marker which has been shown to be universally associated with mature tissue macrophages in a murine model (Gautier *et al.,* 2012). Within the tumour microenvironment however, a study of a murine model of breast carcinoma demonstrated that tumour-associated macrophages are derived from blood monocytes rather than originating from the tissue-resident population of macrophages (Franklin *et al*., 2014). It is yet to be shown whether these findings can be translated into studies of human tissues as well as those of other tissues.

1.2.4 **Tumour-supportive stroma**

Tumour-associated macrophages (TAM) display many pro-tumour effector functions; they secrete TNF for cell proliferation, release matrix metalloproteinases (MMPs) and tumour growth factor β (TGFβ) to promote matrix deposition and remodelling, and promote angiogenesis through secretion of vascular endothelial growth factor (VEGF), fibroblast growth factor 2 (FGF2) and TNF. TNF and MMPs released by TAM also promote metastasis

and secretion of IL-10 and TGFβ to create an immunosuppressive environment (Quatromoni and Eruslanov, 2012). Fibroblasts are the most abundant cell type in the connective tissue and their interaction with macrophages is key in developing a tumour-supportive stroma. They play a role in TAM recruitment which propagates wound healing responses of fibroblasts to further promote invasion, metastasis and matrix deposition. Hence, the cross-talk between fibroblasts, epithelial cells, malignant cells and immune cells is crucial for the maintenance of a tumour microenvironment (MaasSzabowski and Fusenig, 1996).

Tumour-associated macrophage recruitment

Stromal cells, such as fibroblasts, as well as tumour cells drive monocyte recruitment through chemokines such as monocyte chemotactic protein 1 (MCP-1) and chemokine ligands 3 and 5 (CCL3 and CCL5, Murdoch *et al.,* 2008). These have been observed at increased levels in tumours, and implicated in oral cancer with roles including promotion of metastasis and cell migration (Bektas-Kayhan *et al.,* 2012; Chuang *et al.,* 2009; Silva *et al.,* 2007). Increased TAM infiltration between malignant tumour cells in the connective tissue stroma and at the invasive front of the tumour is associated with higher histopathological grades in oral cancer (El-Rouby, 2010).

The role of tumour-associated macrophages in cancer invasion

Granulocyte-macrophage colony-stimulating factor (GM-CSF) and granulocyte colony-stimulating factor (G-CSF) play a key role in the differentiation of monocytes to macrophages and in the maintenance of homeostasis (Rosas *et al.,* 2007). These are secreted by stromal and epithelial cells, and have been observed to upregulate the expression of MMPs 1 and 2 in head and neck squamous cell carcinoma (HNSCC, Gutschalk *et al.,* 2006). These MMPs degrade collagenase IV in the basement membrane, facilitating tumour invasion and metastasis (Sugimoto *et al.,* 2001). Blocking the effects of GM-CSF with antibodies resulted in an inhibition of tumour cell invasion in both three-dimensional (3D) organotypic cultures and in nude mice (Gutschalk *et al.,* 2006). Concerns have

therefore been raised regarding the use of GM-CSF and G-CSF to prevent chemotherapy-induced neutropenia (Dale, 2002).

Among other roles in tumour promotion, TGFβ secreted by macrophages plays a leading role in promoting epithelial-mesenchymal transition (EMT) that promotes cancer invasion and metastasis. EMT describes the process in which epithelial cells reduce their expression of cell-to-cell adhesion proteins, such as E-cadherin, and begin to migrate away from the epithelium and acquire properties associated with mesenchymal cells, such as matrix deposition (Heldin *et al.,* 2012; Lamouille *et al.,* 2014; Xu *et al.,* 2009). The addition of TGFβ to *in vitro* cultured OSCC cell lines has been shown to induce EMT and promote bone invasion (Quan *et al.,* 2013). TGFβ has also been reported to activate macrophages to an M2 phenotype (Gong *et al.,* 2012).

The role of tumour-associated macrophages in tumour metastasis

In the first evidence for synergy between tumour cells and macrophages, macrophage colony-stimulating factor (M-CSF, known to stimulate CD163 expression in macrophages) was shown to stimulate chemotaxis and migration of tumour cells to promote metastasis (Wyckoff *et al.,* 2004). This was confirmed by a study using genetic and chemical ablation of macrophages to reduce the efficiency of cancer cell metastasis in an *in vivo* breast cancer model (Qian *et al.,* 2009). In oral cavity squamous cell carcinoma, a higher percentage of macrophages was found in metastatic patients, which correlated with reduced patient survival times, compared to non-metastatic cancers (Costa *et al.,* 2013). These macrophages were found to be IL10+ TGFβ+ and those in non-metastatic patients were $IFN\gamma^{high}$ (Costa *et al.,* 2013).

Whilst TNF typically plays a role in promoting inflammation, this macrophage-secreted cytokine has displayed immune-suppressing functions and a number of tumour-promoting roles. High levels of TNF have previously been measured in serum from HNSCC patients and in OSCC cell lines (Koontongkaew, 2013). TNF secretion has been linked to a reduction in E-cadherin expression on tumour cells, stimulating EMT, and increased expression of TGFβ

and MMPs (Smith and Kang, 2013). Treatment of human oral cancer cells with TNF promoted expression of CD163 by macrophages and resulted in increased epithelial invasion into a myoma model (Pirila *et al.,* 2015). Lung and liver metastases in mouse models of carcinoma could both be prevented by blocking TNF binding to its receptor (Balkwill, 2006). The TNF-dependent metastasis of cancer cells is likely due to activation of the NF-κB signalling pathway that results in activation of MMPs, particularly MMPs 2 and 9 (Hagemann *et al.,* 2005).

MMPs are proteases essential for extracellular matrix (ECM) turnover; in tumour progression, their role of matrix degradation enables malignant cell invasion and metastasis. Macrophages secrete large amounts of MMPs, and in particular, MMPs 2 and 9 have been implicated in oral cancer metastasis as they can degrade collagen IV, a major component of the basement membrane (Patel *et al.,* 2005). A published study found significantly higher levels of both macrophages and MMP9 in OSCC patients correlating with lymph-node metastasis (Dai *et al.,* 2007). In addition, plasma MMP9 levels were found to be significantly lower in patients responding to treatment (Patel *et al.,* 2007). These authors also found that the activation of MMP2 was higher than MMP9 in malignant tissues and suggest these enzymes may be used as prognostic markers.

The role of tumour-associated macrophages in angiogenesis

TAM have been shown to accumulate in hypoxic areas of tumours through chemoattraction by endothelin-2 (Grimshaw *et al.,* 2002). Within the hypoxic region, they promote angiogenesis through the release of angiogenic factors such as VEGF, FGF and TGFβ in a positive feedback loop (Bingle *et al.,* 2002). A strong correlation was found between TAM accumulation and microvessel density in oral cancer, in agreement with similar studies on breast and cervical cancer (El-Rouby, 2010). However, a later study showed that whilst there were high numbers of TAM in oral cancer, their role in angiogenesis may be more due to macrophage phenotype than numbers of cells infiltrating (Boas *et al.,* 2013).

VEGF mediates the 'angiogenic switch' in order to promote angiogenesis. This 'switch' results in an increase in the number of blood vessels which provides the growing tumour with additional nutrients, and facilitates metastasis (Carmeliet, 2005; Hicklin and Ellis, 2005). In a small study, expression of VEGF was higher in OSCC samples compared to normal tissues and correlated with tumour grading (Kim *et al.,* 2015). In contrast, Kukreja *et al.,* found that VEGF expression and MVD were independent of tumour grade, however this study also found that OSCC samples expressed high levels of VEGF (Kukreja *et al.,* 2013). Additional angiogenic factors, such as FGFs, are involved in the cross-talk between epithelial and stromal cells to promote angiogenesis. In particular, FGF2 has been shown to play a role in EMT and migration as well as angiogenesis (Hasina *et al.,* 2008) and has been identified as a potential prognostic marker for malignant transformation of leukoplakia to OSCC (Nayak *et al.,* 2015). Several studies have indicated that VEGF and FGF may act synergistically to promote angiogenesis (Korc and Friesel, 2009).

The role of tumour-associated macrophages in immunosuppression

To promote tumour progression, TAM take an active role in immune suppression, due to their secretion of IL-10 and TGFβ. Both these cytokines promote the polarisation of macrophages to an M2 phenotype, that has been found to be immunosuppressive by reducing the antigen presentation capabilities of immune cells (Hao *et al.,* 2012; Noy and Pollard, 2014). An additional immunosuppressive mechanism employed by cancer cells involves the recruitment of myeloid-derived suppressor cells (MDSC), including monocytic-MDSCs, that prevent dendritic cell maturation, suppress T cell responses and secrete high levels of TGFβ to further promote immunosuppression (Noy and Pollard, 2014).

IL-10 is an anti-inflammatory cytokine, and thus downregulates the expression of pro-inflammatory cytokines, such as TNF, IL-6 and IL-12, as part of the innate immune response. It prevents antigen presentation by downregulating the expression of major histocompatibility complex II (MHCII) and co-stimulatory molecules (Martinez *et al.,* 2008). In addition, IL-10 prevents maturation of dendritic cells (further reducing antigen presentation) and promotes differentiation of macrophages, specifically to an M2

phenotype (Hao *et al.,* 2012). Meanwhile, TGFβ may inhibit cytolytic activity of natural killer cells and T lymphocytes whilst simultaneously preventing dendritic cell migration and promoting apoptosis (Hao *et al.,* 2012). This further reduces antigen presentation and subsequent attack of cancer cells by the immune system. TGFβ also promotes differentiation of T lymphocytes to Th2 cells, further promoting M2 polarisation of macrophages and stimulates Treg differentiation for peripheral tolerance of malignant cells (Hao *et al.,* 2012; Mori *et al.,* 2011; Noy and Pollard, 2014).

1.2.5 Tumour-associated macrophages in oral cancer

TAM have been widely implicated in the development of a tumour microenvironment and can form up to 65 % of the tumour mass (Liu *et al.,* 2008). A high number of TAM is associated with a favourable prognosis in colorectal and prostate cancer, however they are considered a poor prognostic indicator in glioma, lymphoma, melanoma, sarcomas, breast carcinoma, lung carcinoma and HNSCC (Balermpas *et al.,* 2014; Costa *et al.,* 2013). Macrophages are highly plastic, responding to environmental cues to adopt various activation states. Whilst macrophages *in vivo* tend to fit along a spectrum of activation states, *in vitro* the polarisation status of macrophages has been simplified to classically or alternatively activated macrophages. It has recently been observed that TAM do not fit into either polarisation category, and instead express features of both activation states in response to micro environmental cues (Martinez and Gordon, 2014; Qian and Pollard, 2010).

Tumour-associated macrophage phenotype

In 2000, two distinct subsets of macrophages were described and termed M1 and M2 due to their differential metabolism of arginine (Mills *et al.,* 2000). During differentiation from monocytes, macrophages were found to become either classically or alternatively activated and termed M1 or M2 respectively to reflect the Th1 and Th2 subsets of T lymphocytes that secreted the cytokines thought to be responsible for this polarisation (Mantovani *et al.,* 2002; Stein *et al.,* 1992; Steinman and Idoyaga, 2010; Murray *et al.,* 2014). Additionally,

depending on whether macrophages were cultured in GM-CSF (M1) or M-CSF (M2) they displayed very different transcriptomes (Fleetwood *et al.,* 2009; Joshi *et al.,* 2014) that could not be categorized as M1 or M2 (Murray *et al.,* 2014).

Classically activated macrophages (M1) are considered pro-inflammatory as they are activated by pro-inflammatory cytokines such as interferon-γ (IFNγ), TNF and GM-CSF, or PAMPS such as LPS, to which they respond by secreting further inflammatory cytokines such as IL-1β, IL-12, TNF and IL-6. They express high levels of CD80 and CD86, MHCII co-stimulatory molecules and low levels of CD206. M1 macrophages display microbicidal properties, promote tissue destruction and display anti-tumour functions for the effective depletion of cancer cells (Mills *et al.,* 2000). *In vitro*, M1 macrophages can be induced using various combinations of LPS, IFNγ, GM-CSF and TNF (Chanput *et al.,* 2013; Goerdt and Orfanos, 1999; Mantovani *et al.,* 2005; Mantovani *et al.,* 2002; Martinez and Gordon, 2014; Martinez *et al.,* 2008; Mosser, 2003; Muraille *et al.,* 2014; Murray *et al.,* 2014).

On the other hand, alternatively activated macrophages (M2) typically respond to IL-4, IL-10, IL-13 and immune complexes to release anti-inflammatory cytokines such as IL-10 and TGFβ. These typically express high levels of CD36, CD163 and CD206 and display pro-tumour functions such as promotion of angiogenesis, tissue remodelling and immunosuppression as well as resolution of inflammation and parasite encapsulation (Goerdt and Orfanos, 1999; Mantovani *et al.,* 2005; Mantovani *et al.,* 2002; Martinez and Gordon, 2014; Martinez *et al.,* 2008; Muraille *et al.,* 2014; Murray *et al.,* 2014). Macrophages are a heterogeneous population and it has been proposed that they are further categorised as M1a-M1b and M2a-M2d (Martinez *et al.,* 2008); M1a and M1b may distinguish between classically and alternatively activated macrophages, with M2a used to describe macrophages activated by IL-4 or IL-13, M2b used to describe macrophages activated by immune complexes, IL-1β or LPS, or M2c used to describe those activated by IL-10, TGFβ or glucocorticoids (Lewis and Pollard, 2006; Martinez and Gordon, 2014; Mosser, 2003). Whilst these categories provide information regarding the phenotype of macrophages, they cannot be used identify distinct subtypes as macrophage gene and

protein expression can vary so widely depending on environmental stimuli (Mantovani *et al.,* 2004; Roszer, 2015).

Plasticity between M1 and M2 macrophages has been observed and polarisation often depends on the chemokine environment macrophages found themselves in (Davis *et al.,* 2013; Lewis and Pollard, 2006; Mills *et al.,* 2000). However, M2 macrophages typically prevent polarisation of macrophages to an M1 phenotype (Hofkens *et al.,* 2011) and TAM are often described as displaying an M2 phenotype. The most commonly used markers for macrophage polarisation and their physiological roles are described in **Table 1.1**. The phenotypes of macrophages in oral diseases reflects that found in other diseases and is reviewed in detail here (Merry *et al.,* 2012).

Antigen	Alternative names	M1/M2 macrophage	Receptor binding partner	Role	Reference
CD14	-	M1 and M2	Microbial ligands	Pattern recognition receptor to activate innate immunity	(Poussin *et al.,* 1998)
CD36	SCARB3	M2	Thrombospondin, oxLDL, collagen	Promotion of cell adhesion and scavenger receptor to protect from oxidative damage	(Duque and Descoteaux, 2014)
CD45	Leukocyte common antigen (LCA)	M1 and M2	Galectin-1	Promotion of B and T lymphocyte development	(Roach *et al.,* 1997; St-Pierre and Ostergaard, 2013)
CD80	B7-1, CD28LG	M1	CD28, CTLA-4	Induction of T lymphocyte proliferation and cytokine production	(Iwasaki and Medzhitov, 2004)
CD86	B7-2, CD28LG	M1	CD28, CTLA-4	Activation of T lymphocytes	(Iwasaki and Medzhitov, 2004)
CD163	Haemoglobin scavenger receptor	M2	Haptoglobin-haemoglobin complexes	Scavenger receptor to protect from oxidative damage	(Duque and Descoteaux, 2014)
CD206	Mannose receptor type 1 (MRC1)	M2	Bacterial carbohydrates	Mediates endocytosis, phagocytosis, macrophage activation and antigen presentation	Chavez-Galan *et al.,* 2015; Duque and Descoteaux, 2014)

Table 1.1. Cell surface antigens for the characterisation of monocytes and macrophages. The table lists cell surface markers used to identify monocytes and macrophages, markers for monocyte to macrophage differentiation and markers to detect polarisation of macrophages. The cells which express these proteins, the receptor binding partner and the role of each protein is also shown.

CD14 binds microbial ligands such as LPS to initiate an inflammatory response (Poussin *et al.,* 1998). This is followed by expression of co-stimulatory molecules such as CD80 and CD86 that bind CD28 and cytotoxic T-lymphocyte-associated protein 4 (CTLA-4) to activate T lymphocytes (Iwasaki and Medzhitov, 2004). CD36 and CD163 are scavenger receptors that bind thrombospondin and oxidised LDLs (CD36) and haptoglobin-haemoglobin complexes (CD163), protecting cells from oxidative damage (Duque and Descoteaux, 2014). The transcription of CD36 and CD163 is stimulated by IL-10 binding to its receptor which also stimulates upregulation of CD206 to bind bacterial carbohydrates for antigen presentation (Chavez-Galan *et al.,* 2015; Duque and Descoteaux, 2014). CD45 is expressed by all leukocytes for the activation of B and T lymphocytes. It also plays a role in macrophage adhesion and migration (Roach *et al.,* 1997; St-Pierre and Ostergaard, 2013).

Prognostic value of tumour-associated macrophages in oral cancer

A correlation between a high TAM number and poor prognosis in OSCC has been observed (Bagul *et al.,* 2016; Balermpas *et al.,* 2014; Boas *et al.,* 2013; Li *et al.,* 2002; Mori *et al.,* 2011; Lu 2010). However, alternative research has shown a large infiltration of TAM specifically into the tumour stroma correlates with poor overall disease-free survival suggesting that TAM micro-localisation, rather than number, may have a role to play in OSCC outcome (Ni *et al.,* 2015). In addition, TAM number, measured by CD68, was found to be higher in all pathological grades, but did not correlate with pathological grade (Bagul *et al.,* 2016) which contradicted previously published research (Lo Muzio *et al.,* 2010). A limitation of these studies is the use of CD68 alone as a marker of TAM.

Comparisons between the expression of CD68 and CD163 with regards to overall patient survival showed that whilst CD68 staining showed no correlation with overall survival, CD163 showed potential as a prognostic marker in oral cancer (Fujii *et al.,* 2012; He *et al.,* 2014). CD163 has also been shown to correlate with an unfavourable prognosis particularly after chemotherapy in HPV-negative patients (Balermpas *et al.,* 2014). Expression of CD163 at the invasive front in combination with serum IL-8 and N status was even shown to successfully predict tumour relapse and correlate with histological grade (Fujita *et al.,* 2014; Mori *et al.,* 2011; Weber *et al.,* 2014). In oral cancer, high numbers of CD163+ macrophages

were shown to correlate with lymph node metastasis (Wehrhan *et al.,* 2014) and the number of these was found to increase between pre-operative incision biopsy samples and tumour resection (Weber *et al.,* 2014). In addition to the use of CD163 as a marker of TAM, some success has been observed with the use of CD206 expression, particularly in the case of metastatic oral carcinoma, even at an early stage (Fujita *et al.,* 2014; Weber *et al.,* 2014; Weber *et al.,* 2016).

Expression of CD163 is emerging as a potential diagnostic and prognostic marker in oral cancer. The important role that CD163 plays in cancer progression in general has led to its use as a diagnostic marker in a variety of human cancers, including carcinomas of the breast, endometrium, ovaries, non-small cell lung and colon, in addition to Hodgkin's and angioimmunoblastic T cell lymphomas (Espinosa *et al.,* 2010; Forssell *et al.,* 2007; Harris *et al.,* 2012; Hu *et al.,* 2009; Medrek *et al.,* 2012; Niino *et al.,* 2010; Ohri *et al.,* 2011). A lack of understanding in the role that macrophages play in oral cancer compared to the role they play in other cancers, is limiting the potential use of these cells for clinical benefit.

1.2.6 **Macrophages in cancer therapy**

Macrophages are an attractive target for cancer therapies as their genome is more stable than that of tumour cells, reducing the chance of drug resistance developing (Qian and Pollard, 2010). However, similarly to their pro- and anti-tumour roles in cancer progression, macrophages have demonstrated both favourable and detrimental effects in response to cancer treatments and therapy (Mantovani and Allavena, 2015).

Macrophages as therapeutic targets

In murine models of breast, melanoma and colon carcinoma, anti-macrophage receptor with collagenous structure (MARCO) antibodies were used to selectively target TAM resulting in reduced metastatic spread, reduced tumour volume and weight, and a shift in macrophage polarisation from M2 to M1 (Georgoudaki *et al.,* 2016). Alternatively, anti-M-CSF antibodies have been investigated to halt macrophage development. This has been shown to reduce metastasis and increase the sensitivity of murine models to chemotherapy

(Cheng *et al.,* 2010; Morandi *et al.,* 2011). Additionally, the use of a chemokine receptor type 2 (CCR2) inhibitor in murine models of breast and pancreatic cancer reduced the number of macrophages from both the primary and metastatic tumour, and resulted in a decrease in the tumour growth and a reduction in metastasis (Qian *et al.,* 2011; Sanford *et al.,* 2013). However, data published more recently has shown that whilst CCL2 inhibition initially prevented development of macrophages from the bone marrow to prevent metastasis, removing inhibition resulted in a rapid increase in metastasis and more rapid death (Bonapace *et al.,* 2014).

Further uses of myeloid cells as therapeutic targets include the blockade of recruitment of these cells to tumours using an anti-CD11b/CD18 antibody, resulting in increased sensitivity of squamous cell carcinoma to radiotherapy in a murine model (Ahn *et al.,* 2010). Additionally, activation of macrophages using a CD40 antibody agonist resulted in macrophages adopting a tumoricidal phenotype, characterised by high expression of CD86, to infiltrate a murine model of pancreatic cancer resulting in disaggregation of the tumour stroma (Beatty *et al.,* 2011). Aside from antibody therapies, bisphosphonates have been shown to promote re-polarisation of M2 macrophages to an M1 phenotype. In addition, the use of zoledronic acid to stimulate apoptosis of TAM has reduced their survival and has been successful in prolonging the disease-free survival of patients (Coleman *et al.,* 2011; Rogers and Holen, 2011). Further strategies for re-polarising M2 macrophages to an M1 phenotype remain one of the most promising therapeutic options (Mills *et al.,* 2016) and additional uses of macrophages as therapeutic targets have previously been reviewed (Panni *et al.,* 2013).

Macrophages for drug delivery

As well as providing promising therapeutic targets in the fight against cancer, macrophages can be modified for use as agents for drug delivery. Liposomes are commonly used to target macrophages for drug delivery as these are readily taken up by macrophages through interactions with scavenger receptors and liposome properties can easily be tailored specifically to modify the drug and the efficiency of its delivery (Kelly *et al.,* 2011). In

particular, CD163 plays a key role in the uptake of drugs for targeted delivery (Graversen and Moestrup, 2015). In order to further improve this method of drug delivery, Cao *et al.,* have coated liposomes with an isolated macrophage membrane. This has not only enabled the coated liposomes to specifically target breast cancer cells, but also enhanced uptake of the liposomes by metastatic cells through increased integrin expression. This had the effect of reducing cancer cell viability and metastasis (Cao *et al.,* 2016). Similarly, macrophage membranes have been used to coat upconversion nanoparticles for effective targeting of cancer, and for the purpose of *in vivo* cancer imaging (Rao *et al.,* 2016).

The use of therapeutic nanoparticles also aims to provide more targeted tumour cytotoxicity in order to prevent the unfavourable systemic side effects that results in poor patient compliance to chemotherapy. Although successful alone, a study showed that the uptake of drug-loaded nanoparticles by TAM resulted in a 37 % increase in accumulation of the chemotherapeutic agent within the tumour mass resulting in sustained and targeted drug delivery that was diminished when TAM numbers were depleted (Miller *et al.,* 2015). The chemotaxis of macrophages towards cancer cells has also been used to attract macrophage-based 'microbots' containing drug-loaded magnetic nanoparticles to spheroids in murine models of colon and mammary gland carcinoma to induce targeted cytotoxicity of the tumour cells (Han *et al.,* 2016).

An alternative approach is the use of macrophages as vehicles for gene therapy (Burke *et al.,* 2002). Recent advances include the use of oncolytic viruses, under the regulation of a hypoxia inducible construct, contained within macrophages. In regions of hypoxia, oncolytic viruses were able to replicate and specifically target prostate tumour cells in a xenograft model (Muthana *et al.,* 2011). When this approach was combined with chemotherapy and radiotherapy, which are typically followed by a marked increase in macrophage infiltration into tumours, metastasis and tumour regrowth were suppressed resulting in the increased survival of mice (Muthana *et al.,* 2013). Immunosuppressive Tie2-expressing monocytes have been specifically targeted for tumour therapy (Coffelt *et al.,* 2011) and with the inclusion of *Ifnα1* gene resulted in a reduction in tumour growth and

metastasis in murine models of glioma and mammary carcinoma without the toxicity previously seen with systemic administration of IFNα (De Palma *et al.,* 2008).

1.3 Pre-clinical Models in Oral Health Research

1.3.1 Pre-clinical models

Monolayer models

Traditionally, cells are cultured as monolayers in tissue culture-treated flasks. However, in 2D culture, cells are flattened, lack cell-to-cell and cell-to-matrix interactions as the ECM component is missing (Mazzoleni *et al.,* 2009). *In vivo*, oral keratinoyctes form a multi-layered epithelium at an air-liquid interface (ALI), however this cannot be achieved in 2D culture which prevents the formation of a stratified epithelium (Kriegebaum *et al.,* 2012). In addition, the many oral cell types cultured in close proximity *in vivo* release signals to enable oral mucosa formation, but typically only a single cell type can be cultured in 2D. Therefore, in 2D, oral keratinocytes do not have a representative structure or function (Cukierman *et al.,* 2001).

Animal models

There are many different *in vivo* animal models of oral cancer; oral cancer can be chemically induced, tumours can be transplanted or transgenic animals can be used (Mognetti *et al.,* 2006). *In vivo* models are essential but, similarly to *in vitro* models, they have limitations. Evidence has shown that there are many inter-species differences between humans and animal models, and with limited conserved features, disease modelled in animals may not truly represent disease in humans (Kimlin *et al.,* 2013). Specifically, pathogenicity and liver toxicity have shown large differences between mice and humans (Mazzoleni *et al.,* 2009). 'Humanised' rodents have been developed for use when animal models are unrepresentative and human trials are not possible (Brusevold *et al.,* 2010), however the results from these experiments are often variable (Gaballah *et al.,* 2008). In particular,

evidence confirming any similarities between macrophages in animals compared to those in humans is lacking (Qian and Pollard, 2010). Macrophages in murine models, used in the majority of studies, differ markedly from those in the human immune system (Murray and Wynn, 2011; Roszer, 2015). Whilst in mice iNOS is a prototypical M1 marker, CD64, indoleamine 2,3-dioxygenase (IDO), suppressor of cytokine signalling 1 (SOCS1) and CXCL10 proteins are more typically used in human studies. CD206 and TGM2 have both been used as an M2 marker in both human and mouse studies, however other markers used in human studies, such as CD23 and CCL22 are not used in murine studies (Martinez and Gordon, 2014). A lack of humanised pre-clinical models makes the translation of therapies into clinical use difficult.

3D spheroid models

Spheroid models are formed by aggregation of cells in culture by using various methods; hanging drop, using spinner flasks, static liquid overlay technique (LOT) or by centrifugation (Fennema *et al.,* 2013). Spheroids provide a useful model for hypoxia in the tumour microenvironment, within the necrotic core (Sutherland *et al.,* 1981), but as the simplest 3D model, they typically do not represent a multi-layered tissue architecture which is essential for engineering oral mucosa (Kimlin *et al.,* 2013).

1.3.2 Tissue-engineered models

Structure of the oral mucosa

The oral mucosa forms a protective barrier from mechanical or microbial damage to underlying tissues (Squier and Kremer, 2001). It consists of the epithelium and connective tissue which are separated by the basement membrane (**Figure 1.4**).

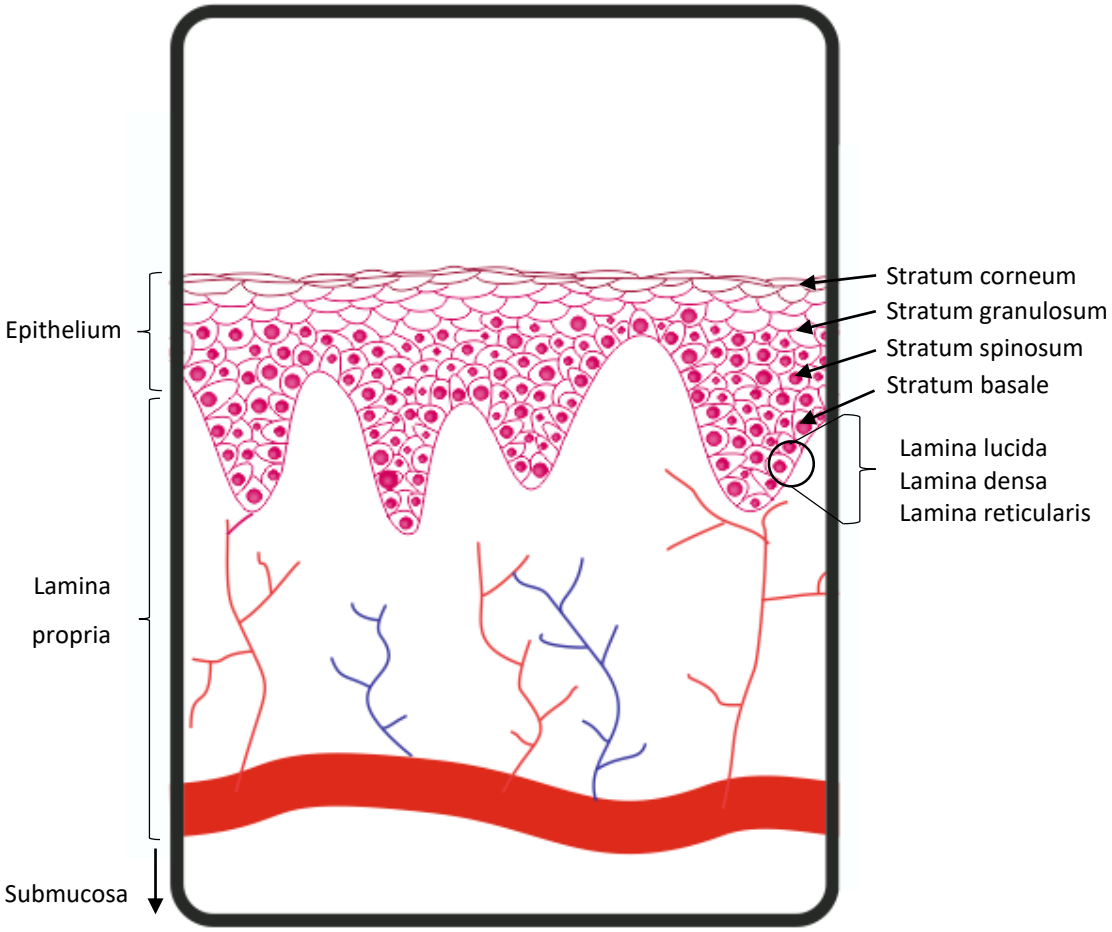

Figure 1.4. Structure of the oral mucosa. Components of the epithelium, basement membrane and connective tissue are represented diagrammatically and labelled.

The oral mucosa epithelium separates the oral cavity and deeper tissues, and consists of keratinocytes which form a stratified squamous epithelium. Depending on location within the oral cavity, this epithelial layer can take on different characteristics, such as non-keratinised (e.g. buccal mucosa and ventral surface of the tongue) or keratinised (e.g. on the hard palate and gingivae).

Within a keratinised oral epithelium are four layers: the stratum basale which contains a single layer of cuboidal cells in contact with the basement membrane, which are rapidly proliferating; the stratum spinosum which is several cell layers thick; the stratum granulosum is formed of several layers of flat cells containing keratohyaline granules which

help form the impermeable keratin layer; and the stratum corneum characterised by a-nuclear cells containing keratin filaments. Cells of the stratum corneum are continuously replaced by proliferating cells in the stratum basale which differentiate upwards through the epithelial layers, with oral mucosa renewed every 41-57 days (Dongari-Bagtzoglou and Kashleva, 2006). In a non-keratinised oral epithelium, the stratum corneum and stratum granulosum layers are absent and are replaced by the stratum intermedium (an epithelial structure closely associated with the inner dental epithelium) and stratum superficiale, where stratified squamous epithelial cells have reached maturity and as such are flat and non-proliferative cells (Koyama *et al.,* 2001).

The basement membrane is a specialised extracellular matrix containing many glycoproteins alongside collagen, integrins and proteoglycans, which forms a barrier between the epithelium and the connective tissue (Merker, 1994). Components of the basement membrane have been shown to have an influence on the adjacent epithelium, such as collagen IV and laminin which have been shown to be important in the differentiation of oral keratinocytes in 3D culture (Kim *et al.,* 2001). Three different layers of the basement membrane can be identified and these include; the lamina lucida on the epithelial side, lamina reticularis on the lamina propria side and lamina densa sandwiched in between.

The connective tissue is also split into layers, with the lamina propria nearest the basement membrane, and the submucosa in limited areas of the mouth such as cheeks and lips. The lamina propria contains blood and lymphatic vessels, nerves, fibroblasts and immune cells within the papillary and reticular layers all within a supportive inter-cellular matrix. Fibrous proteins in the inter-cellular matrix include fibronectin, elastin and collagen, where collagen type 1 is the most abundant. The submucosa provides attachment of the lamina propria to bone and muscle, and contains minor salivary glands.

Scaffolds for tissue engineering

In vitro 3D culture has been shown to promote increased cell proliferation when compared to 2D culture (Li *et al.,* 2013) and creates a more physiologically relevant structural architecture with the use of natural or artificial scaffolds (Lee *et al.,* 2008). This enables cells cultured in 3D *in vitro* to replicate more closely the gene and protein expression profiles of cells *in vivo* (Abbott, 2003). 3D culture provides a superior culture method to 2D culture as these changes in cell behaviour have produced more accurate and predictive cell-based assays, improving clinical trial outcomes (Kimlin *et al.,* 2013).

3D models have not only become a useful tool with which to culture cells in a more physiologically relevant environment, but they also bridge the gap between *in vivo* animal models and human applications (Mazzoleni *et al.,* 2009). The European Chemicals Legislation have identified a need for development of representative *in vitro* models to reduce the use of *in vivo* models to produce more data related to humans (Lilienblum *et al.,* 2008).

Hydrogels can be formed from natural, synthetic or a combination of natural and synthetic molecules. They aim to simulate the ECM component of tissue, enabling 3D cell culture. These substrates of highly cross-linked polymers have a high water content allowing rapid diffusion of oxygen, nutrients and waste products between cells and the surrounding culture medium (Nguyen and West, 2002). Collagen is the major structural component of the ECM where its main role is in mechanical integrity (Rajan *et al.,* 2006). It has therefore been used in the engineering of many different 3D models containing cells of different origin, including; intestinal (Viney *et al.,* 2009), endothelial (Koh *et al.,* 2008), dermal (Smola *et al.,* 1998) and oral (Dongari-Bagtzoglou and Kashleva, 2006) either in mono-culture or as co-cultures. Bovine, equine, rat-tail and plant-derived collagen is available, which can be combined with other components such as glycosaminoglycans (GAG)-chitosan to alter properties of the ECM (Griffon *et al.,* 2006). Apligraf is a commercially available collagen-based skin substitute which combines collagen with dermal fibroblasts and human keratinocytes and is used clinically to promote wound healing.

Synthetic polymers have also been used to produce scaffolds on which cells can be cultured. These have an advantage over naturally-derived scaffolds as they are more reproducible. They can be derived from polymers such as poly-(L)-lactic acid (PLLA), polyglycolic acid (PGA) and polystyrene (Yang *et al.,* 2001). Commercially available oral mucosa models which incorporate a synthetic scaffold include MatTek and Skinethic, however these both lack an essential connective tissue component including fibroblasts (Moharamzadeh *et al.,* 2008).

Examples of scaffolds used for *in vitro* 3D oral mucosa models include de-epidermised dermis (DED), hydrogels, synthetic scaffolds and spheroids which can be used for modelling disease and drug testing, for example. One of the limiting factors for 3D models however is the need for standardisation and the development of protocols to separate cells from the model for analysis (Mazzoleni *et al.,* 2009).

Tissue engineered models of the oral mucosa

The use of *ex vivo* oral mucosa is popular for use as a scaffold in oral mucosa models as its architecture cannot always be recapitulated by engineered tissues. Whilst porcine and bovine buccal mucosa can be used, human *ex vivo* tissue is the most relevant for modelling human disease. Due to the limited size of human oral mucosa, human skin provides a useful alternative. DED is produced by using skin grafts which are de-cellularised to remove the epidermis, leaving the basement membrane intact. The collagen IV and laminin components of the basement membrane allow attachment of different cell types to the DED to produce a tissue engineered oral mucosa (Hearnden *et al.,* 2009). Whilst DED models may provide the most physiologically relevant tissue architecture, there is vast patient variability between grafts and a lack of immune cell components (Colley *et al.,* 2011). Alloderm is a commercially available matrix based on DED which is used clinically to support tissue regeneration, particularly in dental applications.

1.3.3 **Towards improved full-thickness oral mucosa models**

The tumour microenvironment is a complex interplay of multiple cell types residing within a specific ECM. In 1863, Virchow first noted the link between leukocytes and cancer as he observed a large number of infiltrating cells into tumours (Virchow, 1863). Since then, evidence has shown that the tumour stroma is more than just an observer to tumour progression, with fibroblasts, macrophages, other immune cells and secreted cytokines shown to play a role (Mueller and Fusenig, 2004). Three-dimensional *in vitro* models are being developed which represent the tumour microenvironment more accurately than traditional monolayer cell culture, *ex vivo* and *in vivo* models. Suggestions for improvements to currently available oral cancer models are described below.

Oral mucosa models containing haematopoietic cells

Haematopoietic stem cells (HSCs) that originate in the bone marrow, differentiate into all other mature blood cell types via either the common myeloid or lymphoid progenitors. Some studies have developed 3D models of the haematopoietic niche in order to further understand the mechanisms involved in haematopoiesis (Cook *et al.,* 2012; Leisten *et al.,* 2012; Pietrzyk-Nivau *et al.,* 2015). Immune cells, that originate from HSCs, aid the oral mucosa in its role as a protective barrier. The connective tissue component of oral mucosa contains dendritic cells, mast cells and macrophages in order to provide innate immunity (Feller *et al.,* 2013). These release cytokines, chemokines and antimicrobial peptides to protect the oral cavity against microbial invasion. Mast cells and neutrophils are white blood cells which initiate inflammation in response to microbial products. Dendritic cells have a primary role in antigen presentation accompanied by macrophages which also aid microbial clearance using phagocytosis (Feller *et al.,* 2013).

In order to further understand the role that immune cells play within tissues, in addition to how they develop and mature in the bone marrow, a need for an immune cell component within 3D tissue engineered *in vitro* models has been identified. So far, immune cells have been incorporated into a limited number of models. Monocyte-derived macrophages

(MDM) and dendritic cells within an intestinal mucosa collagen-transwell-based model have been used to improve drug delivery in inflammatory bowel disease (Leonard *et al.,* 2010). This model was further developed to include THP-1 or MUTZ-3 cells in order to improve the reproducibility of the model (Julia Susewind, 2015, published dissertation). Macrophages have also been co-cultured with tumour spheroids in a colon carcinoma model to assess tumour invasion, migration and the inflammatory response (Hauptmann *et al.,* 1993).

For the purpose of dermal research, Bechetoille *et al.,* showed that macrophages within a bovine collagen, chitosan and chondroitine 4-6 sulfate solid scaffold secreted anti-inflammatory cytokines in response to LPS (Bechetoille *et al.,* 2011). Dermal models have also been developed using commercially available dendritic cells (Uchino *et al.,* 2009) and THP-1 monocyte cell line in a skin sensitisation model (Uchino *et al.,* 2013). TAM have been monitored within a 3D *in vitro* dermal model in which macrophages were incorporated within a collagen hydrogel (Linde *et al.,* 2012). In addition, a single co-culture system investigating the crosstalk between dermal keratinocytes and T cells has been identified, which uses a de-cellularised DED (van den Bogaard *et al.,* 2014). A comprehensive literature search failed to show any studies using 3D *in vitro* culture of neutrophils, likely due to their short life-span. However, promyelocytic HL60 cells differentiated along the granulocytic pathway have been used as a replacement (Hirz and Dumontet, 2016). Other areas of research which have successfully incorporated macrophages into 3D *in vitro* models include collagen hydrogels using lung adenocarcinoma cell lines (Liu *et al.,* 2016) and a tetra-culture of fibroblasts, adipocytes, primary human monocytes or macrophages and breast carcinoma cell lines cultured under perfusion flow (DesRochers *et al.,* 2015, published abstract). These are summarised in **Table 1.2**.

Disease model	Immune cell	Scaffold	Analyses	Reference
Inflammatory bowel disease	MDM; monocyte-derived dendritic cells	Collagen-coated transwell	TEER; IHC-P; IF; CBA	(Leonard *et al.,* 2010)
Healthy dermal equivalent	MDM	Bovine collagen, chitosan and chondroitine 4-6 sulfate-coated insert	ELISA; IHC; IF; fluorescent bead phagocytosis	(Bechetoille *et al.,* 2011)
	Monocyte-derived dendritic cell	Collagen vitrigel membrane	IHC; Ellman's test	(Uchino *et al.,* 2009)
	THP-1	Collagen vitrigel membrane	ELISA; cytotoxicity assay	(Uchino *et al.,* 2013)
Dermal squamous cell carcinoma	MDM	Collagen hydrogel	IF; IHC; zymography	(Linde *et al.,* 2012)
Dermal inflammation	Primary T cells	DED	IHC; ELISA; qPCR	(van den Bogaard *et al.,* 2014)
Leukaemia	HL60; Kasumi-1; MV411	PGA/PLLA 90/10 co-polymer discs	IHC; flow cytometry; cytotoxicity assay; fluorescent dextran diffusion assay	(Aljitawi *et al.,* 2014)
Lung adenocarcinoma	Not specified	Collagen hydrogel	IF; ELISA; Western blot	(Liu *et al.,* 2016)
Blood-brain-barrier	Astrocytes	Collagen hydrogel	IF; dextran diffusion assay	(Tourovskaia *et al.,* 2014)

Table 1.2. *In vitro* 3D models containing an immune cell component. Transepithelial electrical resistance (TEER), immunohistochemistry (IHC), cytokine bead array (CBA), immunofluorescence (IF), enzyme-linked immunosorbent assay (ELISA), quantitative polymerase chain reaction (qPCR).

Whilst other fields have reported successes with 3D *in vitro* models containing immune cells, to the best of our knowledge, primary human immune cells have yet to be incorporated into a long-term collagen-based 3D *in vitro* oral mucosa model. Examples of simple co-cultures include; an indirect co-culture combining peripheral blood monocytic cells (PBMC) and OSCC cell lines cultured in inserts (Essa *et al.,* 2016), phorbol 12-myristate 13-acetate (PMA)-treated THP-1 pro-monocytes seeded directly onto a mucoepidermoid carcinoma cell line monolayer (Chiu *et al.,* 2014; Lee *et al.,* 2014) or the use of PMA-treated THP-1 cells seeded onto chamber slides in combination with human oral squamous cell carcinoma cancer cell lines. More complex tissue-like models have also used alternatives to primary human cells, including MUTZ-3 dendritic cell line which has been cultured in collagen hydrogel-based models of the human gingiva to investigate the maturation and migration of Langerhans cells (Kosten *et al.,* 2015). Mono Mac 6 (MM6) cell line has been perfused into an oral infection model of the periodontal pocket (Bao *et al.,* 2015b). In the only use of primary human immune cells within a 3D oral model that could be found, PBMC were seeded into a gingival model on gelatin-coated ThinCerts™ 24 hours before the end point to investigate the effect of radiation on modelled gingiva (Tschachojan *et al.,* 2014). It has also been shown that macrophages could be detected in a myoma scaffold bearing human oropharyngeal squamous cell carcinoma cells (Nurmenniemi *et al.,* 2009), and although the addition of exogenous immune cells to this scaffold has not been explored, the addition of conditioned media from PMA-treated THP-1 cells polarised to M2-type resulted in increased invasion and secretion of cytokines associated with OSCC (Pirila *et al.,* 2015). Oral mucosa models containing commercially available immune cell lines are listed in **Table 1.3**.

Disease model	Immune cell	Culture method	Reference
Healthy gingival equivalent	MUTZ-3	3D collagen hydrogel	(Kosten *et al.,* 2015)
Periodontal pocket	MM6	3D collagen sponge	(Bao *et al.,* 2015a)
Immortalised gingival equivalent	PBMC	Gelatin-coated ThinCerts™	(Tschachojan *et al.,* 2014)
Tongue SCC	THP-1	Myoma punch biopsy	(Pirila *et al.,* 2015)

Table 1.3. *In vitro* 3D models of oral tissue containing an immune cell component.

Previously published 3D models containing macrophages have shown dramatic differences in the proliferation, differentiation, morphology and cellular functions of macrophages cultured compared to those cultured as monolayer (Liu *et al.,* 2016).

Oral mucosa models containing stromal cells

Fibroblasts and pericytes are the most common cell type in the stroma. Fibroblasts are responsible for the turnover of the extracellular matrix, and pericytes are contractile cells which surround endothelial cells that make up the vasculature. Fibroblasts are commonly used in tissue-engineered models as they secrete factors, such as keratinocyte growth factor (KGF), required for differentiation and stratification of an epithelium, and they contribute to the integrity of the scaffold used (Latkowski *et al.,* 1995). Models devoid of fibroblasts, but with exogenous application of KGF, produce a thick, but undifferentiated epithelium due to increased keratinocyte proliferation (Costea *et al.,* 2003). Stimulation of fibroblasts cultured in 2D can enable them to secrete enough of their own ECM to support culture of dermis in a tissue engineered model (Berning *et al.,* 2015).

Pericytes however are typically only used in models of angiogenesis. There a number of methods for their isolation from primary tissue and commercially available pericyte cell lines, although their widespread use is limited by the lack of pericyte-specific markers. There is, however, an example of their successful incorporation into a collagen hydrogel

modelling the blood-brain-barrier in the only co-culture of pericytes with an immune component that could be found (Tourovskaia *et al.,* 2014). Other models containing pericytes in co-culture with endothelial cells are reviewed here (Gokcinar-Yagci *et al.,* 2015). Of interest, a tissue-engineered model of angiogenesis containing both fibroblasts and pericytes showed that pericytes were recruited from fibroblasts, due to platelet-derived growth factor (PDGF, Berthod *et al.,* 2012).

Vascularisation of tissue-engineered models

The rich vascular network present in the human body is essential for tissue growth and repair. Evidence has also shown the importance that the vasculature has in tumour growth as it supplies nutrients, oxygen and removes waste. In addition, it provides cancer cells with a route to enter circulation for metastasis and enables a constant supply of immune cells to extravasate from circulation to further support tumour development. The vasculature is so essential to a malignancy that cancer cells employ many different mechanisms to promote angiogenesis (Nagy *et al.,* 2009). Many anti-cancer therapies aim to target angiogenesis, however in order to understand more about the mechanisms involved and test potential therapies, humanised tissue engineered models of cancer require a vasculature in order to best represent the *in vivo* situation.

Vascularisation of tissue-engineered models typically involves the use of moulds, guides and sacrificial lattices to form channels where endothelial cells can be cultured into perfusable channels. For example, to model angiogenesis and the blood-brain-barrier, a chip can be used into which endothelial cells are seeded to form vessels that are surrounded by an ECM containing stromal cells (Tourovskaia *et al.,* 2014). Alternatively, networks of 3D printed carbohydrate glass encapsulated within a polyethylene glycol (PEG) hydrogel containing the cells of interest, can be used to form a vessel template which later dissolves and can be lined with endothelial cells (Miller *et al.,* 2012). Mimetas offer a commercially available pump-free, perfusable 3D vasculature surrounded by a collagen gel.

Vascularisation of tissue-engineered models can also be achieved using the spontaneous sprouting observed by endothelial cells cultured within an appropriate scaffold (typically collagen). A pre-vascularised tumour model has described co-cultures of breast or colon cancer cells with endothelial cells within tumour spheroids, embedded into a fibrin gel containing fibroblasts. This model not only models angiogenesis, but also intravasation of tumour cells under the influence of hypoxia (Ehsan *et al.,* 2014). Tubule formation assays are becoming increasingly popular and have the potential for incorporation into 3D *in vitro* models. Tubule formation assays involve the culture of endothelial cells within Cultrex Basement Membrane Extract, where they begin to form tubules under the influence of exogenous stimuli, such as VEGF, PDGF, epidermal growth factor (EGF) and FGF2 (Arnaoutova and Kleinman, 2010; DeCicco-Skinner *et al.,* 2014). ThermoFisher offer an assay which supplies a gel and 'positive inducer' to promote tubule formation.

Alternatively, a microvascular system has been developed which uses a micropump to induce flow around glass circuits which become covered with endothelial cells after 4 days (Schimek *et al.,* 2013). This technology can be incorporated into existing 'human on a chip' models to create more physiologically relevant model systems.

1.4 Hypothesis and Aims

Immunohistochemical studies have shown that macrophages, specifically those which are CD163+, correlate with a poor prognosis in OSCC. However, due to a lack of reproducible models containing primary human immune cells, the role that macrophages play in oral cancer progression remains largely unknown. *In vitro* 3D models are increasingly bridging the gap between basic and translational research due to their increased complexity compared to monolayer cultures, and increased clinical relevance and reduced cost compared to *in vivo* models. The hypothesis of this study is that *in vitro* 3D models of the oral mucosa containing an immune component will improve understanding of the role TAM play in oral cancer progression. Currently, to the best of our knowledge, there are no published models of the oral mucosa which incorporate primary human monocytes or macrophages. In addition, to enable the analysis of macrophages cultured within

engineered tissues, molecular tools and rapid isolation methods are required to preserve the underlying phenotype of these highly plastic cells (Murray *et al.,* 2014).

Therefore, this thesis aims to address these problems, by:

a) Generating a tissue-engineered 3D *in vitro* model of the oral mucosa containing primary human immune cells;
b) Developing a multi-colour flow cytometry panel for the quantitative analysis of macrophage protein expression;
c) Optimising the use of the multi-colour flow cytometry panel on macrophages isolated from tissue-engineered models of the oral mucosa.

2 Chapter 2: Materials and Methods

2.1 Materials

Manufacturers and product names for all reagents used in this work are described in the text.

2.2 2D cell culture

2.2.1 Cell lines

THP-1 (ATCC® TIB-202™)

THP-1 cells, a promonocytic cell line originally isolated from a male infant with acute monocytic leukaemia (Tsuchiya *et al.,* 1980), were maintained in suspension in Roswell Park Memorial Institute (RPMI) 1640 medium (Sigma Aldrich, Dorset, UK) supplemented with 100 IU/mL penicillin (Sigma Aldrich, Dorset, UK), 100 µg/mL streptomycin (Sigma Aldrich, Dorset, UK) and 10 % batch-tested foetal bovine serum (FBS, v/v; Biosera, East Sussex, UK).

Mono Mac 6

Mono Mac 6 cells, established from a patient with acute monoblastic leukaemia (AML, Zieglerheitbrock *et al.,* 1988), were cultured in suspension in RPMI 1640 supplemented with 100 IU/mL penicillin, 100 µg/mL streptomycin, 10 % batch-tested FBS (v/v), 1-2x non-essential amino acids (NEAA, v/v; Life Technologies, Paisley, UK) and 10 % OPI supplement (containing oxaloacetate, pyruvate and insulin, v/v; Sigma Aldrich, Dorset, UK).

H357

Human epithelial OSCC cell line, H357, isolated from the tongue of a 74 year old male (Prime *et al.,* 1990) were cultured adherent to tissue culture plastic in Dulbecco's modified Eagle's medium (DMEM; Gibco, Paisley, UK) supplemented with 100 IU/mL penicillin, 100 µg/mL streptomycin and 10 % batch-tested FBS (v/v).

NIH/3T3 (ATCC® CRL-1658™)

3T3 murine fibroblast cells were cultured adherent to tissue culture plastic in RPMI 1640 supplemented with 100 IU/mL penicillin, 100 µg/mL streptomycin and 10 % iron-fortified calf bovine serum (Sigma Aldrich, Dorset, UK).

For irradiation of 3T3, cells were exposed to 60 Grays using a cobalt-60 source irradiator to arrest cell growth and cryopreserved. Irradiated 3T3s were resurrected immediately prior to use and referred to as 'i3T3' cells.

FNB6 hTERT

Human telomerase immortalised epithelial cell line, FNB6, isolated from a healthy volunteer were maintained in adherent culture on an i3T3 feeder layer in Green's medium (**Table 2.1**).

Component	Volume	Stock conc.	Final conc.	Storage
DMEM	330 mL	-	66 %	4°C
Ham's F12	108 mL	-	21.6 %	4°C
FCS	50 mL	-	10 %	-20°C
Penicillin/streptomycin	5 mL	-	1%	-20°C
Amphotericin B	1.25 mL	250 µg/mL	0.625 µg/mL	-20°C
Adenine	2 mL	6.25 µg/mL	0.025 µg/mL	-20°C
Insulin	2.5 mL	1 mg/mL	5 µg/mL	4°C
3, 3, 5-Tri-iodothyronine (T_3)	0.5 mL	136 µg/mL	136 ng/mL	-20°C
Apo-transferrin	0.5 mL	5 mg/mL	5 µg/mL	-20°C
Hydrocortisone	80 µL	2.5 mg/mL	4 µg/mL	4°C
Epidermal Growth Factor (EGF)	25 µL	100 µg/mL	5 ng/mL	-20°C
Cholera toxin	500 µL	8.47 µg/mL	8.47 ng/mL	4°C

Table 2.1. Green's medium. Table lists the volume, stock and final concentrations and storage conditions for the components required in Green's medium used for FNB6 and NOK cells. Adapted from Hearnden, V thesis, January 2011.

2.2.2 Primary cells

Normal oral keratinocyte isolation

Normal oral keratinocytes (NOK) were isolated from the oral mucosa during routine dental procedures with written informed consent (ethical approval number 09/H1308/66) as previously described (Hearnden *et al.,* 2009). Briefly, biopsies were incubated overnight at 4 °C in 0.05 % trypsin/0.02 % ethylenediaminetetraacetic acid (EDTA) supplemented with 100 IU/mL penicillin, 100 µg/mL streptomycin and 0.625 µg/mL amphotericin B (Sigma Aldrich, Dorset, UK). Following enzymatic digestion, the connective tissue was separated from the epithelium; keratinocytes were gently scraped from the surface of the biopsy and collected for subsequent culture. Following centrifugation, NOK cells were cultured in

Green's medium (**Table 2.1**) and maintained adherent to tissue culture plastic on an i3T3 feeder layer until passage 3, where cells were discarded (Rheinwald and Green, 1975).

Normal oral fibroblast isolation

Primary human normal oral fibroblasts (NOF) were isolated from the oral mucosa during routine dental procedures with written informed consent (ethical approval number 09/H1308/66) as previously described (Hearnden *et al.,* 2009). Briefly, biopsies were incubated overnight at 4 °C in 0.05 % trypsin/0.02 % EDTA supplemented with 100 IU/mL penicillin, 100 µg/mL streptomycin and 0.625 µg/mL amphotericin B (Sigma Aldrich, Dorset, UK). Following enzymatic digestion, the connective tissue was separated from the epithelium and finely minced, followed by digestion with 0.5 % collagenase A (w/v; Sigma Aldrich, Dorset, UK) overnight in a humidified environment at 37 °C and 5 % CO_2. Following centrifugation, NOF cells were cultured adherent to tissue culture plastic in DMEM supplemented with 100 IU/mL penicillin, 100 µg/mL streptomycin (v/v) and 10 % batch-tested FBS (v/v) until passage 9, where cells were discarded.

Human peripheral blood monocyte isolation

Human peripheral blood monocytes (PBM) were isolated from buffy coats (ethical approval number 012597) by Ficoll-hypaque (GE Healthcare, Buckinghamshire, UK) density gradient centrifugation. Blood cells were mixed 1:1 with Hank's balanced salt solution (HBSS, without Ca^{2+} and Mg^{2+}; Fisher Scientific, Leicestershire, UK), carefully overlayed onto Ficoll-hypaque and centrifuged at 400 x *g* for 40 minutes at room temperature with reduced deceleration. The monocyte layer (between the upper serum and lower Ficoll layers) was removed by aspiraton using a Pasteur pipette and washed several times in HBSS. In order to further enrich the monocyte population, a human pan monocyte isolation kit was used according to the manufacturer's instructions (Miltenyi). Briefly, CD14+CD16+ cells were negatively selected using a cocktail of antibodies bound to microbeads. Magnetically labelled CD14-CD16- cells remained bound to an LS column, enabling CD14+CD16+ cells to be collected. Monocyte purity was assessed by flow cytometry ($CD14^+$). Human monocytes

were cultured, initially in suspension until they became adherent to tissue culture, in Iscove's modified Dulbecco's medium (IMDM; Gibco, Paisley, UK) supplemented with 2 % human AB serum (v/v; Sigma Aldrich, Dorset, UK), 100 IU/mL penicillin and 100 µg/mL streptomycin.

2.2.3 Passaging, cryogenic preservation and recovery of cells

Passaging of cells in suspension culture

THP-1 cells were sub-cultured when cell concentration reached $0.8x10^6$ cells/mL, by centrifugation for 5 minutes at 190 x *g* and cells were resuspended at $0.2\text{-}0.4x10^6$ cells/mL in fresh, supplemented media. MM6 cells were sub-cultured when cell concentration reached $1x10^6$ cells/mL, by centrifuging for 5 minutes at 190 x *g* and re-suspending cells at $0.6\text{-}0.8x10^6$ cells/mL in fresh, supplemented media. Cells were passaged every 2-3 days and cell concentration never exceeded $1x10^6$ cells/mL.

Passaging of cells in monolayer culture

H357, FNB6 and NOF cells were passaged at 90% confluence by removing media and washing twice with calcium and magnesium-free phosphate buffered saline (PBS; Sigma Aldrich, Dorset, UK) before incubating with 0.05 % trypsin/0.02 % EDTA (Sigma Aldrich, Dorset, UK) at 37 °C for 10 minutes, or until cells were detached. Medium containing 10 % FBS was added at a 1:1 (v/v) ratio to prevent further enzymatic activity. Cells were centrifuged at 190 x *g* for 5 minutes, re-suspended at the required concentration (**Table 2.2**) of appropriate cell culture medium and seeded into 75 cm^2 tissue culture flasks (Greiner-Bio-One, Germany). At 80 % confluence, NIH/3T3 were passaged as above. All cells were cultured in a humidified environment at 37 °C in 5 % CO_2 and routinely tested for mycoplasma contamination. Media was refreshed every 2-3 days.

Cell type	Seeding density
H357	$5x10^3/cm^2$
FNB6	$13x10^3/cm^2$
NIH/3T3	$3x10^3/cm^2$

Table 2.2. Seeding densities of cell lines. The seeding density of cell lines H357, FNB6 and NIH/3T3 is described.

Cells were counted using a Neubauer haemocytometer (Weber Scientific International, Middlesex, UK) using the equation below (**Equation 2.1**):

$$Concentration\ of\ cells\ per\ mL = \frac{Number\ of\ cells\ x\ 10{,}000}{Number\ of\ squares\ x\ dilution\ factor}$$

Equation 2.1. Equation to determine cell number. The relationship between number of cells counted with a haemocytometer and the total concentration of cells is described.

Freezing cells for cryogenic preservation

For long term storage, cells were passaged (as above) and resuspended at $1x10^6$ cells/mL in freezing medium (90 % FBS (v/v) with 10 % dimethyl sulfoxide (DMSO, v/v; Sigma Aldrich, Dorset, UK)). One millilitre of this solution was added to each cryovial (Greiner bio-one, Gloucestershire, UK) for cryopreservation. Cryovials were placed in a Mr. Frosty™ freezing container (Thermo Scientific, Leicestershire, UK) which achieves a cooling rate of 1 °C per minute to -80 °C prior to long-term storage in liquid nitrogen for optimal cell preservation.

Recovery of frozen cells

When required, cells were thawed and immediately re-suspended in appropriate supplemented cell culture media, centrifuged at 190 x *g* for 5 minutes to remove DMSO and the pellet re-suspended in media and seeded into 75 cm^2 tissue culture flask.

2.2.4 Differentiation of monocytes to macrophages

Human monocyte-derived macrophages

Human PBM in suspension were cultured in 75 cm^2 tissue culture flasks, where they immediately became adherent. Adherent monocytes were washed twice with PBS every 3 days and cultured in fresh supplemented IMDM to remove non-adherent cells. PBM were differentiated to MDM for between 7 and 14 days.

THP-1 macrophages

THP-1 monocytes were seeded at $5x10^5$ cells/mL and treated with 200 nM PMA (Sigma Aldrich, Dorset, UK) as previously described (Daigneault *et al.,* 2010). Briefly, cells were incubated with PMA for 3 days followed by a resting phase for 5 days in a humidified environment of 5 % CO_2 at 37 °C.

Mono Mac 6 macrophages

To differentiate MM6 cells into a macrophage-like cell, adherence was induced as previously described (Zieglerheitbrock and Ulevitch, 1993). Briefly, cell culture 24-well plates were pre-coated with 50 % (v/v) human serum diluted in PBS and incubated for 1 hour at 37 °C. With pre-coating serum removed, 1 mL of cell culture medium containing $0.5x10^6$ cells/mL was added to each well and cultured for 72 hours in the presence or absence of 10-50 ng/mL PMA.

2.2.5 Polarisation of macrophages

To promote polarisation, MDM were treated with supplemented IMDM with the addition of human recombinant cytokines and *E.coli* LPS. To polarise MDM to an M1 phenotype, 10 ng/mL GM-CSF (Peprotech, London, UK) was added, or for M2 polarised MDM 25 ng/mL M-CSF (Peprotech, London, UK) was added, for a total of 7 days with media and cytokines refreshed on days 3 and 6 (Zhang *et al.,* 2013). For the final 24 hours of the 7-day culture period, cell culture media was further supplemented with 100 ng/mL LPS (Sigma Aldrich, Dorset, UK) and 20 ng/mL IFNγ (Peprotech, London, UK) for M1 polarised MDM (Zhang *et*

al., 2013). Alternatively, for M2a polarised MDM, 25 ng/mL IL-4 (Peprotech, London, UK) was added for the final 24 hours of culture (Zhang *et al.,* 2013) or for M2c polarised MDM, 20 ng/mL IL-10 (Peprotech, London, UK) was added (Mia *et al.,* 2014). This is summarised in **Table 2.3**.

<table>
<tr><th></th><th>M0</th><th>M1</th><th>M2a</th><th>M2c</th></tr>
<tr><td>6 days</td><td>-</td><td>10 ng/mL GM-CSF</td><td>25 ng/mL M-CSF</td><td>25 ng/mL M-CSF</td></tr>
<tr><td rowspan="2">24 hours</td><td rowspan="2">-</td><td>100 ng/mL LPS</td><td rowspan="2">25 ng/mL IL-4</td><td rowspan="2">20 ng/mL IL-10</td></tr>
<tr><td>20 ng/mL IFNγ</td></tr>
</table>

Table 2.3. Polarisation of monocyte-derived macrophages. The supplements used for polarisation of MDM to M0, M1, M2a and M2c phenotypes are described.

2.3 3D cell culture

2.3.1 Use of a collagen hydrogel

Isolation of rat-tail type 1 collagen

Rat-tail type 1 collagen was isolated from rat tails kindly donated by research groups led by Professor Boissonade, Professor Paul Hatton and Mrs Christine Freeman, The University of Sheffield, at the end of licensed studies and stored at -20 ºC. When required, these were thawed and processed as previously described (Rajan *et al.,* 2006). Briefly, under sterile conditions, tails were folded and twisted to expose the underlying bone and tendons. Bones were removed, and exposed tendons were cut and washed in PBS. Tendons were then dissolved for 7 days in 0.1 M sterile acetic acid (Sigma Aldrich, Dorset, UK) at 4 ºC. The resultant collagen solution was freeze-dried (VirTis Benchtop K Manifold freeze drier, SP Scientific, Suffolk, UK) and re-dissolved in 0.1 M acetic acid to a stock concentration of 5 mg/mL and stored at 4 ºC for use in collagen hydrogel preparation.

Preparation of collagen hydrogel

Collagen hydrogels were prepared as previously described (Dongari-Bagtzoglou and Kashleva, 2006). Briefly, keeping everything on ice, rat-tail type 1 collagen was mixed on ice with 10x DMEM, reconstitution buffer (a mixture of N-2-Hydroxyethylpiperazine-N-2-ethane sulfonic acid (HEPES; Sigma Aldrich, Dorset, UK), sodium hydroxide (Sigma Aldrich, Dorset, UK) and sodium bicarbonate (Sigma Aldrich, Dorset, UK), FBS and L-glutamine (Sigma Aldrich, Dorset, UK; **Table 2.4**). This solution was neutralised to pH 7.4 with 0.1 M sodium hydroxide (Sigma Aldrich, Dorset, UK) before addition of cells. One millilitre of the thoroughly mixed collagen mixture was then distributed to each well of a 24-well plate (Greiner-Bio-One, Germany) and incubated at 37 °C in a humidified environment for 20 minutes, allowing the collagen hydrogel to set.

Component	Final Concentration
10x RPMI	13.8 mg/mL
Sodium bicarbonate	2.25 mg/mL
HEPES	2 mM
1M NaOH	6.3 mM
FBS	8.5% v/v
L-glutamine	2.1 mM
Rat tail collagen, type 1	3.365 mg/mL

Table 2.4. Preparation of collagen hydrogels. The final concentration of components used in the preparation of collagen hydrogels. 4-(2-hydroxyethyl)-1-piperazinethanesulfonic acid (HEPES), sodium hydroxide (NaOH).

Mono-culture of monocytes and macrophages within collagen hydrogels

One million monocytes (either PBM, THP-1 or MM6) or macrophages (MDM or PMA-treated THP-1) were added per millilitre of collagen hydrogel mixture and cultured with 1 mL per well of either supplemented IMDM (PBM and MDM) or RPMI 1640 (THP-1, MM6, and PMA-treated THP-1). Cell-containing hydrogels were cultured for 14 days in a humidified atmosphere of 5 % CO_2 at 37 °C. Media was refreshed every 2-3 days.

Preparation of tissue-engineered oral mucosa

Collagen hydrogels were prepared as described previously (Dongari-Bagtzoglou and Kashleva, 2006), with the addition of 0.05-0.2x10^6 NOF within the collagen hydrogel. For models containing an immune component, either 0.5x10^6 THP-1 or 1-4x10^6 MDM were also added within the hydrogel mixture. Once the hydrogel had set, 0.5x10^6 epithelial cells (FNB6, NOK or H357) in relevant cell culture media were seeded on top. Engineered mucosa was incubated for 24 hours before lifting to an air-liquid interface (ALI) within a 6 well plate using perforated metal grids, with a fine mesh separating the grid and hydrogel (**Figure 2.1**). 6mL of cell culture media, appropriate to the epithelial cell type, was used to fill each well to meet the underside of the engineered mucosa. Media was refreshed every 2-3 days for 14 days.

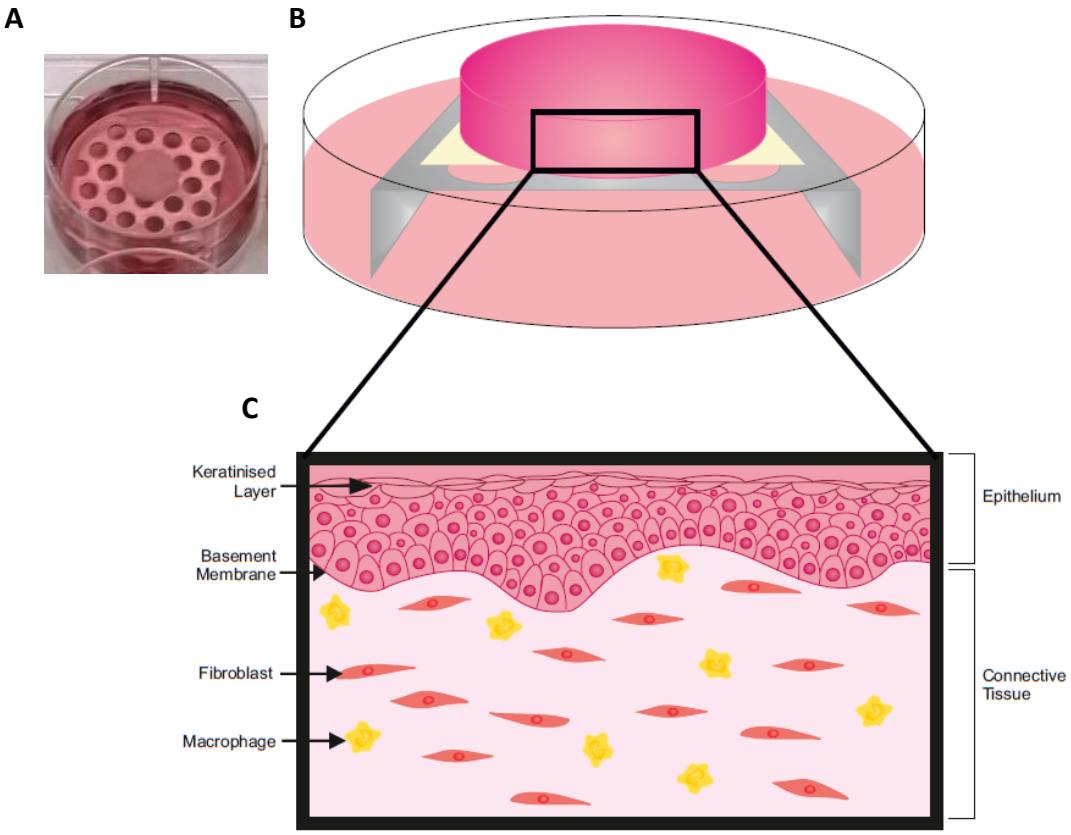

Figure 2.1. Production of tissue-engineered oral mucosa. Image shows a collagen hydrogel containing cells, cultured at air-to-liquid interface on top of a perforated metal grid, separated by a fine mesh (**A**). Diagram (**B**) is a graphic representation of image A. Diagram (**C**) is a schematic example section of a collagen hydrogel populated with fibroblasts and macrophages with an overlying stratified epithelium.

2.3.2 Physical analyses of cell-containing collagen hydrogels

Contraction assay

After 14 days of culture, images of contracted hydrogels were taken using a background of graph paper. The surface area was measured using ImageJ, and scale set using the graph paper (Schneider *et al.,* 2012). Results are reported as surface area measurements (mm^2).

Rheological examination

A rheometer (Bohlin Gemini, Malvern instruments, UK) was used to collect data measuring the elastic modulus. Samples were loaded, with epithelium facing upwards, between 20 mm parallel plate and peltier plate heated to 37 °C. Samples were surrounded by Green's medium and 1.0 g of thrust was applied to maintain grip on the sample. An oscillatory test (frequency sweep from 1.0-0.1 Hz, 0.02 strain) was undertaken, with elastic modulus and gap size measurements recorded. In order to normalise the differences in sample size, surface area measurements from the contractility assay were related to the elastic modulus at 0.1 Hz by the following equation (**Equation 2.2**):

$$Stiffness = \frac{area\ of\ parallel\ plate\ (314.16mm^2)}{surface\ area\ of\ model\ (mm^2)}\ x\ measured\ elastic\ modulus\ (Pa)$$

Equation 2.2. Equation to determine stiffness. The relationship between stiffness, sample surface area and elastic modulus is described.

Results from oscillatory tests are reported as elastic modulus (Pa) and gap size (mm^2).

2.4 Histological analysis

2.4.1 Formalin-fixed paraffin-embedded

Preparation of formalin-fixed paraffin-embedded blocks

To visualise tissue morphology, collagen hydrogels were fixed in 10 % PBS-buffered formalin (v/v) for 24 hours, processed overnight using a Leica TP1020 benchtop tissue processor (Leica TP1020 benchtop tissue processor, Leica Microsystems, Germany; **Table 2.5**), bisected and embedded perpendicular to the bottom of the mould in paraffin wax (Leica EG1160 embedding centre, Leica Microsystems, Germany). Formalin-fixed paraffin-embedded (FFPE) blocks were stored at room temperature until use.

Solution	Time in Solution
10 % neutral buffered formalin	1 hour
70 % alcohol	1 hour
70 % alcohol	1 hour
90 % alcohol	1 hour
90 % alcohol	1 hour
Absolute alcohol	1 hour
Absolute alcohol	1 hour
Absolute alcohol	1 hour
Xylene	1 hour 30 mins
Xylene	1 hour 30 mins
Paraffin wax I	2 hours
Paraffin wax II	2 hours

Table 2.5. Histological processing schedule. Table shows the solutions and length of time FFPE samples spent in each solution for histological processing.

Preparation of 4 µm sections

FFPE blocks were cooled on ice blocks for 30 minutes prior to sectioning. Initially, blocks were trimmed in 10 µm sections until the sample was exposed at the surface of the wax block. Four micrometer sections were prepared in levels, 40 µm apart (Leica RM2235 microtome, Leica Microsystems, Germany), floated on a paraffin section mounting bath (Barnstead Electrothermal, Staffordshire, UK), transferred to a Superfrost plus micro slide (VWR, West Sussex, UK) and incubated at 55 °C for 20 minutes to ensure the section was fully adhered to the slide.

Haematoxylin and eosin staining

Haematoxylin and eosin (H&E) staining was performed (Leica ST4040 Shandon Linear Stainer, Leica Microsystems, Germany; **Table 2.6**). Haematoxylin is a basic dye which stains the acidic cell nucleus blue, whereas eosin counterstain is an acidic dye which stains the nucleus of cells pink. Once stained, slides were mounted with Dibutyl phthalate, polystyrene, xylene (DPX) and samples were covered with an appropriately sized coverslip. Once DPX was set, slides were imaged using an Olympux BX51 microscope and colour view Illu camera with associated Cell^d SOFTWARE (Olympus soft imaging solutions, GmbH, Münster, Germany).

Order	Solution
1	Xylene
2	Xylene
3	Xylene
4	99 % IDA
5	99 % IDA
6	99 % IDA
7	Distilled water
8	Distilled water
9	Harris' haematoxylin (Shandon)
10	Harris' haematoxylin (Shandon)
11	Harris' haematoxylin (Shandon)
12	Harris' haematoxylin
13	Running tap water
14	0.1 % acid alcohol
15	Running tap water
16	Scott's tap water substitute
17	Running tap water

18	Eosin Y – aqueous (Shandon)
19	Eosin Y – aqueous (Shandon)
20	Eosin Y – aqueous (Shandon)
21	Running tap water
22	99 % IDA
23	99 % IDA
24	99 % IDA
25	Xylene
26	Xylene
27	Xylene
28	Xylene

Table 2.6. Histological staining schedule. Table describes the order and solutions used for histological staining of organotypic co-culture sections. Industrial denatured alcohol (IDA).

Immunohistochemistry

Immunohistochemistry (IHC) staining to determine the expression of CD68, E-cadherin, AE1/3, vimentin, Ki67, collagen IV and isotype-matched controls was performed by the core facility. Staining was visualised using light microscopy and 3 fields of view for each section, cut in levels 40 µm apart, were analysed under the supervision of an oral pathologist.

2.5 Molecular analyses

2.5.1 Protein expression analysis using flow cytometry

Flow cytometry was used to analyse single cell expression of key macrophage markers of 2D and 3D cultured cells. Both single colour and polychromatic staining methods were used.

Sample preparation

Adherent cells were gently scraped using a cell scraper (Fisher Scientific, UK). Non-adherent monocytes (THP-1, PBM and MM6) and detached macrophages (PMA treated THP-1 and

MDM) were centrifuged at 1800 x *g* for 5 minutes and re-suspended at $1x10^6$ cells/mL in cold staining buffer (PBS supplemented with 1 % bovine serum albumin (BSA; Fisher Scientific, UK) and 0.1 % sodium azide (Sigma Aldrich, Dorset, UK)). Alternatively, for 3D-cultured cells, collagen hydrogels were enzymatically digested using 2 mg/mL collagenase IV (Sigma Aldrich, Dorset, UK) and incubated at 37 ºC with shaking at 100 rpm for 1.5 hours. Once digested, the resulting solution was passed through a 40 µm cell strainer (SLS, Nottinghamshire, UK) before washing twice with staining buffer. All sample staining was performed on ice to reduce the metabolic activity of cells, prevent apoptosis and prevent receptor shedding or internalisation during staining.

Single-colour sample staining

One millilitre of cell suspension containing 1 million cells was transferred to individual microtubes and pelleted for staining. For single-colour antibody staining of cell-surface markers, cell pellets were incubated for 20 minutes with either; primary followed by fluorescein-isothiocyanate (FITC)-conjugated secondary antibody (Life Technologies, Paisley, UK); or 20 minutes with directly conjugated antibody (Abcam, Cambridgeshire, UK); or mouse immunoglobulin G (IgG) isotype-matched control diluted in staining buffer (**Table 2.7**). Samples were incubated on ice, in the dark for 20 minutes. Cells were washed with cold staining buffer and finally re-suspended in 350 µL staining buffer on ice.

Specificity	Antibody	Fluorochrome	Vendor	Dilution
CD14	Primary (and secondary)	PE	Abcam	1:5 (1:10)
CD45	Directly conjugated	FITC	eBioscience	1:20
CD80	Directly conjugated	FITC	Abcam	1:5
CD163	Directly conjugated	APC	eBiosceince	1:20
CD206	Primary (and secondary)	FITC	Abcam	1:50 (1:25)
CPM	Primary (and secondary)	FITC	Abcam	1:50 (1:25)

Table 2.7. Antibodies used for single-colour staining. The antibodies and fluorochromes used for single-colour flow cytometry analysis of key monocyte and macrophage cell surface markers are detailed. Phycoerythrin (PE), fluorescein-isothiocyanate (FITC) and allophycocyanin (APC).

Single-colour sample analysis

For single-colour flow cytometry, samples were analysed using a FACSCalibur flow cytometer (BD Biosciences, Oxfordshire, UK) with 10 000 events collected. Fifty µg/mL Propium Iodide (PI; Sigma Aldrich, Dorset, UK) was added immediately before sample analysis for dead cell exclusion; cells staining positively for PI (based on gates set using unstained cells cultured and treated under the same conditions as test samples) were excluded from the analysis. Data was analysed using FlowJo software (TreeStar). Cell populations were gated using forward scatter (FSC) and side scatter (SSC) voltages for size and granularity respectively. A threshold for positively fluorescent cells was set using cells stained with an isotype-matched control. Normalised median fluorescence index (nMFI) was determined as previously described (Chan *et al.,* 2013) by the following equation (**Equation 2.3**):

$$nMFI = \frac{MFI\ positive\ staining}{MFI\ negative\ staining}$$

Equation 2.3. Equation to determine nMFI. The relationship between median fluorescence intensity (MFI) of positive and negative staining in relation to normalised MFI (nMFI) is described.

Polychromatic sample staining

The selected directly-conjugated macrophage markers were titrated in order to determine the optimal staining concentration. Antibodies were used at the manufacturer recommended concentrations and with the following dilution factors: 1:5 (v/v) followed by serial dilutions of 1:2 (v/v). Staining index was determined (**Equation 2.4**) and used to produce an antibody saturation curve to identify optimal antibody staining, shown on concatenated dot plots of the titrated antibody samples (red boxes, **Figure 2.2**).

$$Staining\ index = \frac{MFI\ positive - MFI\ negative}{2\ x\ standard\ deviation}$$

Equation 2.4. Equation to determine staining index. The relationship between standard deviation and median fluorescence intensity (MFI) of positive and negative samples to determine staining index for a selected fluorchrome is described.

Cells dispersed in a single cell suspension were washed in staining buffer and re-suspended at $0.5x10^6$ cells/mL with 1 mL transferred to individual microtubes. Samples were centrifuged at 1800 x *g* for 2 minutes, and supernatant discarded. Cells were re-suspended in 40 µL staining buffer with 10 µL FcR blocking reagent and incubated for 15 minutes at 4 °C. A titrated amount of each fluorochrome-conjugated antibody was added and the total volume made up to 100 µL with staining buffer (**Table 2.8**). Samples were incubated for 20 minutes on ice, and protected from light. Cells were washed twice in 1 mL of staining buffer and amine-reactive blue live/dead stain was used according to the manufacturer's instructions. Cells were washed twice in 1 mL staining buffer and finally re-suspended in 350 µL 1 % (w/v) paraformaldehyde diluted in PBS. Samples were analysed within 48 hours of staining.

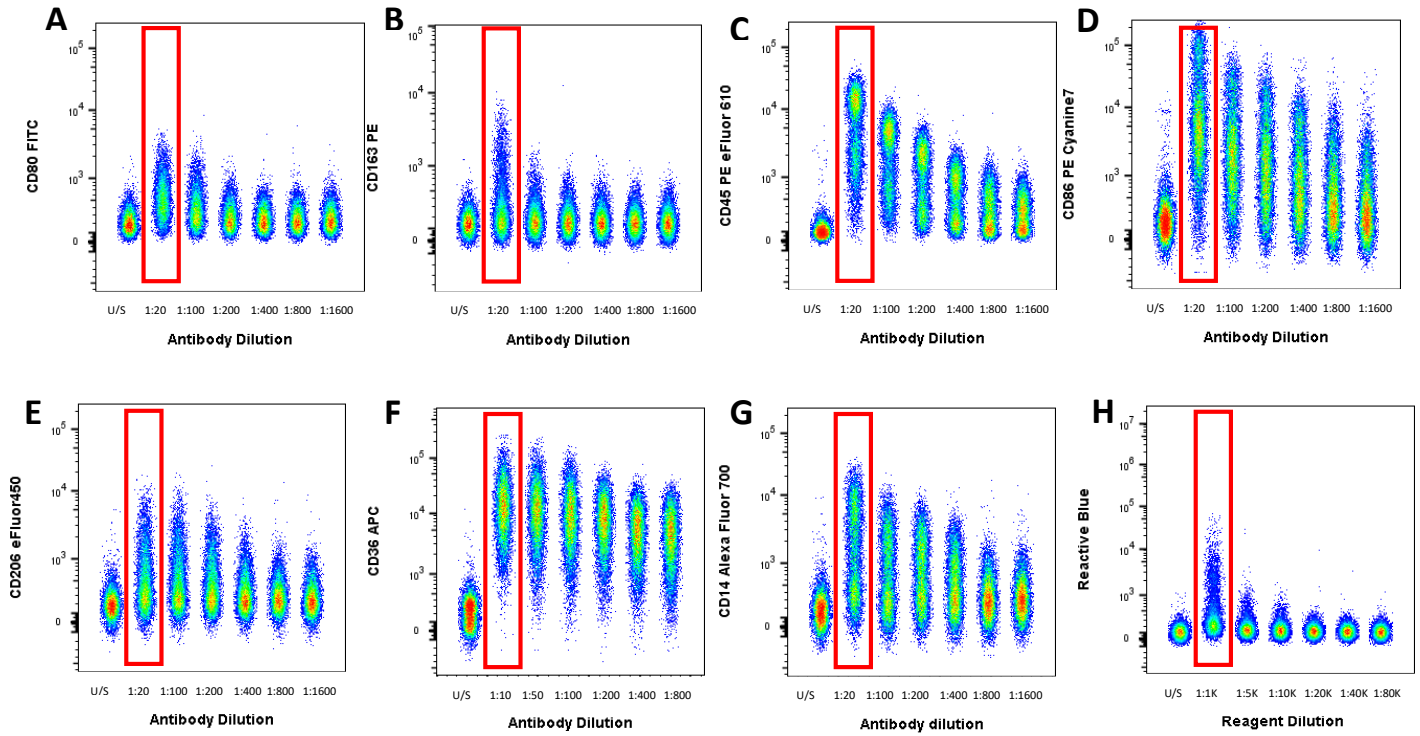

Figure 2.2. Concatenate displays of antibody conjugates and non-antibody reagents. Monocyte-derived macrophage gates were set based on FSC-SSC dot plots, followed by exclusion of doublets and non-viable cells. Concatenate displays of titrations for $CD80^{FITC}$ (**A**), $CD163^{PE}$ (**B**), $CD45^{PE\ eFluor\ 610}$ (**C**), $CD86^{PE\ Cyanine7}$ (**D**), $CD206^{eFluor\ 450}$ (**E**), $CD36^{APC}$ (**F**), $CD14^{Alexa\ Fluor\ 700}$ (**G**), and amine-reactive blue (**H**), where each concatenated dot plot represents all concentrations of each antibody ranging from 1:10 to 1:1600 dilutions, are compared to the measured fluorescence for each fluorochrome. Titres used for optimal staining conditions are highlighted (red box).

Specificity	Fluorochrome	Antibody clone	Vendor	Catalogue no.	Stock concentration	Dilution
CD14	Alexa Fluor® 700	61D3	eBioscience	56-0149	0.050 µg/µL	1:20
CD36	APC	AC106	MACS Miltenyi Biotec	130-100-307	0.055 µg/µL	1:10
CD45	PE eFluor® 610	HI30	eBioscience	61-0459	0.050 µg/µL	1:20
CD80	FITC	2D10.4	eBioscience	11-0809	0.200 µg/µL	1:20
CD86	PE Cyanine7	IT2.2	eBioscience	25-0869	0.025 µg/µL	1:20
CD163	PE	eBioGHI/61	eBioscience	12-1639	0.050 µg/µL	1:20
CD206	eFluor® 450	19.2	eBioscience	48-2069	0.050 µg/µL	1:20
Viability	Amine-reactive blue	n/a	Life Technologies	L23105	n/a	1:1000

Table 2.8. Flow cytometry reagent information. Detailed information on the commercially available antibodies and non-antibody reagents used. Not applicable (n/a).

Polychromatic sample analysis

A customised LSRII flow cytometer (BD Biosciences, California, USA) with the configuration shown in **Table 2.9** was used to collect all polychromatic flow cytometry data.

Laser (type)	Wavelength (nm)	Laser power (mW)	Spectral range for detector (nm)	Long pass (nm)	Band pass (nm)	Fluorochrome
Coherent® Sapphire™ (solid state)	488 (Blue)	20	515-545	505	530/30	FITC
			562-588	550	575/26	PE
			600-630	600	610/20	PE-eFluor 610
			750-810	755	780/60	PE-Cyanine7
Coherent Radius™ 405 (solid state)	405 (Violet)	25	425-475	-	450/50	eFluor 450
Lightwave Xcyte™ (solid state)	355 (UV)	20	425-475	-	450/50	Reactive blue
JDS Uniphase™ 1344P (helium-neon (HeNe) gas)	633 (Red)	17	650-670	655	660/20	APC
			707.5-752.5	-	730/45	Alexa Fluor 700

Table 2.9. LSRII Instrument configuration. The polychromatic flow cytometry panel was set up using a customised BD LSR II with the listed lasers and filters.

Data was analysed using FlowJo software and the following gating strategy applied to all stained samples (**Figure 2.3**). FSC and SSC gating was used to remove debris, anti-CD14 and anti-CD45 antibodies were used to selected the cells of interest and single cells were selected to remove doublet events. A time gate was used to check for stable flow of cells and viability gate was used to remove non-viable cells stained with amine-reactive blue viability stain. Flow cytometry data in this work is presented with both percentage of cells positive and nMFI values reported. Together these values provide an accurate summary of

the results; percentage positive gates (set based on <1 % positive cells in unstained samples) alone reduce the resolution of the data as they can be skewed to outliers and do not account for changes in fluorescence intensity. This information is provided by nMFI values (Chan *et al.,* 2013).

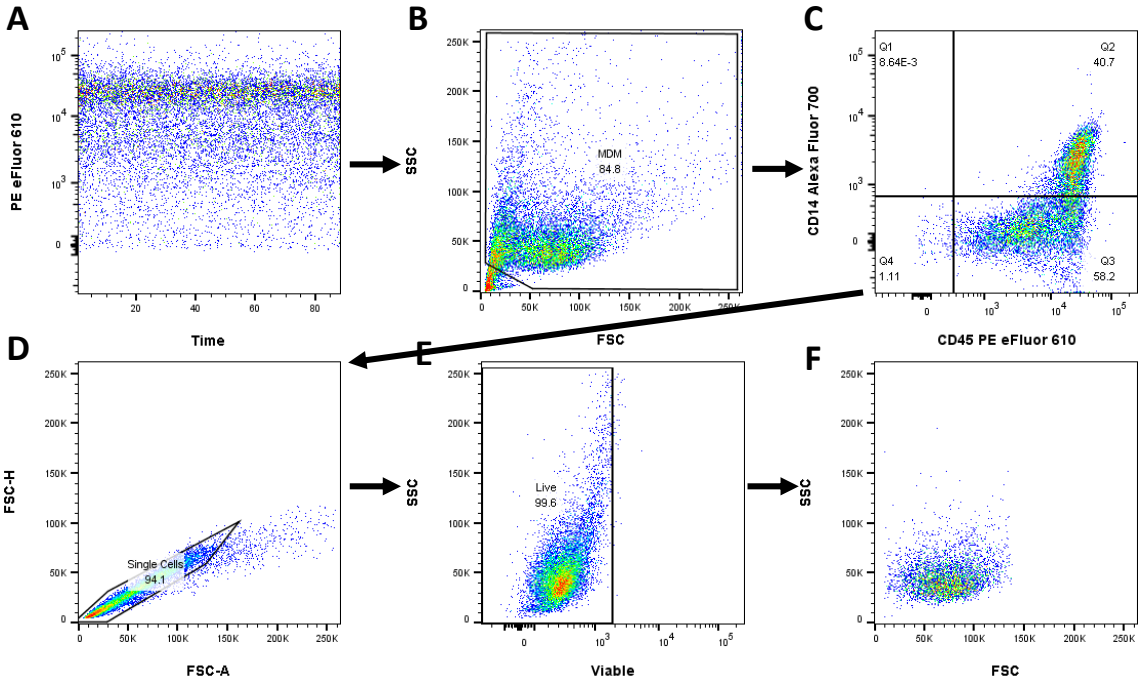

Figure 2.3. Gating strategy used for polychromatic flow cytometry analysis. Monocyte-derived macrophages were stained with 7 fluorochrome-conjugated antibodies in addition to an amine-reactive viability stain. Areas of stable flow were selected (**A**) and debris was excluded from the analysis (**B**). Any $CD14^{-}CD45^{-}$ events were excluded (**C**) before single (**D**) and viable (**E**) cells were selected. The remaining cell population (**F**) is used for analysis.

Compensation and fluorescence-minus-one controls

During cell staining, CompBeads and ArC Compensation Beads were stained according to the manufacturer's instructions and re-suspended into 500 µL 1 % paraformaldehyde in PBS. In addition, a sample of dead cells was prepared by incubating cells for 15 minutes in 100 % (v/v) ethanol at room temperature. These were mixed with the same number of viable cells and stained with amine-reactive blue viability stain according to the manufacturer's instructions. These samples were used to compensate for spillover of fluorochromes in polychromatic stained samples. An example compensation matrix is provided (**Table 2.10**). Fluorescence-minus-one (FMO) controls were used to set gating for all selected fluorochromes as shown (**Figure 2.4**).

		Coherent® Sapphire™				Coherent Radius™ 405	Lightwave Xcyte™	JDS Uniphase™ 1344P	
		Blue 530/30	Blue 575/26	Blue 610/20	Blue 780/60	Violet 450/50	UV 450/40	Red 660/20	Red 730/45
Coherent® Sapphire™	Blue 530/30	-	43.3357	18.2063	1.6358	0.000	0.2610	0.000	0.3025
	Blue 575/26	0.5077	-	42.7495	4.9803	0.0000	0.0246	0.0000	0.0508
	Blue 610/20	18.59	42.79	-	0.38	0.00	0.33	0.01	0.04
	Blue 780/60	0.00	5.00	11.01	-	0.00	0.20	0.21	1.09
Coherent Radius™ 405	Violet 450/50	0.10	0.00	0.03	0.00	-	19.37	0.00	0.00
Lightwave Xcyte™	UV 450/40	0.30	0.02	0.00	0.45	2.72	-	0.02	0.00
JDS Uniphase™ 1344P	Red 660/20	0.00	0.04	0.35	0.08	0.19	1.32	-	0.46
	Red 730/45	0.00	0.00	0.00	0.00	0.00	0.02	33.34	-

Table 2.10. Compensation matrix. The Compensation matrix applied by BD LSRII using BD™ CompBead and ArC™ Amine Reactive Compensation Beads.

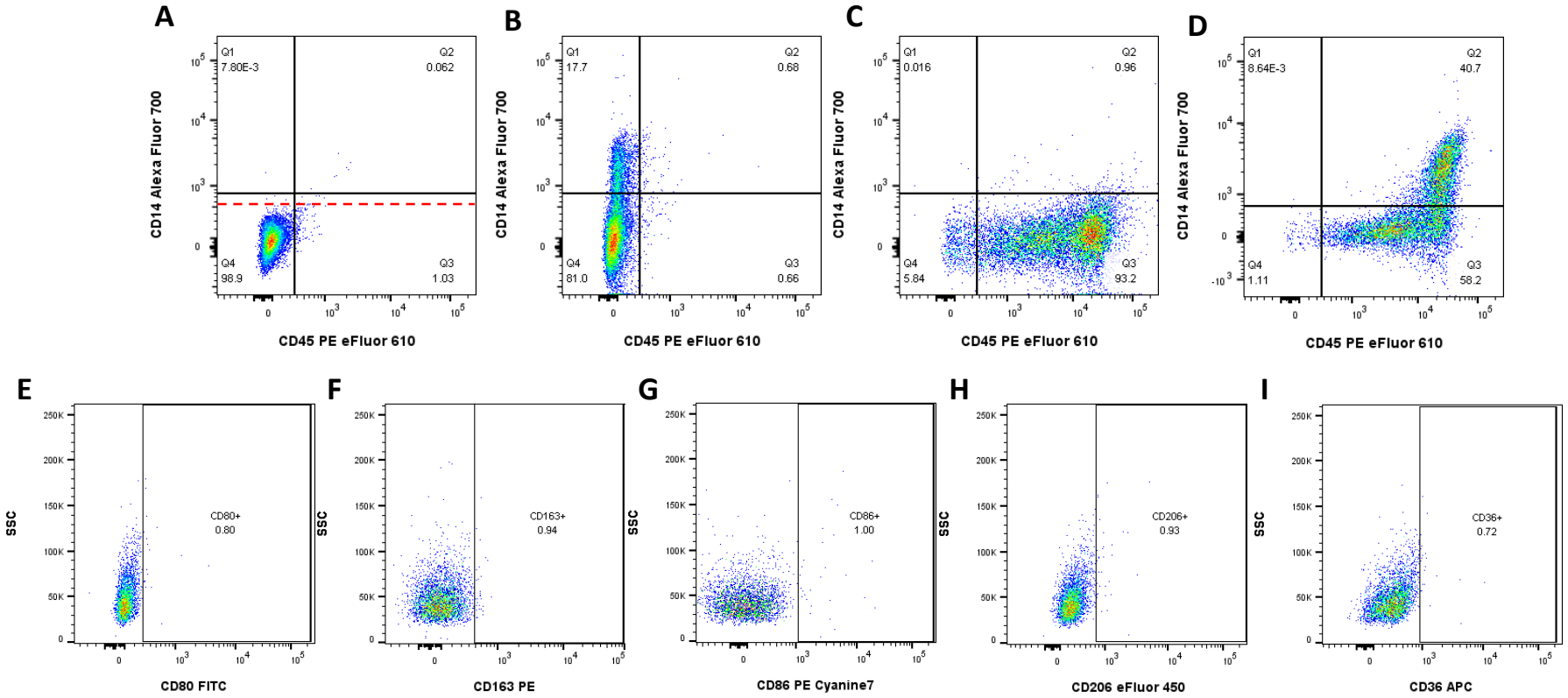

Figure 2.4. Fluorescence-minus-one controls. Fluorescence-minus-one (FMO) controls excluding $CD45^{PE\ eFluor\ 610}$ (**B**) and $CD14^{Alexa\ Fluor\ 700}$ (**C**) were used to accurately gate CD14- and CD45-positive cells (**D**). The use of unstained cells alone to draw gates (red dotted line, **A**) would have resulted in selection of CD14-negative cells as false-positive. FMO controls excluding FITC (**E**), PE (**F**), PE Cyanine7 (**G**), eFluor 450 (**H**) and APC (**I**) were also used for the correct positioning of gates.

2.6 Analysis of model culture media

Cell culture media was collected from MDM in adherent culture (2D) following 7 days of differentiation from monocytes, or from collagen hydrogels containing MDM alone or oral mucosa models containing FNB6 and NOF in addition to MDM (3D) following 14 days of culture. Cell culture media was centrifuged for 5 minutes at 1800 x *g*, aliquoted and stored at -80 °C until analysis. These samples were analysed using enzyme-linked immunosorbent assay (ELISA) and a lactate dehydrogenase release (LDH) assay, as described below.

Enzyme-linked immunosorbent assay

Conditioned media was collected and analysed for the presence of IL-6 protein by ELISA using an BD OptEIA™ IL-6 ELISA set (BD Biosciences, California, USA) following the manufacturer's instructions. Presence and concentration of IL-6 protein was determined using a spectrophometer (Tecan, Männedorf, Switzerland) at 450nm (with wavelength correction at 570nm) and analysed according to the manufacturer's instructions using Microsoft Excel. The concentration of protein was determined by comparison to a standard curve using a range of IL-6 of known concentrations.

Lactate dehydrogenase assay

The CytoTox 96® non-radioactive cytotoxicity assay (Promega, UK) was used to detect lactate dehydrogenase (LDH) release as a measure of cell death as lactate dehydrogenase is released upon cell lysis. In this assay, LDH released from lysed cells results in the conversion of iodonitrotetrazolium chloride (INT salt) into a red formazan product. Cell culture conditioned media was used to detect LDH release following the manufacturer's instructions. The amount of red colour formed was proportional to the number of lysed cells and can be measured at an absorbance wavelength of 490 nm by spectrophotometer (Tecan, Männedorf, Switzerland).

2.6.1 Gene expression analysis

RNA isolation

Total RNA was isolated from cell pellets of PBM immediately following magnetic cell sorting, or from cell pellets of MDM cultured for 7 days adherent to tissue culture plastic, in the absence or presence of M-CSF or GM-CSF using Isolate II RNA mini kit (Bioline) according to the manufacturer's instructions. RNA quantity and quality was measured using a NanoDrop spectrophotometer (Fisher Scientific) to assess the ratio of absorbance at 260 nm and 280 nm (only samples with a ratio of approximately 2.0 were used). RNA was stored at -80 °C until use.

Preparation of cDNA

Complementary DNA (cDNA) was prepared from isolated RNA using a high capacity cDNA reverse transcription kit (Applied Biosystems) according to the manufacturer's instructions. Using a 2720 thermal cycler (Applied Biosystems), gene-specific and oligo dT priming was enabled at 25 °C for 10 mins, followed by 120 mins at 37 °C for optimal reverse transcription of RNA and 5 mins at 85 °C for termination of the reaction. cDNA was stored at -20 °C until use.

Quantitative real-time PCR

cDNA was subsequently analysed using quantitative real-time polymerase chain reaction (qRT-PCR) by the addition of cDNA to qRT-PCR master mix containing 1x SYBR Green mixture (Applied Biosystems) with 0.5 µM gene specific forward and reverse primers (Sigma). Small nucleolar RNA U6 (TaqMan probe) was used as an endogenous control for all qRT-PCR assays. Assays were performed in triplicate using 7900 HT Fast real time PCR equipment (Applied Biosystems) and measured using SDS version 2.4. Forty cycles comprising of 95 °C for 15 s to enable cDNA strand denaturation, 60 °C for 60 s to enable primer annealing and strand elongation, and 95 °C for 15 s for strand termination were used. Cycle threshold (CT) values were recorded using RQ manager version 1.2.1 and the difference in CT values between the target gene and endogenous control was recorded as ΔCT. ΔΔCT values were

calculated by normalising ΔCT values to untreated samples. Primer sequences are indicated in **Table 2.11**.

Primer Name	Forward sequence	Reverse sequence
CPM	5'-AAGGTGGAATGCAAGATTAC	3'-GGATATTTACAGCATGACAGC

Table 2.11. Oligonucleotide sequences.

The melt curve of designed SYBR Green primer is provided in the appendix.

2.7 Statistical analyses

Error bars are not typically recommended for experiments where n=3 or less, therefore individual data points have been plotted where possible. To draw comparisons between control and experimental data, standard error mean bars have been shown for independently repeated experiments (n=3 or more) and the number of repeated measures have been indicated (Cumming *et al.,* 2007). The length of these inferential error bars can give a graphic depiction of uncertainty in the data, as opposed to descriptive error bars, such as range and standard deviation, which show the spread of the data. Where representative experiments are shown (i.e. n=1) statistics have not been presented.

As repeats in this work are typically limited to n=3, the distribution of the data cannot be determined. Therefore, parametric tests have been used as it is recommended that non-parametric tests are only used when $n \geq 10$ in the absence of normally distributed data due to the Central Limit Theorum. In addition, non-parametric tests, whilst making fewer assumptions than parametric tests, often provide higher p values, resulting it difficulties identifying true differences, especially in the case of small sample sizes. For small sample sizes, statistical tests are not robust, and can only give an indication of whether the null hypothesis may be rejected or accepted.

GraphPad Prism 7 was used for all statistical analysis.

One-sample T-test

A one-sample T-test compares the mean of data to a hypothetical value. A small p value suggests that differences between the mean and hypothetical value are unlikely to be due

to coincidence and so may be statistically significant. Conversely, a large p value suggests there is no evidence for difference between the mean of the data and a hypothetical value.

Unpaired T-test

An unpaired T-test has been used to compare the means between two different groups. A small p value suggests that the differences observed between the two means are not a coincidence. A large p value here suggests that there is not enough evidence to show that the means of the data differ.

One-way ANOVA with Tukey's post-test

A one-way analysis of variance (ANOVA) compares three or more un-matched groups and determines whether or not random sampling would result in equal means. With the addition of Tukey's post-test for multiple comparisons, a one-way ANOVA provides more robust statistical analysis that accumulating results from multiple T-tests. A small p value suggests any differences observed between means are unlikely to be due to random sampling.

Linear regression

Linear regression was calculated to determine the best-fit line and hence determine collagen concentration from matrix stiffness **Figure 5.9**.

3 Chapter 3: Development of 2D Culture Methods for Primary and Cell Line Monocytes and Macrophages

3.1 Introduction

Monocyte cell lines are often used in place of primary cells due to the challenges of acquiring ethical approval, collecting patient samples and isolating cells from samples. Although there is an abundance of published research using both primary and cell line monocytes and macrophages, a huge variety of methods are cited. Therefore, the two-dimensional (2D) culture methods of both primary and cell line monocytes and macrophages required optimisation.

3.2 Isolation and purification of peripheral blood monocytes

3.2.1 Isolation of peripheral blood monocytes from whole blood

Whole blood is mostly made up of plasma (55 %) containing electrolytes, nutrients, organic waste and proteins dissolved in water. This aids the transport of erythrocytes (45 %) and peripheral blood mononuclear cells (<1 %). Monocytes are found in the buffy coat layer, along with small numbers of other leukocytes (neutrophils, eosinophils and basophils) and platelets.

Whole blood from healthy volunteers was stained with PE-conjugated anti-CD14 antibody, erythrocytes lysed and samples analysed by flow cytometry to determine the percentage of monocytes present (**Figure 3.1**). A CD14+ gate was drawn based on an unstained sample.

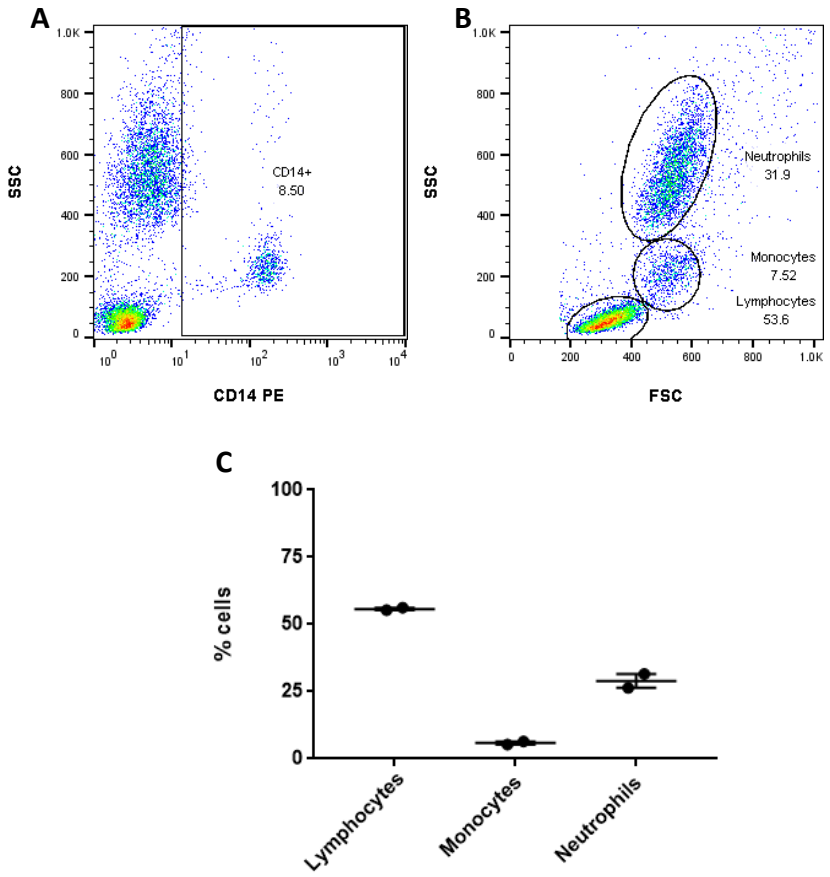

Figure 3.1. Leukocyte composition of whole blood. CD14+ events in whole blood (**A**) are labelled as monocytes and shown separated from lymphocytes and neutrophils by FSC and SSC (**B**) with percentage numbers of cells in whole blood displayed. Gates were set based on unstained cells. Dot plots are representative of two independent experiments, measured in duplicate (n=2) and summarised in scatter plot (**C**) where error bars show standard error mean.

A distinct population of cells stained positive for CD14 and could easily be separated from the rest of the cells in the whole blood preparation. The nMFI of monocytes was 16.4 compared to 1.03 for lymphocytes and 2.34 for neutrophils. Separation of monocytes, based on CD14 expression, from lymphocytes and neutrophils (subsequently gated based on FSC and SSC) shows that samples of whole blood were composed of 55.7 % lymphocytes, 29.0 % neutrophils and 5.9 % monocytes.

3.2.2 **Isolation and purification of peripheral blood monocytes from buffy coats**

Buffy coat layers are separated from plasma and erythrocytes through the centrifugation of whole blood and the use of these for isolation of PBM may result in a higher yield of CD14+ cells. Additionally, a pan monocyte isolation kit using negative selection by depletion of magnetically labelled, non-monocyte cells, can further enrich the number of CD14+ cells (**Figure 3.2**).

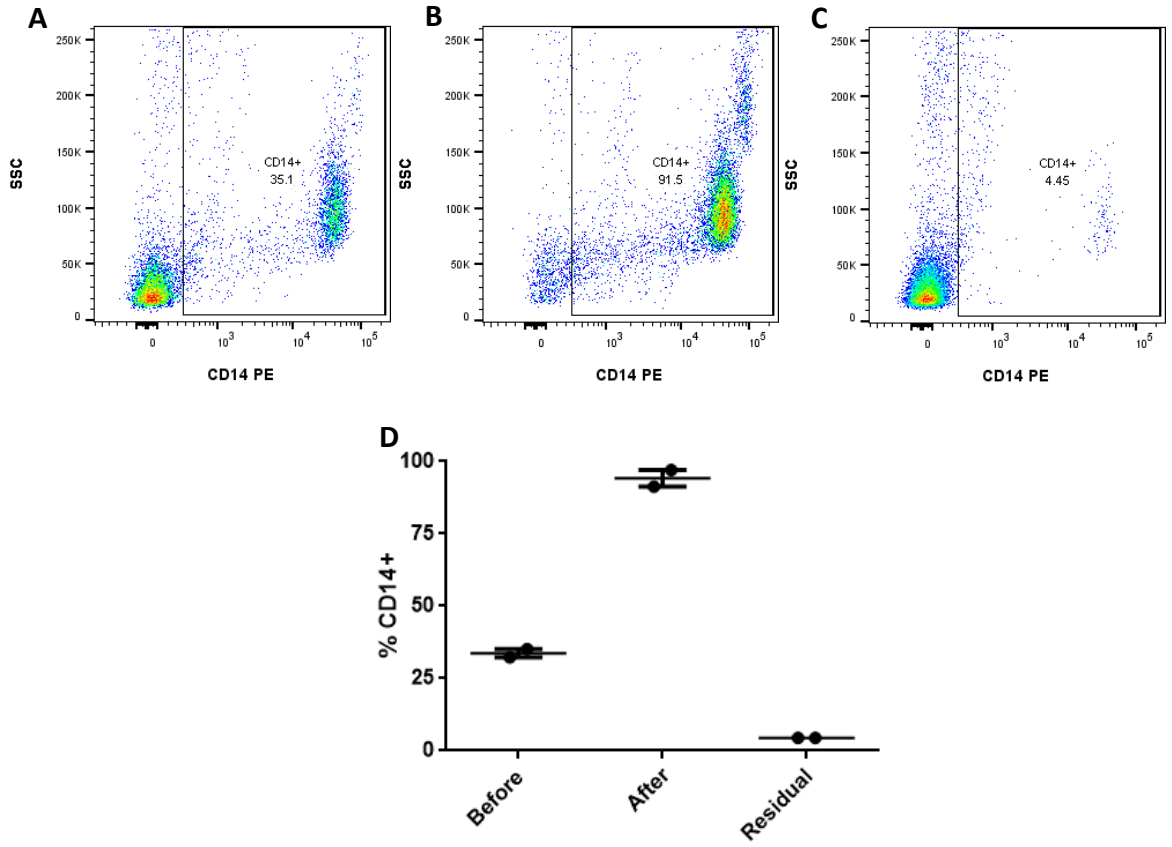

Figure 3.2. Purification of peripheral blood monocytes isolated from buffy coats. The percentage of CD14+ cells in buffy coat layers before use of a magnetic purification column (**A**), after magnetic separation (**B**) and residual cells remaining bound to the magnetic column (**C**). Dot plots are representative of two independent experiments, measured in duplicate (n=2) and summarised in scatter plot (**C**). Error bars show standard error mean.

Isolation of monocytes from buffy coats using Ficoll-hypaque centrifugation resulted in an increase of CD14+ cells from 5.9 % in whole blood to 33.7 % in the peripheral blood

mononuclear cell preparation. The additional use of a magnetic purification column resulted in a marked increase in the percentage of CD14+ cells to 94.2 % with only 4.5 % CD14+ cells residually bound to the column after its use.

3.3 Monocyte to macrophage differentiation

Monocytes are small, spherical cells with a reniform nucleus and very few granules (Auffray *et al.,* 2009; Geissmann, 2010; Ginhoux and Jung, 2014; Terry and Miller, 2014). In response to MCP-1, monocytes are recruited to sites of injury where they extravasate into the tissue, from the blood stream, and differentiate into macrophages. This change can be characterised by a morphological change where cells increase in size and granularity (Chang *et al.,* 2012). *In vitro*, human monocyte to macrophage differentiation can be stimulated through plastic adherence or the use of exogenous cytokine stimulation, such as M-CSF or GM-CSF.

3.3.1 Differentiation of peripheral blood monocytes to monocyte-derived macrophages *in vitro* in 2D

PBMC isolated from buffy coats through Ficoll-hypaque density centrifugation were seeded at $1x10^6$ cells/mL (v/v) to $5x10^6$ cells/mL (v/v) to determine an optimal seeding density, with $3x10^6$ cells/mL frequently reported in the literature and found here to provide a good yield of MDM per $75cm^2$ tissue culture flask. As monocytes adhere rapidly to tissue culture plastic, PBMC were washed after 3 hours, 24 hours, and every 3 days thereafter for up to 14 days to remove contaminating lymphocytes.

Detachment of monocyte-derived macrophages from cell culture plastic

In order to determine purity and viability of MDM, cells required detachment from tissue culture plastic. Previous literature mostly omitted information relating to cell detachment, therefore a variety of methods were tested, including the use of cell scrapers into flow cytometry staining buffer or cell culture media, low adherence plates, macrophage detachment solution, EDTA alone or in combination with trypsin and cell dissociation solution. Detachment methods were compared in terms of MDM recovered as a

percentage of the total events, and the percentage of these that were viable, determined by staining with PI (**Figure 3.3**).

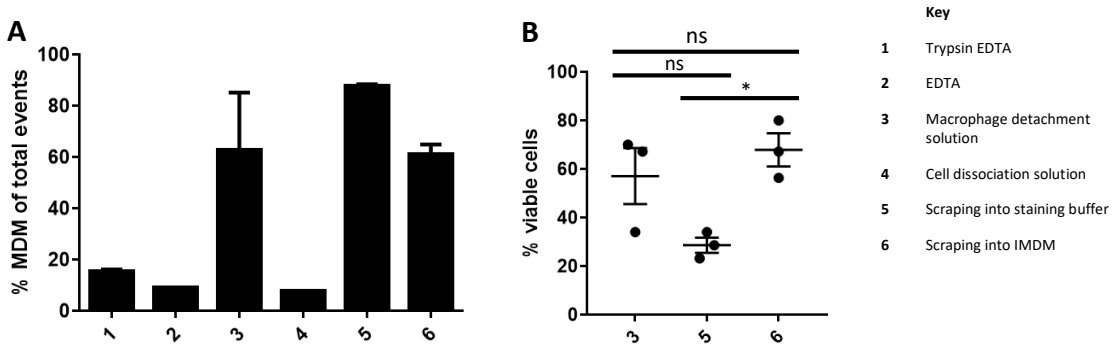

Figure 3.3. Recovery of viable 2D *in vitro* cultured monocyte-derived macrophages using a variety of detachment methods. Following monocyte to macrophage differentiation over 14 days of adherent culture, monocyte-derived macrophages (MDM) were recovered using a variety of methods (shown in key). Recovered MDM were stained with propium iodide for dead cell exclusion and percentages of total events (**A**) and percentages of viable cells (**B**) reported. Gates were set based on unstained cells treated under the same detachment conditions. Data shown are for three independent experiments (n=3) and error bars show standard error mean.

Low adherence plates prevented monocytes from adhering in the first instance resulting in unsuccessful culture of MDM. The use of EDTA alone (9.1 %) or in combination with trypsin (15.5 %), or cell dissociation solution (7.9 %) led to recovery of a very low percentage of intact MDM. The use of macrophage detachment solution (62.7 %) and scraping into PBS (87.8 %) or IMDM (61.0 %) enabled improved recovery of intact MDM. Of the three detachment methods that yielded the highest percentages of intact MDM, scraping into IMDM resulted in the highest percentage of viable cells (67.9 %) compared to macrophage detachment solution (57.5 %) and scraping into flow cytometry staining buffer (28.6 %). Statistical analysis using a one-way ANOVA with Tukey's multiple comparisons showed a significantly higher percentage of viable MDM after scraping into IMDM compared to scraping into staining buffer ($p=0.0301$). However, there was no statistically significant difference in the percentage of viable MDM through scraping into macrophage detachment solution compared to either scraping into staining buffer ($p=0.0983$) or scraping into IMDM

(0.6261). For all further experiments, MDM were recovered using scraping into IMDM due to improved recovery of intact MDM and percentage of viable MDM recovered following adherent culture in 2D, compared to other detachment methods tested.

Percentage of monocyte-derived macrophages expressing CD14+ over 14 days

CD14 binds microbial ligands such as LPS to initiate an inflammatory response (Poussin *et al.,* 1998). It is often used as a marker for monocytes and macrophages. Literature frequently cites culture of MDM from 7 to 14 days in order to acquire a population of MDM >95 % CD14+. In order to determine the optimum cell culture time for >95 % CD14+ cells, PBMC were differentiated to macrophages for up to 14 days. Purity was assessed using anti-CD14 antibody staining and analysis by flow cytometry, after 3 hours, 24 hours, 7 days and 14 days of culture. The percentage of CD14+ events was compared to those found in whole blood and immediately after Ficoll-hypaque density centrifugation. Gates used were based on unstained samples from the same time point (**Figure 3.4**).

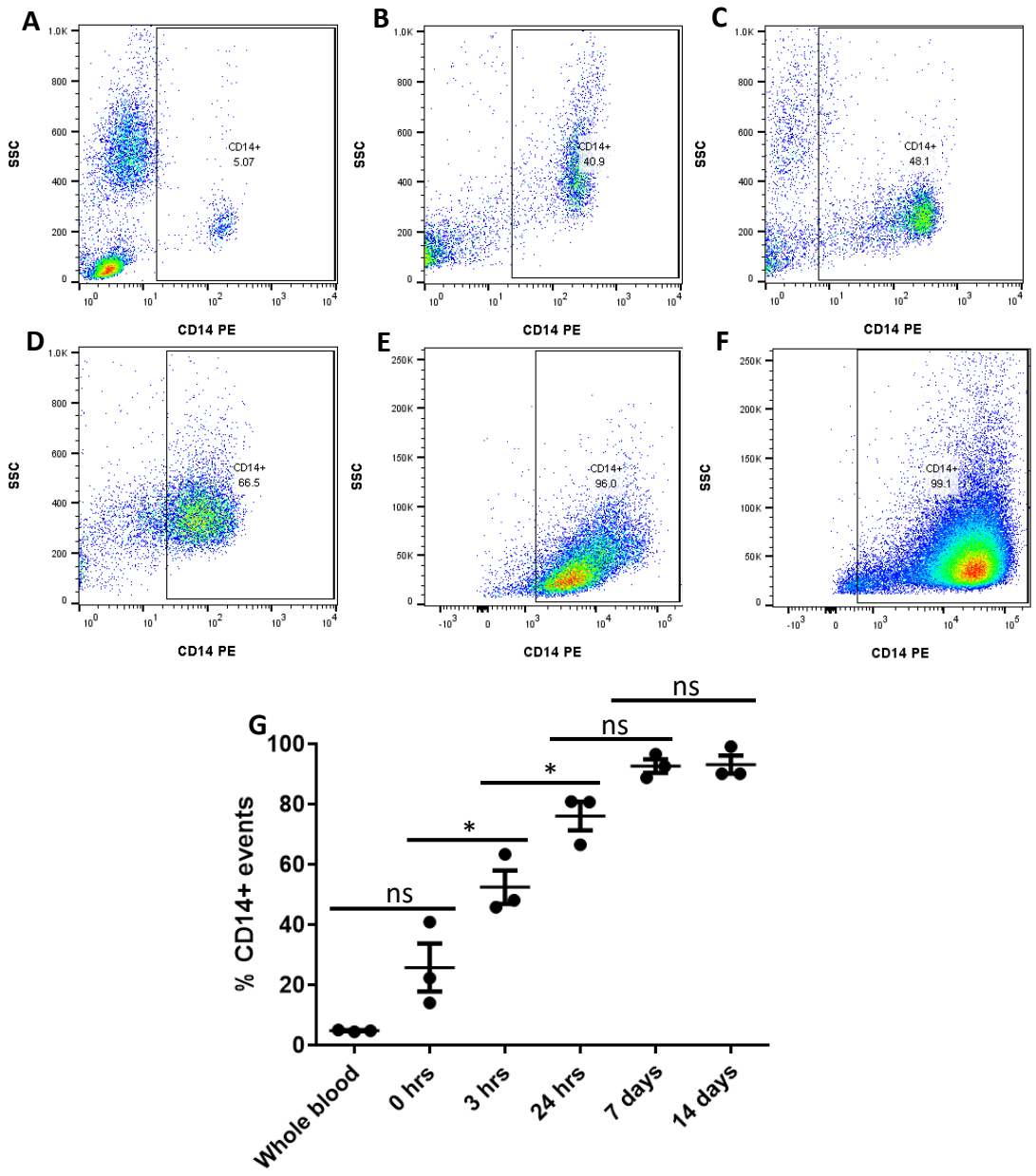

Figure 3.4. Percentage of monocyte-derived macrophages expressing CD14 following isolation and culture. The percentage CD14+ events in whole blood (**A**) or immediately after Ficoll-hypaque density centrifugation (0hrs, **B**), and subsequent culture for 3 hours (**C**), 24 hours (**D**), 7 days (**E**) and 14 days (**F**) of plastic adherent culture. Following culture of various times, cells were stained using anti-CD14^{PE} antibodies and analysed using flow cytometry, following dead cell exclusion using propium iodide. Gates were set using unstained cells cultured under the same conditions. Data are summarised in scatter plot (**G**) and dot plots are representative of three independent experiments (n=3), error bars show standard error mean and significance was determined using results from a one-way ANOVA with Tukey's multiple comparisons (* = $p<0.05$).

The percentage of CD14+ events analysed by flow cytometry increased from whole blood (4.8 %), again following density centrifugation (25.7 %) and again following culture for 3 hours (52.4 %), 24 hours (76.0 %), 7 days (92.6 %) and 14 days (93.1 %). The size of individual cells and spread of the whole population also increased over 14 days. There was no significant difference in the percentage of CD14+ events identified between whole blood and 0 hours ($p=0.0675$), 3 hours and 24 hours of culture ($p=0.0346$), 24 hours and 7 days of culture ($p=0.1938$) or 7 days and 14 days of culture ($p=>0.9999$), however there was a marked increase in CD14+ events from 76.0 % after 24 hours to 92.6 % after 7 days. There was also a significant increase in the percentage of CD14+ detected between 0 hours and 3 hours of culture ($p=0.0157$) and 3 hours and 24 hours of culture ($p=0.0346$). Consequently, MDM were cultured for 7 days in ensuing experiments.

Carboxypeptidase M gene expression by monocyte-derived macrophages in 2D

The cell surface expression of carboxypeptidase M (CPM) by macrophages has been shown to be increased compared to expression by monocytes. CPM has therefore become a widely used marker of monocyte to macrophage differentiation (Rehli *et al.,* 1995). The expression of CPM by PBM isolated from buffy coats and purified using magnetic separation was compared to the expression of CPM by MDM cultured in the presence of either GM-CSF, M-CSF or un-stimulated for 7 days. The expression of CPM was measured using qRT-PCR (**Figure 3.5**).

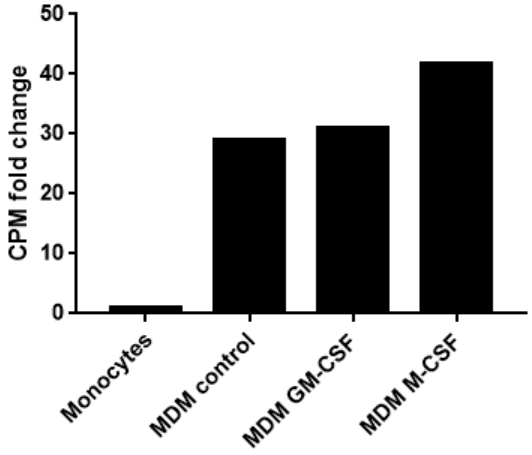

Figure 3.5. Monocyte-derived macrophages appear to express higher levels of carboxypeptidase M than peripheral blood monocyte. Expression of CPM by peripheral blood monocytes (PBM), or monocyte-derived macrophages (MDM) cultured for 7 days in the absence or presence of cytokines (M-CSF or GM-CSF) was compared using fold change determined by qPCR. Data are representative of two independent experiments (n=2).

Compared to monocytes, which expressed very low levels of CPM, MDM expressed 29-fold more CPM. In addition, stimulation with GM-CSF and M-CSF resulted in even higher levels of CPM expression, with a 31-fold and 41-fold increase in expression respectively compared to monocytes. In proceeding experiments, GM-CSF and M-CSF were used in M1 and M2-stimulated cultures of MDM, respectively, and compared to MDM cultured in the absence of additional cytokine stimulation used to promote differentiation (**Table 2.3**).

3.3.2 **Differentiation of Mono Mac 6**

Previous literature has shown that MM6 monocytes could be differentiated to display characteristics of macrophages, such as reduced proliferation and increase phagocytosis through the use of prostaglandin E2, LPS or PMA (Zieglerheitbrock *et al.,* 1994). However, this study was unable to successfully differentiate MM6 cells and replicate published results.

3.4 Preliminary comparison between THP-1, Mono Mac 6 and peripheral blood monocytes

THP-1 and MM6 commercially available monocytes are often used in research to represent PBM, however there is limited evidence comparing the expression of key markers in these cells. THP-1 and MM6 monocytes cultured in suspension were compared to PBM in relation to size, granularity and cell surface expression of key monocyte and macrophage markers using flow cytometry.

3.4.1 Differences in morphology of THP-1, Mono Mac 6 and peripheral blood monocytes

PBM, THP-1 and MM6 monocytes in cell culture medium were visualised using light microscopy and analysed by flow cytometry. Monocytes were gated based on FSC and SSC to exclude contaminating lymphocytes in the mononuclear cell preparation and cell debris from all samples. The size and granularity of the different monocyte cell types was compared (**Figure 3.6**).

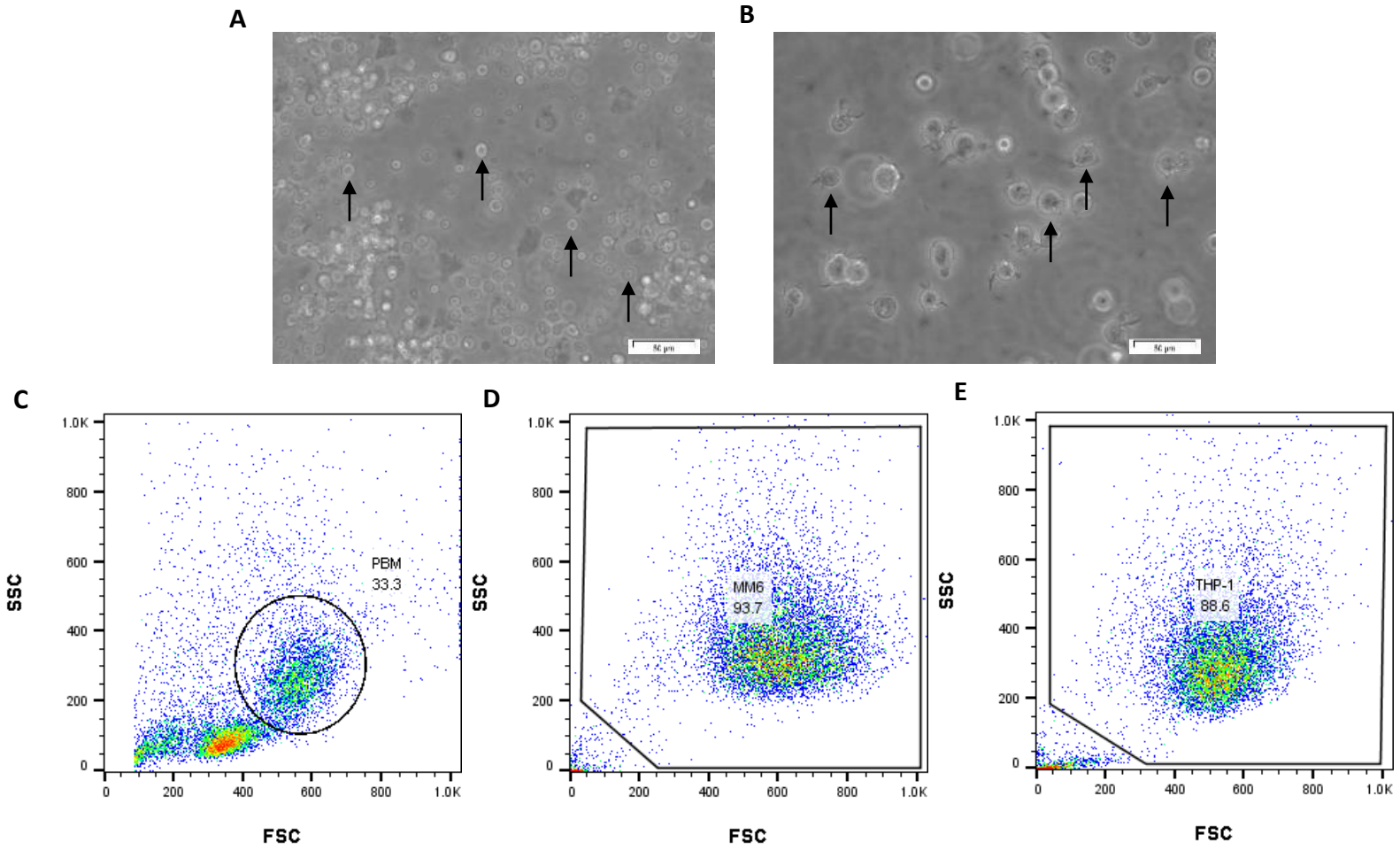

Figure 3.6. Differences in morphology of peripheral blood monocytes, THP-1 and Mono Mac 6. Peripheral blood monocytes (PBM) immediately following isolation and magnetic cell sorting, or THP-1 and Mono Mac 6 (MM6) cells cultured in suspension were imaged and analysed using flow cytometry. Light microscopy images show the differences in size of PBM (**A**), MM6 and THP-1 (**B**) cells. Dot plots show differences in size (FSC) and granularity (SSC) of PBM (**C**), MM6 (**D**) and THP-1 (**E**) cells, with gates used for analysis displayed, following dead cell exclusion using propium iodide. Arrows indicate PBM (**A**) and THP-1 (**B**) in suspension, and figures display data from a single experiment (n=1).

Light microscopy showed visible differences in size between blood monocytes (6 µm) and THP-1 cells (16 µm, Chitra *et al.,* 2014). Forward scatter data collected using flow cytometry was measured as 553, 512 and 456 for PBM, THP-1 and MM6 respectively, and side scatter was measured as 254, 269 and 342, respectively.

3.4.2 Differential protein expression in THP-1, Mono Mac 6 and peripheral blood monocytes

To determine whether THP-1 or MM6 monocytes could accurately represent PBM in the expression of key monocyte and macrophage markers, flow cytometry using antibodies targeting CD14, CD45, CD80, CD163, CD206 and CPM was used. PBM, THP-1 and MM6 monocytes were stained with primary and fluorochrome-conjugated secondary antibodies or fluorochrome-conjugated primary antibodies and analysed by flow cytometry to detect cell surface expression of selected markers (**Figure 3.7**).

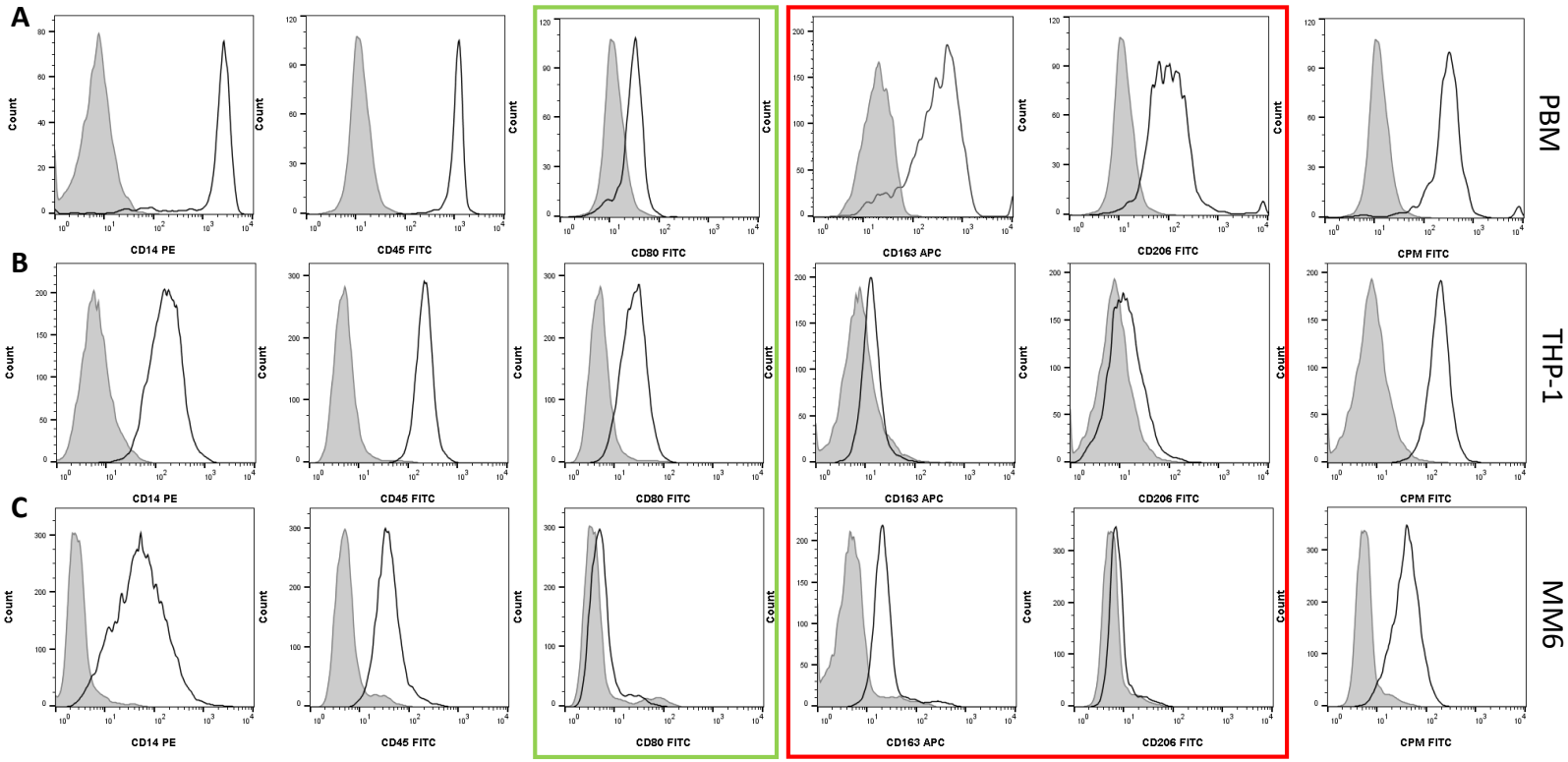

Figure 3.7. Differential expression of key monocyte and macrophage markers in THP-1, Mono Mac 6 and peripheral blood monocytes. Peripheral blood monocytes (PBM) directly following isolation and THP-1 or Mono Mac 6 (MM6) monocytes cultured in suspension were labelled with antibodies to detect expression of CD14, CD45, CD80, CD163, CD206 and carboxypeptidase M (CPM) through flow cytometry analysis. Black, unfilled histograms show expression of markers for PBM (**A**), THP-1 (**B**) and MM6 (**C**) cells, compared to an isotype-matched control (grey, filled histogram) in the absence of FcR blocking reagent. Gates used for analysis are as shown in **Figure 3.6**, where cells are gated on size and granularity in the absence of dead cell exclusion. Green box highlights M1 marker, CD80, and red box highlights M2 markers, CD163 and CD206. Data are shown for a single experiment (n=1).

As expressed by nMFI values, PBM expressed high levels of CD14 (327.8), CD45 (92.7), CD163 (14.3) and CD206 (6.8) with lower levels of CPM (21.0) and CD80 (2.5). Comparatively, THP-1 monocytes expressed lower levels of CD14 (25.8), CD45 (41.8), CD163 (1.8) and CD206 (1.6) but higher levels of CPM (23.5) and CD80 (5.0). MM6 monocytes expressed the lowest levels of CD14 (18.3), CD45 (9.7), CD206 (1.3), CPM (6.9) and CD80 (1.4) but expressed higher levels of CD163 (4.4) compared to THP-1 cells, although this was still considerably lower than for PBM cells.

3.5 Preliminary comparison between THP-1 PMA and monocyte-derived macrophages

Although THP-1 PMA cells are often used to represent MDM, it has previously been reported that they do not show the same increases in size, granularity or cytoplasmic-to-nuclear ratio as those seen in MDM (Daigneault *et al.,* 2010). 2D-cultured THP-1 PMA were compared to MDM in relation to size, granularity and cell surface expression of key monocyte and macrophage markers.

3.5.1 Differences in morphology of THP-1 PMA and monocyte-derived macrophages

Once differentiated, THP-1 PMA and MDM were compared using light microscopy and analysed by flow cytometry. A gate excluded smaller events likely to be cell debris and the two cell types were compared using FSC and SSC as measures of size and granularity respectively (**Figure 3.8**).

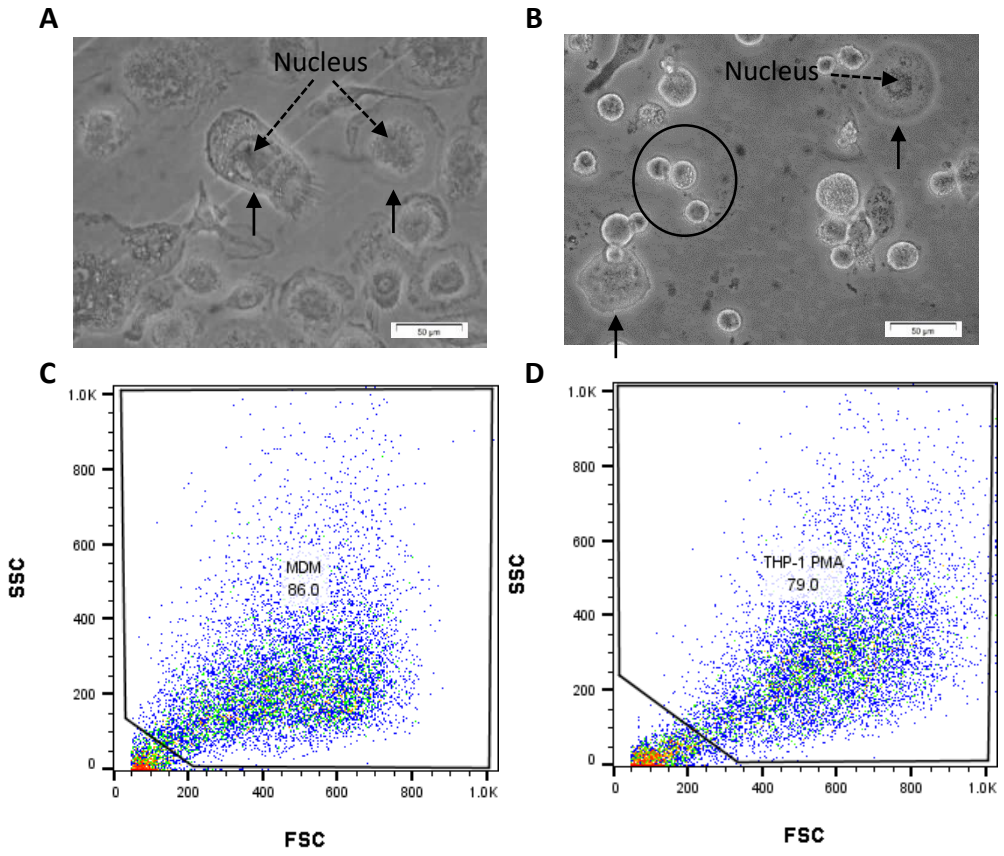

Figure 3.8. PMA-treated THP-1 monocytes appear to display a difference in morphology to monocyte-derived macrophages. Monocyte-derived macrophages (MDM) cultured for 7 days in adherent culture or THP-1 monocytes treated with PMA for 8 days in adherent culture were imaged and analysed using flow cytometry. Light microscopy images show the differences in size of monocyte-derived macrophages (MDM, **A**) and PMA-treated THP-1 (THP-1 PMA, **B**) cells. Dot plots show differences in size (FSC) and granularity (SSC) of MDM (**C**) and THP-1 PMA (**D**) cells, with gates used for analysis displayed following dead cell exclusion with propium iodide. Block arrows indicate macrophages, dashed arrows indicate nuclei and non-adherent cells are highlighted in circle. Figures display data from a single experiment (n=1).

The visible differences between THP-1 monocytes and PBM were again apparent between THP-1 PMA and MDM. Through light microscopy, MDM were visualised as a homogeneous population will large, flat cells displaying a large nucleus and cytoplasmic-to-nuclear ratio. In contrast, THP-1 PMA formed a heterogeneous population with some cells displaying features of differentiated macrophages, whilst others appeared un-affected by PMA treatment. In addition, the large differences in size between MDM (31µm) and THP-1 PMA

(23µm) could be observed (Chitra *et al.,* 2014). Flow cytometry measured FSC for MDM as 462 and 615 for THP-1 PMA. SSC was measured as 214 for MDM and 287 for THP-1 PMA, indicating that MDM were larger and more granular than THP-1 PMA.

3.5.2 Differential protein expression of THP-1 PMA and monocyte-derived macrophages

To determine whether THP-1 macrophages could accurately represent MDM in the expression of CD14, CD45, CD80, CD163, CD206 and CPM, flow cytometry was performed. THP-1 PMA and MDM were stained with primary and fluorochrome-conjugated secondary antibodies or fluorochrome-conjugated antibodies for cell surface expression of selected markers to enable comparisons to be drawn between the two cell types (**Figure 3.9**).

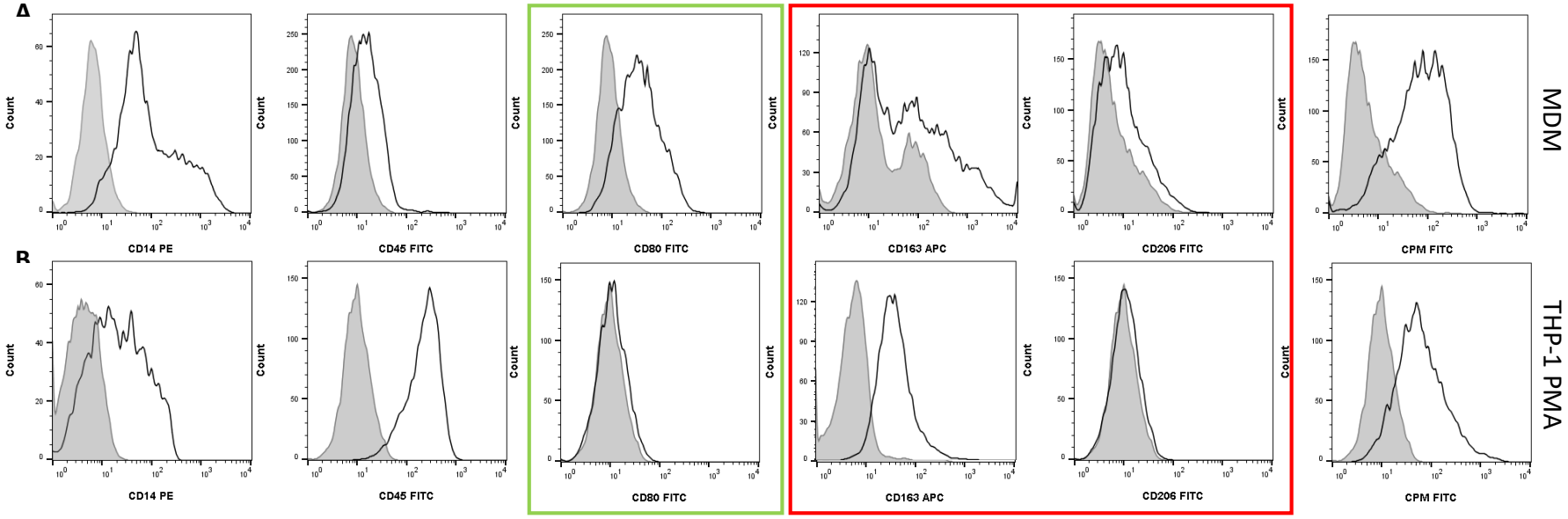

Figure 3.9. Differential expression of key monocyte and macrophage markers in PMA-treated THP-1 and monocyte-derived macrophages. THP-1 monocytes treated with PMA (THP-1 PMA) for 8 days or monocyte-derived macrophages (MDM) cultured for 7 days in adherent culture were detached using scraping into IMDM and labelled with antibodies to detect the expression of CD14, CD45, CD80, CD163, CD206 and carboxypeptidase M (CPM). Black, un-filled histograms show the expression of markers by MDM (**A**) and THP-1 PMA (**B**), compared to an isotype-matched control (grey, filled histograms) in the absence of FcR blocking reagent. Gates used for analysis are as shown in **Figure 3.8**, where cells were selected using size and granularity, in the absence of dead cell exclusion. Green box highlights M1 marker, CD80, and red box highlights M2 markers, CD163 and CD206. Data are shown for a single experiment (n=1).

Measured by nMFI, MDM showed high expression of CD14 (9.7), CD80 (1.8), CD206 (14.9) and CPM (14.9) with lower expression of CD45 (4.1) and CD163 (4.6) compared to THP-1 PMA which expressed lower levels of CD14 (4.2), CD80 (1.1), CD206 (1.0) and CPM (5.2) but higher expression of CD45 (23.9) and CD163 (6.3).

3.5.3 Preliminary comparison of monocyte to macrophage differentiation of THP-1 to THP-1 PMA and peripheral blood monocytes to monocyte-derived macrophages

The nMFI values of the panel of markers used to characterise PBM, THP-1, MM6, MDM and THP-1 PMA cells were used to draw comparisons in the expression of selected markers between PBM and MDM, and THP-1 and THP-1 PMA (**Figure 3.10**).

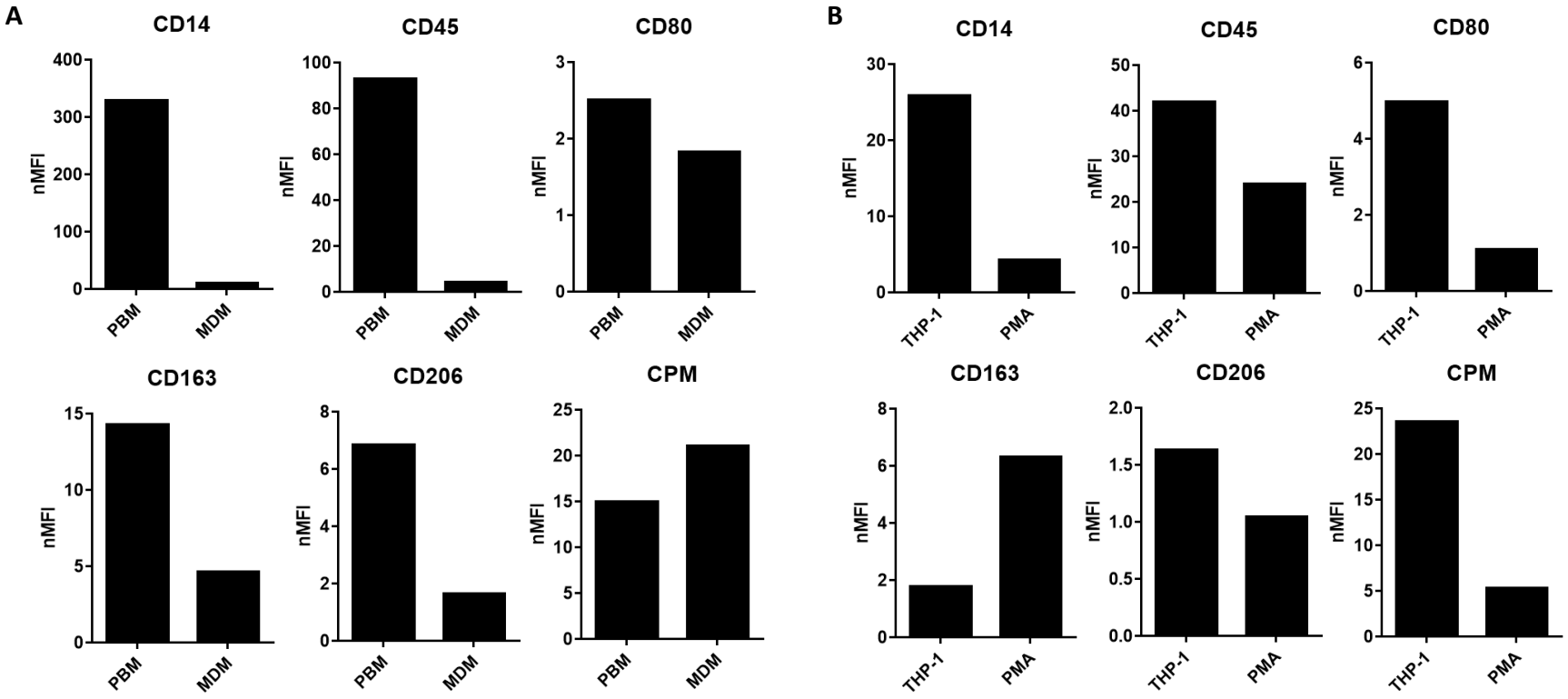

Figure 3.10. Changes in expression levels of key monocyte and macrophage markers through differentiation of peripheral blood monocytes to monocyte-derived macrophages, and THP-1 to THP-1 PMA. Peripheral blood monocytes (PBM) immediately following isolation and magnetic purification, THP-1 monocytes cultured in suspension, THP-1 monocytes treated with PMA (THP-1 PMA) for 8 days or monocyte-derived macrophages (MDM) cultured for 7 days in adherent culture were detached using scraping into IMDM (THP-1 and MDM only) and labelled with antibodies to detect the expression of CD14, CD45, CD80, CD163, CD206 and carboxypeptidase M (CPM). Normalised median fluorescence intensity (nMFI) values for CD14, CD45, CD80, CD163, CD206 and CPM are displayed as bar charts to compare PBM with MDM (**A**) and THP-1 with THP-1 PMA (**B**). Data shown are for a single experiment (n=1).

As measured by nMFI values, a decrease in the expression of CD14 (327.8 to 9.7), CD45 (92.7 to 4.1), CD80 (2.5 to 1.8), CD163 (14.3 to 4.6) and CD206 (6.8 to 1.0) was observed in PBM and MDM respectively. An increase in the expression of CPM was observed from 14.9 in PBM to 21.0 in MDM. A comparison between THP-1 and THP-1 PMA showed a decrease in the expression of CD14 (25.8 to 4.2), CD45 (41.8 to 23.9), CD80 (5.8 to 1.1), CD206 (1.6 to 1.0) and CPM (23.5 to 5.2), and an increase in CD163 expression (1.8 to 6.3), respectively.

3.6 Discussion

There are many barriers in research preventing scientists from using primary cells in all experiments; ethical approval, primary tissue availability, patient-patient variation, longer protocols and added costs, to name just a few. Therefore, cell lines are often used as alternatives due to ease of culture and increased reproducibility. However, cells lines are in most cases derived from malignancies and are therefore not representative of primary, normal cells in many aspects. The results in this chapter have shown the optimisation of methods for the isolation and culture of primary monocytes and macrophages, and a preliminary comparison to their cell line equivalents has been drawn. These results will now be discussed in light of the published literature.

3.6.1 Isolation of peripheral blood monocytes

Monocytes are the precursors to macrophages; monocytes can be found circulating in peripheral blood, whereas macrophages can be found terminally differentiated and residing in tissues. Typically, monocytes are isolated from peripheral blood and differentiated to macrophages *in vitro*. This is mostly due to difficulties in acquiring macrophage-containing primary tissue and a lack of tools available to specifically isolate macrophages from primary tissue.

CD14 is commonly used as a specific monocyte and macrophage marker and is often used to assess the purity of primary monocyte preparations using flow cytometry. In whole blood, CD14+ cells represented just 5.9 % of the population, slightly less than is typically reported. CD14 is not expressed by lymphocytes, and is expressed at only very low levels

by neutrophils. However, it is expressed on dendritic cells which may therefore can result in contamination of the monocyte population.

Firstly, to improve the yield of monocytes retrieved, the percentage of CD14+ cells isolated from buffy coats was compared to that from whole blood. Ficoll-hypaque density fractionation of whole blood resulted in the separation of a buffy coat layer containing peripheral blood mononuclear cells such as lymphocytes, monocytes and dendritic cells, from other components of whole blood, such as erythrocytes and polymorphonuclear cells such as eosinophils and neutrophils. Flow cytometry analysis of the PBMC preparation resulted in an increase in the percentage of CD14+ cells from 5.9 % in whole blood to 33.7 % in the buffy coat layer. In addition, fractionation of whole blood to separate the buffy coat layer removes much of the dendritic cell contamination which can be found representing <1 % of the buffy coat layer (Freudenthal and Steinman, 1990). Neutrophils and lymphocytes are very short-lived, and are typically dead after 48 hours (AntalSzalmas *et al.,* 1997).

In order to further purify monocytes from the PBMC preparation, the use of magnetic purification was explored. A negative monocyte isolation kit was used to prevent activation of monocytes by binding of the CD14 receptor. This uses an antibody cocktail to specifically label all non-monocyte cells. These biotin-conjugated antibodies bind to anti-biotin magnetic beads, that with the use of a magnet, results in the binding of non-monocyte cells to a purification column, whilst monocytes elute through the column for collection. The additional use of magnetic purification resulted in an increase in CD14+ cells to >90 %, with <5 % of CD14+ remaining bound to the column after purification. However, the yield of PBM following this purification step was consistently $\leq 1x10^6$ cells which is too low for many applications. This highlighted a real need for methods to isolate and purify primary cells, in large quantities.

3.6.2 Differences between THP-1 and Mono Mac 6 cell lines and peripheral blood monocytes

The THP-1 pro-monocytic cell line is often used as an alternative to PBM in various experimental procedures, often because of ease of culture and difficulty in isolating primary cells from blood (Qin, 2012). However, there is limited published evidence to show that their phenotype is similar to that of PBM. Therefore, the morphological characteristics and expression levels of key cell surface monocyte and macrophage markers were examined to determine if THP-1 and MM6 share similar phenotypes with PBM. Flow cytometry and light microscopy were used to compare the size and granularity of THP-1, MM6 and PBM and flow cytometry was used to assess the expression profiles of CD14, CD45, CD80, CD162, CD206 and CPM in the three monocyte types.

Light microscopy showed that PBM from healthy volunteers were visibly smaller than both THP-1 and MM6 cell lines. However, this could not be confirmed using flow cytometry due to changes in voltages during data collection. During haematopoiesis, monocytes become smaller, compared to monoblasts and promonocytes, and as an immature monocyte, it follows that THP-1 monocytes will be larger than PBM. Therefore, the data presented here confirms previously published data (Chitra *et al.,* 2014).

In addition to differences in size and granularity, PBM from healthy volunteers expressed high levels of the pan-leukocyte marker CD45 and the monocyte markers CD14 and CD163, as has been previously described (Curat *et al.,* 2004; Griffin *et al.,* 1981; Zhang *et al.,* 2013). In contrast, expression of these important cell surface markers on THP-1 and MM6 cells was markedly lower. THP-1 and MM6 monocyte cell lines are derived from patients suffering from acute myeloid leukaemia (AML) and monoblastic leukaemia respectively, where leukocytes from these cancer patients are typically characterised by low levels of CD45 compared to healthy subjects (Deszo *et al.,* 2001; Lacombe *et al.,* 1997). Both THP-1 and MM6 cells are immature pro-monocytes as a result of premature release from the bone marrow into the circulation.

The expression of CD14 has been shown to increase as pro-monocytes develop into mature blood monocytes (Fraser *et al.,* 2006) providing an explanation for the higher expression of cell surface CD14 on PBM from volunteers than on both pro-monocytic cell lines. In addition, the expression of low levels of CD163 on THP-1 cells compared to PBM has been previously described (Neu *et al.,* 2013). The marked differences in the expression of the classical leukocyte/monocyte markers, CD14, CD45 and CD163 between PBM and the pro-monocytic cell lines may cause marked differences in the cell biology exhibited by these cells. For example, CD14 is a receptor for bacterial-derived LPS and so differences in the expression of this receptor may alter the immune response of THP-1/MM6 cells compared to PBM. CD45 is crucial for T cell receptor activation and so there may also be significant differences in immune signalling and T cell activation. Similarly, CD163 is a scavenger receptor with essential roles in homeostasis and adhesion, binding both endothelial cell adhesion molecules and haemoglobin (Kowal *et al.,* 2011). Low expression of this molecule in the pro-monocyte cell lines may perturb cell function.

Expression of CPM and CD80 was similar in PBM and THP-1 cells but lower for MM6, suggesting that similarities in marker expression exist between PBM and THP-1 cells. In all cases, expression of key cell surface markers was very low on MM6 suggesting that these are most different phenotypically from PBM.

The differences in the expression of important cell surface molecules suggests that the pro-monocytic cell lines have a different phenotype to PBM and may therefore not be appropriate cells to model PBM in these experiments. Whilst this comparison provided only preliminary data to show the differences in expression of key markers between PBM, THP-1 and MM6, it also highlighted the need for a robust flow cytometry panel for in depth characterisation of monocytes. In addition, due to abundant expression of FcγR on the surface of monocytes, essential in facilitating their roles in immune surveillance, data highlighted the need for an FcγR blocking step in sample preparation for flow cytometry; non-specific binding of the isotype-matched control can be observed in **Figure 3.7**

particularly in the staining of MM6 cells and **Figure 3.9** in samples stained with $CD163^{APC}$ and isotype-matched controls.

3.6.3 *In vitro* monocyte to macrophage differentiation

During monocyte to macrophage differentiation, monocytes become larger with increasingly large cytoplasms, increase in granularity and nuclei change in shape from reniform to spherical. Previous literature cites differentiation time periods ranging from 7 to 14 days resulting in a pure (> 95 % CD14+) population of CD14+ cells (Chitra *et al.,* 2014; Eligini *et al.,* 2013; Kreutz and Andreesen 1990; Martinez *et al.,* 2006; Rehli *et al.,* 2000; Vogt and Nathan, 2011). This can be stimulated *in vitro* using plastic adherence or exogenous cytokines (Kelley *et al.,* 1987). The addition of GM-CSF or M-CSF has previously been reported to promote monocyte to macrophage differentiation, but has also been reported to promote macrophage polarization to M1 or M2 phenotype.

Published literature describing research involving MDM largely omits information relating to macrophage detachment from cell culture plastic. For flow cytometry analysis of cell surface receptors, the use of non-enzymatic detachment of cells is recommended as enzymes, such as trypsin, may cleave the protein of interest from the cell surface (Zhang *et al.,* 2012). MDM are highly adherent and consequently many different products are marketed for the easy detachment of viable macrophages following *in vitro* culture. Many of these are non-enzymatic, including the macrophage detachment solution tested in this work (PromoCell, Heidlberg, Germany). In addition, cell culture plastic with special coatings are marketed for non-adherent or low-adherent cultures. Attempts to culture MDM using non-adherent or low-adherent culture plates were unsuccessful, and of the detachment methods tested, scraping into IMDM resulted in the highest percentage of viable MDM.

Whilst cell scraping has previously been shown to increase the expression of annexin V associated with apoptosis (Bundscherer *et al.,* 2013), it has also been shown by SEM that membrane domain structures are minimally altered, even if the integrity of the membrane as a whole may become mechanically damaged (Batista *et al.,* 2010). This is re-iterated in

the data presented in this thesis, as while cell viability is decreased with cell scraping (although it retains the highest viability of MDM of the methods tested), the events collected by flow cytometry are consistently found in the MDM gate, rather than in the region where cell debris and extracellular vesicles are found. For some applications it may be that enzymatic detachment such as the use of trypsin is optimal, however this must be determined by the investigator for different purposes (Mutin *et al.,* 1996).

The culture of MDM *in vitro* is often cited as taking between 7 and 14 days and whilst the purity of the resulting cell populations is reported as a percentage CD14+, to the best of our knowledge, the changes in percentage expression of CD14 by MDM over 14 days has never been measured. It is important for the resulting MDM population to have a high percentage of CD14+ cells, however the use of MDM in subsequent long-term cultures planned in this work requires shorter differentiation protocols.

This work has shown that the percentage of CD14+ cells increases over time, throughout 14 days from 25.7 % after density centrifugation to 93.1 % after 14 days. At first, there are significant increases in the percentage of CD14+ cells between 0 and 3 hours, and 3 hours and 24 hours. Between 24 hours and 7 days, no statistically significant difference in the percentage of CD14+ was observed, however 92.6 % CD14+ cells were identified after 7 days. Whilst not of statistical significance, this increase is scientifically important. Very little increase in the percentage of CD14+ cells was subsequently found between 7 days and 14 days. Consequently, MDM were cultured for 7 days for the remainder of this work.

During the *in vitro* differentiation of monocytes to macrophages, regular washing of the cells to remove non-adherent cells is recommended by most published protocols. Non-adherent cells are typically lymphocytes as the other major leukocyte cell types, such as neutrophils, have a short lifespan and are often non-viable in buffy coat preparations.

Unlike PBM, THP-1 monocytes do not become spontaneously adherent or differentiate to macrophages. Instead, they require stimulation from exogenous stimuli, such as Phorbol myristate acetate (PMA) or 1,25-dihydroxyvitamin D_3 which promote adherence,

phagocytosis, and expression of CD14, whilst preventing proliferation in order to imitate a differentiated macrophage-like state through the activation of protein kinase C (Schwende *et al.,* 1996). PMA is a protein kinase C (PKC) agonist, which activates the Raf/MEK/ERK pathway in THP-1 monoblastic cells for transcription of genes involved in differentiation (Traore *et al.,* 2005).

There are many different protocols available for the *in vitro* generation of macrophage-like cells from THP-1 using PMA treatment; over 24 hours (Smith *et al.,* 2015), 48 hours (Chanput *et al.,* 2013; Park *et al.,* 2007), 3 days of treatment followed by 1 day of rest (Mittar *et al.,* 2011), and 3 days of treatment followed by 5 days of rest (Daigneault *et al.,* 2010). The method developed by Daigneault *et al.,* was used in this work as their data showed these THP-1 macrophages more closely resembled MDM than THP-1 differentiated using alternative protocols. In particular, their comparisons focussed on the increase in cytoplasmic-to-nuclear ratio and downregulation of CD14 expression, associated with MDM differentiation from monocytes.

In the work presented here, differentiated MDM appeared as a mildly heterogeneous population, with cells ranging from circular to spindle-shaped. However, they all displayed a spherical nucleus and large cytoplasmic-to-nuclear ratio. In comparison, THP-1 PMA appeared as a highly heterogeneous population, with some very small cells, that were lightly adherent, and some that resembled MDM with a large cytoplasmic-to-nuclear ratio, spherical nucleus and flattened morphology. This is in accordance with previously published data (Daigneault *et al.,* 2010).

THP-1 monocytes treated with PMA and plastic-adherent PBM displayed changes in cell morphology, becoming larger and more granular indicating differentiation to macrophages, confirming previously published data (Bosque *et al.,* 1997). However, the different methods used to achieve this is reflected in the differential expression of the differentiation marker, CPM. CPM is a specific marker of monocyte to macrophage differentiation and previous studies have shown that cell surface expression of CPM increases as monocytes differentiate into macrophages (Rehli *et al.,* 1995). This is confirmed by gene expression

data which showed a 29-fold increase in CPM expression in MDM compared to PBM. In the presence of GM-CSF and M-CSF, this was further increased.

Importantly, the protein expression of CPM by PMA-treated THP-1 macrophages was much lower than that by MDM. Accordingly, cell surface expression of CPM increased as PBM were differentiated to MDM. However, although CPM expression was detected on THP-1 cells, its expression decreased with PMA treatment. Since CPM expression correlates with macrophage maturation, it is likely that the low levels of CPM observed on the surface of THP-1 macrophages are due to their immature phenotype (Rehli *et al.,* 2000). The failure to increase expression of this key differentiation marker suggests that PMA-differentiated THP-1 cells do not adequately model the monocyte to macrophage differentiation of primary cells *in vitro*. Regarding the differentiation of MM6 cells, attempts to confirm previously published data by Zieglerheitbrock *et al.,* were unsuccessful (Zieglerheitbrock *et al.,* 1994).

3.6.4 **Differences between THP-1 PMA and monocyte-derived macrophages**

The expression of CD14 and CD45 has previously been shown to decrease during monocyte to macrophage differentiation (Zieglerheitbrock and Ulevitch, 1993). As previously described, both PBM and THP-1 monocytes displayed decreased expression of CD14 upon differentiation to macrophages (Ambarus *et al.,* 2012). However, whilst PBM also displayed decreased expression of CD45 upon differentiation, PMA-treated THP-1 cells showed an increase in CD45 expression. Taken together, these data suggest that PMA-treated THP-1 cells show dramatically altered expression of differentiation markers compared to peripheral blood MDM. This may be due to the actions of the potent protein kinase C stimulator (PMA) used to initiate the differentiation process.

3.7 Conclusion

Due to the 2D culture methods optimised in this chapter, large numbers of CD14+ PBM and MDM can be isolated and viably cultured *in vitro* and detached for use in downstream applications. In addition, a preliminary comparison has been drawn between primary and

cell line monocytes and macrophages. However, a more robust, multi-colour flow cytometry panel may enable a more thorough characterisation of the protein expression profiles of these different cell types to confirm any differences in expression. Additionally, the expression of a range of markers using qRT-PCR could provide further understanding in differences at the gene expression level. Whilst THP-1 and MM6 have been preliminarily compared in this work, further work could also compare other human monocyte cell lines such as AML-193, established from a young female with AML with lymphoblast morphology and GM-CSF dependency (Lange *et al.,* 1987); HL-60, a promyeloblast cell line which has the capacity for differentiation to a macrophage-like cell, established from the peripheral blood leukocytes of a female with AML (Collins, 1987); Kasumi-3 derived from the blast cells of an adult male with myeloperoxidase-negative acute leukaemia, which is capable of maturation of a monocytic lineage (Asou *et al.,* 1996); and U-937 derived from an adult male with histiocytic leukaemia and can be terminally differentiated (Sundstrom and Nilsson, 1976).

In conclusion, due to the important differences in morphology and protein expression observed in THP-1 and MM6 cell lines compared to primary cells (particularly of key markers CD45, CD14 and CD163) PBM and MDM will be used in the ensuing experiments. However, as very few optimized protocols are available for the 3D culture of primary monocytes and macrophages, cell lines will be used for method development, and these methods will then be applied to the 3D culture of primary cells.

4 Chapter 4: 3D Culture of Functional and Viable Macrophages

4.1 Introduction

Tissue-engineering is increasingly used in regenerative medicine for improved wound healing and several companies offer tissue-engineered oral mucosa for use in the clinic (Moharamzadeh *et al.,* 2012). In addition, tissue-engineering is becoming a more widespread technique in research as it provides several benefits compared to 2D and mono-culture experiments which are very simple, quick, and cost-effective, but lack the complexity of *in vivo* tissues. As such, 2D monolayer experiments have been shown repeatedly to fail to represent the *in vivo* environment (Cukierman *et al.,* 2001; Kriegebaum *et al.,* 2012; Mazzoleni *et al.,* 2009). Animal models are often used to test drugs for clinical application, however, due to the differences between humans and animals, results from these experiments are not always transferable (Gaballah *et al.,* 2008; Kimlin *et al.,* 2013; Mazzoleni *et al.,* 2009; Qian and Pollard, 2010). Therefore, there is an increased demand for accurate models of human tissues, which can represent an *in vivo* environment and therefore inform future clinical trial decisions and further understanding of disease progression. *In vitro* 3D co-culture models offer the benefits of including multiple cell types to more accurately represent human tissues, whilst providing a cost-effective, clinically relevant alternative to *in vivo* models and at the same time retaining the ease of use and reproducibility of 2D culture.

However, there are very few examples of 3D cultured immune cells, and of these, even fewer use primary human immune cells. As macrophages are shown to have an increasingly important role in the development and progression of oral cancer, this project aims to develop methods for the 3D culture of viable and functional macrophages in order to further develop existing *in vitro* 3D models of oral cancer.

4.2 Viable 3D culture of THP-1 monocytes

THP-1 cells are an established cell line which are often used to represent primary monocytes as they do not require lengthy isolation procedures, proliferate in culture and can be differentiated using PMA to produce a macrophage-like cell. This commercially available

cell line was initially used in this research to optimise methods for the 3D culture of monocytes and macrophages within a collagen hydrogel.

4.2.1 **Changes in proliferation of THP-1 cells cultured in a collagen hydrogel**

In order to show viable 3D culture of THP-1 cells over an experimental time course, an appropriate viability assay was required which did not involve cell lysis. AlamarBlue® is a non-toxic cell viability assay which measures cell proliferation through the reduction of non-fluorescent, membrane-permeable resazurin into resorufin during cell metabolism. Cell culture media surrounding collagen hydrogels in the presence or absence of THP-1 cells was sampled over 14 days (on days 1, 4, 7, 10 and 14) and the red fluorescence of resorufin was measured at 570 nm by a spectrophotometer (Tecan, Männedorf, Switzerland).

A collagen hydrogel was prepared as previously described (Dongari-Bagtzoglou and Kashleva, 2006) into which $1x10^6$ THP-1 cells were incorporated. Once set, hydrogels were cultured with 1 mL supplemented RPMI 1640 for 14 days. Cell culture media with the addition of alamarBlue® was sampled and analysed for changes in resorufin absorbance on days 1, 4, 7, 10 and 14. Media from THP-1-containing hydrogels was compared to media from cell-free hydrogels maintained under the same conditions (**Figure 4.1**).

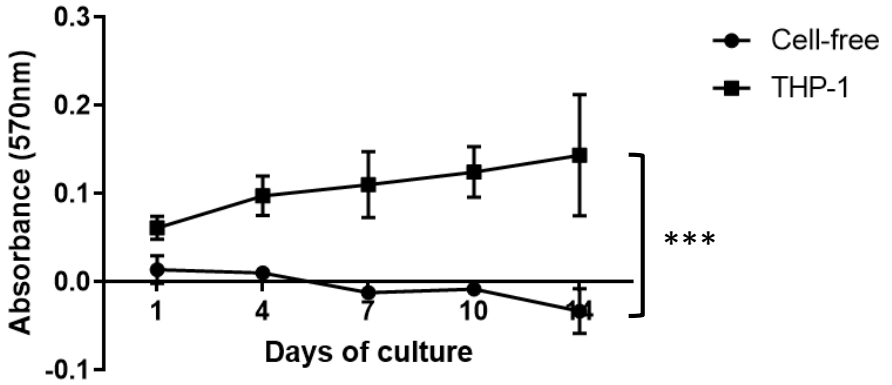

Figure 4.1. Absorbance of alamarBlue® over 14 days. THP-1-containing or cell-free collagen hydrogels were cultured for 14 days and absorbance of alamarBlue® was measured at 570nm on days 1, 4, 7, 10 and 14. Samples from six independent experiments were measured in triplicate (n=6), error bars show standard error mean, and significance was determined using an unpaired two-tailed T-test (*** = $p<0.005$).

Over 14 days, cell-free models showed no conversion of resazurin into resorufin, however, there was a small increase in resorufin in media surrounding THP-1-containing models suggesting an increase in the number of proliferating cells (**Figure 4.1**). After 14 days, an unpaired two-tailed T-test was carried out and concluded that collagen hydrogels containing THP-1 cells showed a significant increase in absorbance at 570 nm ($p=0.0001$) compared to a cell-free hydrogel.

4.2.2 Preparation of 3D cultured THP-1 cells for flow cytometry

Flow cytometry is a technique which uses lasers to interrogate individual cells in a fluid sample stream in order to detect scattered light relating to the physical characteristics (such as size, complexity and expression of proteins labelled with fluorochrome-conjugated antibodies) of the cells in a sample. Previous data suggested that THP-1 monocytes spontaneously differentiated to macrophages when cultured within a collagen hydrogel (Jennings, L., unpublished data). Therefore, flow cytometry was selected to detect changes in cell size and granularity which are associated with monocyte to macrophage

differentiation. However, a single-cell suspension was required for flow cytometry analysis. In addition, viability stains could be incorporated into flow cytometry sample staining methods for precise quantification of cell viability.

The concentration of collagen for hydrogel preparation was tested between 3-7 mg/mL in order to optimise formation of a hydrogel suitable for manipulation, viable cell culture and to enable rapid digestion of the hydrogel. In addition, incubation times of varying lengths were tested for rapid digestion of models, with and without the use of shaking or additional co-factor molecules such as calcium chloride ions, which stabilise the enzyme and promote its activity by facilitating its binding to collagen. Incubation of 2 mg/mL collagenase IV diluted in cold DMEM for 1.5 hours at 37 °C with shaking at 100 rpm enabled visible disaggregation of the collagen hydrogel. After 14-days of culture, THP-1-containing collagen hydrogels were digested using collagenase IV to release individual cells. However, un-digested collagen fibres prevented a THP-1 cell pellet forming upon centrifugation. Therefore, the use of a cell strainer to remove un-digested fibres was explored. THP-1 monocytes, cultured in 3D for 14 days, before and after use of a cell strainer were compared to a suspension of THP-1 monocytes cultured in 2D and a collagen hydrogel preparation devoid of cells that had not been subjected to processing with a cell strainer (**Figure 4.2**). These samples were analysed using flow cytometry.

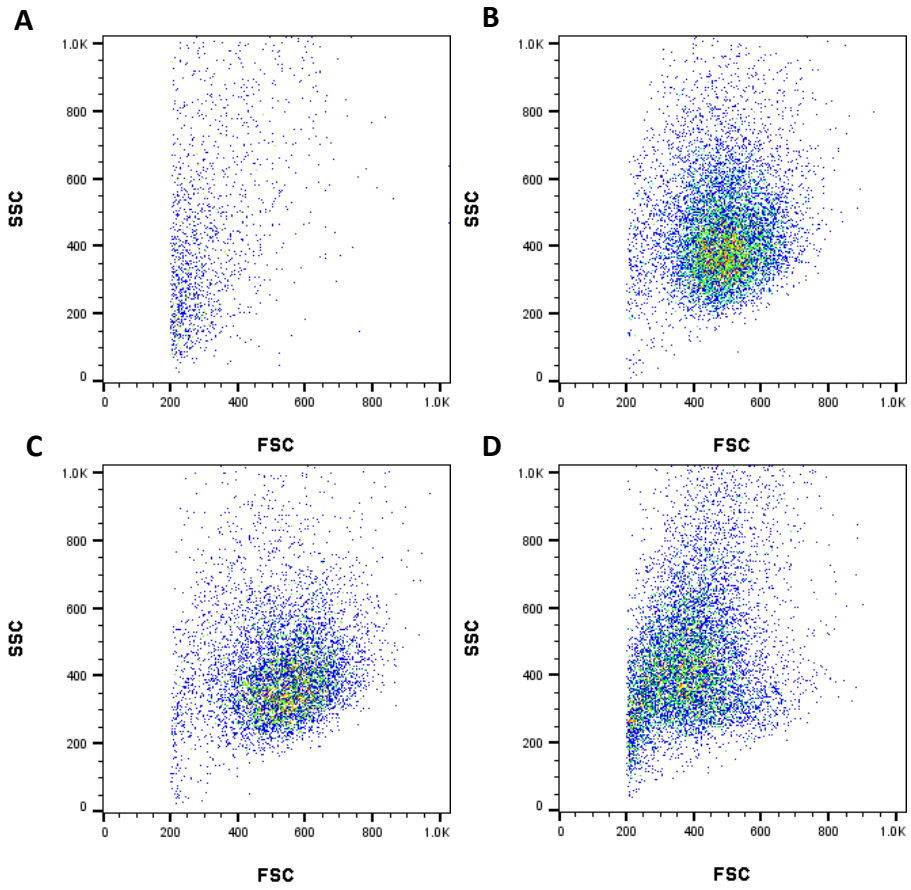

Figure 4.2. Preparation of a single-cell suspension suitable for flow cytometry. THP-1 monocytes cultured in 3D for 14 days were prepared into a single cell suspension suitable for flow cytometry using a cell strainer to eliminate contaminating un-digested collagen fibres. Dot plots show forward scatter (FSC) and side scatter (SSC) data measured using flow cytometry. The removal of undigested collagen molecules, such as those present in hydrogels devoid of cells (**A**) from disaggregated collagen hydrogels produced a homogeneous single-cell suspension suitable for flow cytometry (**B**), comparable to THP-1 cells cultured in suspension (**C**), without the collagen contamination which was previously observed (**D**). Dot plots show representative data from three independent experiments, measured in duplicate (n=3).

A collagen hydrogel devoid of cells, digested with collagenase IV and prepared for analysis by flow cytometry, without prior processing with a cell strainer, retained particles of undigested collagen that were falsely detected as cells during flow cytometry analysis. Once this sample had passed through a cell strainer, no events were detected by the flow cytometer (data not shown). The use of a cell strainer removed this undigested collagen contamination from THP-1 monocytes cultured in 3D resulting in detection of a

homogeneous THP-1 cell population using flow cytometry, which was comparable to that of THP-1 cells cultured in 2D. All subsequent samples of 3D-cultured cells for flow cytometry analysis were processed using a cell strainer before staining with antibodies.

4.2.3 **Viability of THP-1 cells cultured in 3D**

In order to quantitatively determine the viability of THP-1 cells cultured in 3D over 14 days, single-cell suspensions of THP-1 monocytes released from a digested collagen hydrogel were stained with propium idodide (PI). However, repeated, high levels of cell death were observed. Different aspects of hydrogel preparation were investigated to determine if gel dehydration during gelation, gel disaggregation using collagenase IV, cell culture media used, or gel pH were responsible for cell death. For the preparation of the hydrogel, the published protocol described neutralisation according to 'if the solution looks acidic (judged visually by the color of the phenol red…)' (Dongari-Bagtzoglou and Kashleva, 2006). However, this resulted in a mixture of pH 9.1, as determined by pH probe analysis. The preparation of a hydrogel of pH 7.4 required a reduced quantity of NaOH, displaying a subtle change in colour of phenol red (**Figure 4.3**).

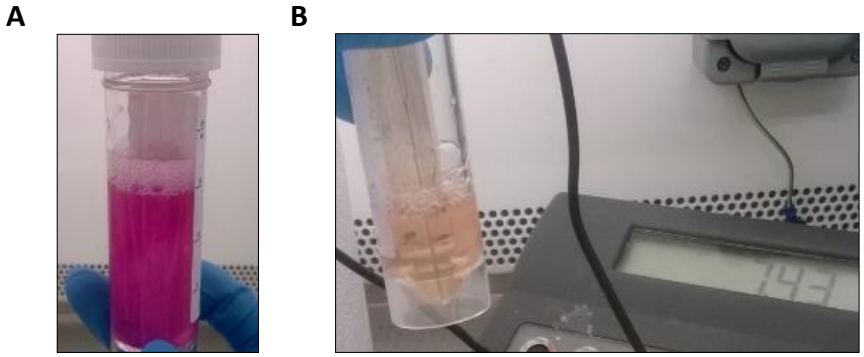

Figure 4.3. Preparation of collagen hydrogels of different pH. Images show the colour difference of solutions of pH 9.1 (**A**) and pH 7.4 (**B**) used for collagen hydrogel preparation.

Collagen hydrogels prepared under the guidance of a colour change of phenol red resulted in a hydrogel pH of 9.1. To determine whether this highly alkaline pH affected cell viability

during 3D cell culture, THP-1 monocytes were cultured in gels prepared at pH 9.1 and pH 7.4, and viability analysed by flow cytometry using PI (**Figure 4.4**).

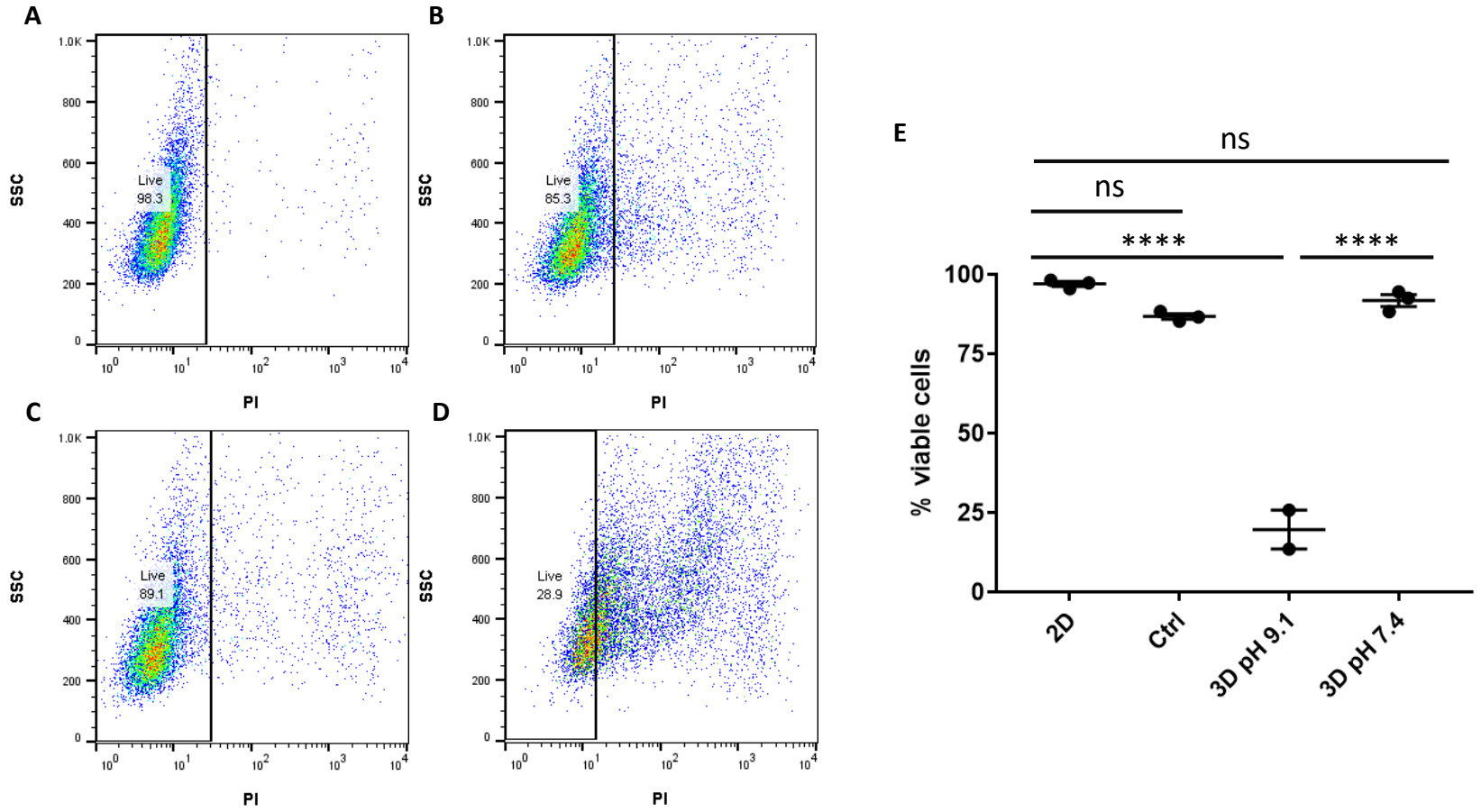

Figure 4.4. Viability of THP-1 monocytes cultured within a collagen hydrogel. THP-1 monocytes cultured in suspension (**A**), with the additional treatment of collagenase IV as a control (Ctrl, **B**) and in 3D, in a collagen hydrogel of either pH 7.4 (**C**) or pH 9.1 (**D**) for 14 days were analysed using flow cytometry. Viability assessed by dead cell exclusion using propium iodide is summarised in scatter plot (**E**). Gates were set based on unstained samples treated under the same condition. Samples from three independent experiments were measured in duplicate (n=3) where dot plots show representative data. Error bars show the standard error mean and significance was determined using a one-way ANOVA with Tukey's multiple comparisons (**** = $p<0.0001$).

THP-1 monocytes cultured in 2D showed 97.0 % viability as measured with PI and analysed by flow cytometry. Preparation of collagen hydrogels of pH 7.4 enabled recovery of a significant increase in the percentage of viable THP-1 cells recovered after 14 days compared to hydrogels of pH 9.1, up to 91.8 % from 19.7 % respectively ($p=<0.0001$). THP-1 cells cultured in 3D within collagen hydrogels of pH 7.4 showed no significant decrease in viability compared to THP-1 cells cultured in a 2D suspension ($p=0.4045$). THP-1 cells cultured in a 2D suspension treated with collagenase IV, used as a control (Ctrl), showed 86.4 % viability and also showed no significant decrease in viability compared to THP-1 cells cultured in 2D without treatment with collagenase IV ($p=0.0543$). Subsequently, all ensuing collagen hydrogel mixtures were pH-probed before addition of cells to ensure a pH of 7.4.

4.2.4 **Visualisation of THP-1 cells cultured in 3D**

In order to visualise THP-1 monocytes cultured within the collagen hydrogel, formalin-fixed hydrogels containing THP-1 cells after 14 days of culture were processed, bisected and paraffin-embedded. Haematoxylin and eosin (H&E) stains were used to identify cell nuclei and cytoplasms respectively, and cell distribution overall (**Figure 4.5**).

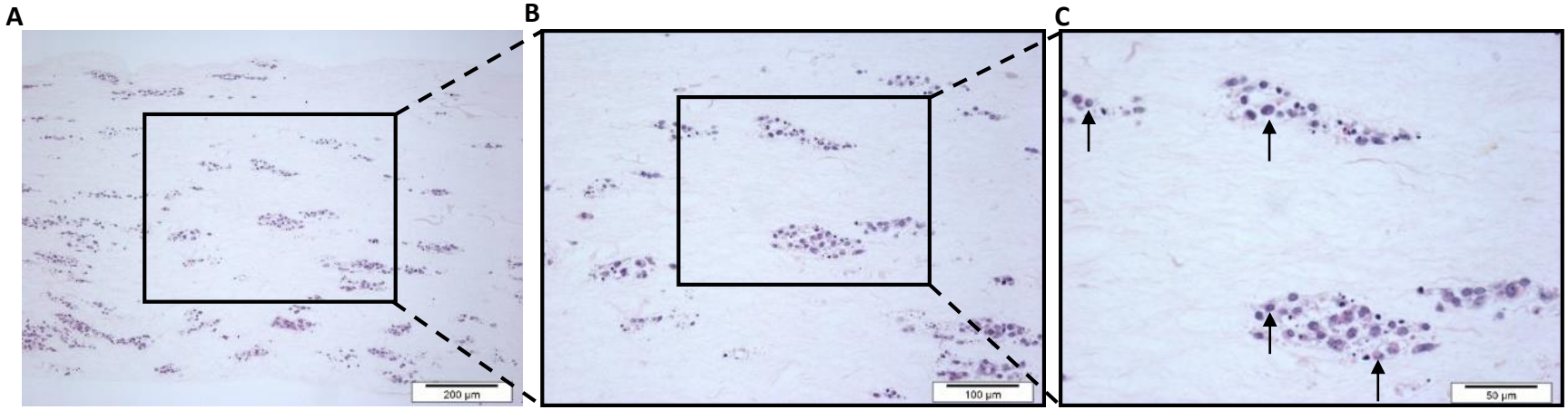

Figure 4.5. H&E stained THP-1 cells cultured within a collagen hydrogel. Collagen hydrogels containing THP-1 monocytes cultured for 14 days were formalin fixed, sectioned and stained using H&E. Images taken at 10x (**A**), 20x (**B**) and 40x (**C**) magnification are representative of three independent experiments (n=3). Monocytes with typical morphology are exemplified (arrows). Scale bars indicate 200 µm (**A**), 100 µm (**B**) and 50µm (**C**).

Following 14 days of culture within a collagen hydrogel, evenly dispersed clusters of THP-1 cells stained with H&E can be observed. Here, THP-1 cells can be observed as small, spherical cells with a reniform nucleus and very few granules.

4.2.5 Changes in proliferation of viable THP-1 cells cultured in a collagen hydrogel

Previous data in this chapter showed that THP-1 monocytes cultured in 3D, stained with PI and analysed by flow cytometry were viable. Additionally, the use of alamarBlue® over the time course of 14 days to measure cell proliferation, combined with the use of PI at the end of the cell culture period to measure cell viability was explored. Culture media of collagen hydrogels containing THP-1 cells with or without the addition of alamarBlue® were sampled (**Figure 4.6**) and compared to samples from THP-1 cells cultured in suspension.

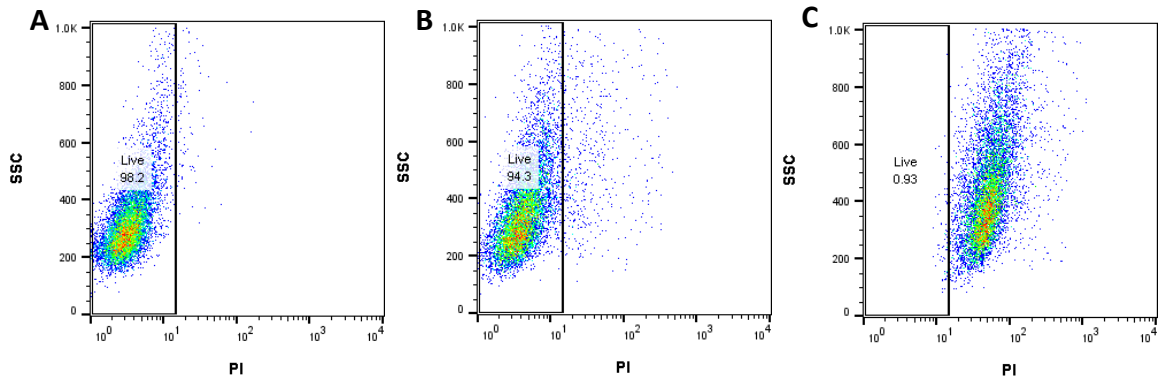

Figure 4.6. Viability of THP-1 cells cultured within a collagen hydrogel treated with alamarBlue®. THP-1 cells cultured in suspension (**A**), or in a collagen hydrogel for 14 days in the absence (**B**) or presence of alamarBlue® (**C**) were analysed by flow cytometry using propium iodide dead cell exclusion. Gates were set based on unstained samples treated under the same conditions. Dot plots are representative of two independent experiments measured in duplicate (n=2).

THP-1 monocytes cultured in 2D or in 3D without the addition of alamarBlue® showed >90 % viability, however those treated with alamarBlue® showed <1 % viability measured with PI.

4.2.6 **THP-1 monocytes cultured in 2D and 3D show no differences in size and granularity**

Previous evidence suggested that monocytes cultured in 3D spontaneously differentiate to macrophages in a manner representative of circulating monocyte differentiation to macrophages within tissues *in vivo* (Jennings, L., unpublished). Monocyte to macrophage differentiation is characterised by a morphological change as cells increase in size, cytoplasmic-to-nuclear ratio and number of cytoplasmic granules to increase production of hydrolytic enzymes (Chang *et al.,* 2012). Previous data determined monocyte to macrophages differentiation visually by light microscopy and H&E staining of 4 µm FFPE sections. However, with methods now developed for analysis of 3D-cultured THP-1 monocytes by flow cytometry, changes in size (FSC) and granularity (SSC) of THP-1 cells, indicative of monocyte to macrophage differentiation, could be compared between those cultured in 2D and 3D. THP-1 cells cultured within a collagen hydrogel for 14 days were retrieved using collagenase IV digestion and a single-cell suspension was prepared using a 40 µm cell strainer (**Figure 4.7**).

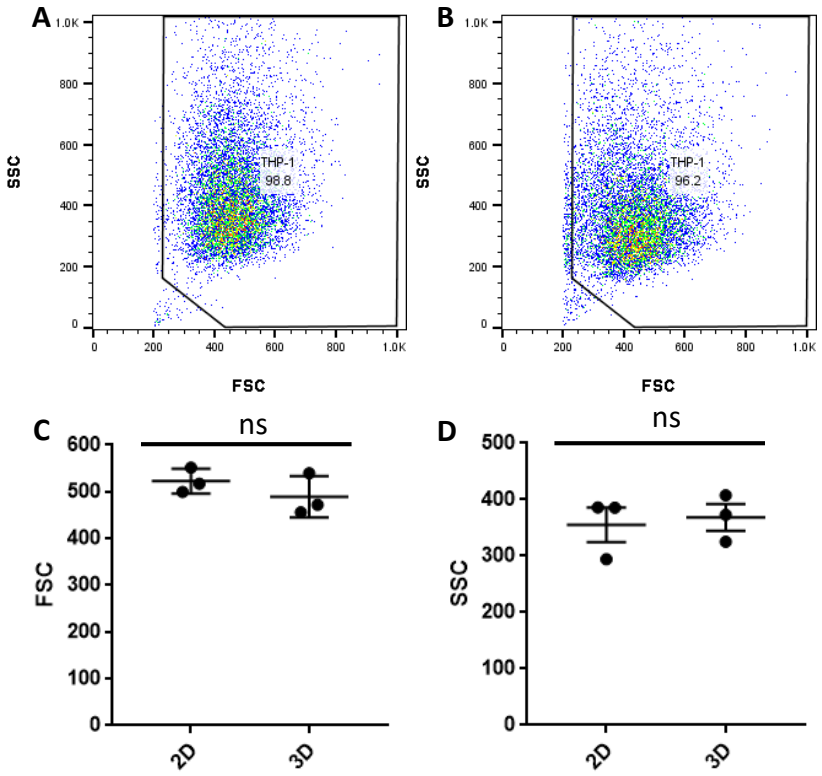

Figure 4.7. Comparison of size and granularity of THP-1 cells cultured in 2D and 3D. Forward scatter (FSC) and side scatter (SSC) data of THP-1 cells cultured in a 2D suspension (**A**) or in a 3D collagen hydrogel for 14 days (**B**) was measured using flow cytometry following dead cell exclusion using propium iodide, and compared using summarised data in scatter plots (**C** and **D**) for FSC and SSC respectively. Gates were set based on unstained samples. Samples from three independent experiments were measured in duplicate (n=3), error bars show standard error mean and significance was determined using an unpaired T-test.

FSC values of THP-1 monocytes cultured in 2D were measured as 522.7 ± 15.28 compared to those cultured in 3D which were measured as 489.2 ± 25.59. SSC values were measured as 355.3 ± 30.42 in 2D-cultured THP-1 monocytes, and 368.5 ± 23.92 in those cultured in 3D. An unpaired T-test showed that THP-1 cells cultured in 2D and 3D showed no significant difference in size or granularity (p=0.3238 and p=0.7508 respectively).

4.3 3D culture of peripheral blood monocytes

Following the successful culture of THP-1 monocytes in 3D within a collagen hydrogel for 14 days, the 3D culture of PBM was explored. Monocytes were isolated from buffy coats using density centrifugation and purified using magnetic separation. One million of the resulting

cells were incorporated into a collagen hydrogel for 3D culture and cultured with supplemented IMDM for 14 days.

Due to poor yields of purified populations of monocytes using magnetic separation, it was not possible to acquire enough primary monocytes for analysis of 3D cultures by flow cytometry. Of the pooled samples that were tested, viability was very low after 24 hours, and no viable cells could be detected following 14 days of culture (data not shown).

4.4 3D culture of Mono Mac 6

Whilst THP-1 cells are regularly used to represent PBM, a need for a more mature monocyte cell line was addressed by Ziegler-Heitbrock *et al.,* who established a new human monocyte cell line, Mono Mac 6, which expressed phenotypic and functional features more similar to mature monocytes than THP-1 or U937 monocyte cell lines (Zieglerheitbrock *et al.,* 1988). However, MM6 cells are also derived from a patient with monoblastic leukaemia, so while they may be preferential in some aspects of monocyte biology compared to THP-1 cells, they may not be representative in other aspects.

Due to the limitations in the viable 3D culture of PBM, the use of MM6 monocytes was explored as an improvement to THP-1 monocytes. In a similar way to THP-1 cells, MM6 are cultured in suspension and rapidly proliferate once established in culture. Therefore, it is possible to culture large numbers of these cells to prepare 3D cultures.

A collagen hydrogel was prepared into which $1x10^6$ MM6 cells were incorporated. After 14 days, MM6 cells were retrieved from the collagen hydrogel using collagenase IV digestion, prepared into a single cell suspension using a cell strainer, and stained with PI for flow cytometry analysis. Alternatively, models were fixed in formalin, embedded in paraffin and stained with H&E (**Figure 4.8**).

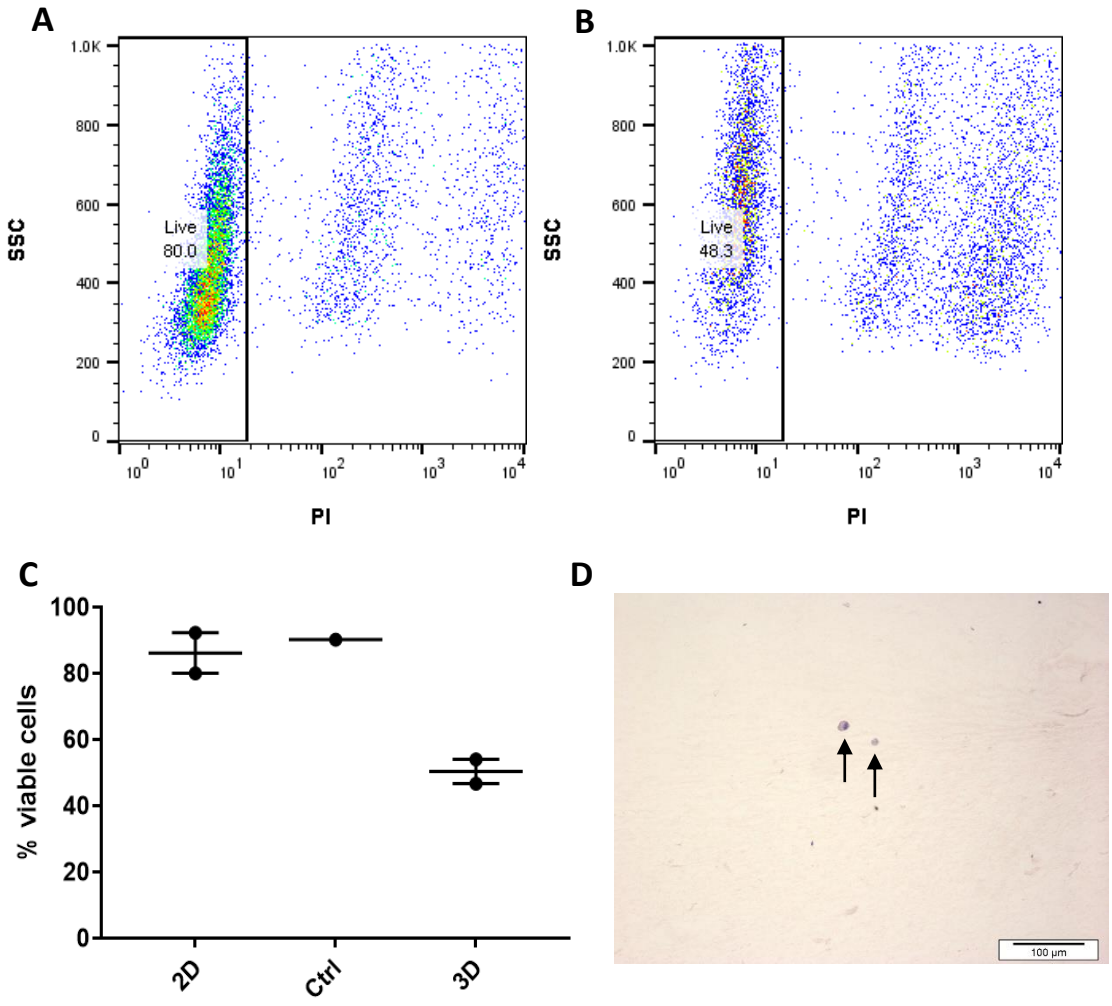

Figure 4.8. Viability of 3D-cultured Mono Mac 6. Mono Mac 6 (MM6) were cultured in 3D within a collagen hydrogel for 14 days and compared to those cultured in suspension (2D). For flow cytometry analysis, cells were selected based on dead cell exclusion and gates set based on unstained samples cultured under the same conditions. For histological analysis, models were formalin fixed, sectioned and stained with H&E. Viability of MM6 cell line cultured in 2D (**A**) or within a 3D collagen hydrogel (**B**) is summarised in scatter plot (**C**). H&E stained MM6 cultured in 3D (**D**) and dot plots are representative of two independent experiments (n=2). Error bars shows standard error mean and arrows indicate MM6 cells sparsely populating the hydrogel.

Viability of MM6 cells cultured in a 2D suspension, measured using PI and analysed by flow cytometry, dropped from 86.2 % to 50.4 % when cultured in 3D. However, 2D-cultured MM6 monocytes treated with collagenase IV only resulted in 10 % loss in viability (data not

shown). MM6 cells cultured in 3D and stained with H&E can be observed sparsely distributed throughout the hydrogel.

4.4.1 Differentiation of peripheral blood monocytes to monocyte-derived macrophages *in situ* within collagen hydrogel

CPM cleaves terminal arginine and lysine residues on peptides to control binding of growth factors and hormones on the cell surface and degradation of cell-surface peptides. Importantly here, it is a marker of monocyte to macrophage differentiation as its expression levels are higher in macrophages than in monocytes. In the literature, GM-CSF and M-CSF are often used to promote monocyte to macrophage differentiation and therefore to stimulate an increase in the expression of CPM. An increase in expression of CPM was used to indicate monocyte to macrophage differentiation on monocytes and macrophages cultured in 2D and 3D and in the presence or absence of GM-CSF or M-CSF.

Carboxypeptidase M gene expression in 3D

One million PBM isolated from buffy coats and purified using magnetic separation were incorporated into a collagen hydrogel and cultured with supplemented IMDM for 14 days, in the presence or absence of GM-CSF or M-CSF. After 14 days, cells were retrieved using collagenase IV digestion of the hydrogel and processed using a cell strainer to remove undigested collagen fibres. RNA was extracted from cell pellets and yield determined.

Due to poor yields of purified populations of monocytes using magnetic separation, and loss of cells during the processing of 3D cultures, negligible amounts of RNA were acquired and it was therefore not possible to analyse gene expression of CPM by PBM cultured in 3D.

Carboxypeptidase M protein expression in 3D

One million PBM isolated from buffy coats and purified using magnetic separation, or MDM were incorporated into a collagen hydrogel and cultured with supplemented IMDM for 14 days. After the culture period, hydrogels were fixed, paraffin-embedded and stained with

H&E and immunohistochemically stained with anti-CPM antibody and counter-stained with haematoxylin (**Figure 4.9**).

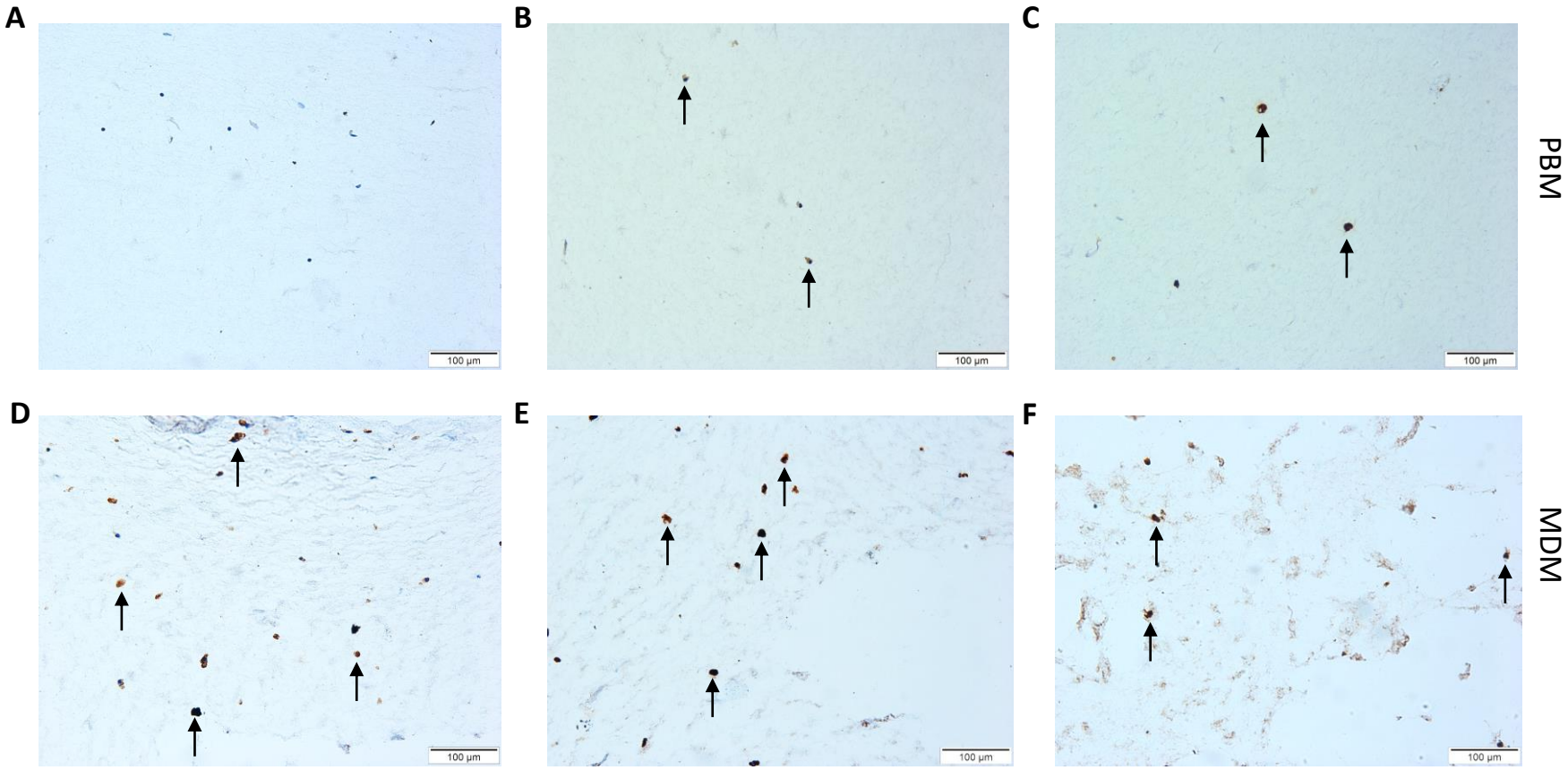

Figure 4.9. Carboxypeptidase M expression of peripheral blood monocytes and monocyte-derived macrophages on day 1 and day 14 of 3D culture. Immediately following isolation and purification of peripheral blood monocytes (PBM, **A-C**) or following 7 days of adherent culture of monocyte-derived macrophages (MDM, **D-F**), cells were cultured within a collagen hydrogel. Models were cultured in the absence (**A** and **D**) or presence of GM-CSF (**B** and **E**) or M-CSF (**C** and **F**) for 14 days. Light microscopy images display collagen hydrogels containing PBM on days 1 (**A** and **D**) and 14 (**B**, **C**, **E** and **F**) of culture stained using anti-CPM antibodies and counter-stained with haematoxylin. Images are representative of two independent experiments (n=2). Arrows indicate areas of staining positive for CPM and scale bars indicate 100 µm.

PBM appeared visibly smaller than MDM on day 1, however they were of comparable size by day 14. Additionally, increased amounts of CPM staining could be visualised in MDM samples compared to PBM samples. Whilst no CPM staining could be observed in models containing PBM on day 1, small amounts could be detected on day 14 in the presence of GM-CSF, which was further increased in the presence of M-CSF.

4.5 3D culture of THP-1 PMA

To determine whether THP-1 PMA could be viably cultured in 3D, THP-1 monocytes were stimulated with PMA in 2D for 8 days (Daigneault *et al.,* 2010). After differentiation, $1x10^6$ THP-1 PMA were incorporated into a collagen hydrogel and cultured for 14 days with supplemented RPMI. After 14 days, cultures were formalin-fixed, processed, stained with H&E and visualized using light microscopy. Additionally, hydrogels were disaggregated using collagenase IV, processed using a cell strainer, and stained with PI for assessment of cell viability using flow cytometry (**Figure 4.10**).

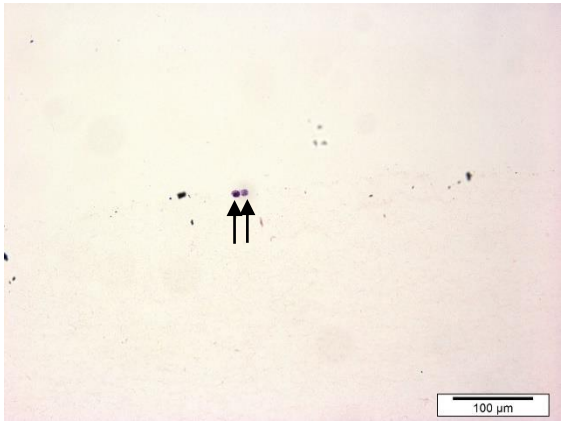

Figure 4.10. Viability of 3D-cultured THP-1 PMA. THP-1 monocytes treated with PMA (THP-1 PMA) for 8 days were recovered using cell scraping and cultured within a collagen hydrogel for 14 days. H&E stained sections of THP-1 PMA cultured in 3D are representative of three independent experiments (n=3). Arrows indicate THP-1 PMA and scale bar indicates 100 µm.

Two cells can be visualized in the uppermost layer of the hydrogel. H&E staining shows a large nucleus and minimal cytoplasm. Due to the low numbers of THP-1 PMA recovered following 14 days of 3D culture, it was not possible to perform viability analysis using flow

cytometry. Of the pooled samples that were tested after 24 hours, <30 % of cells were viable (data not shown).

4.6 3D culture of monocyte-derived macrophages

Small numbers of macrophages have previously been cultured within a collagen hydrogel model of the dermis (Linde *et al.,* 2012). However, this has not been successfully combined with a tissue-engineered model of the oral mucosa. With so many differences identified between MDM and THP-1 PMA, it was essential to determine methods for the viable 3D culture of MDM. In order to determine whether MDM could be cultured in 3D, a variety of methods to incorporate MDM within a collagen hydrogel were tested; monocytes were seeded into wells or on top of models and allowed to differentiate for 7 days as it was hypothesized that differentiated MDM may extravasate into the collagen hydrogel. However, MDM remained on the surface of the hydrogel and could not be visualized within the hydrogel (data not shown).

4.6.1 Viability of monocyte-derived macrophages cultured in 3D

Monocytes differentiated to MDM in 2D over 7 days were detached using gentle scraping into IMDM. One million MDM were incorporated into the collagen hydrogel mixture, and once set, cultured for 14 days with supplemented IMDM. After 14 days, cells were retrieved from the hydrogel using collagenase IV, processed using a cell strainer and viability measured using PI and analysed using flow cytometry. Alternatively, hydrogels were formalin-fixed, processed, paraffin-embedded, stained with H&E and visualized using light microscopy (**Figure 4.11**).

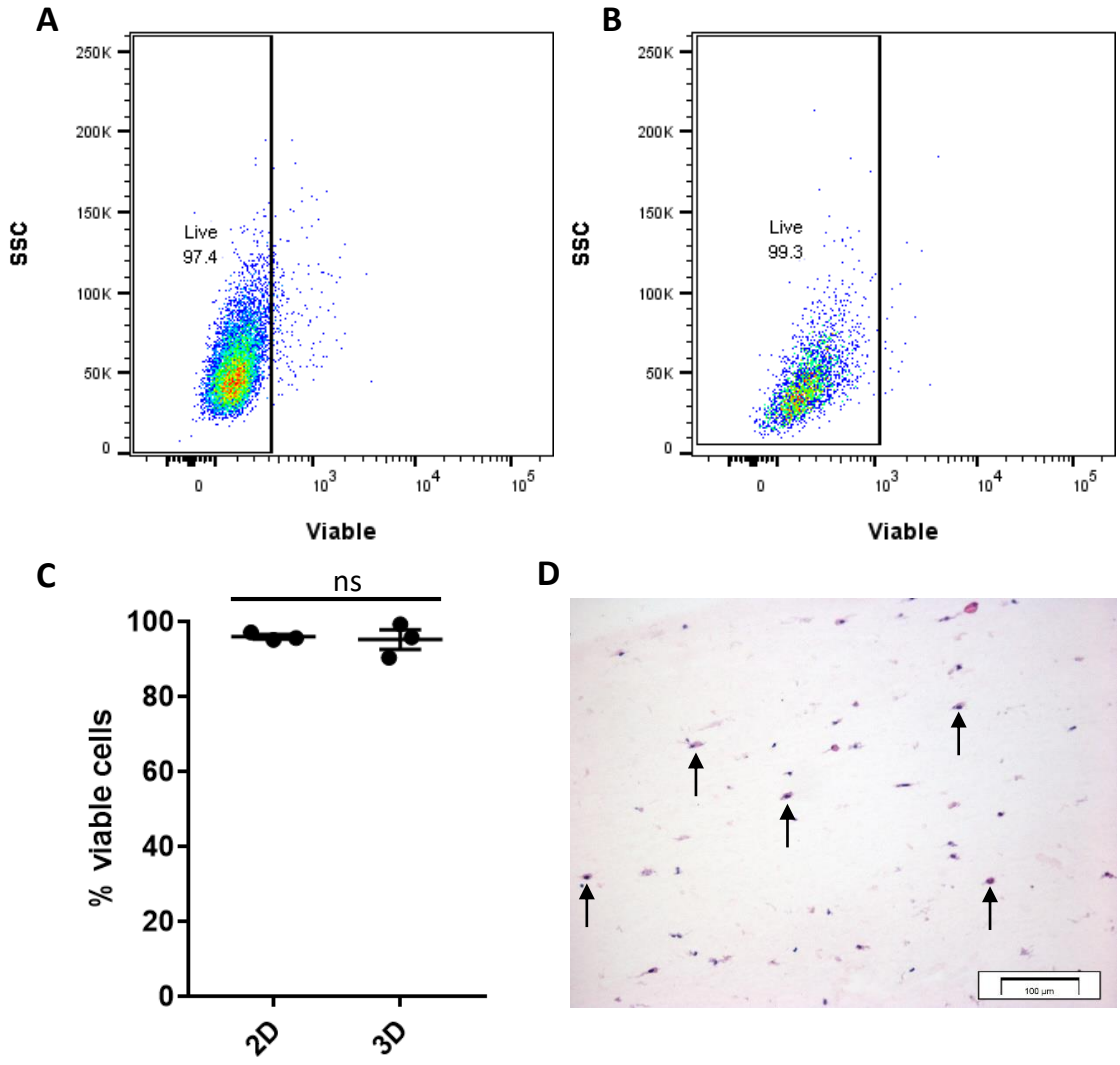

Figure 4.11. Viability of 3D-cultured monocyte-derived macrophages. Monocyte-derived macrophages (MDM) cultured for 7 days in adherent culture were recovered using cell scraping and analysed using flow cytometry. Viability of MDM cultured in 2D (**A**) or within a 3D collagen hydrogel (**B**) is summarised in scatter plot (**C**). H&E stained MDM cultured in 3D (**D**) and dot plots are representative of three independent experiments (n=3). Error bars shows standard error mean. Arrows indicate MDM and scale bar indicates 100 µm.

Following 14 days of 3D culture, >95 % of MDM were measured as viable using flow cytometry. An unpaired two-tailed T-test concluded that there was no significant difference in viability observed between MDM cultured in 2D and 3D (p=0.7978). Compared to unstained samples, viability gates were set at different positions for 2D and 3D samples, suggesting that the auto-fluorescence, FSC and SSC were altered in MDM cultured in 3D

compared to 2D. Staining of hydrogels with H&E showed an even distribution of MDM throughout the hydrogel. These cells appeared as large, irregular-shaped cells with a darkly stained spherical nucleus.

4.6.2 **MDM cultured in 3D release inflammatory cytokines in response to LPS**

Macrophages play a key role in host defences, providing the first line of defence against invading pathogens. LPS is the major component of the outer membrane of gram-negative bacteria which binds to CD14 on the surface of macrophages, resulting in the production of an inflammatory response. This is characterised by the release of pro-inflammatory cytokines, such as IL-6.

To demonstrate that MDM are not only viable in 3D culture, but can also respond to exogenous stimuli in a manner representative of their role *in vivo*, LPS was added to fresh media on 2D and 3D cultured MDM on days 7 and 14 of culture respectively. After 24 hours, cell culture media was collected and assayed for any cytotoxic effects of LPS through LDH release, and evidence of a pro-inflammatory response was detected using ELISA to measure IL-6 release (**Figure 4.12**).

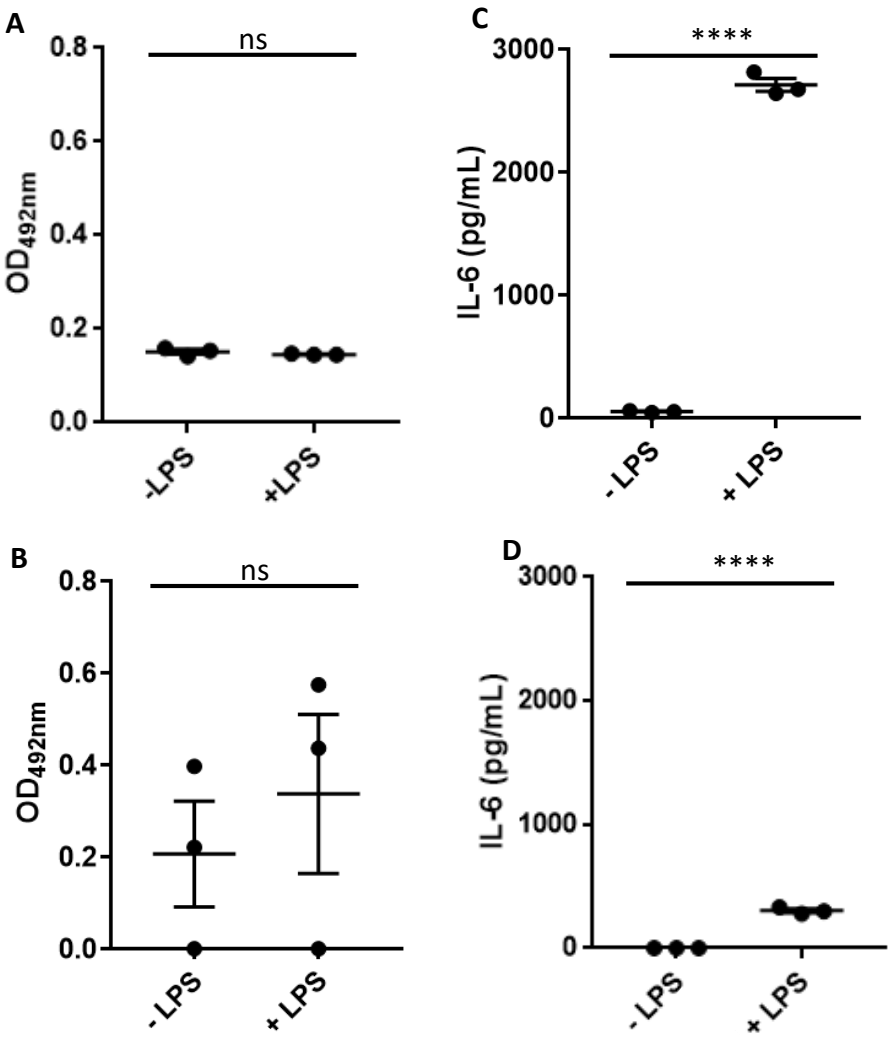

Figure 4.12. Monocyte-derived macrophages cultured in 2D and 3D release IL-6 in response to lipopolysaccharide. Monocyte-derived macrophages (MDM) were cultured for 7 days in adherent culture, and recovered using cell scraping (2D). For 3D cultures, MDM were additionally cultured for 14 days within a collagen hydrogel. Lactate dehydrogenase (LDH) release (**A** and **B**) and IL-6 release (**C** and **D**) of MDM cultured in 2D (**A** and **C**) or 3D (**B** and **D**) were measured using LDH assay and ELISA respectively. Data are representative of three independent experiments measured in triplicate (n=3) and error bars show standard error mean. Significance was determined using an unpaired T-test (****=p<0.0001).

The addition of LPS did not result in an increase in release of LDH from MDM in both 2D and 3D cultures (p=0.3782 and p=0.5678, respectively) as determined by an unpaired two-tailed T-test. However, the amount of LDH released from MDM cultured in 3D was higher than

that of MDM cultured in 2D. In both 2D and 3D cultures, there was a significant increase in IL-6 released in response to stimulation of MDM with LPS ($p<0.0001$). However, the amount of IL-6 released from 2D cultures was almost 10-fold higher than that released by 3D cultures.

4.7 Discussion

Collagen is the main component of the ECM and as such can be used to form a hydrogel for the 3D culture of cells to mimic the ECM. Whilst it lacks the complexity of other scaffolds, such as DED, cells can easily be incorporated into the mixture whilst it is still viscous. This makes it ideal for the 3D culture of cells which typically reside within the ECM, such as macrophages. In order to best represent tissue resident macrophages *in vivo*, this research sought to model monocyte to macrophage differentiation *in situ* within the gel. Previous data suggested that monocytes cultured within a 3D hydrogel may spontaneously differentiate to macrophages in response to culture within a 3D environment (Jennings, L., unpublished).

Published studies that have incorporated monocytes into tissue-engineered models typically use THP-1 or MM6 cell lines (**Table 1.2**); no studies could be found incorporating primary human monocytes into a collagen hydrogel. In this chapter, the viable 3D culture of primary human monocytes within a collagen hydrogel is explored. Due to the challenges presented by isolating primary cells, 3D culture methods were developed using THP-1 cell line which is often used to represent primary monocytes. However, results from Chapter 3 demonstrated important differences between PBM, THP-1 and MM6. Consequently, optimised methods were then applied to the 3D culture of primary cells.

4.7.1 Viable 3D culture of THP-1

No published articles could be found describing the culture of THP-1 monocytes within a collagen hydrogel. Previous H&E data showed that THP-1 monocytes cultured in 3D appeared larger with a macrophage-like appearance suggesting differentiation of THP-1

monocytes to macrophages (Jennings, L., unpublished). This work also identified challenges in maintaining the viability of THP-1 cells in 3D culture.

To measure cell viability within the collagen hydrogel over the 14-day culture period, an assay for measuring cell viability was required. Commonly used cell viability reagents include (3-4,5-dimethylthiazol-2-yl)-2,5-diphenyltetrazolium bromide) tetrazolium (MTT), PrestoBlue®, Resazurin and alamarBlue®. An MTT assay involves cell lysis, making it an end-point assay so it cannot be used to measure cell viability over time. Resazurin, PrestoBlue® and alamarBlue® are all resazurin-based reagents and so can be used interchangeably depending on reaction times required. AlamarBlue® was selected to measure THP-1 viability on days 1, 4, 7, 10 and 14. Published models of the oral mucosa, using DED, are cultured for 14 days, hence, the viable culture of THP-1 in 3D was sought for 14 days (Colley *et al*., 2011; Hearnden *et al*., 2014).

AlamarBlue® detects cell viability as a measure of metabolic activity. The modest increase in absorbance of alamarBlue® over 14 days indicates a modest increase in metabolic activity of the cells within the hydrogel. Macrophages are less metabolically active than monocytes, so through differentiation, little increase in metabolic activity would be detected using alamarBlue®. This supported previous data suggesting that in response to a 3D environment, THP-1 monocytes were differentiating to macrophages.

Flow cytometry can not only detect changes in size and granularity of cells, or morphological changes associated with monocyte to macrophage differentiation, but could also be used to quantitatively measure cell viability and expression levels of proteins associated with monocyte to macrophage differentiation, such as CPM. In order for flow cytometry analysis to be possible, a single-cell suspension was required. This involved the disaggregation of the collagen hydrogel using collagenase IV to retrieve cells contained within it. Whilst conditions were optimised for the visible disaggregation of the collagen hydrogel, un-digested collagen fibres prevented a pellet of THP-1 monocytes from forming upon centrifugation and also resulted in collagen fragments falsely detected as cells during flow cytometry analysis. Cell strainers are often used in flow cytometry, particularly for cells

which typically form adherent junctions, such as keratinocytes, to prevent clogging of the flow chamber. In this case, a cell strainer was effective in removing contaminating un-digested collagen fibres to produce a single-cell suspension of THP-1 monocytes suitable for flow cytometry analysis.

Previous data has shown an increase in the size and granularity of PMA-treated THP-1 cells compared to THP-1 monocytes (Daigneault *et al.,* 2010) and therefore changes in FSC and SSC respectively could indicate monocyte to macrophage differentiation. Flow cytometry analysis comparing the size and granularity of THP-1 cells cultured in 2D and 3D showed no significant difference. Histological analysis of 3D cultured THP-1 using H&E staining revealed evenly distributed clusters of cells indicative of cell proliferation. Further analysis using proliferation markers, such as Ki67, may indicate whether THP-1 cells are proliferating. However, it is widely considered that macrophages are terminally differentiated and therefore do not proliferate within tissues, although unless treated with PMA, or other differentiation-inducing stimuli, THP-1 monocytes are not considered terminally differentiated.

Analysis of THP-1 monocytes cultured in 3D using flow cytometry also enabled quantitative measurement of viability over 14 days. PI is a membrane impermeant intercalating dye which penetrates cells with damaged or permeable membrane to bind to the DNA, thus enabling dye exclusion of non-viable cells excited at 488 nm and detected at emission wavelength of 617 nm. It is often used to assess viability using flow cytometry. This showed that cells cultured in 3D for 14 days were non-viable. The decrease in metabolic activity identified by alamarBlue® thought to indicate monocyte to macrophage differentiation was in fact due to cell death. However, probing of the collagen hydrogel mixture identified a pH of 9.1, that is not supportive to maintaining viable cells. Altering the pH to 7.4 resulted in successful, viable culture of THP-1 monocytes for 14 days within a collagen hydrogel.

Resazurin, in the alamarBlue® reagent, fluoresces at the same wavelength as PI, with 71 % overlap in emission spectra, resulting in cells treated with alamarBlue® measured falsely as non-viable by flow cytometry. Whilst there are alternative viability dyes available for flow

cytometry, a major component of this project is the development of a polychromatic flow cytometry panel for detailed characterisation of macrophages. The use of alamarBlue® limits the number of fluorochromes available for use in the multi-colour panel, as its fluorescence emission spectra demonstrates spectral overlap with many commonly used reagents (such as 24 % overlap with FITC, 87 % overlap with PE and 63% overlap with Texas Red). By using separate hydrogels for each time point and/or analysis, the benefits of using a live cell assay would be lost. In addition, the manufacturer reports that alamarBlue® is metabolized by leukocytes making it difficult to interpret results (ThermoFisher). Therefore, in ensuing experiments, flow cytometry will be used to quantitatively measure cell viability during extended culture.

4.7.2 3D culture of peripheral blood monocytes

In order to develop an *in vitro* culture system truly representative of the *in vivo* environment, the use of primary cells is preferred. No published articles could be found describing the 3D culture of PBM within a collagen hydrogel. As methods had previously been developed for the 3D culture of commercially available monocytes, attempts were made using PBM isolated from healthy volunteers. PBM were purified using magnetic separation and cultured for 14 days within a collagen hydrogel. However, due to the limited number of PBM resulting from magnetic purification, few PBM were available for seeding into the collagen hydrogel. H&E staining identified cells sparsely populating the hydrogel, and after 14 days, no events were detected using flow cytometry. After just 24 hours in 3D culture, cell viability was <20 % suggesting that large-scale cell death was occurring over 14 days. A previously published study incorporated PBMC into a ThinCert™ coated with gelatin for 24 hours, but did not assess viability of cells (Tschachojan *et al.,* 2014).

Within human tissues, monocytes extravasate from the blood stream into tissues where they differentiate to macrophages. With the use of exogenous stimuli, the differentiation of PBM to macrophages *in situ* within the hydrogel was explored. It was hypothesized that differentiation of PBM to MDM may improve the poor viability of PBM cultured in 3D observed previously, by more accurately replicating the *in vivo* transition from circulating

monocyte to resident tissue macrophage. CPM is used as a marker of monocyte to macrophage differentiation (Rehli *et al.,* 2000) and whilst immunohistochemical staining of CPM provided some evidence that monocytes could be stimulated to differentiate to macrophages within the models, the numbers of monocytes available after magnetic purification were too low and hydrogels were sparsely populated with cells. Using currently available methods of monocyte isolation and purification, it was not possible to seed the required number of PBM into the hydrogel in order for sufficient cells to be recovered for measurement of viability by flow cytometry.

4.7.3 **Viable 3D culture of Mono Mac 6**

To test methods of 3D monocyte culture optimized for THP-1 cells, and as a more mature monocyte alternative in the absence of success with 3D culture of PBM, the 3D culture of MM6 was assessed. MM6 cells are also an alternative to primary monocytes, but as shown previously in Chapter 3, display many differences to PBM. H&E stained sections of 3D cultured THP-1 monocytes showed large clusters of cells, indicative of cell proliferation, that were absent in the 3D cultures of MM6. Instead, cells were found sparsely populating the hydrogel, with low percentages of viability measured using flow cytometry. As previous work had identified that MM6 may not be representative of PBM in size, granularity, and protein expression profile, and with the additional challenges in their culture compared to THP-1 monocytes, they were discarded.

4.7.4 **3D culture of THP-1 PMA**

As insufficient numbers of PBM could be isolated to prepare 3D cultures at physiologically relevant concentrations of cells, the use of macrophages in 3D cultures was explored. Again, due to the challenges accompanying the isolation and purification of primary tissue-resident macrophages, this work sought to use 2D *in vitro* generated MDM. However, there are also challenges posed during the isolation and culture of MDM, which during method development were overcome by using PMA-treated THP-1 to represent macrophages. PMA-treated THP-1 have previously been shown to be representative of MDM in

characteristics such as resistance to apoptosis, phagocytosis and increased cytoplasmic-to-nuclear ratio (Daigneault *et al.,* 2010). However, data presented in Chapter 3, showed that the expression of key markers was markedly different between THP-1 and primary macrophages. Crucially, for method development in this work, THP-1 PMA are adherent and similar methods for cell detachment and subsequent incorporation into the collagen hydrogel are required as for MDM.

The protocol selected for the generation of macrophage-like cells from THP-1 using PMA resulted in low yields of differentiated cells compared to the high numbers of cells seeded at the beginning of the 8-day differentiation protocol. In addition, even fewer cells were recovered using collagenase after 14 days of culture within a hydrogel. As a result, too few cells could be detected using flow cytometry to accurately determine viability. However, the cells could be visualised, sparsely populating a 3D hydrogel. Interestingly, single cells were visualised within the gel, compared to the clusters of cells visualised in models containing un-stimulated THP-1 cells. This could indicate terminal differentiation of THP-1 following treatment with PMA, or that cells are non-viable. TUNEL or immunohistochemistry to detect caspase expression could be used to determine cell viability or cells undergoing apoptosis. No other examples of THP-1 PMA cultured within a collagen hydrogel could be found.

4.7.5 **Viable 3D culture of functional monocyte-derived macrophages**

Compared to 3D culture of THP-1 PMA, MDM responded very positively to culture within a collagen hydrogel. Not only was there a high percentage of viable cells measured after 14 days, but MDM could be found evenly dispersed throughout the gel. The 3D culture of THP-1 monocytes showed evenly dispersed clusters of cells indicating proliferation. However, these were not observed in the 3D cultures of MDM. In large amounts of the literature, MDM are considered to be terminally differentiated, and therefore do not proliferate, although this is still a subject for debate (Jenkins *et al.,* 2011; Klappacher *et al.,* 2002). Of those models which had previously incorporated MDM, authors either did not measure viability directly (Leonard *et al.,* 2010; Linde *et al.,* 2012) or cells were largely non-viable (Liu

et al., 2016). The only study that detected viable MDM in 3D culture used calcein AM, analysed using immunofluorescence (Bechetoille *et al.,* 2011). By using flow cytometry to measure cell viability however, it is possible to quantify precisely the viable cells and exclude non-viable cells from further analysis.

Macrophages are integral to the innate immune response to invading pathogens and thus play a key role in the initiation and maintenance of inflammation. In response to PAMPs binding PRRs, macrophages release pro-inflammatory cytokines such as IL-6, IL-8 and TNF (Rosso *et al.,* 2011). In order to assess the functionality of MDM in 3D culture, *E.coli* LPS was applied to cell culture media for 24 hours, following 14 days of culture. LPS is often used to activate macrophages and the release of IL-6, among other pro-inflammatory cytokines, can be measured using ELISA.

Previous literature has shown that in response to 100 ng/mL LPS, in comparison to lower concentrations of LPS, macrophages secreted significantly increased amounts of TNF which further stimulated release of IL-6 (Thorley *et al.,* 2007). In addition, incubation of macrophages with LPS released more pro-inflammatory cytokines after 24 hours than time points at 6, 12 and 18 hours. Data presented here shows a similar pattern, with a significantly increased amount of IL-6 released by macrophages cultured in 2D and 3D following stimulation with LPS compared to those which were un-stimulated. Interestingly, higher amounts of IL-6 were measured in cell culture media from 2D cultures compared to 3D cultures. Due to the differences in culture techniques between 2D and 3D culture, macrophages were cultured at a higher concentration in 3D cultures. Therefore, the lower amounts of measured IL-6 in cell culture media may be due to capture of the cytokine within the collagen scaffold. Previously published literature has found that cytokines diffuse through the ECM faster than through cell culture media unless they bind to the ECM (Mittal, 2012). It has previously been observed that IL-6 does not bind to ECM proteins, but TNF can bind tightly to ECM proteins such as laminin and fibronectin, and to a lesser amount to collagen (Alon *et al.,* 1994). The use of a collagen hydrogel to measure cytokine diffusion rates is generally popular as it accurately models those rates found *in vivo* (Ramanujan *et*

al., 2002). Therefore, in future experiments the collagen hydrogel was degraded using collagenase and the solution stored for future analysis.

4.8 Conclusion

The 3D culture of THP-1, THP-1 PMA, MM6, PBM and MDM was explored in this chapter. Ultimately, MDM were selected for addition into ensuing 3D cultures as they demonstrated superior viability compared to the other cell types, as well as increased physiological relevance. Following 14 days of culture in 3D, not only did flow cytometry detect that these macrophages were viable, but ELISA also demonstrated a significant release of IL-6 in response to LPS challenge suggesting that MDM are functional within the hydrogel. Following the successful mono-culture of MDM within a collagen hydrogel, the incorporation of MDM into a tissue-engineered model of the oral mucosa can now be attempted.

5 Chapter 5: Development of a 3D *In Vitro* Oral Mucosa Model Containing Macrophages

5.1 Introduction

The 3D culture of cells is becoming increasingly popular due to the limitations of 2D cell culture and *in vivo* models. 3D *in vitro* models provide a more physiologically relevant culture environment compared to 2D culture which enable cells cultured in 3D to more accurately represent cells *in vivo* (Abbott, 2003; Kimlin *et al.,* 2013; Lee *et al.,* 2008; Li *et al.,* 2013; Mazzoleni *et al.,* 2009). In addition, European legislation has identified a need for more and improved *in vitro* models to produce more clinically relevant data and reduce the numbers of animals used in research (Lilienblum *et al.,* 2008). An increasing number of culture systems modelling the oral mucosa have become available, however, very few of these contain an immune component and none contain primary human immune cells cultured for more than 24 hours (Bao *et al.,* 2015b; Kosten *et al.,* 2015; Pirila *et al.,* 2015; Tschachojan *et al.,* 2014). In addition, the analyses possible on the individual cells within these models is often limited to IHC or IF microscopy.

Chapter 4 described methods for the 3D culture of monocytes and macrophages. However, in order to determine the role that TAM play in oral cancer progression, the next aim of the project was to further develop this mono-culture collagen hydrogel culture system into a co-culture model of oral cancer which contains immune cells. In addition, methods for detailed analyses of the individual cells, and their interactions with other cells of the tumour microenvironment, and engineered tissue as a whole would need to be optimised.

The following data will present the development of tissue-engineered oral mucosa models using an oral keratinocyte cell line established from a malignant biopsy (H357) and an immortalised 'normal' oral keratinocyte cell line (FNB6).

5.2 Incorporation of THP-1 cells into an oral mucosa model containing H357 oral squamous cell carcinoma cell line

Initially, an oral mucosa model containing H357 oral squamous cell carcinoma cell line and THP-1 monocyte cell line was used for method development; the H357 cell line was established from the tongue of a patient suffering from oral squamous cell carcinoma, and

the THP-1 monocyte cell line was established from a patient with acute myeloid leukaemia. Based on previously published literature, $0.2x10^6$ NOF were incorporated into a collagen hydrogel in the absence or presence of $0.2x10^6$ THP-1 cells (Dongari-Bagtzoglou and Kashleva, 2006; Linde *et al.,* 2012). Five hundred thousand H357 cells were seeded on top, and the model system was cultured for 14 days at an air-to-liquid interface. After 14 days, models were fixed in formalin, processed, paraffin-embedded, sectioned and stained either with haematoxylin and eosin (H&E), or immunohistochemically stained using anti-CD68, anti-Ki67 and pan-cytokeratin (AE1/3) antibodies and counter-stained with haematoxylin. These were compared to isotype-matched controls. Mounted and stained sections 40 µm apart were analysed using light microscopy and staining assessed visually under the supervision of an oral pathologist (**Figure 5.1**).

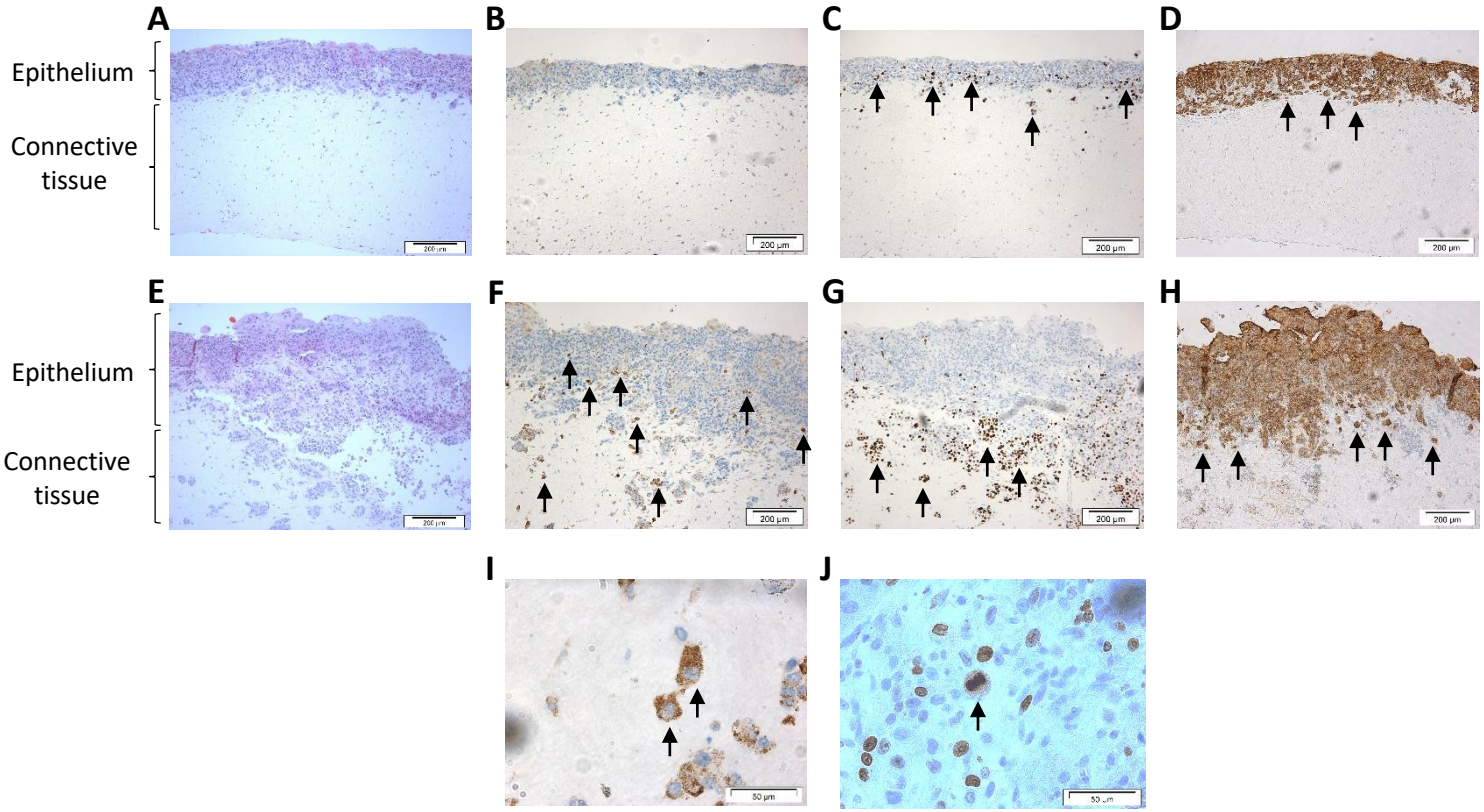

Figure 5.1. Addition of THP-1 monocytes to oral mucosa models containing OSCC cell line, H357, appeared to increase epithelial invasion. Tissue-engineered oral mucosa models containing oral squamous cell carcinoma cell line, H357, and normal oral fibroblasts (NOF) were cultured at air-liquid interface in the absence (**A-D**) or presence (**E-H**) of THP-1 monocytes. Following 14 days of culture, models were fixed and sections were stained with H&E (**A** and **E**), and immunohistochemically stained to show the expression of CD68 (**B**, **F** and **I**), Ki67 (**C**, **G** and **J**) and AE1/3 (**D** and **H**), and counter-stained with haematoxylin. Images I and J show examples of CD68+ and Ki67+ cells in high resolution, with the latter demonstrating a mitotically dividing cell. Arrows indicate areas positive for protein expression. Data are shown for a single experiment (n=1) and scale bars indicate 200 µm (**A-H**) and 50 µm (**I** and **J**).

H&E staining showed an even distribution of NOF within the hydrogel, with many cells visible in each section. H357 cell line formed a thick, multi-layered epithelium in both the presence and absence of THP-1 cells, however this did not appear as a stratified epithelium; cells were not organised into rows, nuclei were present throughout the epithelium and proliferating cells, indicated by staining with antibodies targeting Ki67, could be found throughout the epithelium. In particular, models containing THP-1 monocytes showed an even more disorganised epithelium and in addition displayed an increase in the invasion of the epithelium into the connective tissue component of the model where cells expressing proliferation and cytokeratin markers (Ki67 and AE1/3) could be found penetrating much deeper within the connective tissue. Arrows in figure indicate tumour invasion visualised as tumour islands (**Figure 5.1, D** and **H**). Models devoid of THP-1 monocytes did not stain positively for CD68.

Epithelial invasion in the presence of THP-1 monocytes did not appear to be a result of the high numbers of cells present as even the inclusion of only $7.5x10^4$ THP-1 monocytes, resulted in the invasion of both H357 and FNB6 cell lines (**Figure 5.2**).

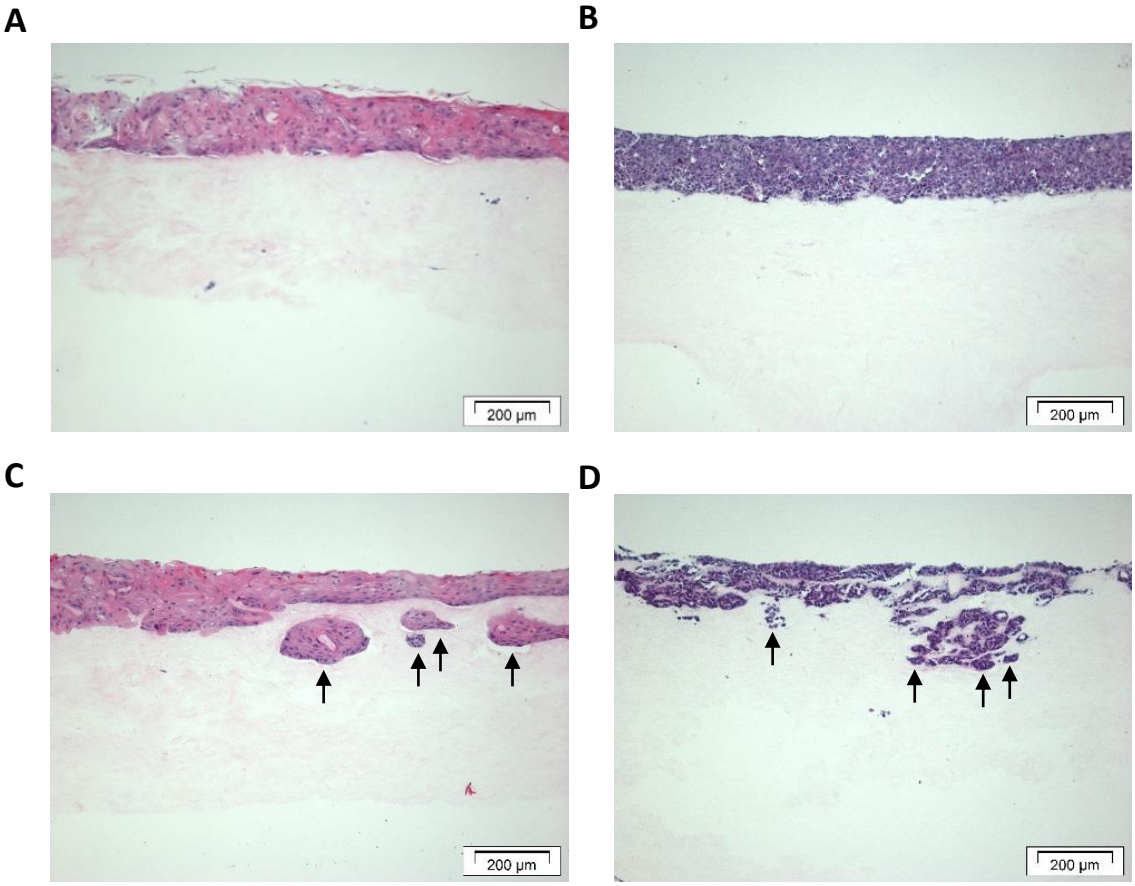

Figure 5.2. Addition of THP-1 monocytes to oral mucosa models containing FNB6 and H357 keratinocytes, even in reduced numbers, appeared to increase epithelial invasion. Tissue-engineered oral mucosa models containing immortalised FNB6 keratinocyte cell line (**A** and **C**) or oral squamous cell carcinoma cell line, H357, (**B** and **D**) were cultured in the absence (**A**-**B**) or presence (**C**-**D**) of THP-1 monocytes. Following 14 days of culture at air-liquid interface, models were fixed and stained with H&E. Data are shown for a single experiment (n=1) and scale bars indicate 200 µm. Arrows indicate areas of epithelial invasion visualised as tumour islands.

H&E staining showed a sparsely populated hydrogel, with stromal cells rarely visualised in sections. Both FNB6 and H357 cell lines formed a thick, multi-layered epithelium in both the presence and absence of THP-1 monocytes, however this did not appear as a stratified epithelium. As seen previously in **Figure 5.1**, the addition of THP-1 monocyte, albeit in reduced numbers, resulted in an increase in epithelial invasion into the collagen hydrogel which could be visualised as tumour islands in the connective tissue component of the

model. In addition, preliminary experiments used the culture media from THP-1 cells alone, or after simple 2D co-culture of THP-1 and NOF, on oral mucosa models containing keratinocytes and NOF alone. In these, no epithelial invasion was visualised in the absence of intact cells (data not shown). Further repeats of this work were performed using THP-1 cells cultured at low passage and results could not be confirmed.

5.3 Incorporation of monocyte-derived macrophages into an oral mucosa model containing FNB6 cell line

H357 keratinocytes originate from an oral cancer biopsy, and THP-1 monocytes originate from a leukaemia patient. Therefore, as these cell lines are derived from malignancies, the use of FBN6 cell line (an immortalised 'normal' keratinocyte cell line) and MDM was explored in order to produce an oral mucosa model which more closely represents malignancy-free oral mucosa. Monocytes were differentiated to MDM *in vitro* using plastic adherence over 7 days and recovered into supplemented cell culture medium using cell scraping. A collagen hydrogel mixture containing NOF was prepared and models were prepared either additionally containing or devoid of MDM. Once set, FNB6 cells were seeded upon the hydrogels and cultured at ALI for 14 days. Models were fixed, processed and stained using H&E or analysed using immunohistochemistry and counter-stained with haematoxylin to measure the expression of CD68 and E-cadherin (**Figure 5.3**); pan-cytokeratins (AE1/3), vimentin and Ki67 (**Figure 5.4**); or collagen IV and compared to isotype-matched controls (**Figure 5.5**). Mounted sections were analysed using light microscopy.

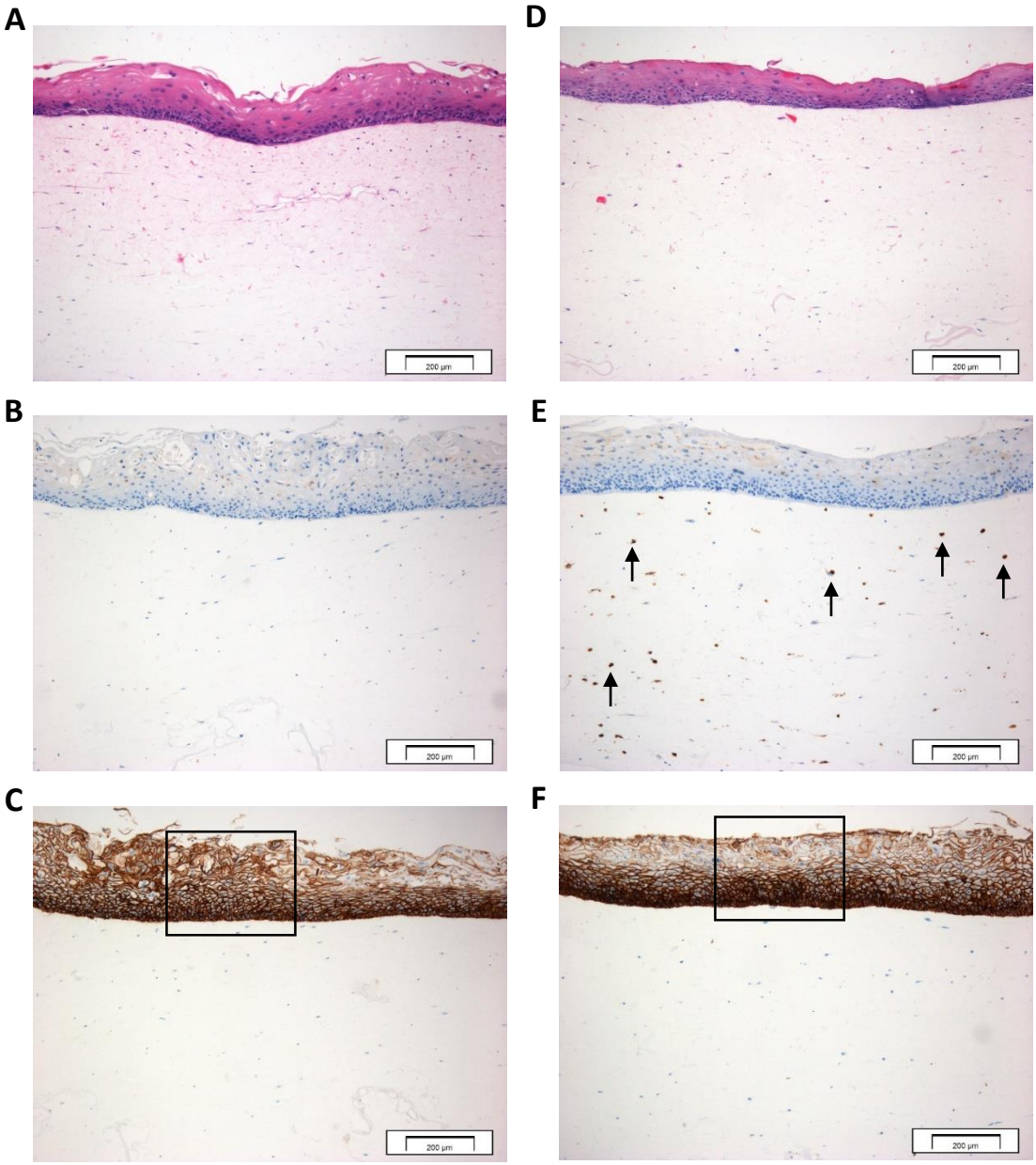

Figure 5.3. H&E, CD68 and E-cadherin expression of tissue-engineered oral mucosa models containing immortalised keratinocyte cell line, FNB6, normal oral fibroblasts and monocyte-derived macrophages. Tissue-engineered oral mucosa models containing immortalised keratinocyte cell line, FNB6, and normal oral fibroblasts (NOF), were cultured at air-liquid interface in the absence (**A**-**C**) or presence (**D**-**F**) of monocyte-derived macrophages (MDM). Following 14 days of culture, models were fixed and sections were stained with H&E (**A** and **I**) or immunohistochemically stained to show the expression of CD68 (**B** and **E**) and E-cadherin (**C** and **F**) and counter-stained with haematoxylin. Images are representative of three independent experiments (n=3) and scale bars indicate 200 µm. Arrows indicate CD68+ staining and boxes highlight areas of E-cadherin expression.

H&E staining showed an even distribution of NOF in the connective tissue component of the model and a stratified epithelium resembling that of normal tissue; cells were organised into layers, with cuboidal cells forming a stratum basale and cells devoid of nuclei forming a stratum corneum. The extracellular matrix was stained pink, suggesting ECM deposition has occurred. Stratification is a good maker of epithelial maturation (Schroeder, 1981).

CD68 is a classical macrophage marker. Models containing MDM stain positively for CD68, however those devoid of MDM are absent of CD68 staining. CD68+ cells can be observed throughout the connective tissue component, but not within the epithelial compartment of the model, and can be viewed abundantly in every section.

E-cadherin, as a marker of cell adhesion, can be viewed in the epithelium, but not in the connective tissue of the model. Expression of E-cadherin is highest in the basal cells of the epithelium and it is present at the periphery of individual cells, where these form adherent junctions with other keratinocytes in the epithelium. There does not appear to be a difference in staining for E-cadherin in models containing or devoid of MDM.

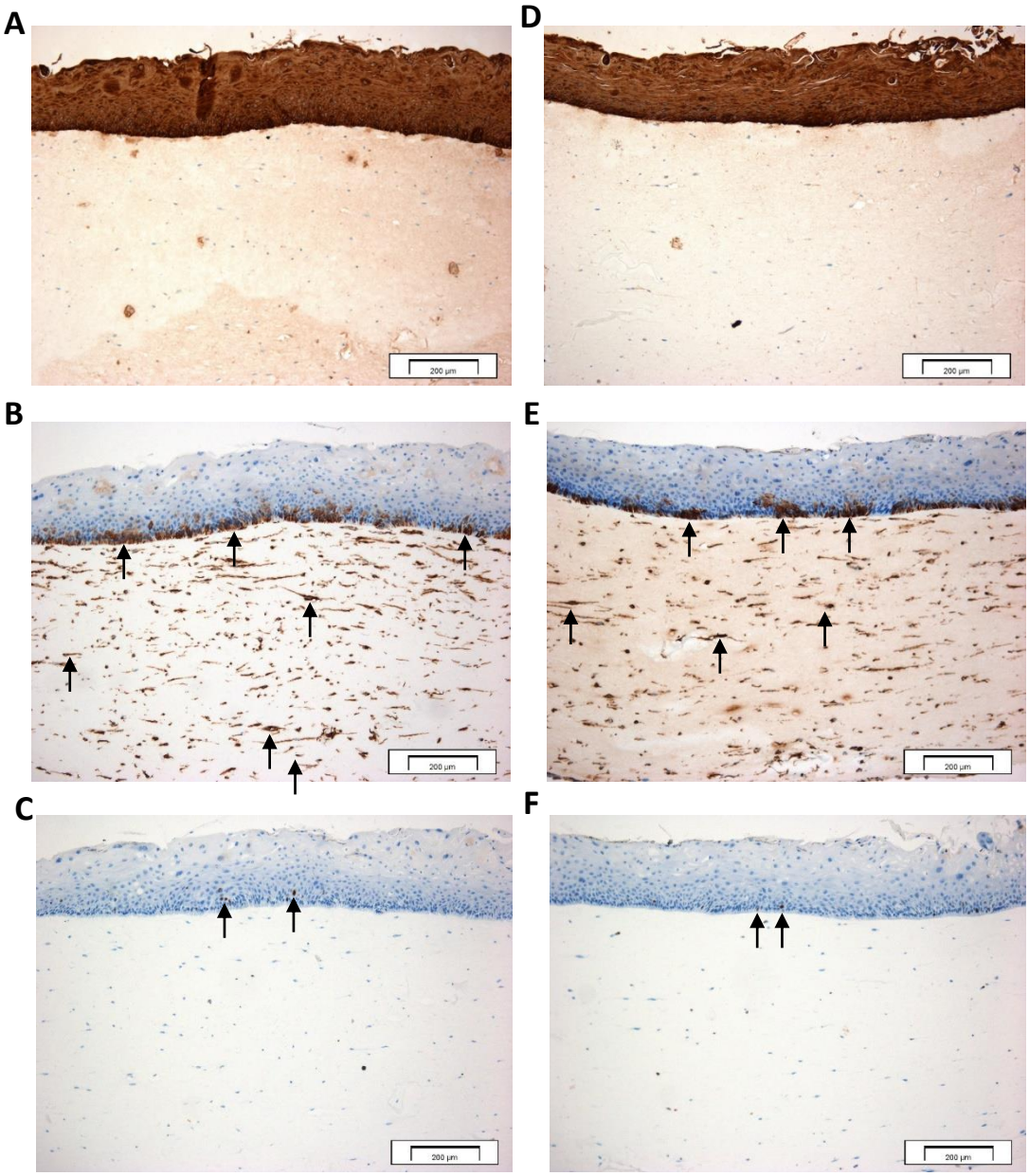

Figure 5.4. Cytokeratin, vimentin and Ki67 expression of tissue-engineered oral mucosa models containing immortalised keratinocyte cell line, FNB6, normal oral fibroblasts and monocyte-derived macrophages. Tissue-engineered oral mucosa models containing immortalised keratinocyte cell line, FNB6, and normal oral fibroblasts (NOF), were cultured at air-liquid interface in the absence (**A**-**C**) or presence (**D**-**F**) of monocyte-derived macrophages (MDM). Following 14 days of culture, models were fixed and sections were immunohistochemically stained to show the expression of cytokeratins (AE1/3, **A** and **D**), vimentin (**B** and **E**) and Ki67 (**C** and **F**) and counter-stained with haematoxylin. Images are representative of three independent experiments (n=3) and scale bars indicate 200 µm. Arrows indicate areas of positive staining.

Pan-cytokeratin staining using AE1/3 shows that the epithelium is entirely composed of cells expressing cytokeratins. No specific staining of AE1/3 can be seen in the connective tissue of the model indicating that there is no invasion of keratinocytes into the connective tissue in either the absence or presence of MDM.

Vimentin is an intermediate filament typically expressed by mesenchymal cells, of which only fibroblasts are present in this model. Both models containing and devoid of MDM show abundant expression of vimentin in the connective tissue, but additionally it is expressed in the stratum basale of the epithelium.

Ki67 is used to specifically distinguish cells in the active phases of the cell cycle from those in resting phase (G_0). Its presence therefore indicates cells which are actively proliferating. Few cells positive for Ki67 can be observed in the epithelium of both models containing and devoid of MDM. These are primarily in the bottom-most layers of the epithelium.

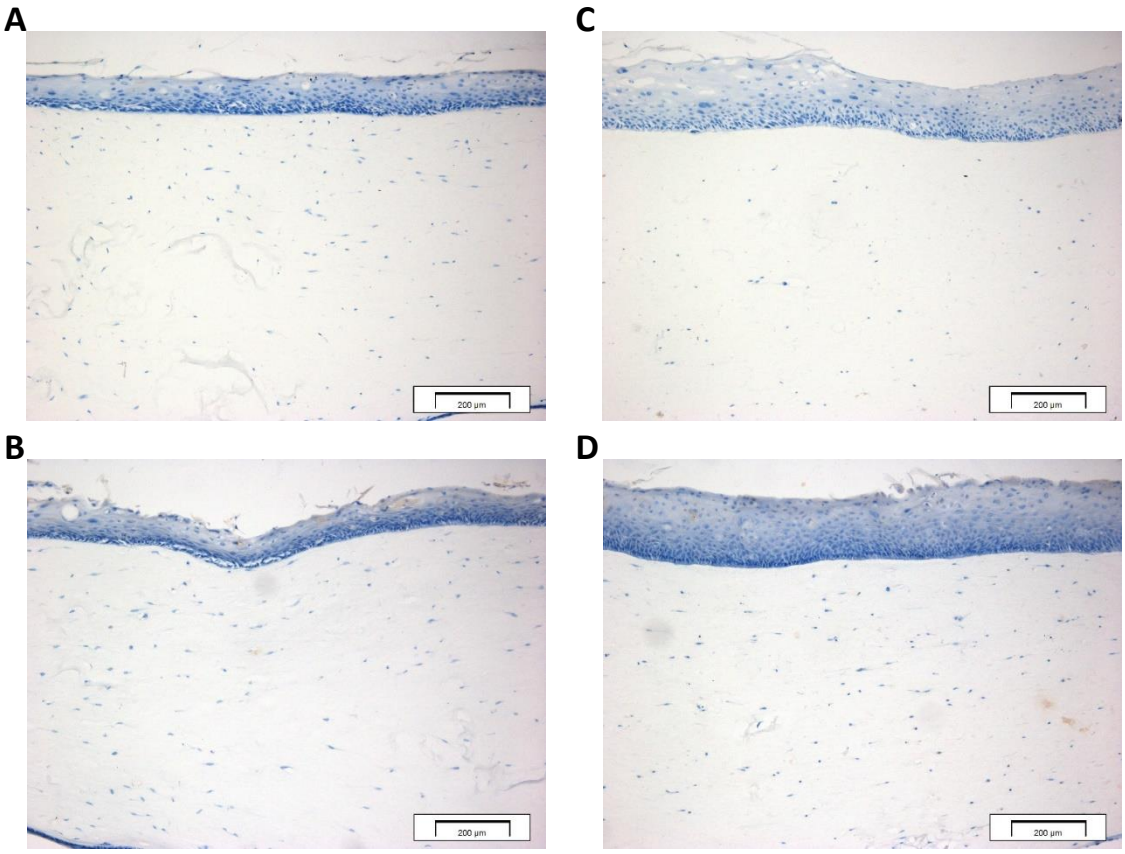

Figure 5.5. Collagen IV expression of tissue-engineered oral mucosa models containing immortalised keratinocyte cell line, FNB6, normal oral fibroblasts and monocyte-derived macrophages compared to an isotype-matched control. Tissue-engineered oral mucosa models containing immortalised keratinocyte cell line, FNB6, and normal oral fibroblasts (NOF), were cultured at air-liquid interface in the absence (**A**-**B**) or presence (**C**-**D**) of monocyte-derived macrophages (MDM). Following 14 days of culture, models were fixed and sections were immunohistochemically stained to show the expression of collagen IV (**A** and **C**) compared to isotype-matched controls (**B** and **D**) and counter-stained with haematoxylin. Images are representative of three independent experiments (n=3) and scale bars indicate 200 µm.

Type IV collagen is a major constituent of the basement membrane, however no positive staining for collagen IV can be observed in models either in the absence or presence of MDM.

5.3.1 Monocyte-derived macrophages cultured within a tissue-engineered oral mucosa model release inflammatory cytokine, IL-6, in response to lipopolysaccharide

Macrophages rapidly respond to the binding of PAMPs, such as LPS present on the membrane of gram-negative bacteria, to their PRRs by releasing pro-inflammatory cytokines. To determine whether MDM cultured within an oral mucosa model retained the ability to respond to pathogen challenge, LPS was added to the cell culture media of models containing an FNB6 epithelium for an additional 24 hours following 14 days of culture at ALI. Response was determined by measuring the release of pro-inflammatory cytokine IL-6 using ELISA and compared to models devoid of MDM. Additionally, models were fixed, processed and stained with H&E, and the cytotoxic effect of LPS on models was analysed using an LDH assay.

Lipopolysaccharide does not have a significant cytotoxic effect on oral mucosa models containing monocyte-derived macrophages

After treatment of models with LPS for 24 hours, cell culture media was aspirated and analysed using an LDH assay (**Figure 5.6**).

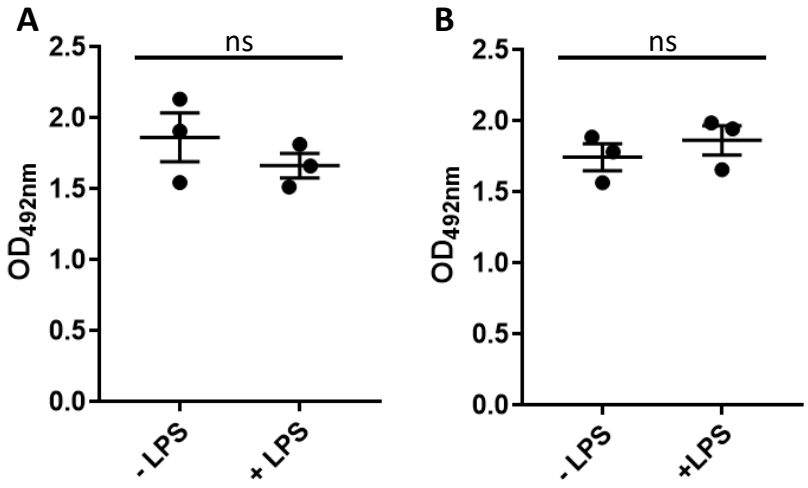

Figure 5.6. Lactate dehydrogenase release by tissue-engineered oral mucosa models containing FNB6 cells, normal oral fibroblasts and monocyte-derived macrophages stimulated with lipopolysaccharide. Tissue-engineered models of the oral mucosa containing immortalised keratinocyte cell line, FNB6, and normal oral fibroblasts (NOF) in the absence or presence of monocyte-derived macrophages (MDM) were cultured at air-liquid interface. Following 14 days of culture, cell culture medium was sampled and lactate dehydrogenase release in response to lipopolysaccharide (LPS) measured in the absence (**A**) or presence (**B**) of MDM. Data are representative of three independent experiments measured in triplicate (n=3) error bars show standard error mean and statistical significance was determined using an unpaired T-test.

There was no significant difference in the amounts of LDH released in the presence or absence of LPS treatment in both models devoid of or containing MDM (p=0.3755 and p=0.4464, respectively).

Models containing monocyte-derived macrophages release interleukin-6

After treatment of models with LPS for 24 hours, cell culture media was aspirated and analysed using ELISA to detect release of IL-6 (**Figure 5.7**).

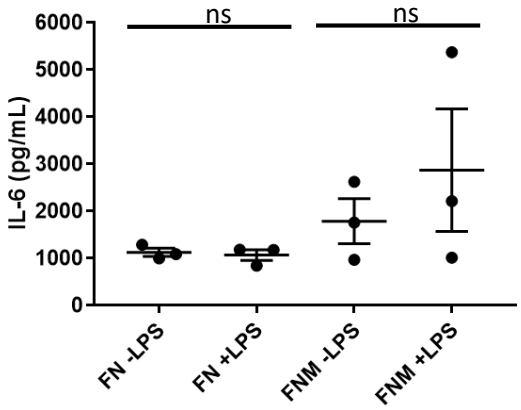

Figure 5.7. Tissue-engineered oral mucosa models containing immortalised keratinocyte cell line, FNB6, in the absence or presence of monocyte-derived macrophages release IL-6 in response to lipopolysaccharide. Tissue-engineered oral mucosa models containing immortalised keratinocyte cell line, FNB6, and normal oral fibroblasts (NOF), in the absence (FN) or presence (FNM) of monocyte-derived macrophages (MDM) were cultured at air-liquid interface. Following 14 days of culture, models were stimulated with lipopolysaccharide for 24 hours, after which cell culture media was collected and IL-6 release was measured by ELISA. Data are representative of three independent experiments measured in triplicate (n=3), error bars show standard error mean and statistical significance was determined using an unpaired T-test.

Models devoid of MDM released low levels of IL-6, which was unaltered in the presence of LPS stimulation. However, in the presence of MDM, IL-6 release increased even in un-stimulated models. The addition of both MDM and LPS to oral mucosa models resulted in the release of the highest concentration of IL-6. However, an unpaired two-tailed T-test did not identify a significant difference in the levels of IL-6 released in response to LPS in models devoid of MDM (p=0.7056) or containing MDM (p=0.4783). Interestingly, models containing MDM, but in the absence of LPS stimulation also released an increased amount of IL-6 compared to compared to models devoid of MDM.

5.4 Optimising cell numbers within oral mucosa model

In order to develop an oral mucosa model truly representative of *in vivo* oral mucosa, the numbers of cells used required optimisation.

5.4.1 **Optimising the number of normal oral fibroblasts**

Within the connective tissue, NOF are responsible for matrix deposition. Whilst collagen type I is the main constituent of the extracellular matrix, and thus the source of the hydrogel used in this culture system, the ECM *in vivo* contains many other proteins, including elastin, fibronectin and laminin. Within the collagen hydrogel in 3D, fibroblasts release many of these proteins, thus improving the physiological relevance of the ECM compared to the use of a collagen hydrogel devoid of fibroblasts (Costea *et al.,* 2003; Latkowski *et al.,* 1995). In addition, biological tissues are well populated with cells, so the optimisation of NOF number was explored.

A collagen hydrogel was prepared with either $0.05x10^6$, $0.1x10^6$ or $0.2x10^6$ NOF and seeded with $0.5x10^6$ FNB6. Models were cultured for 14 days at ALI and subsequently formalin-fixed, paraffin-embedded, sectioned, H&E stained and analysed using light microscopy (**Figure 5.8**).

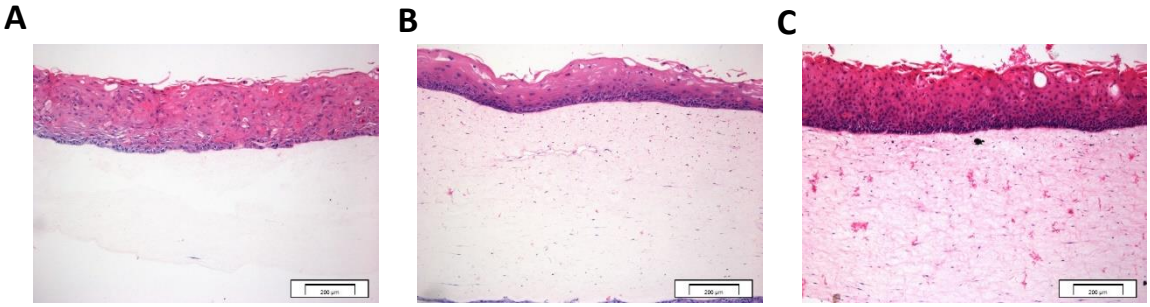

Figure 5.8. Optimisation of normal oral fibroblast number in oral mucosa models. Normal oral fibroblasts (NOF) were cultured in 3D with $0.05x10^6$ (**A**), $0.1x10^6$ (**B**) or $0.2x10^6$ (**C**) cells per model with an FNB6 epithelium. H&E stained sections are representative of three independent experiments (n=3) and scale bars indicate 200 µm.

Models containing $0.05x10^6$ NOF were visibly acellular and NOF were identified in very few sections and fields of view. In contrast, NOF could be found more frequently and evenly distributed in models containing $0.1x10^6$ NOF. The highest frequency of NOF could be visualised in sections of models containing $0.2x10^6$ NOF. Additionally, the ECM of these

models was stained the darkest pink compared to models containing $0.1x10^6$ and $0.05x10^6$ NOF.

5.4.2 Optimising the number of monocyte-derived macrophages

The number of macrophages present in a biological sample varies greatly depending on the tissue, and state of health or disease. Therefore, it was not possible to determine an absolute number of MDM to represent primary tissue. Due to limitations of cell culture, it was not possible to include more than $4x10^6$ MDM per model, however in stained sections of these models, many MDM could be visualised per field of view, and from these it was possible to isolate sufficient numbers of cells for gene and protein analyses.

5.5 Measuring the stiffness of tissue-engineered oral mucosa

Tissue stiffness can vary greatly in health and disease, between different sites of the oral cavity and between patients (Chen *et al.,* 2015; Handorf *et al.,* 2015; Paszek *et al.,* 2005). In particular, changes in the microenvironment during tumour development alter the stiffness of a tissue, largely due to changes in matrix deposition and activation of myofibroblasts (Bagul *et al.,* 2015; Mason *et al.,* 2011). To measure stiffness, the use of a rheometer was explored to perform a frequency sweep.

To determine the sensitivity of the rheometer for measuring the stiffness of tissue-engineered oral mucosa, collagen was prepared at a range of concentrations (2.5-15.0 mg/mL) and the elastic modulus was measured in order to draw a standard curve (**Figure 5.9**).

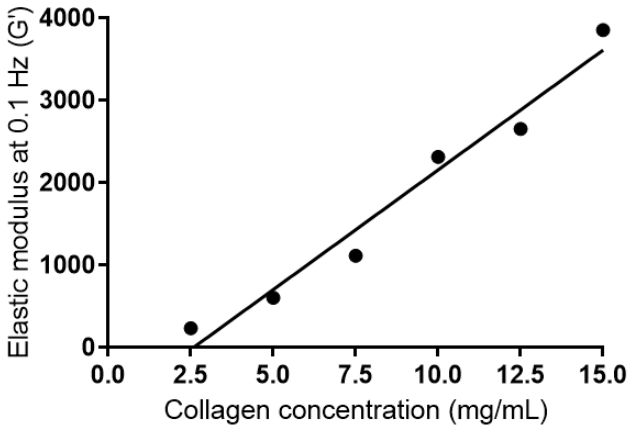

Figure 5.9. Rheometry was used to measure the stiffness of collagen hydrogels composed of collagen at varying concentrations. Collagen hydrogels composed of collagen ranging from 2.5-15.0 mg/mL were prepared and stiffness measured as elastic modulus at 0.1 Hz (G') using rheometry.

As the concentration of collagen increases, so does the value of the elastic modulus measured at 0.1 Hz (R^2 = 0.9675, p=0.0004). Tissue-engineered models of the oral mucosa containing NOF and FNB6 were prepared and analysed individually. The elastic modulus was measured at 716 ± 59.67 and gap size measured at 1.14 ± 0.07. A one-sample T-test showed no significant variance in stiffness or gap size (p=0.25 and p=0.5, respectively) between different biological samples prepared under the same conditions. Therefore, no technical repeats, only biological repeats, were performed on proceeding samples.

To determine if oscillation of the tool on the rheometer may cause damage to the epithelium of the tissue-engineered mucosa, post-rheometry samples of tissue-engineered oral mucosa models containing NOF and FNB6 cells were formalin-fixed, processed, sectioned and stained with H&E. These were compared to samples prepared under the same conditions that had not been subjected to oscillatory tests (**Figure 5.10**).

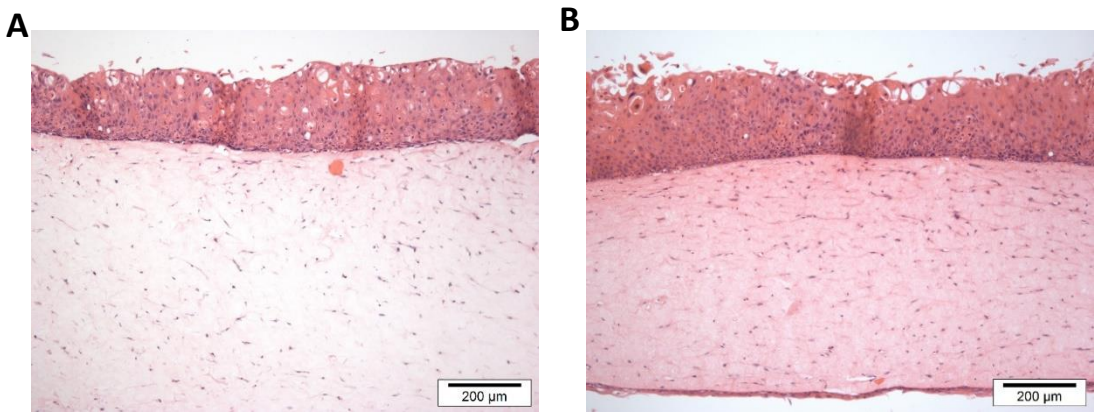

Figure 5.10. Rheometry does not cause visible damage to the epithelium of tissue-engineered oral mucosa. Tissue-engineered oral mucosa models containing FNB6 immortalised keratinocytes and normal oral fibroblasts (NOF) were compared without (**A**) and after analysis by rheometry (**B**). H&E stained sections are representative of three independent experiments (n=3) and scale bars indicate 200 µm.

Stained sections of tissue-engineered oral mucosa showed no visible differences in epithelial integrity or signs of shearing of the stratum granulosum in samples analysed using rheometry, compared to those which had not. Following the optimisation of methods presented here, comparisons between models containing or devoid of MDM and those containing NOK, FNB6 or H357 epithelia are discussed in Chapter 7.

5.6 Discussion

Due to the important role that macrophages play in cancer progression, they are used as diagnostic and prognostic markers in breast and colon carcinomas, for example (Hu *et al.,* 2009; Medrek *et al.,* 2012). An increasing number of studies have identified a correlation between TAM and poor patient prognosis, suggesting they may play an important role in oral cancer progression (Bagul *et al.,* 2016; Balermpas *et al.,* 2014; Boas *et al.,* 2013; Li *et al.,* 2002; Mori *et al.,* 2011). Although oral cancer research has readily adopted the use of 3D models as an improvement to 2D models, very few models have incorporated immune cells and of those, none have incorporated primary human macrophages (Bao *et al.,* 2015b; Kosten *et al.,* 2015; Pirila *et al.,* 2015; Tschachojan *et al.,* 2014). With macrophages forming more than 65 % of the tumour mass, the inclusion of macrophages in tissue-engineered

models of the oral mucosa is essential (Liu *et al.,* 2008). In addition, macrophages are a highly secretory cell, and the cytokines they release play an important role in altering the tissue environment to promote tumour progression. Therefore, new and improved tools are required to further understand the interactions that macrophages have with other cells of the tumour microenvironment. The results presented in this chapter aim to demonstrate the development of one such tool; a tissue-engineered model of the oral mucosa containing macrophages.

5.6.1 **THP-1 monocytes may promote epithelial invasion**

Previously, 2D co-cultures of THP-1 monocytes and oral cancer cell lines (YD38 and OE) has shown that co-culture with monocytes promotes cancer cell invasion and migration relative to malignancy (Lee *et al.,* 2014). In this study, THP-1 monocytes were co-cultured with NOF and the oral cancer cell line, H357, at an air-liquid interface for 14 days. Results show that incorporation of THP-1 monocytes promoted an increase in invasion of oral cancer into the connective tissue component of 3D *in vitro* oral cancer models. In addition, observations demonstrated that their inclusion promoted contraction of collagen within the extracellular matrix compared to a control excluding THP-1 monocytes. This was also observed in models containing FNB6 immortalised keratinocytes. However, when repeated with low passage THP-1 monocytes, the amount of invasion was markedly lower. It is possible that THP-1 monocytes in the initial experiment had undergone phenotypic drift through repeated passaging, promoting their pro-tumour phenotype. In addition, preliminary data incorporating THP-1 macrophages or conditioned media from THP-1 monocytes cultured in 2D alone or in combination with NOF showed no invasion of the epithelium into the connective tissue. Therefore, it is likely that epithelial invasion is a result of secreted proteins involved in the cross-talk between fibroblasts, monocytes or macrophages and keratinocytes, either all together or in various combinations (Comito *et al.,* 2014). In any case, this line of thought requires further investigation.

5.6.2 Tissue-engineered normal oral mucosa containing monocyte-derived macrophages

Previous data in chapter 3 showed that THP-1 and MM6 cell lines were not necessarily representative of primary monocytes and macrophages in morphology and the expression of key markers. Therefore, following the 3D culture of MDM, which were shown to be viable and responsive to LPS, MDM were included within an oral mucosa model containing normal immortalized keratinocytes.

Unlike models containing THP-1 monocytes, the presence of MDM did not result in invasion of the epithelium into the connective tissue. However, the use of FNB6 cells to replace H357 cells resulted in the formation of a stratified epithelium, although some nuclei could be visualized in the outermost layers of the epithelium, indicative of moderate dysplasia (Geetha *et al.,* 2015). Immunohistochemical staining of these models showed that E-cadherin, AE1/3 and Ki67 were restricted to the epithelial component of the models, and CD68 staining was restricted to the connective tissue component of models containing MDM which confirmed previously published data of normal oral mucosa (Colley *et al.,* 2011; Helal and Wahba, 2016; Sridevi *et al.,* 2015). However, Ki67 staining was not restricted to the stratum basale, indicating proliferation of cells beyond the basal cells, indicative of dysplasia (Colley *et al.,* 2011).

Vimentin, a marker of stromal cells, was expressed in the stratum basale of the epithelium and not restricted to the connective tissue component. This did not match previous data which showed no expression of vimentin in the epithelium of normal oral mucosa compared to low expression of vimentin in OSCC (Balasundaram *et al.,* 2014). Vimentin is often used as a marker of EMT and published data using a breast carcinoma cell line suggests that these intermediate filaments play a key in role in reorganization of the cytoskeleton, adhesion, stiffness and motility of epithelial cells undergoing EMT which is associated with their decreased expression of E-cadherin (Liu *et al.,* 2015; Mendez *et al.,* 2010). However, positive staining for E-cadherin was observed in the model presented here in a similar pattern to that found in normal oral mucosa, and was not found to be downregulated as in

the case of EMT (Balasundaram *et al.,* 2014). Previously published data has shown that aberrant vimentin expression correlated with histopathological grade of dysplasia (Sawant *et al.,* 2014).

Collagen IV and laminin are deposited by fibroblasts residing in the connective tissue and represent the major components of the basement membrane (Sanderson *et al.,* 1986). The basement membrane separates the epithelial and connective tissue components of the oral mucosa (Squier and Kremer, 2001). However, during cancer progression, epithelial cells breach the basement membrane, and at this point the cancer is considered invasive (Bradley *et al.,* 2010; Scully and Bagan, 2009a). Collagen IV was used to identify the basement membrane in the model, however, no positive staining was observed in these, in contrast to positively stained positive control samples. This is in contrast to previously published data that showed the deposition of laminin, integrin α6 and collagen IV in organotypic models containing macrophages, fibroblasts and dermal keratinocytes. In those models, a continuous basement membrane did not form as had been observed in murine models, particularly in the presence of MDM (Linde *et al.,* 2012). In addition, models containing many more fibroblasts resulted in the deposition of both laminin and collagen IV which formed a basement membrane, especially following further addition of KGF (Costea *et al.,* 2003). A previous model of the oral mucosa devoid of macrophages and using DED showed strong positive staining for collagen IV at the interface of the epithelium and connective tissue (Colley *et al.,* 2011). Commercially available basement membrane substitutes, such as Matrigel, as well as other materials, can be used to mimick the protein expression of the basement membrane (Bye *et al.,* 2014). The importance of the basement membrane was shown in a previous study which used a collagen type I scaffold coated with laminin and collagen IV to produce a tissue-engineered oral mucosa. These additions promoted the differentiation of keratinocytes into a stratified epithelium (Kim *et al.,* 2001).

The oral mucosa model presented in this thesis demonstrated similarities in protein expression and tissue architecture compared to previously published data analysing patient oral mucosa biopsies (Colley *et al*., 2011). In addition, the aim of this research was to

include viable and functional macrophages within this tissue-engineered oral mucosa. The primary role of macrophages is in defence against invading pathogens, providing innate immunity (Sheel and Engwerda, 2012; Shi and Pamer, 2011; Wrigley *et al.,* 2011; Yang *et al.,* 2014a). Macrophages respond to PAMPs, such as LPS on the surface of gram-negative bacteria, by releasing pro-inflammatory cytokines, such as IL-6, IL-8 and TNF (Rosso *et al.,* 2011). The release of these co-ordinates additional immune cells to respond to the pathogen challenge.

Therefore, to determine whether macrophages may retain some functionality when cultured in 3D, models were treated with LPS for 24 hours, following 14 days of culture at ALI. Following LPS stimulation, culture media was collected and an LDH assay was used to detect LDH release in response to LPS, to detect cell death. ELISA was also used to measure release of pro-inflammatory cytokine, IL-6, in response to LPS stimulation. Similarly, to Haw *et al.,* who analysed the activation of BV2 microglia in a 3D collagen hydrogel, results show that low LDH release was observed following stimulation of models with LPS (Haw *et al.,* 2014). Additionally, this published study used a cytokine bead array and qPCR to analyse the expression of IL-6 at both the gene and protein level 6 hours and 48 hours post stimulation. A significant increase in IL-6 was detected following LPS stimulation. An alternative model measured the activation of RAW 264.7 murine macrophages when co-cultured within a 3D tissue-engineered skin model. Here, LPS stimulation induced increased expression of IL-6 measured by ELISA in both the absence and presence of co-culture with engineered skin (Chung *et al.,* 2014). Whilst not statistically significant, in this work ELISA measured a marked increase in IL-6 release following LPS stimulation, confirming that macrophages are functional within this model, in line with previously published results.

5.6.3 **Collagen hydrogel contraction**

During wound healing, fibroblasts become activated and contractile. Gel contraction assays are often used to measure the activation of fibroblasts. Whilst informative, within a tissue-engineered oral mucosa model based on a collagen gel scaffold, fibroblast contraction posed challenges to tissue disaggregation. The addition of fibroblasts is key for the

proliferation and stratification of the epithelium (Latkowski *et al.,* 1995). However, observations suggested that models containing an increased number of NOF experienced increased amounts of contraction. The number of NOF added required balancing between the amount of matrix deposition (for improved physiological relevance and to prevent the connective tissue from being too acellular) and contraction. Too much contraction resulted in poor disaggregation of the models using collagenase IV and prevented analysis using flow cytometry. The amount of matrix deposition could be detected using haematoxylin staining and appeared as pink staining in the connective tissue component of the model (Fischer *et al.,* 2008). An alternative approach for reducing the amount of contraction, rather than reducing the number of fibroblasts, may be found in addition of Src kinase inhibitor PP2 (Fletcher *et al.,* 2011). Results show that the addition of $0.2x10^6$ NOF generated a well populated connective tissue. A decreased amount of contraction was found to enable disaggregation of the tissue for analysis by flow cytometry. Importantly, the inclusion of MDM, in contrast to THP-1, within the model resulted in a reduced amount of contraction.

5.6.4 **The stiffness of tissue-engineered oral mucosa**

During normal development and during disease progression, the stiffness of tissues around the body can vary enormously. In particular, malignant tissues increase in stiffness compared to normal tissue and can be used in screening for potential malignancies; for example, an increase in stiffness of mammary tissue associated with breast carcinoma can be detected as a hard lump (Boyd *et al.,* 2014; Paszek *et al.,* 2005). This increase in stiffness of malignant tissues is likely due to abnormal matrix deposition and the contraction of myofibroblasts (Bagul *et al.,* 2015). In turn, changes in tissue stiffness can alter the proliferative, migratory and invasive phenotypes of cells, resulting in a positive feedback loop (Mason *et al.,* 2011). Preliminary observations of oral cancer models containing THP-1 monocytes and H357 oral squamous cell carcinoma cells suggested that these were more contracted following 14 days of culture, compared to models devoid of THP-1 monocytes. In addition, these models appeared stiffer than those which had not contracted. Therefore, the use of rheometry and contraction assays was explored to quantitate these changes. The

stiffness of a material can be analysed using a variety of methods (Canovic *et al.,* 2016). For the analysis of biological samples however, indentation and rheometry are most commonly used. In this chapter, the suitability of rheometry to detect changes in collagen hydrogel stiffness was explored. Results showed that oscillatory tests performed by the rheometer caused minimal damage to the epithelium of models, and changes in stiffness of collagen hydrogels containing increasing concentrations of collagen could be detected. Therefore, rheometry may be useful in detecting changes in the stiffness of models containing a variety of components from the tumour microenvironment.

6 Chapter 6: Development of an 8-colour Flow Cytometry Panel for the Analysis of Macrophage Polarisation Status

6.1 Introduction

Flow cytometry uses lasers to interrogate individual cells for specific markers which can be identified by bound fluorochrome-conjugated antibodies. It can not only quantitatively identify changes in protein expression of individual cells, but also changes in expression of the entire cell population as a whole. This provides a quantitative analysis of both intracellular and extracellular proteins, and any changes in expression in response to various stimuli. Recent advances in technology have enabled researchers to analyse multiple protein markers at the same time using polychromatic flow cytometry. Whilst an increasing number of fluorochrome conjugates have become available recently, the number of antibodies targeting macrophage-specific cell surface proteins remains limited.

The development of polychromatic flow cytometry panels requires thorough optimisation of every step of the experiment; from reagent selection, to equipment configuration, to data analysis. In view of this, flow cytometry journal, Cytometry, Part A, preferentially publishes such panels under a unique category of 'Optimized Multicolor Immunofluorescence Panel'. Since the first of these was published in 2010, 34 have been published in total. These typically feature cells of the immune system, such as T cells, natural killer cells and B cells, however none to date have been directed towards macrophages.

In addition to a limited choice of reagents targeting macrophage-specific proteins, with a limited range of fluorochrome conjugates, flow cytometry analysis of macrophages is challenging due to the high levels of auto-fluorescence that they display which limits the choice of suitable fluorochromes even further. The aim of this work was to develop a novel polychromatic flow cytometry panel that could be used to quantitatively analyse the expression of key macrophage markers on macrophages cultured within a 3D model of the oral mucosa. As with previous chapters, cell lines were used for the initial optimisation of methods. These optimised methods were later applied to primary cells.

6.1.1 **Separating macrophages from fibroblasts and keratinocytes**

The model of the oral mucosa presented in this thesis contains fibroblasts and keratinocytes in addition to macrophages. Human macrophages are typically a large cell between 20-30 microns in diameter compared to fibroblasts at 10-15 microns and keratinocytes around 10 microns. The differences in size and granularity of different cell types can often be used to distinguish between the cells using flow cytometry. For example, monocytes can easily be identified from lymphocytes and neutrophils in flow cytometry samples prepared from whole blood (**Figure 3.1**). However, as the example shows (**Figure 6.1**), THP-1 monocytes overlap in size and granularity with keratinocytes and fibroblasts.

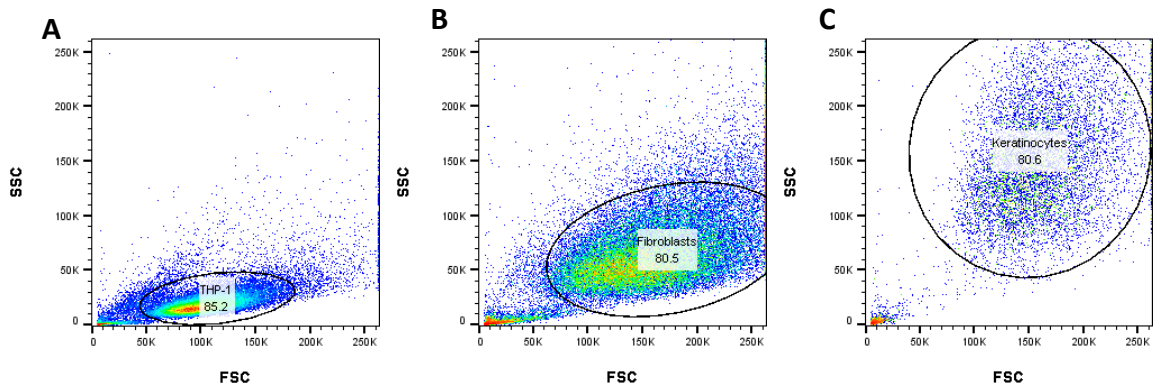

Figure 6.1. Separation of THP-1 monocytes from normal oral fibroblasts and H357 keratinocytes using size and granularity. THP-1 monocytes cultured in suspension, or normal oral fibroblasts (NOF) and oral squamous cell carcinoma cell line, H357, cultured in adherent culture were analysed using flow cytometry. Gates were set to measure forward scatter (FSC) and side scatter (SSC), for size and granularity respectively, of THP-1 (**A**), (NOF (**B**) and H357 (**C**). Data are shown for a single experiment (n=1) following dead cell exclusion with propium iodide.

In addition, as macrophages can vary greatly in size depending on environmental cues due to their plastic nature, the separation of these immune cells from other cells within the model based on FSC and SSC is not suitable. Therefore, unique markers were required for the identification and separation of macrophages from fibroblasts and keratinocytes.

6.2 Selection of reagents for polychromatic flow cytometry

The aim of the polychromatic flow cytometry panel was to firstly identify macrophages within a co-culture of macrophages, fibroblasts and keratinocytes, and subsequently enable characterisation of macrophage phenotype using a range of M1 and M2 markers. To select fluorochromes for serial gating, reagents were given priority ratings in order that the brightest fluorochromes could be assigned to the highest prioritised antigens for gating purposes (**Table 6.1**). Furthermore, the panel was designed so that CD antigens with the smallest selection of commercially available antibodies were assigned the most commonly available fluorochromes.

Priority Rating	Category	Rationale	Reagents
1	Identification of leukocytes and specifically, macrophages	To remove any cells not relevant to the analysis	CD45, CD14
2	Viability	To exclude dead and highly auto-fluorescing cells	Amine-reactive blue
3	Polarisation 1	Key macrophage protein involved in oral cancer	CD163
4	Polarisation 2	Further polarisation markers to characterise the macrophage population	CD36, CD80, CD86, CD206

Table 6.1. Development strategy of the multi-colour flow cytometry panel.

For the identification of macrophages from fibroblasts and keratinocytes, CD14 and pan-leukocyte marker CD45 were selected. Due to its emerging role as a marker for poor prognosis in oral cancer (Balermpas *et al.,* 2014; Fujii *et al.,* 2012; Fujita *et al.,* 2014; He *et al.,* 2014; Mori *et al.,* 2011; Weber *et al.,* 2014; Wehrhan *et al.,* 2014), CD163 was selected as the highest prioritised macrophage polarisation marker, followed by CD80 and CD86 (M1 markers), and CD36 and CD206 (M2 markers). As with previous work in this thesis, THP-1 monocytes were initially used for the optimisation of techniques that were later applied to

primary human macrophages; following **Figure 6.2** and **Figure 6.3**, all the following data in chapter 6 has been collected using primary human MDM based on optimisation of methods presented in the preceding chapters.

6.2.1 Selection of antibodies for the identification of monocytes

CD14 is a monocyte and macrophage cell surface marker that is not expressed by NOF. Therefore, fluorochrome-conjugated anti-CD14 antibodies were used to separate monocytes from fibroblasts using flow cytometry. As one of the highest prioritised markers, CD14 required conjugation to a bright fluorochrome, such as PE, to enable clear separation of CD14+ from CD14- events.

Separation of monocytes from fibroblasts using CD14 expression

To determine the efficacy of CD14 expression to separate monocytes from NOF, purified PBM from healthy volunteers and THP-1 or MM6 monocytes cultured in suspension were combined in equal number with NOF cultured in 2D stained with anti-$CD14^{PE}$ antibodies (**Figure 6.2**) and the results analysed using flow cytometry.

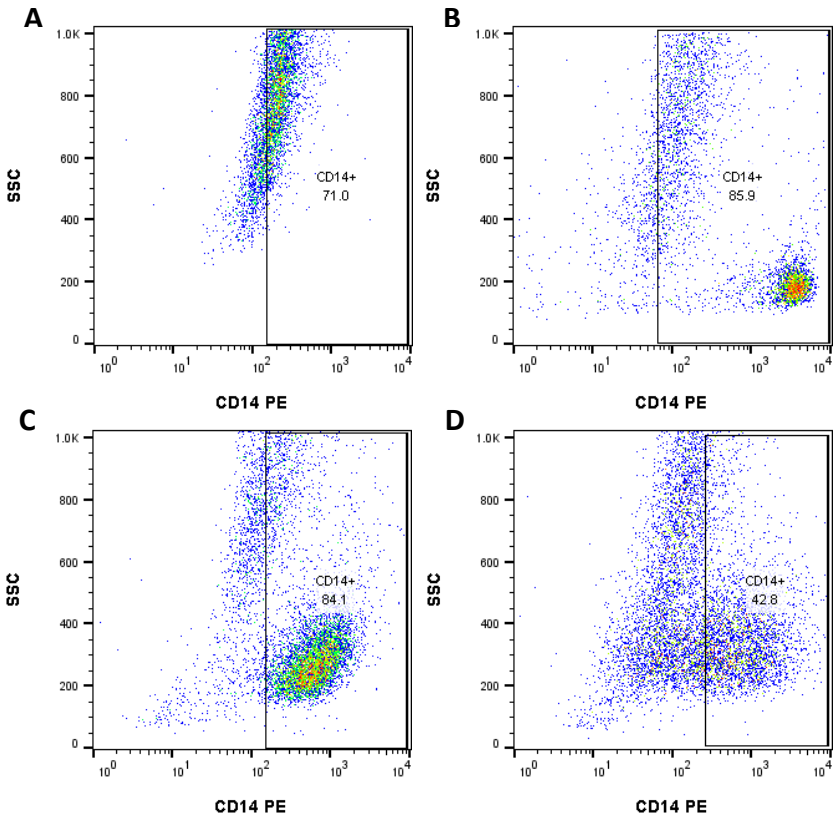

Figure 6.2. Separation of monocytes from normal oral fibroblasts using PE-conjugated anti-CD14 antibody. Peripheral blood monocytes immediately following isolation and purification; THP-1 or Mono Mac 6 (MM6) monocytes cultured in suspension; or normal oral fibroblasts (NOF) cultured in adherent culture were recovered, mixed and labelled using anti-CD14 antibodies and analysed using flow cytometry. Gates were set based on unstained samples of relevant cells to identify CD14+ events in NOF alone (**A**), and mixtures of NOF with peripheral blood monocytes (**B**), THP-1 (**C**) or MM6 (**D**) monocytes. Data are shown for a single experiment (n=1) following dead cell exclusion with propium iodide.

Dot plots show that NOF alone showed high levels of auto-fluorescence at the same wavelength as PE, resulting in a high percentage of events recovered in the CD14+ gate, in the absence of monocytes. As shown previously (**Page 87**), PBM express higher levels of CD14 than both THP-1 or MM6 monocytes, and the three cell types differ in size and granularity (**Page 85**). Dot plots here show that the high expression of CD14 on PBM and the difference in size of PBM and NOF, enabled the two cell types to be clearly separated. THP-1 monocytes, although larger than PBM and expressing lower levels of CD14, could still

be separated from NOF by size and CD14 expression. However, due their larger size and markedly lower levels of CD14 expression, MM6 and NOF could not be clearly segregated.

In parallel, it was observed that the expression of CD14 decreased during monocyte to macrophage differentiation in both primary cells and THP-1 cell line (**Page 93**). Therefore, the additional use of CD45 leukocyte marker was assessed for the separation of monocytes and macrophages from NOF by flow cytometry.

Separation of THP-1 from normal oral fibroblasts and H357 using CD45 expression

As an alternative to anti-CD14 antibodies, anti-$CD45^{FITC}$ antibodies were explored to enable the identification of the THP-1 monocytes from NOF and keratinocytes used within the tissue-engineered oral mucosa developed in parallel (**Page 137**). THP-1, NOF and H357 cells were cultured individually in 2D or in various combinations of 3D co-cultures using a collagen hydrogel. Hydrogels were cultured at an air-to-liquid interface for 14 days and models processed into single-cell suspensions using collagenase IV and a cell strainer. Viable cells were selected using Topro3, which contains a carbocyanine dye that enters dead cells through compromised cell membranes, causing them to fluoresce. The expression of $CD45^{FITC}$ was analysed using flow cytometry (**Figure 6.3**).

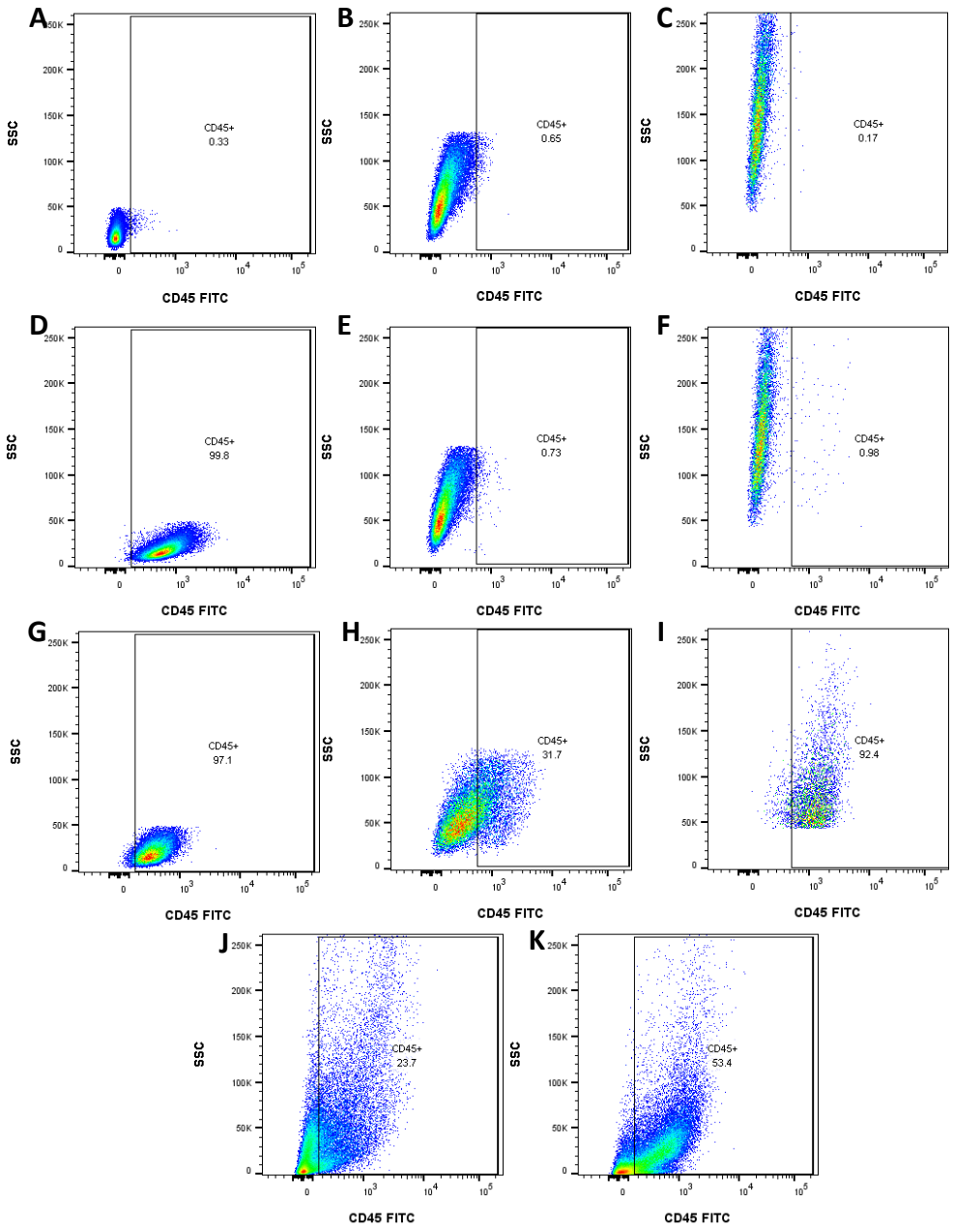

Figure 6.3. Separation of THP-1 monocytes from normal oral fibroblasts and H357 keratinocytes, in 2D and 3D using FITC-conjugated anti-CD45 antibody. THP-1 monocytes cultured in suspension, or normal oral fibroblasts (NOF) and oral squamous cell carcinoma cell line, H357, cultured in adherent culture, were retrieved and used, unstained, to set gates (**A-C**) respectively. Samples labelled with anti-CD45^{FITC} were analysed for each cell type individually (**D-F**) for THP-1, NOF and H357 respectively. Additionally, cells were cultured within a collagen hydrogel for 14 days either individually (**G-I**) for THP-1, NOF and H357 respectively, or in co-culture; THP-1 with NOF (**G**) or THP-1, NOF and H357 (**H**). Data are shown for a single experiment (n=1) following dead cell exclusion using propium iodide.

THP-1 monocytes expressed high levels of CD45, with >99 % of THP-1 cells cultured alone in 2D appearing in the CD45+ gate. In contrast, NOF and H357 keratinocytes cultured alone in 2D showed no expression of CD45 and hence <1 % of events appeared in the CD45+ gate. However, once cultured alone within a collagen hydrogel, 31.7 % NOFs and 92.4 % H357 cells appeared within the CD45+ gate. This resulted in a high percentage of CD45+ events appearing in 3D co-cultures omitting THP-1 cells and poor separation of THP-1 monocytes from H357 cells and NOFs in 3D tri-cultures.

Parallel experiments enabling the viable culture of MDM in 3D (**Page 124**) resulted in the 3D culture of THP-1 being discarded; all subsequent experiments use MDM and data from experiments using THP-1 monocytes were used to inform future experimental design.

6.2.2 Selection of viable monocyte-derived macrophages

MDM auto-fluoresce in every laser channel, and as cells die, the membrane becomes permeable allowing antibodies to penetrate the cell resulting in auto-fluorescence which may be detected as a false positive signal. In addition, MDM require processing in order to produce a single-cell suspension suitable for flow cytometry that can lead to a decrease in cell viability over time. Therefore, a suitable reagent for the gating of viable cells was required. Reagents using Lightwave Xcyte™ laser in the UV detection range were chosen, as this would not affect the selection of other fluorochrome reagents.

Amine dyes are available in a wide choice of colours, including those excited with a UV laser. These dyes bind amine groups which are only accessible once the cell membrane has become permeable. Only a few amine groups are present on the surface of viable cells with intact membranes, therefore these dyes can penetrate non-viable cells to bind the amine groups on proteins inside the cell, resulting in a brighter fluorescence of non-viable cells than those that are viable.

Treatment of viable MDM with saponin or ethanol, heat-shock or freeze-thaw cycles for cell permeabilisation were tested in order to produce a positive control for non-viable cells. Treatment with 100% ethanol for 15 minutes at room temperature enabled clear separation

of viable and non-viable MDM. Fixable Viability Dye eFluor® 455UV (eBioscience, USA) was compared to LIVE/DEAD® Fixable Blue Dead Cell Stain (Life Technologies, UK) using viable and ethanol-treated non-viable macrophages (1:1 v/v ratio) to determine dye efficacy (**Figure 6.4**).

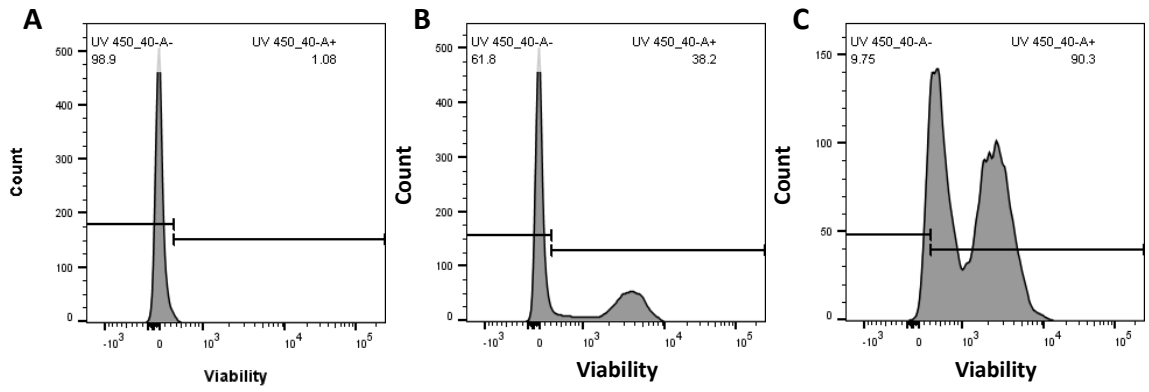

Figure 6.4. Viability stain comparison. Monocyte-derived macrophages (MDM) were adherently cultured for 7 days, retrieved using cell scraping and analysed using flow cytometry. LIVE/DEAD® Fixable Blue Dead Cell Stain (Life Technologies, **B**) and Fixable Viability Dye eFluor® 455UV (eBioscience, **C**) were used to detect viable and ethanol-treated non-viable macrophages mixed in a 1:1 (v/v) ratio to examine reagent performance. Unstained cells, treated under the same conditions as sample cells, were used to set viability gates (**A**). Data representative of three independent experiments (n=3). Gates were set using unstained cells treated with ethanol (**A**).

A gate was set based on unstained cells treated with ethanol, and used to compare the separation of viable and ethanol-treated non-viable MDM. LIVE/DEAD® Fixable Blue Dead cell stain showed a sharp peak of 61.4 ± 2.8 % of cells within the left-hand viable gate with an MFI of 95.8 ± 2.7, and a second peak of 38.33 ± 1.1 % of cells was visible distinctly separated from the first with an MFI of 3094 ± 591.2. Alternatively, Fixable Viability Dye eFluor® 455UV showed a shift in the whole population of cells beyond the left-hand viable gate, where only 9.5 ± 0.5 % of cells were found. Two peaks could be identified with this dye (the first with an MFI of 268.3 ± 49.19 and the second with an MFI of 1688 ± 195.1), however, there was overlap between the two peaks and no clear distinction could be made between the viable and non-viable cell populations. Of the two stains used, LIVE/DEAD®

Fixable Blue Dead Cell Stain showed superior separation of viable and non-viable macrophages and was consequently used in ensuing experiments.

6.2.3 Selection of antibodies for identification of monocyte-derived macrophages

A limiting feature of macrophages, in polychromatic flow cytometry panel design, is their high level of auto-fluorescence that limits the choice of fluorochromes that can be used. In particular, FITC and PE fluorochromes should be avoided for the initial separation of MDM from other cell types as MDM are highly auto-fluorescent at the same wavelength as these fluorochromes.

Selection of anti-CD14 antibodies for polychromatic analysis of monocyte-derived macrophages

To enable separation of MDM from fibroblasts and keratinocytes in co-culture, a suitable anti-CD14 antibody was required. MDM cultured in 2D were stained with anti-CD14 antibodies conjugated to PE, eFluor450 and Alexa Fluor 700 and compared to unstained samples. The normalised median fluorescence intensity (nMFI) for the three antibodies was compared (**Figure 6.5**).

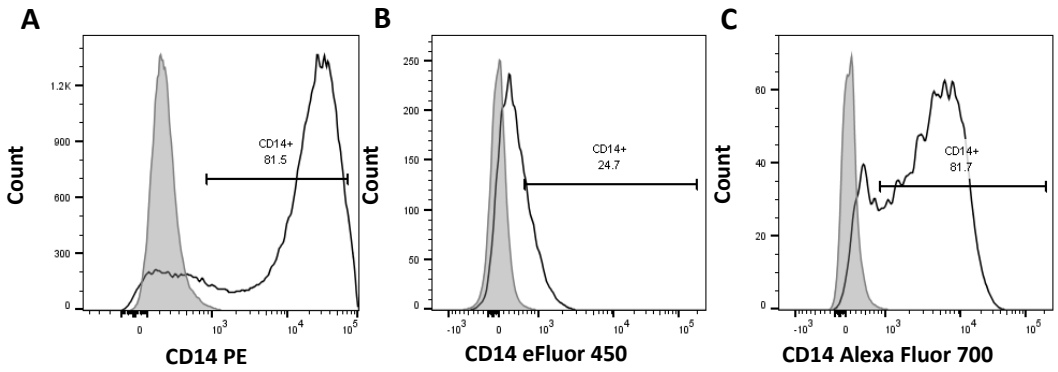

Figure 6.5. Selection of anti-CD14 antibody. Monocyte-derived macrophages (MDM) were cultured for 7 days, retrieved using cell scraping and CD14 expression analysed using flow cytometry. Anti-CD14 antibodies conjugated to PE (**A**), eFluor 450 (**B**) and Alexa Fluor 700 (**C**) were tested and compared using normalised median fluorescence. Filled (grey) histograms show unstained cells, and open histograms show single-stained cells. Data are from a single experiment (n=1) and gates were set based on unstained cells following dead cell exclusion.

Anti-CD14^{PE} displayed the highest MFI (110.14) compared to anti-CD14$^{Alexa\ Fluor®\ 700}$ (7.88) and CD14$^{eFluor®\ 450}$ (1.39). In addition, both anti-CD14^{PE} and anti-CD14$^{Alexa\ Fluor®\ 700}$ showed a CD14^{low} and CD14^{high} population that was not visible with the less bright eFluor 450 fluorochrome.

Selection of anti-CD45 antibodies for polychromatic analysis of monocyte-derived macrophages

Previous data demonstrated that during monocyte to macrophage differentiation, the expression of CD14 decreased. Therefore, the use of both CD14 and CD45 may be used to identify MDM from fibroblasts and keratinocytes in a mixed co-culture. MDM cultured in 2D were stained with anti-CD45 antibodies conjugated to PE eFluor 610 and FITC, and compared to unstained samples. The normalised median fluorescence intensity (nMFI) for the two antibodies was compared (**Figure 6.6**).

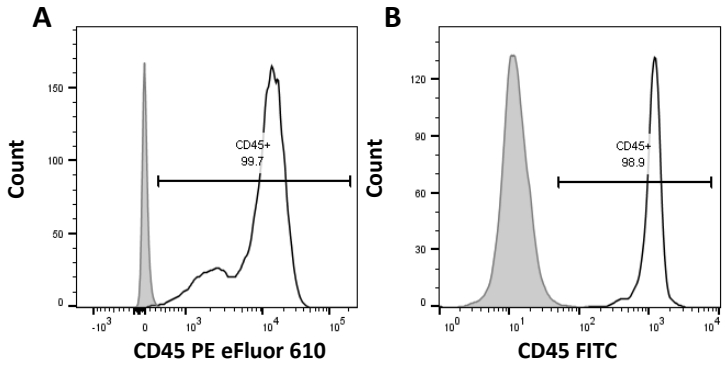

Figure 6.6. Selection of anti-CD45 antibody. Monocyte-derived macrophages (MDM) were cultured for 7 days, retrieved using cell scraping and CD45 expression analysed using flow cytometry. Anti-CD45 antibodies conjugated to PE eFluor 610 (**A**) and FITC (**B**) were tested and compared using normalised median fluorescence. Filled (grey) histograms show unstained cells, and open histograms show single-stained cells. Data are from a single experiment (n=1) and gates were set based on unstained cells following dead cell exclusion.

The use of both anti-CD45$^{PE\ eFluor®\ 610}$ and anti-CD45^{FITC} clearly identified CD45+ events compared to unstained cells, although the MFI of anti-CD45$^{PE\ eFluor®\ 610}$ was higher at 79.56 compared to 1.41 for anti-CD45^{FITC}. In addition, anti-CD45$^{PE\ eFluor®\ 610}$ was able to distinguish between CD45^{high} and CD45^{low} events, and FITC had previously been shown to be unsuitable for use in detecting MDM cultured within a highly auto-fluorescent collagen hydrogel.

Separation of monocyte-derived macrophages from normal oral fibroblasts cultured in 3D

To retrieve cells from the collagen hydrogel, methods using collagenase IV had previously been optimised. However, previously published literature suggested that collagenase IV may cleave cell surface proteins of interest. Therefore, the expression of CD45 and CD14 in MDM cultured in 2D with and without additional treatment with collagenase IV were compared using nMFI to quantify any differences in expression measured by flow cytometry (**Figure 6.7**).

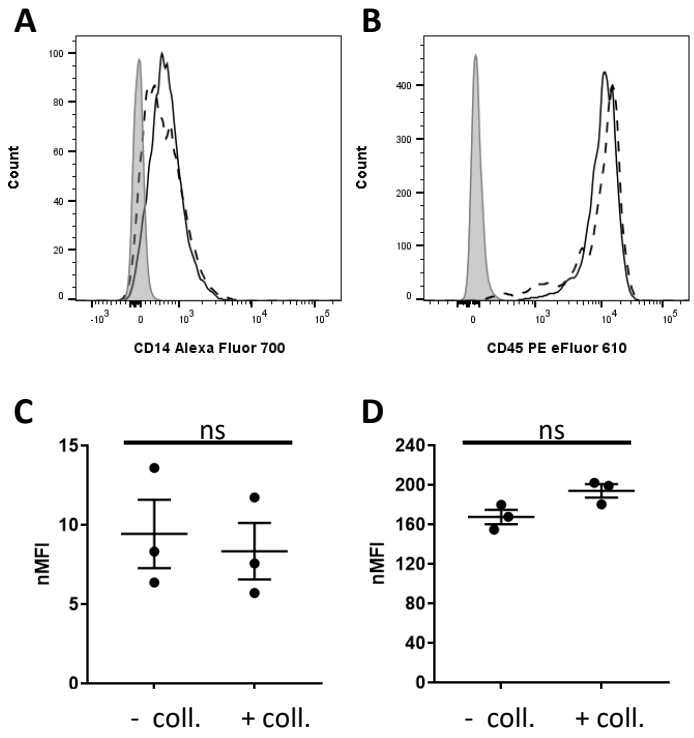

Figure 6.7. Collagenase IV does not affect the expression of CD14 and CD45. Monocyte-derived macrophages (MDM) were adherently cultured for 7 days, and retrieved using cell scraping before analysis using flow cytometry. The expression of CD14 (**A** and **C**) and CD45 (**B** and **D**) by MDM was unaffected by treatment with (+ coll., dotted line) and without (- coll., solid line) collagenase IV. Data are compared as histograms (**A** and **B**) and column charts (**C** and **D**). Grey, filled histograms represent unstained MDM, error bars show standard error mean and significance was determined using an unpaired two-tailed T-test. Data are representative of three independent experiments (n=3).

Histograms showed very similar expression levels of CD14 and CD45 by MDM cultured in 2D either with or without additional treatment with collagenase IV; 9.4 ± 2.2 and 8.3 ± 1.8 for CD14, and 167.5 ± 7.3 and 193.9 ± 8.7 for CD45 in the absence or presence of collagenase treatment, respectively. An unpaired two-tailed T-test showed that MDM treated with collagenase IV displayed no significant difference in the expression of CD14 ($p=0.7165$) or CD45 ($p=0.0578$).

As there was no apparent decrease in expression of CD14 or CD45 by MDM following treatment with collagenase IV, MDM and NOF co-cultured within a collagen hydrogel for 14

days at ALI were stained with both anti-CD14$^{\text{Alexa Fluor® 700}}$ and CD45$^{\text{PE eFluor® 610}}$ to enable separation of MDM from NOF (**Figure 6.8**).

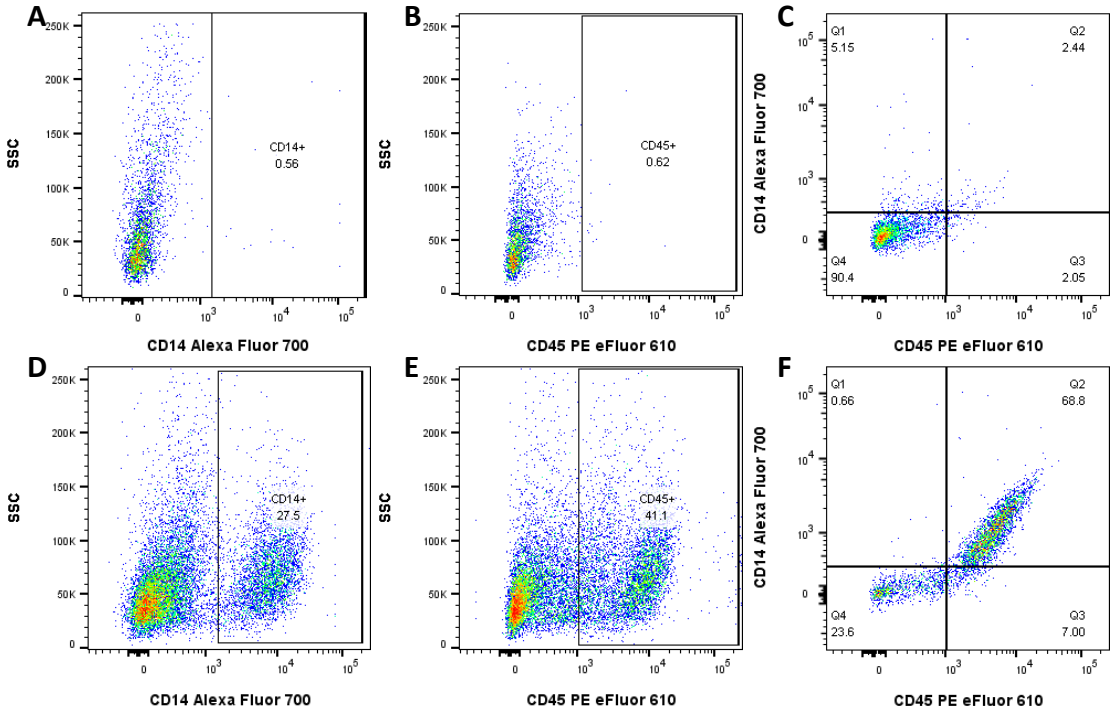

Figure 6.8. Separation of monocyte-derived macrophages from normal oral fibroblasts cultured in 3D. Monocyte-derived macrophages (MDM) cultured for 7 days in adherent culture were retrieved using cell scraping and co-cultured for an additional 14 days with normal oral fibroblasts (NOF) within a collagen hydrogel. Identification of CD14+ (**A** and **D**), CD45+ (**B** and **E**) and CD14+CD45+ (**C** and **F**) cells in 3D collagen hydrogels containing normal oral fibroblasts in the absence (**A-C**) or presence (**D-F**) of MDM. Gates were set based on fluorescence-minus-one controls following dead cell exclusion. Dot plots are representative of three independent experiments (n=3).

Collagen hydrogels devoid of MDM showed 1.8 % of events in the CD14+ gate and 0.6 % of events in the CD45+ gate. In addition, 2.4 % of events appeared in the CD14+CD45+ gate. In contrast, hydrogels containing MDM showed a clear population of cells in both the CD14+ gate (representing 27.5 % of events) and CD45+ gate (representing 41.1 % of events). Analysis of MDM-containing hydrogels showed 68.8 % of events in the CD14+CD45+ gate, that were not present in the hydrogels devoid of MDM.

6.2.4 Polarisation of monocyte-derived macrophages

A huge variety of macrophage polarisation markers have been identified in the literature. In this study, CD80, CD86, CD163 and CD206 were selected as they were the most highly cited and due to antibody availability. In order to generate positive controls for the selected proteins, the use of various exogenous stimuli was required. The published literature cites a variety of different combinations of cytokines to stimulate high expression of CD80, CD86, CD163 and CD206. Therefore, a variety of polarisation protocols were followed, and for many, results did not confirm published data.

Selection of polarisation stimuli

Of the published polarisation protocols, the use of GM-CSF, M-CSF, IL-4, IL-10, LPS and IFNγ appeared frequently. MDM were cultured in 2D for 7 days with the additional presence of GM-CSF combined with LPS and IFNγ for the final 24 hours to induce high expression of CD80 and CD86, and M-CSF combined with either IL-4 or IL-10 to induce high expression of CD163 and CD206. The expression of the selected markers was compared between MDM cultured with different cytokine stimulation, including MDM cultured in the absence of any cytokine stimulation (control, M0) and compared to unstained cells to determine nMFI (**Figure 6.9**).

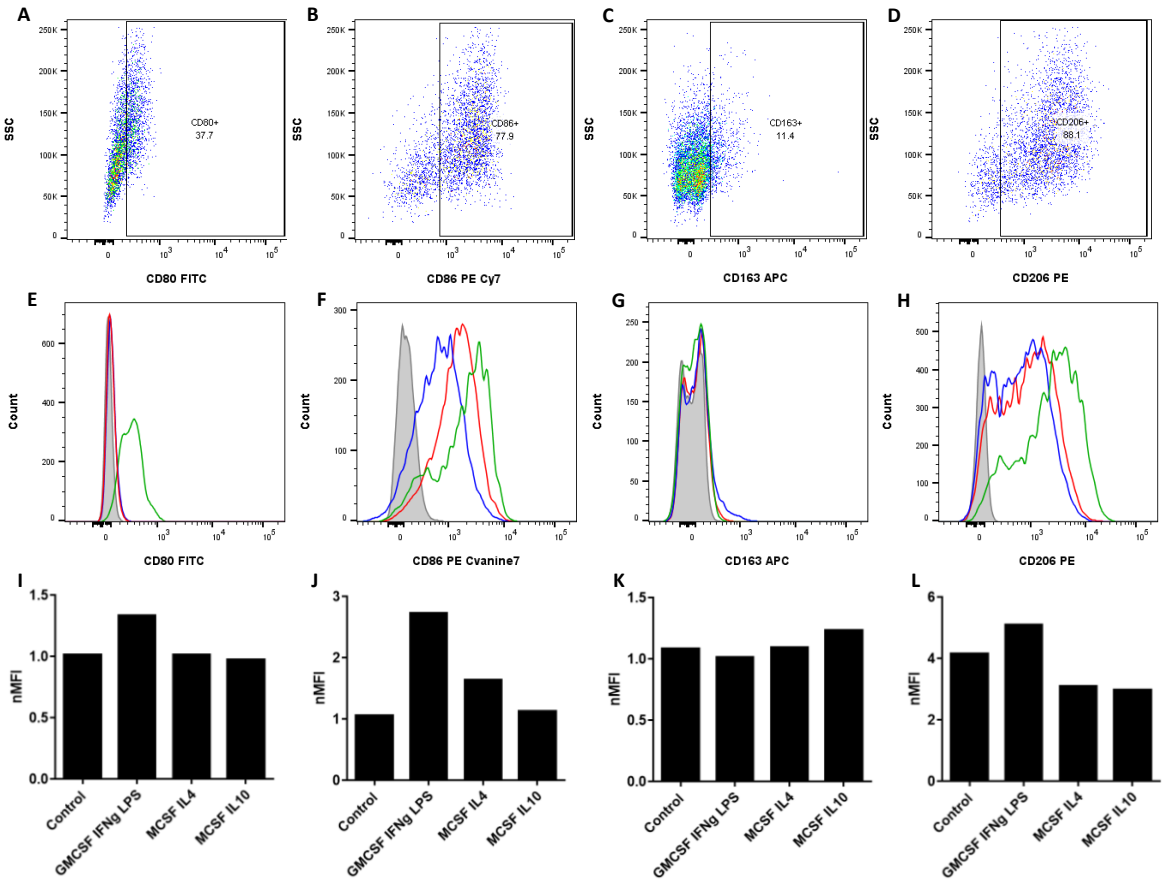

Figure 6.9. Expression of key macrophage polarisation markers following exogenous cytokine stimulation. Monocyte-derived macrophages (MDM) were adherently cultured for 7 days in the absence (control) or presence of M1 (GM-CSF, IFNγ and LPS; green line) or M2 (M-CSF combined with either IL-4 (red line) or IL-10 (blue line) cytokines. The expression of M1 markers, CD80 (**A**, **E** and **I**) and CD86 (**B**, **F** and **J**), and M2 markers, CD163 (**C**, **G** and **K**) and CD206 (**D**, **H** and **L**) on MDM were compared. Dot plots represent M1-stimulated MDM (**A-C**) or M-CSF/IL-10-stimulated MDM (**D**). Stained samples are compared to an unstained control (grey, filled histogram). Histograms (**E-H**) are summarised as bar charts (**I-L**). Data are representative of two independent experiments (n=2). Gates were set based on unstained samples treated under the same conditions following dead cell exclusion.

Dot plots show the percentage expression of the selected marker under conditions to stimulate a positive control, with gates set compared to an unstained sample. These show that after stimulation with GM-CSF, LPS and IFNγ, a high percentage of MDM expressed CD80 and CD86 (37.7 % and 77.9 % respectively). In addition, the levels of CD80 and CD86 expression by the whole MDM population increased resulting in a shift in MFI beyond that of MDM stimulated with M-CSF with IL-4 or IL-10. Stimulation of MDM with M-CSF and IL-10 resulted in 11.4 % of cells expressing CD163, and a small increase in nMFI compared to MDM stimulated with GM-CSF, LPS and IFNγ or M-CSF with IL-4. Stimulation of MDM with M-CSF and IL-4 resulted in 88.1 % of cells expressing CD206, however, the overlay histogram and nMFI values showed that MDM stimulated with GM-CSF, LPS and IFNγ expressed higher levels of CD206 when MDM were stimulated with M-CSF and IL-4. Consequently, CD36 was selected to confirm an M2 phenotype in addition to CD163 in later experiments.

Selection of polarisation marker antibodies

MDM were cultured in 2D for 7 days with the additional presence of GM-CSF combined with LPS and IFNγ for the final 24 hours to induce high expression of CD80, CD86 and CD206, and M-CSF combined with IL-10 to induce high expression of CD36 and CD163. MDM were stained with anti-CD80 antibodies conjugated to FITC; anti-CD163 antibodies conjugated to PE and APC; anti-CD36 antibodies conjugated to PE and APC; anti-CD86 antibody conjugated to PE Cyanine 7; and anti-CD206 antibodies conjugated to eFluor 450 and PE. The expression of marker and fluorochrome combinations was compared to an unstained sample and the nMFI determined (**Figure 6.10**).

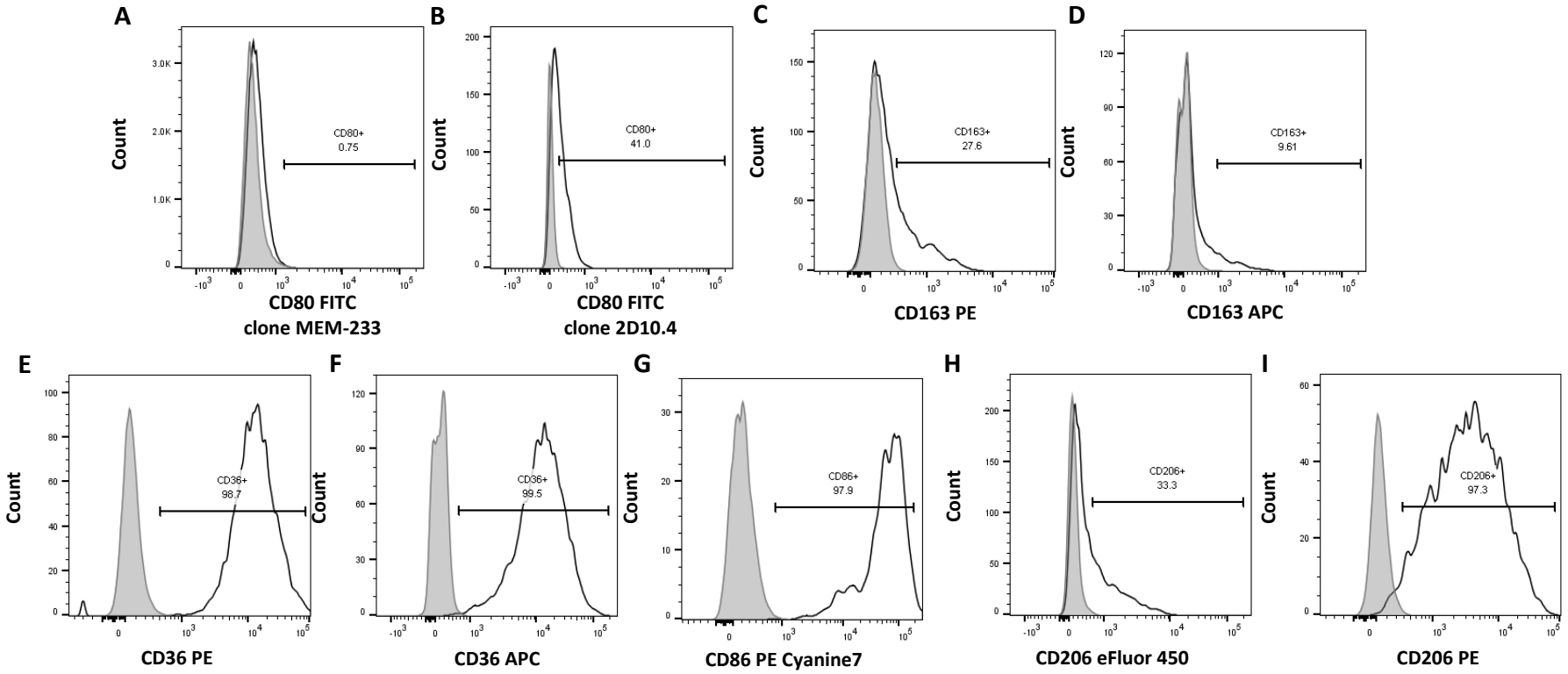

Figure 6.10. Selection of antibodies targeting macrophage polarisation markers. Monocyte-derived macrophages (MDM) were cultured for 14 days, retrieved using cell scraping and CD36, CD80, CD86, CD163 and CD206 expression analysed using flow cytometry. Anti-CD80 antibodies conjugated to FITC, clones MEM-233 (**A**) and 2D10.4 (**B**); anti-CD163 antibodies conjugated to PE (**C**) and APC (**D**); anti-CD36 antibodies conjugated to PE (**E**) and APC (**F**); anti-CD86 antibody conjugated to PE Cyanine7 (**G**); anti-CD206 antibodies conjugated to eFluor 450 (**H**) and PE (**I**) were tested and compared using normalised median fluorescence. Filled (grey) histograms show unstained cells, and open histograms show single-stained cells. Gates were based on unstained cells, following dead cell exclusion. Data are from a single experiment (n=1).

CD163^{PE} displayed a higher nMFI (1.58) than CD163^{APC} (1.36) and as a key marker in this panel, the brightest fluorochrome was allocated to CD163 (**Figure 6.10)**. By this stage, further choices were very limited and fluorochromes were selected according to availability (CD86$^{PE\ Cyanine7}$ and CD80^{FITC}); clone 2D10.4 showed a higher nMFI (2.54) than clone MEM-233 (1.07) for CD80^{FITC} and so was selected in preference. CD36^{APC} showed a lower nMFI (49.93) than CD36^{PE} (70.67), however with PE required for CD163, CD36^{APC} was added to the panel. The nMFI of CD86$^{PE\ Cyanine7}$ was 47.39. Although CD206^{PE} showed a higher MFI (19.87) than CD206$^{eFluor®\ 450}$ (2.01) the latter was selected as the PE fluorochrome was required for CD163.

6.3 Optimisation of FcγR blocking methods

Macrophages express many Fcγ receptors (FcγR) which enable them to recognize and internalize foreign antigens in order to perform their role in antigen presentation to cells of the adaptive immune system. However, the abundance of FcγR present on macrophages results in non-specific (non-epitope) binding of flow cytometry antibodies. In addition, antibodies can penetrate the membrane of non-viable cells and non-specifically bind intracellular targets. For these reasons, it was vital to use FcγR blocking prior to flow cytometry staining of MDM. In order to detect non-specific binding, selected isotype controls were used with the same fluorochrome (at the same F:P ratio), and at the same concentration as the antibody targeted to antigens of interest. FcR blocking reagent was tested at two different concentrations and incubations were performed at 4 °C or on ice for 15 minutes (**Figure 6.11**).

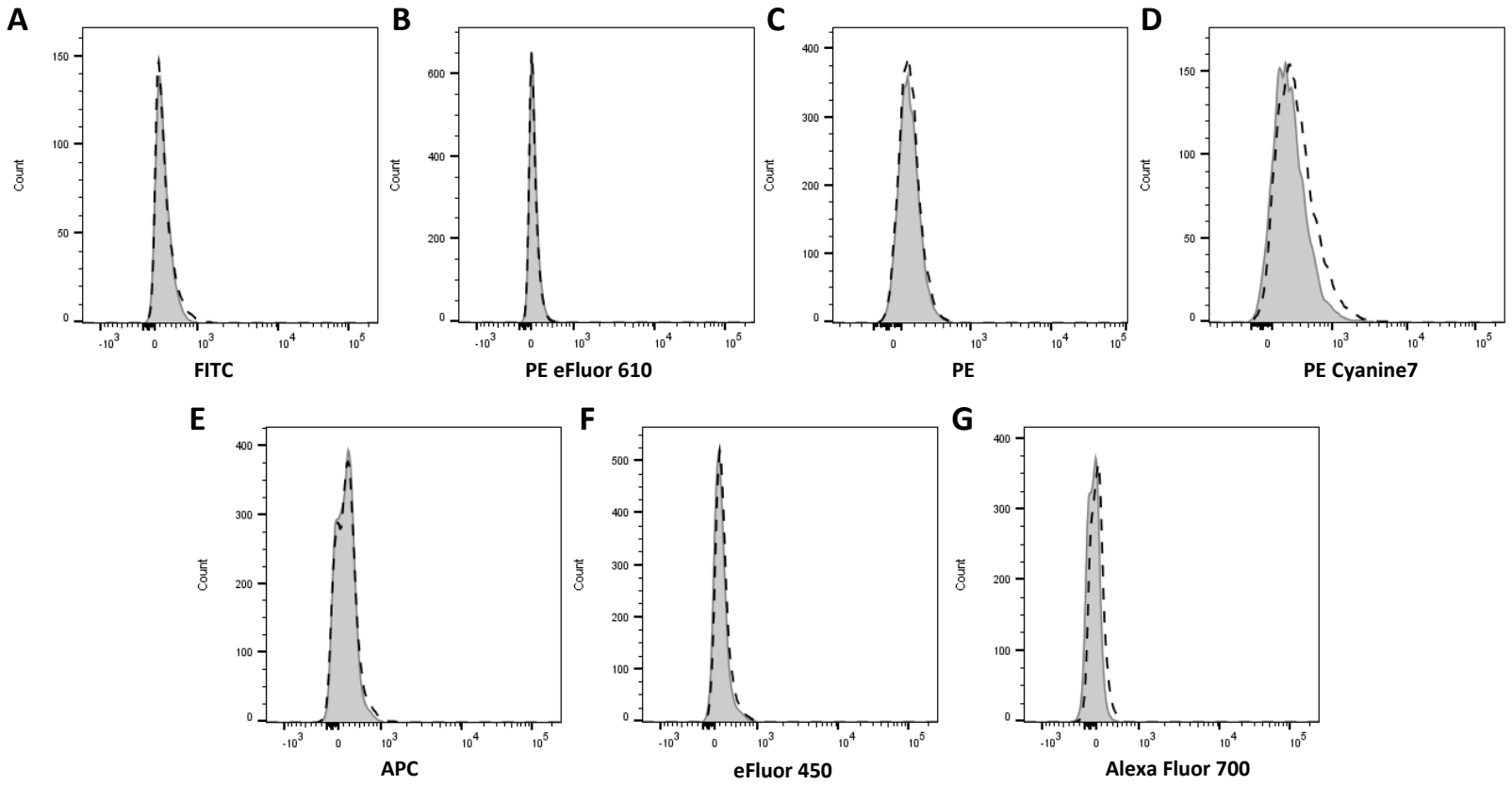

Figure 6.11. Optimisation of FcγR blocking methods. Monocyte-derived macrophages (MDM) were cultured for 14 days, retrieved using cell scraping and analysed using flow cytometry. The fluorescence from an unstained sample is compared to that of a sample stained with isotype control for FITC (**A**), PE eFluor 610 (**B**), PE (**C**), PE Cyanine7 (**D**), APC (**E**), eFluor 450 (**F**) and Alexa Fluor 700 (**G**). Data are representative of three independent experiments (n=3).

Ten microliters of FcR blocking reagent incubated at 4 °C demonstrated improved blocking of non-specific binding of isotype controls, to levels comparable to unstained samples. No difference in nMFI was measured or visible differences in histograms could be visualized between unstained samples and those stained with isotype controls for antibodies conjugated to FITC, PE eFluor 610, PE, APC or eFluor 450. However, a small increase nMFI was observed for PE Cyanine 7 (1.25) and Alexa Fluor 700 (1.47) in isotype-stained samples.

6.4 Phenotypic characterisation of polarised monocyte-derived macrophages cultured in 2D

The fully optimised polychromatic flow cytometry panel could now be used to characterise and compare the expression of key macrophage markers by MDM cultured under the stimulation of various polarising cytokines. MDM were cultured in 2D without additional stimulation or with the addition of GM-CSF with LPS and IFNγ, or M-CSF with IL-10.

6.4.1 Fewer M1 monocyte-derived macrophages are CD14+ compared to M2 monocyte-derived macrophages

The morphological changes of unstimulated MDM and MDM polarised to M1 or M2 phenotypes were compared using light microscopy (**Figure 6.12**), and changes in size and granularity were measured using flow cytometry for CD14+CD45+ (**Figure 6.13**) and CD45+ (**Figure 6.14**) events.

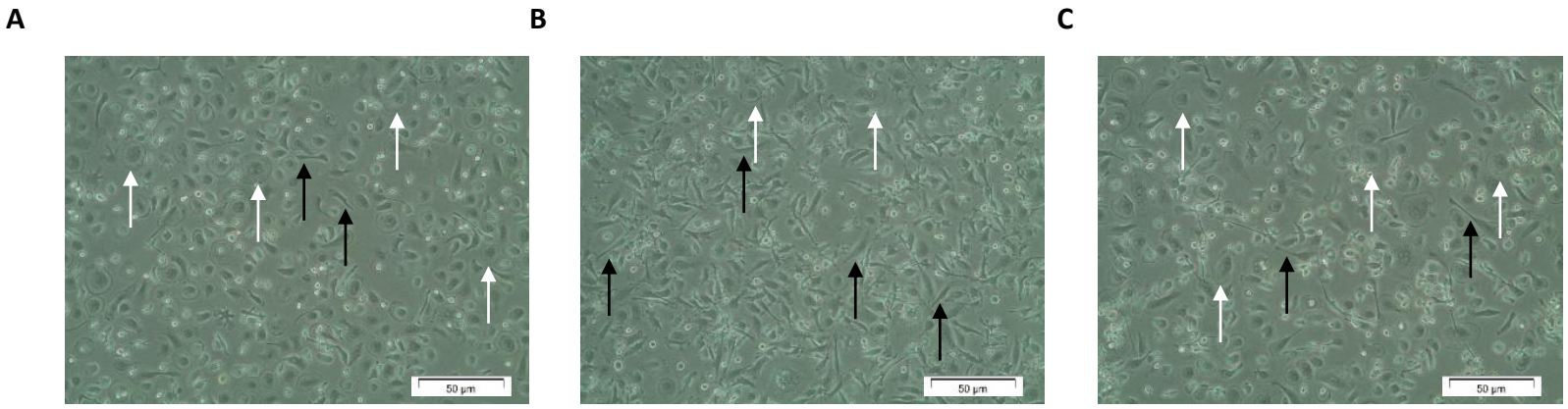

Figure 6.12. Polarised monocyte-derived macrophages undergo morphological changes in 2D. Monocyte-derived macrophages (MDM) cultured for 7 days in the absence of exogenous stimuli (**A**) or in the presence of M1-polarising cytokines GM-CSF, LPS and IFNγ (**B**) or M2-polarising cytokines M-CSF and IL-10 (**C**) were imaged using light microscopy. Data are representative of three independent experiments (n=3) and scale bars indicate 50 µm. White arrows highlight rounded cells, and black arrows highlight spindle-shaped cells.

Unstimulated MDM and those stimulated with M2 cytokines showed a high proportion of flat, round cells (white arrows) compared to spindle-shaped fibroblastoid cells (black arrows). In contrast, those stimulated with M1 cytokines showed an increased representation of fibroblastoid-like cells similar to results described previously (Cassol *et al.,* 2009).

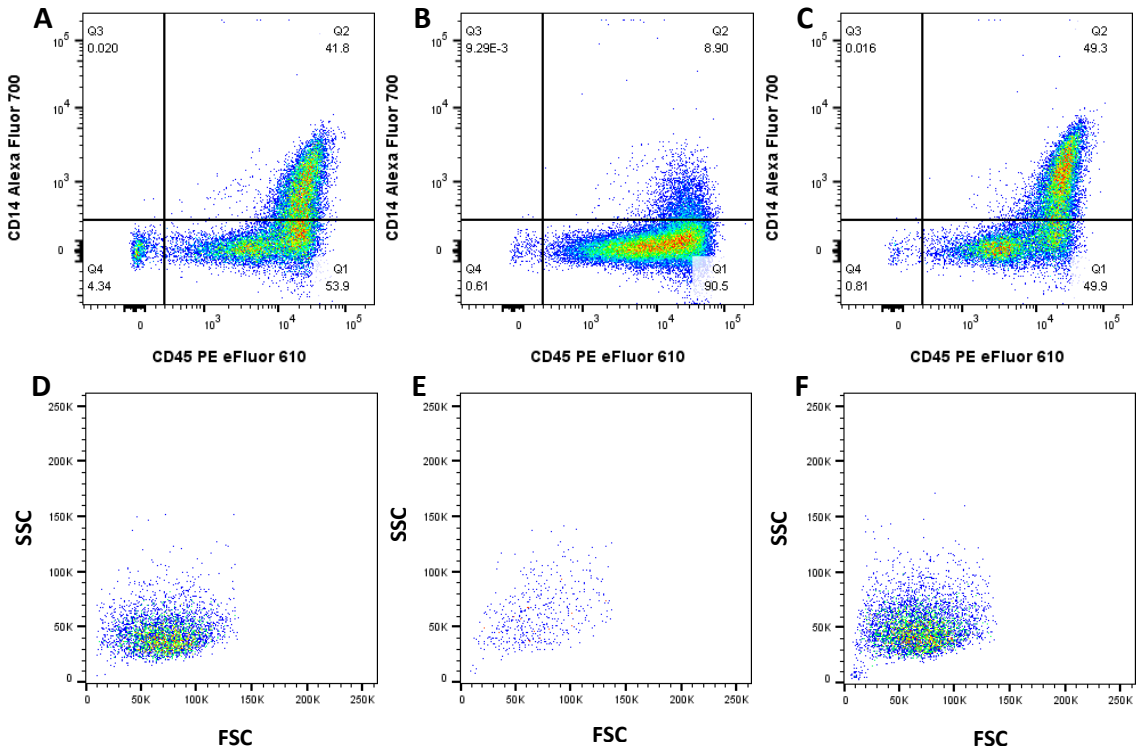

Figure 6.13. Polarised CD14+CD45+ monocyte-derived macrophages undergo physical changes in 2D. Monocyte-derived macrophages (MDM) cultured for 7 days in the absence of exogenous stimuli (**A** and **D**) or in the presence of M1-polarising cytokines GM-CSF, LPS and IFNγ (**B** and **E**) or M2-polarising cytokines M-CSF and IL-10 (**C** and **F**) were analysed using flow cytometry. CD14+CD45+ (**A-C**) events were selected following dead cell exclusion and their size and granularity compared (**D-F**).

Measurements of FSC and SSC of CD14+CD45+ events to examine changes in size and granularity were 80213 ± 4268 and 48021 ± 3484 (M0), 85184 ± 7829 and 78485 ± 9093 (M1), 78059 ± 4950 and 51371 ± 3824 (M2) respectively. This data indicates that MDM stimulated with M1 cytokines were larger and more granular than both those unstimulated and those stimulated with M2 cytokines, with much smaller differences in FSC and SSC observed between the latter. Of the un-stimulated MDM, 40.1 ± 1.2 % were CD14+CD45+ compared to 7.6 ± 0.6 % of M1-stimulated and 51.3 ± 1.9 % of M2-stimulated. However, in all samples, >90 % of events were CD45+, therefore, changes in size and granularity of CD45+ were also compared (**Figure 6.14**).

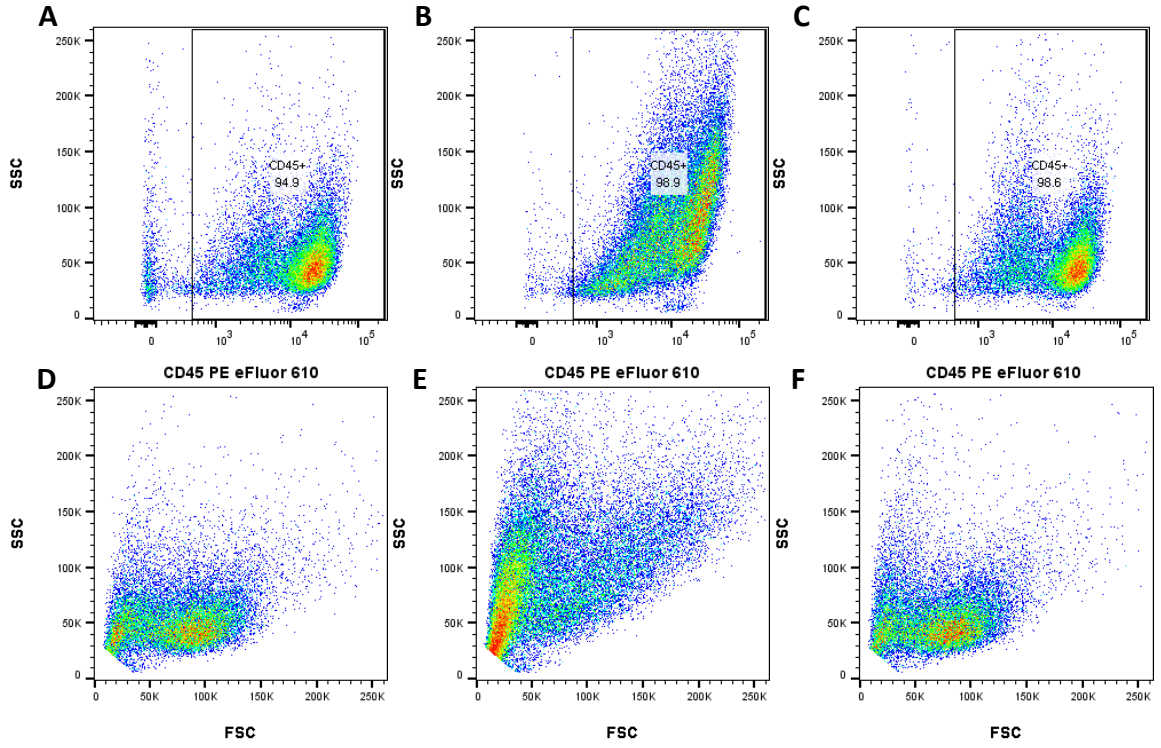

Figure 6.14. Polarised CD45+ monocyte-derived macrophages undergo physical changes in 2D. Monocyte-derived macrophages (MDM) cultured for 7 days in the absence of exogenous stimuli (**A** and **D**) or in the presence of M1-polarising cytokines GM-CSF, LPS and IFNγ (**B** and **E**) or M2-polarising cytokines M-CSF and IL-10 (**C** and **F**) were analysed using flow cytometry. CD45+ (**A-C**) events were selected following dead cell exclusion and their size and granularity compared (**D-F**).

Measurements of FSC and SSC of CD45+ events to examine changes in size and granularity were 65408 ± 10240 and 46176 ± 2400 (M0), 34240 ± 9600 and 57888 ± 9504 (M1), 60768 ± 10080 and 47744 ± 1408 (M2) respectively. This data indicates that M1-stimulated MDM are smaller and more granular than those unstimulated or stimulated with M2 polarising cytokines. This is comparable to data analysed CD14+CD45+ MDM. Interestingly, FSC and SSC dot plots of CD45+ MDM showed two different populations, as opposed to the single, homogeneous population of CD14+CD45+ MDM seen previously.

6.4.2 M1 monocyte-derived macrophages appear to express CD80, CD86 and CD206, whilst M2 monocyte-derived macrophages express CD36 and CD163

The expression of CD36, CD80, CD86, CD163 and CD206 of un-stimulated and M1 or M2-polarised MDM was compared using percentage expression and nMFI for CD14+CD45+ (**Figure 6.15**) events and CD45+ events (**Figure 6.16**).

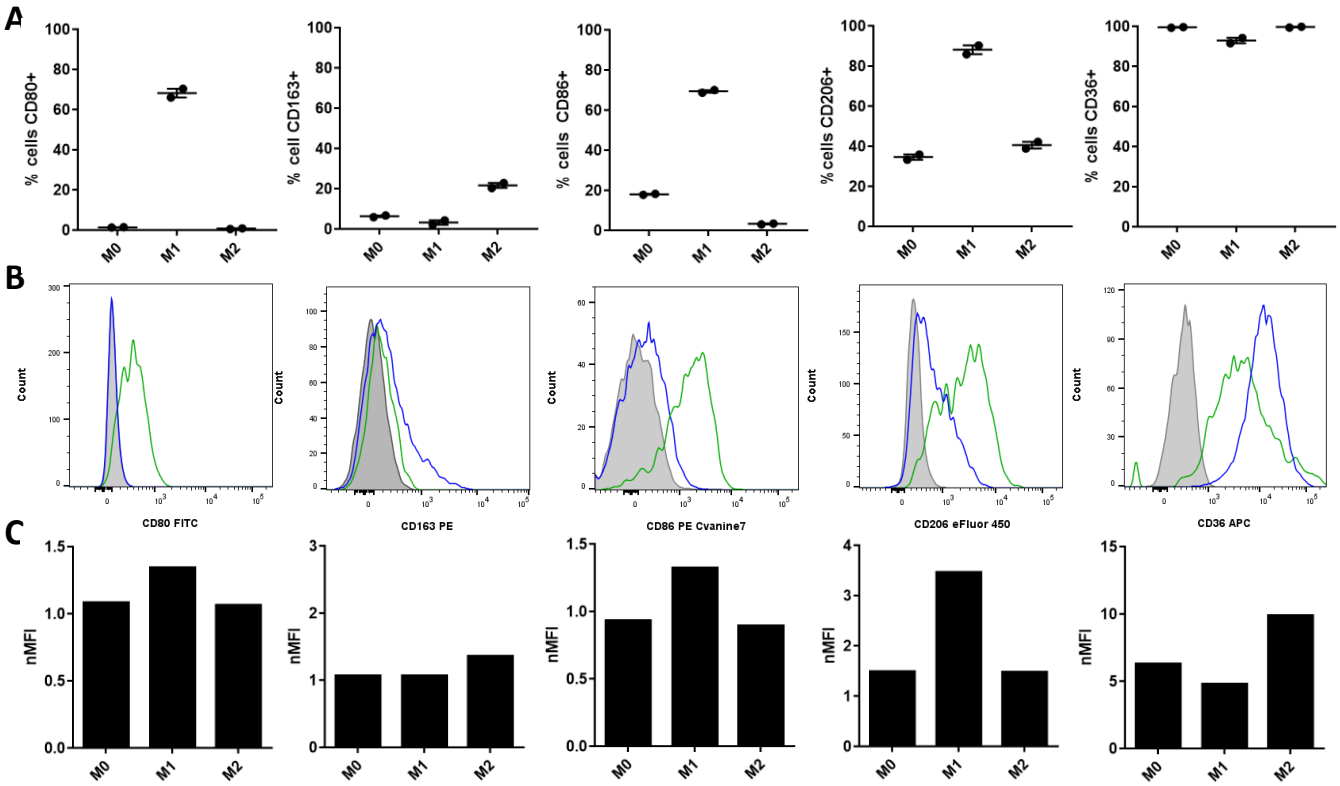

Figure 6.15. Differences in expression of key monocyte and macrophage markers in unstimulated, M1 and M2 CD14+CD45+ monocyte-derived macrophages. Monocyte-derived macrophages (MDM) were adherently cultured for 14 days in the absence (M0) or presence of GM-CSF, IFNγ and LPS (M1), or stimulated with M-CSF and IL-10 (M2). The percentage of CD14+CD45+ events expressing CD80, CD163, CD86, CD206 and CD36 respectively (**A**), the normalised median fluorescence (nMFI, **B**) and nMFI data summarised as column charts (**C**) are shown. Grey, filled histograms represent un-stimulated MDM, green line depicts M1-stimulated and blue line depicts M2-stimulated macrophages. Gates were set based on fluorescence-minus one controls and CD14+CD45+ events were selected as in **Figure 6.13**, following dead cell exclusion. Data are representative of two independent experiments (n=2).

M1-stimulated MDM displayed a higher expression of CD80 (68.2 %), CD86 (69.4 %) and CD206 (88.1 %), compared to un-stimulated MDM (1.4 %, 18.1 % and 34.6 % respectively) and M2-stimulated MDM (0.7 %, 3.3 % and 40.6 % respectively). In addition, M1-stimulated MDM displayed higher average nMFI values for CD80 (2.2), CD86 (6.0) and CD206 (5.8) compared to un-stimulated MDM (1.0, 2.4 and 1.9 respectively) and M2-stimulated MDM (1.1, 5.4 and 1.5 respectively).

A slightly increased percentage of M2-stimulated MDM expressed CD36 (99.6 %) and CD163 (21.7 %) compared to un-stimulated MDM (99.5 % and 6.3 % respectively) and M1-stimulated MDM (92.9 % and 3.2 % respectively). In addition, M2-stimulated MDM displayed higher average nMFI values for CD36 (9.9) and CD163 (1.4) compared to un-stimulated MDM (6.2 and 1.2 respectively) and M1-stimulated MDM (4.7 and 1.2 respectively). Whilst changes in the percentage expression and nMFI were observed through the different polarization stimuli, these changes represented the cell population as a whole, as opposed to the segregation of separate populations of cells.

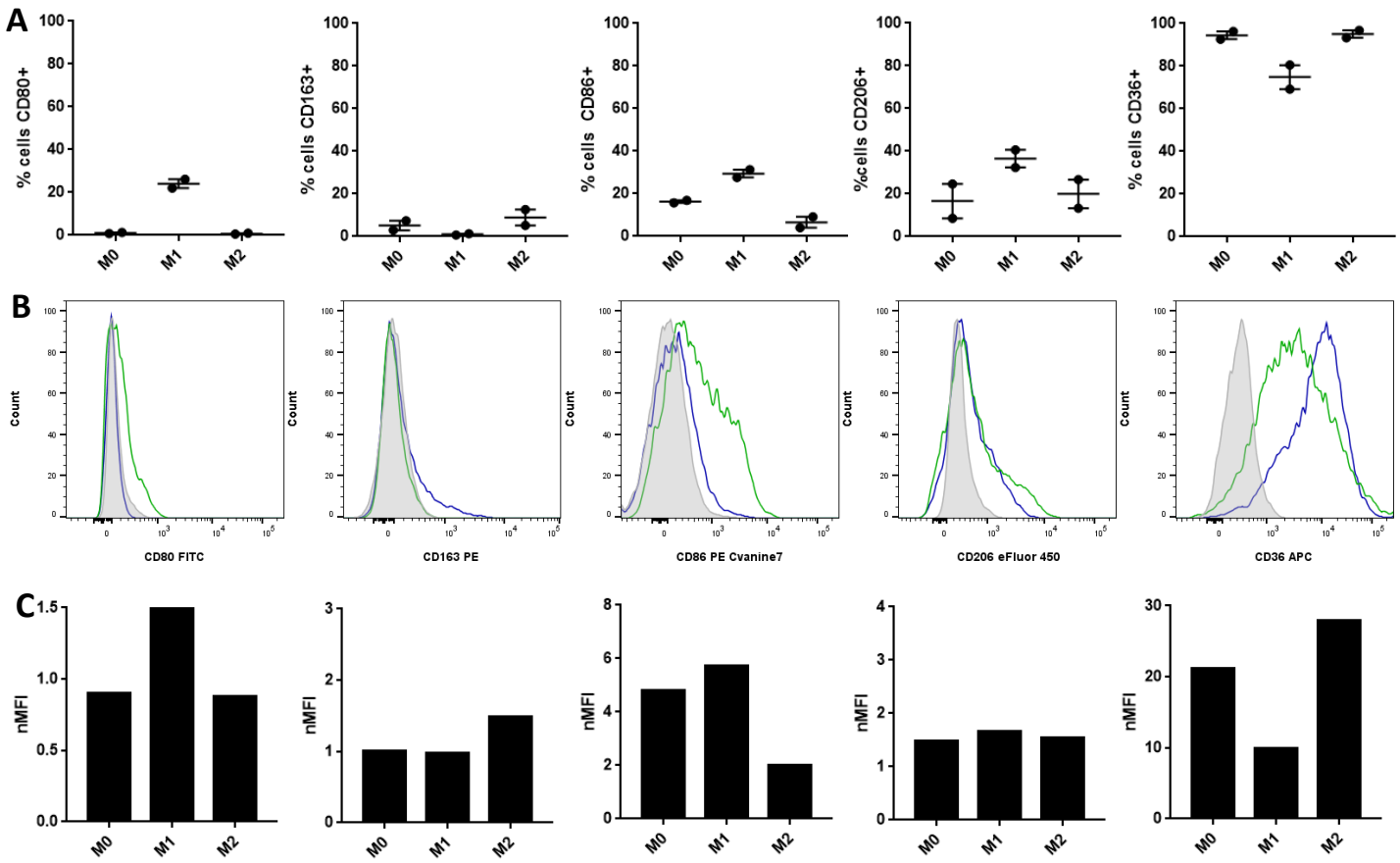

Figure 6.16. Differences in expression of key monocyte and macrophage markers in unstimulated, M1 and M2 CD45+ monocyte-derived macrophages. Monocyte-derived macrophages (MDM) were adherently cultured for 14 days in the absence (M0) or presence of GM-CSF, IFNγ and LPS (M1), or stimulated with M-CSF and IL-10 (M2). The percentage of CD45+ events expressing CD80, CD163, CD86, CD206 and CD36 respectively (**A**), the normalised median fluorescence (nMFI, **B**) and nMFI data summarised as column charts (**C**) are shown. Grey, filled histograms represent un-stimulated MDM, green line depicts M1-stimulated and blue line depicts M2-stimulated macrophages. Gates were set based on fluorescence-minus one controls and CD45+ events were selected as in **Figure 6.14**, following dead cell exclusion. Data are representative of two independent experiments (n=2).

M1-stimulated MDM displayed a higher expression of CD80 (26.1 %), CD86 (97.6 %), CD206 (40.6 %), compared to un-stimulated MDM (0.8 %, 95.7 %, and 8.6 % respectively) and M2-stimulated MDM (0.5 %, 91.1 %, and 13.3 % respectively). In addition, M1-stimulated MDM displayed higher average nMFI values for CD80 (2.4), CD86 (210.0) and CD206 (5.9), compared to un-stimulated MDM (1.1, 81.7, and 1.9 respectively) and M2-stimulated MDM (1.1, 40.4, and 2.4 respectively). This is comparable to analysis of CD14+CD45+ MDM.

A slightly increased percentage of M2-stimulated MDM expressed CD36 (96.7 %) but not CD163 (5.2 %) compared to un-stimulated MDM (96.3 % and 7.3 % respectively) and M1-stimulated MDM (69.2 % and 0.74 % respectively). In addition, M2-stimulated MDM displayed higher average nMFI values for CD36 (60.4) and CD163 (0.3) compared to M1-stimulated MDM (12.7 and 0.1 respectively) but not un-stimulated MDM (72.5 and 0.1 respectively).

6.5 Discussion

To date, no single polychromatic flow cytometry panels have been developed for the quantitative characterisation of human MDM polarization status. Since the start of development of this panel, Tarique *et al.,* published a series of three panels that could be used in parallel to measure various features of classically and alternatively activated macrophages (Tarique *et al.,* 2015). In common with the panel presented here, published work used CD80, CD206 and CD163 to distinguish M1 from M2 macrophages. However, only 2 of the 3 panels used an antigen to distinguish macrophages, CD68, and therefore cannot be used to identify macrophages in a co-culture environment. In addition, the use of intracellular markers limits the use of these panels for live cell sorting. Whilst a 10-colour flow cytometry panel has been previously published to characterise macrophages and dendritic cells in the normal mouse lung (Misharin *et al.,* 2013) and a 6-colour panel for the analysis of mouse adipose tissue macrophages (Cho *et al.,* 2014), there are no multi-colour flow cytometry panels available for the characterisation of human macrophages from *in vitro* 3D culture or patient tissue samples. The polychromatic flow cytometry panel presented here is an essential tool for developing an understanding of the changes in

expression of key macrophage markers in response to changes in culture environment. The development of the panel is discussed below.

6.5.1 **Reagent selection**

Fibroblasts are required within a tissue engineered oral mucosa model as they enable the adherence and proliferation of keratinocytes to the simulated connective tissue in order to form an epithelium (Latkowski *et al.,* 1995). However, to identify the macrophage population for accurate analysis of cell surface protein expression, both fibroblasts and keratinocytes need to be separated from macrophages prior to analysis by flow cytometry. Typically, a 'dump-channel' would be used to remove cells irrelevant to the analysis, such as fibroblasts and keratinocytes. Increasingly, CD90 has been used as a fibroblast marker in flow cytometry experiments. However, CD90 is also expressed by many other cell types, including some T lymphocytes and blast cells signifying poor prognosis in AML (Buccisano *et al.,* 2004; Guillot-Delost *et al.,* 2012; Zhou and Chng, 2014). In addition, previously published data has isolated stromal cells from lymphnodes, and showed the challenges in specifically selecting these for analysis using flow cytometry as a whole range of markers was required (Fletcher *et al.,* 2011). In particular, this paper cites the challenges posed by the highly auto-fluorescence extra-cellular matrix in tissues. Therefore, CD90 alone may not be a suitable dump channel marker for fibroblasts in flow cytometry. Alternative markers include αSMA and vimentin, although these are intracellular markers and their expression varies markedly under different conditions (Gedye *et al.,* 2014; Hsia *et al.,* 2016). The use of PDGFRα has also been explored to isolate cancer-associated fibroblasts from patient samples and may be useful in isolating fibroblasts that are both αSMA positive and negative (Sharon *et al*., 2013). Regarding keratinocytes, these cells express many different markers, but no examples of optimised keratinocyte markers suitable for use in a 'dump channel' could be found.

CD14 is typically regarded as a monocyte- and macrophage-specific marker, although evidence has shown that CD14 may also be expressed by non-myeloid cells (Jersmann, 2005). CD45, otherwise known as leukocyte common antigen, is expressed by all

leukocytes, including macrophages. Neither fibroblasts or keratinocytes are CD14+CD45+ and thus the panel presented here used positive selection for CD14+CD45+ dual positive cells in order to identify macrophages within co-culture with keratinocytes and fibroblasts.

Fluorochrome selection

Macrophages are a highly auto-fluorescent cell type, to such an extent that this has previously been used to identify these cells during *in vitro* generation from PBM using flow cytometry (Njoroge *et al.,* 2001). Cellular auto-fluorescence in animals is mostly derived from chromophores such as flavins, enzymes such as NADH and NADPH and extracellular matrix components such as collagen and elastin (Billinton and Knight, 2001). Initially, anti-CD14 and anti-CD45 antibodies conjugated to FITC and PE were examined for the identification of macrophages from other cell types. However, fibroblasts contain large amounts of collagen which auto-fluoresces around 520nm; within the emission spectra of FITC. Due to the large amounts of overlap in emission spectra of FITC and PE, auto-fluorescence from fibroblasts resulted in both of these fluorochromes proving unsuitable for the separation of macrophages from fibroblasts.

A wide variety of fluorochromes are available for use in flow cytometry experiments; these can vary in brightness and excitation or emission wavelengths, and they can be used alone or in tandem. The brightest fluorochromes (those with the highest stain index) were reserved for the highest prioritised antigens, such as CD14, CD45 and CD163 that were assigned to Alexa Fluor 700, PE eFluor 610 and PE respectively. Directly-conjugated anti-CD14 and anti-CD45 antibodies are commonly used in research, and thus a wide choice of fluorochromes are available. Therefore, the selection of fluorochromes for these antibodies was postponed until fluorochromes had been selected for less commonly available antibodies. Fluorochromes were selected in order to reduce the amount of compensation required to minimize the effects of spectral overlap. However, there was considerable spectral overlap of FITC in the blue 575/26 and blue 610/20 channels; PE into blue 610/20; PE eFluor 610 into blue 530/30 and blue 575/26; and Alexa Fluor 700 into red 660/20

although this never exceeded >50%. Due to spectral overlap, the use of fluorochromes detected by blue 660/20 laser are not recommended for additions to this panel.

Non-viable cells non-specifically bind free antibodies in a staining solution. Therefore, it is essential to use a viability dye during flow cytometry analysis to remove non-viable cells from the analysis that may otherwise be measured as a false-positive result (Tung 2007). The LIVE/DEAD® Fixable Blue Dead Cell Stain used here demonstrated favourable separation of viable and non-viable cells compared to a Fixable Viability Dye eFluor® 455UV. Both these dyes are excited by the Lightwave Xcyte™ laser, for which very few fluorochromes are available. This ensured that as many fluorochromes remained available for the selected markers.

6.5.2 Polarisation of monocyte-derived macrophages

Macrophages are a highly pleiotropic cell type, responding to various environmental stimuli by changing gene and protein expression, as well as shape and size. As macrophages alter their protein expression so rapidly to changes in their environment, there is a need for tools to enable characterisation of macrophages isolated from animals and humans with limited *in vitro* manipulation to further understand their role in disease progression. *In vitro* experiments have shown that the gene expression profile of MDM stimulated with one cocktail of cytokines can rapidly change if a second cocktail of cytokines is added (Murray and Wynn, 2011). Therefore, polychromatic flow cytometry panels are rapidly emerging as promising tools to characterise macrophages isolated from various disease models, however none exist for the characterisation of human macrophages.

There are many different published protocols for the polarisation of MDM using several different cytokines and varying antigens used to measure the direction of polarisation. Typically, changes in protein expression measured by flow cytometry are reported as changes in nMFI (Chan *et al.,* 2013) and will therefore be discussed here, in addition to changes in percentage expression.

It was previously observed that MDM cultures were >95 % CD14+ after 7 days, therefore protocols for polarising MDM over 7 days were used. The most commonly used markers were selected for assessment of macrophage polarisation (**Table 1.1**). Gene and protein expression do not often correlate, but similarly to experiments analysing protein expression, many different combinations of cytokines are used to stimulate gene expression of MDM polarisation antigens. These have previously been summarised (Erbel *et al.,* 2013).

M1 antigens

T lymphocyte activation antigen, CD80, is often used as a marker of M1 macrophage polarisation. Through culture of MDM for 7 days in the presence of GM-CSF with the addition of LPS and IFNγ, expression of CD80 increased compared to MDM cultured without stimulation or in the presence of M2 cytokines, providing similar results to those previously published (Jaguin *et al.,* 2013). However, in this published study, stimulation of MDM by GM-CSF alone, resulted in no significant increase in CD80 observed (Jaguin *et al.,* 2013). This is in direct contrast to Ambarus *et al.,* who found that GM-CSF or IFNγ alone could stimulate an increased expression of CD80 (Ambarus *et al.,* 2012). Whilst the increase in CD80 expression by nMFI was modestly in favour of M1-stimulated MDM, 70 % of cells were found to be CD80+ compared to unstimulated and M2-stimulated MDM that showed 1.4 % and 0.7 % CD80+ cells respectively.

CD86 is a common antigen used for identifying M1 macrophages. In the absence of GM-CSF, but presence of LPS and IFNγ, or IFNγ alone, Vogel *et al.,* found no significant increase in CD86 expression compared to control or M2 polarised MDM (Vogel *et al.,* 2013). As in other previously published protocols (Mia *et al.,* 2014; Zhang *et al.,* 2013), it was found here that CD86 expression could be induced by the culture of MDM for 6 days in the presence of GM-CSF, with an additional 24 hours in the presence of GM-CSF, LPS and IFNγ. This treatment resulted in a similar pattern of increase in both nMFI and percentage expression of CD86+ cells.

During the activation of innate immunity, the binding of LPS to TLR4 leads to a signal transduction pathway that culminates with activation of iNOS and expression of co-stimulatory molecules such as CD80, CD86 and CD40 that results in the activation of T lymphocytes (Iwasaki and Medzhitov, 2004). Activated T lymphocytes and natural killer cells, attracted by IL-12 released by macrophages, secrete IFNγ that binds IFNGR1 resulting in the upregulation of pro-inflammatory cytokines such as TNF and IL-1β whilst increasing the expression of IFNGR1 in a positive feedback loop (Biswas and Mantovani, 2010; Chavez-Galan *et al.,* 2015). Additionally, the binding of LPS to CD14, via the action of LPS binding protein and GM-CSF to GMCSFR results in further upregulation of pro-inflammatory cytokines (Duque and Descoteaux, 2014).

Following stimulation of MDM with GM-CSF, LPS and IFNγ, data showed a decrease in the expression of CD14+ events. This resulted in a decrease in the number of macrophages selected as they were no longer selected in the CD14+CD45+ gate. Previous data showed a decrease in membrane CD14 expression by alveolar macrophages in response to *E.coli* and extracted LPS both *in vivo* and *in vitro* (Lin *et al.,* 2004). With the aid of LPS binding protein (LBP), LPS binds CD14 for internalisation. Whilst there is evidence to support the internalisation of CD14 with LPS (Poussin *et al.,* 1998), there is also evidence to suggest that CD14 does not accompany LPS during internalisation (Vasselon *et al.,* 1999). During inflammation, LBP is secreted from the liver and increases in concentration in peripheral blood. This aids in activating cells devoid of CD14 to respond to exposure to LPS (Fenton and Golenbock, 1998). Whilst many researchers add exogenous LBP to *in vitro* cultures of macrophages to stimulate a response to LPS, CD14 can bind LPS in the absence of LBP, albeit at a very low rate (Fenton and Golenbock, 1998).

M2 antigens

CD36 is a scavenger receptor that is increasingly used to identify M2 macrophages. It is considered essential for the activation of macrophages to an M2 phenotype (Huang *et al.,* 2014). Although its gene expression is commonly measured in macrophage polarising experiments to indicate M2 polarisation, no examples of flow cytometry analysis of CD36

under different polarising conditions could be found. Data showed that MDM stimulated with M-CSF combined with IL-10 expressed higher levels of CD36 compared to both un-stimulated and M1-stimulated MDM. Here, M1-stimulated MDM expressed the lowest levels of CD36, determined by both percentage expression and nMFI, in a similar pattern to previously published gene expression data (Jaguin *et al.,* 2013). However, while nMFI data showed a marked increase in CD36 expression compared to both unstimulated and M1-stimulated MDM, similar percentages of MDM were CD36+ in both un-stimulated and M2-stimulated MDM.

Scavenger receptor CD163 is often used to identify M2 macrophages. In addition, CD163 has been shown in the literature to have an important role in the progression of oral cancer, and can be used as a determinant of poor prognosis (Balermpas *et al.,* 2014; Fujii *et al.,* 2012; Fujita *et al.,* 2014; He *et al.,* 2014; Mori *et al.,* 2011; Weber *et al.,* 2014; Wehrhan *et al.,* 2014). An increase in the expression of CD163 has previously been observed following culture of MDM for 6 days in the presence of M-CSF with an additional 24 hours in the presence of IL-4 (Zhang *et al.,* 2013). This is in direct contrast to research by another group that found no significant increase in CD163 expression by MDM following stimulation with IL-4 (Vogel *et al.,* 2013). In fact, it was found that there was a slight increase in the expression of CD163 in the presence of M1 polarising cytokines. Of note, the use of M-CSF alone has been found to increase the expression of CD163 (Ambarus *et al.,* 2012). In addition, this work showed that CD163 expression was observed to increase in response to stimulation of MDM with M-CSF or IL-10 either alone or in combination (Ambarus *et al.,* 2012). Research presented in this thesis found that the culture of MDM with M-CSF in combination with IL-10 resulted in an increase in CD163 expression compared to un-stimulated MDM and those stimulated with GM-CSF, LPS and IFNγ. The use of M-CSF combined with IL-4 did not result in an increase in expression of CD163 compared to un-stimulated MDM. Whilst a modest increase in nMFI of M2-stimulated MDM was observed, the percentage of CD163+ cells increased by more than 3-fold compared to un-stimulated MDM and more than 7-fold compared to M1-stimulated MDM.

Mannose receptor type 1, otherwise known as CD206, has been well characterised and has many roles in macrophage function. It is often used to identify M2 macrophages, however this study found its expression to increase during polarisation with M1 cytokines. Previous literature has shown that the use of IL-4 can significantly increase the expression of CD206 to demonstrate polarisation of MDM to M2 status (Ambarus *et al.,* 2012; Vogel *et al.,* 2013). However, other research groups found no significant difference in CD206 expression after stimulation of MDM with M-CSF and IL-4 compared to MDM stimulated with M0 or M1 polarising cytokines (Jaguin *et al.,* 2013). However, this was not replicated by their gene expression data that showed a significant increase in CD206 transcription in the presence of IL-4 compared to un-stimulated MDM or those cultured with M1-polarising cytokines. An alternative approach is the use of IL-4 combined with IL-10 or with the further addition of TGFβ that displayed a significant increase in CD206 expression compared to un-stimulated MDM and those stimulated with various combinations of IL-4, IL-10, IL-13, TGFβ, LPS and IFNγ (Mia *et al.,* 2014). In this published study, the use of IL-4 and IL-10 in the absence of TGFβ resulted in the largest increase in CD206 expression. The study presented in this thesis was unable to reproduce these results, and consistently found that CD206 expression increased in the presence of M1 polarising cytokines, as reported by both nMFI and percentage expression.

Of note, data showed that changes in expression of polarisation antigens by MDM was shared by the population as a whole, with shifts in nMFI observed. No evidence of discrete populations of cells emerging as CD36+, CD80+, CD86+, CD163+ or CD206+ was observed. The combination of nMFI and percentage expression was found to provide further insight into the changes in protein expression reported.

Whilst there are many studies analysing the signalling pathways involved in M1 macrophage activation, less information is available for M2 macrophages. IL-10 is an anti-inflammatory cytokine, and the binding of this to its receptor, IL-10R, leads to a signal transduction cascade that culminates in the transcription of anti-inflammatory genes and scavenger receptors CD36 and CD163, and CD206 (Chavez-Galan *et al.,* 2015; Duque and Descoteaux,

2014). Further IL-10 is secreted, and attracts B cells and Treg cells that release more IL-10 in a positive feedback loop (Biswas and Mantovani, 2010). The increased expression of CD36, CD163 and CD206 enables macrophages to bind and scavenge increased amounts of oxidised LDL, hapto-haemoglobin complexes and bacterial carbohydrates resulting from the inflammatory response, respectively (Duque and Descoteaux, 2014). As part of the anti-inflammatory response of M2 macrophages, LPS-dependent pro-inflammatory responses are inhibited (Biswas and Mantovani, 2010).

6.5.3 **Flow cytometry controls**

There are many studies using flow cytometry that have not been found to be reproducible, particularly in the case of large clinical trials with some studies showing more than 20 % variance in results, typically from variation in gating strategies (Maecker *et al.,* 2010). Hence, there has been a focussed effort to raise awareness of the correct controls and approaches to gating to ensure that more data can be reproduced (Alvarez *et al.,* 2010). Consequently, guidelines were developed for the minimum information to be reported alongside published flow cytometry data (Lee *et al.,* 2008). By incorporating suitable controls, accurate gating and data compensation into a study, reproducible data may be achieved. The data presented in this work has followed all published flow cytometry guidelines and used the following controls and quality control steps.

Compensation is used to account for spectral overlap between different fluorochromes. It estimates and subtracts the spectral overlap from the detected signal to estimate the actual signal (Herzenberg *et al.,* 2006). Most software associated with a flow cytometers compute complex algorithms for quantifying spectral overlap using positive controls such as compensation beads (Tung *et al.,* 2007). The fluorochromes selected in the polychromatic panel presented here required compensation due to overlap between the emission spectra. Compensation corrects for reagent spillover, and the gold-standard method combines the use of compensation beads which are always brighter, more accurate and more reproducible than the cells of interest with automatic compensation algorithms (Bagwell

and Adams, 1993). This ensures that only the fluorochrome of interest is measured at any given time, rather than spillover from other fluorochromes (Roederer, 2001).

Compensation beads were used in this thesis to provide maximally bright and maximally dim signals to calculate accurate compensation. Anti-mouse CompBeads and ArC amine reactive beads were used according to the manufacturer's instructions with the selected, titrated fluorochrome-conjugated antibodies. Compensation (**Table 2.10**) was applied by FACSDiva software and applied to all ensuing samples. All compensated samples were manually checked to ensure the median values of negative and positive populations were equal.

Whilst compensation minimises the amount of spectral overlap between different fluorochromes, FMO controls are used to ensure that gates are set to eliminate any fluorescence spread. This is particularly important in the case of highly auto-fluorescent cells, such as macrophages. Each FMO control contains all the panel reagents, except the reagent of interest. Gates can then be applied that ensure only truly positive events are measured (Roederer, 2001; Tung *et al.,* 2007).

Macrophages express many Fcγ receptors (FcγR) which enable them to recognize and internalize foreign antigens in order to perform their role in antigen presentation to cells of the adaptive immune system (Guilliams *et al.,* 2014). However, the abundance of FcγR present on macrophages results in non-specific (non-epitope) binding of flow cytometry antibodies (Andersen *et al.,* 2016). In addition, antibodies can penetrate the membrane of non-viable cells and non-specifically bind intracellular targets. For these reasons, it was vital to use FcγR blocking prior to flow cytometry staining of MDM. MDM bind strongly to IgG1 and IgG2a, but not to IgG2b. However, even this strong binding can be blocked by using an FcγR blocking reagent (Andersen *et al.,* 2016). Isotype controls are typically used to ensure that FcγR blocking methods successfully block non-specific antibody binding. In this work, all flow cytometry reagents were titrated in order to avoid high levels of background staining. In addition, isotype antibodies matched the isotype of the test antibody and both antibodies were purchased from the same vendor to ensure matching F:P ratios. It was

ensured that the background staining of the isotype antibody matched an unstained sample (Maecker and Trotter, 2006).

In some studies, samples stained with isotype controls are used to set gates and as a reference in comparison to stained samples. However, an increasing body of literature advises against the use of isotype controls for this purpose, and instead advises the use of unstained and unstimulated samples as comparisons and FMO controls for setting gates (Andersen *et al.,* 2016; Keeney *et al.,* 1998; Maecker and Trotter, 2006). The use of an isotype control to set gates in a polychromatic flow cytometry experiment does not allow for fluorescence spill over, hence FMO controls are recommended for this purpose (Herzenberg *et al.,* 2006).

6.6 Conclusion

The fully optimised polychromatic flow cytometry panel presented here not only describes a tool that may be used reproducibly to gain further understanding in the expression of specific antigens by MDM cultured under various conditions, the exclusive use of cell surface markers in this panel enables its use for live cell sorting. Whilst the panel has been developed for use on *in vitro* cultured MDM in 2D and 3D, the panel may be further optimised for use on patient biopsies. In any case, the panel provides the opportunity to analyse MDM antigen expression in detail that has not previously been possible.

7 Chapter 7: Preliminary Analysis of an *In Vitro* 3D Model of the Oral Mucosa Using Polychromatic Flow Cytometry

7.1 Introduction

Macrophages have been shown to have an increasingly important role in oral cancer progression. However, the tools available to establish the molecular interactions between primary human macrophages and other cells of the tumour microenvironment have previously been limited to IHC of patient biopsies (Bagul *et al.,* 2016; Balermpas *et al.,* 2014; Boas *et al.,* 2013; Li *et al.,* 2002; Lu *et al.,* 2010; Mori *et al.,* 2011). However, whilst histological analysis provides some detailed information, it only provides a snapshot. The tissue-engineered oral mucosa model containing human MDM developed previously in Chapter 5 may be used to investigate the role that TAM play in oral cancer progression. In this model, the interactions of MDM with fibroblasts and keratinocytes can be explored. The array of tools, such as polychromatic flow cytometry panel and rheometry, optimised in previous chapters may now be optimised and applied specifically to analyse changes in MDM within the tissue-engineered model.

Macrophages are highly plastic and adjust their function in response to environmental stimuli. In the tumour microenvironment, previous data has shown that macrophages change expression of markers in response to cytokines released by tumour cells to promote a tumour-supportive environment. In particular, CD163 is emerging as a potential prognostic marker for oral cancer as its expression has correlated with poor patient survival in a number of studies (Balermpas *et al.,* 2014; Fujii *et al.,* 2012; Fujita *et al.,* 2014; He *et al.,* 2014; Mori *et al.,* 2011; Weber *et al.,* 2014; Wehrhan *et al.,* 2014).

In order to gain an understanding of the changes that macrophages undergo in response to oral cancer cells and consequences to cancer progression, a collagen hydrogel containing fibroblasts with and without MDM was seeded with NOK, FNB6 or H357 keratinocytes. Alternatively, to further understanding of the effects polarised macrophages have on the oral mucosa, hydrogels populated with M0, M1 and M2 MDM were cultured with an FNB6 epithelium in the presence of continuous cytokine stimulation as previously described (Linde *et al.,* 2012). Models were cultured at ALI for 14 days and analysed using an 8-colour flow cytometry panel for the identification of MDM from fibroblasts and characterisation

of macrophage polarisation status, rheometry to measure changes in tissue stiffness and histology to analyse changes in tissue architecture.

7.2 Optimisation of flow cytometry panel for use on tissue-engineered models of the oral mucosa

Chapter 6 of this thesis described the optimisation of a multi-colour flow cytometry panel suitable to quantitatively analyse the expression of CD36, CD80, CD86, CD163 and CD206 on CD14+CD45+ macrophages. To be used on MDM co-cultured in 3D with fibroblasts and a variety of epithelial cells, further methods for the disaggregation of models and analysis of MDM were required.

7.2.1 Effect of collagenase IV on the expression of cell surface markers by 3D-cultured monocyte-derived macrophages

The polychromatic flow cytometry panel presented in this thesis has so far been optimized for use on 2D *in vitro* generated MDM, however, its purpose is to interrogate the expression of key macrophage markers on MDM cultured in 3D, which requires further optimisation. Retrieval of MDM from 3D cultures was previously optimized using collagenase IV and therefore it was essential to ensure that the use of this enzyme did not affect the expression of the selected markers of interest.

MDM were cultured in 2D either un-stimulated or in the presence of M1 or M2 polarising cytokines in order to stimulate the expression of chosen markers of interest. MDM were washed and scraped into fresh IMDM using cell scrapers and expression of markers was compared between MDM treated with collagenase IV and those without treatment. Data are presented as overlay histograms and the nMFI of $CD80^{FITC}$, $CD163^{PE}$, $CD86^{PE\ Cyanine7}$, $CD206^{eFluor450}$ and $CD36^{APC}$ with and without collagenase IV treatment were compared using an unpaired two-tailed T-test (**Figure 7.1**).

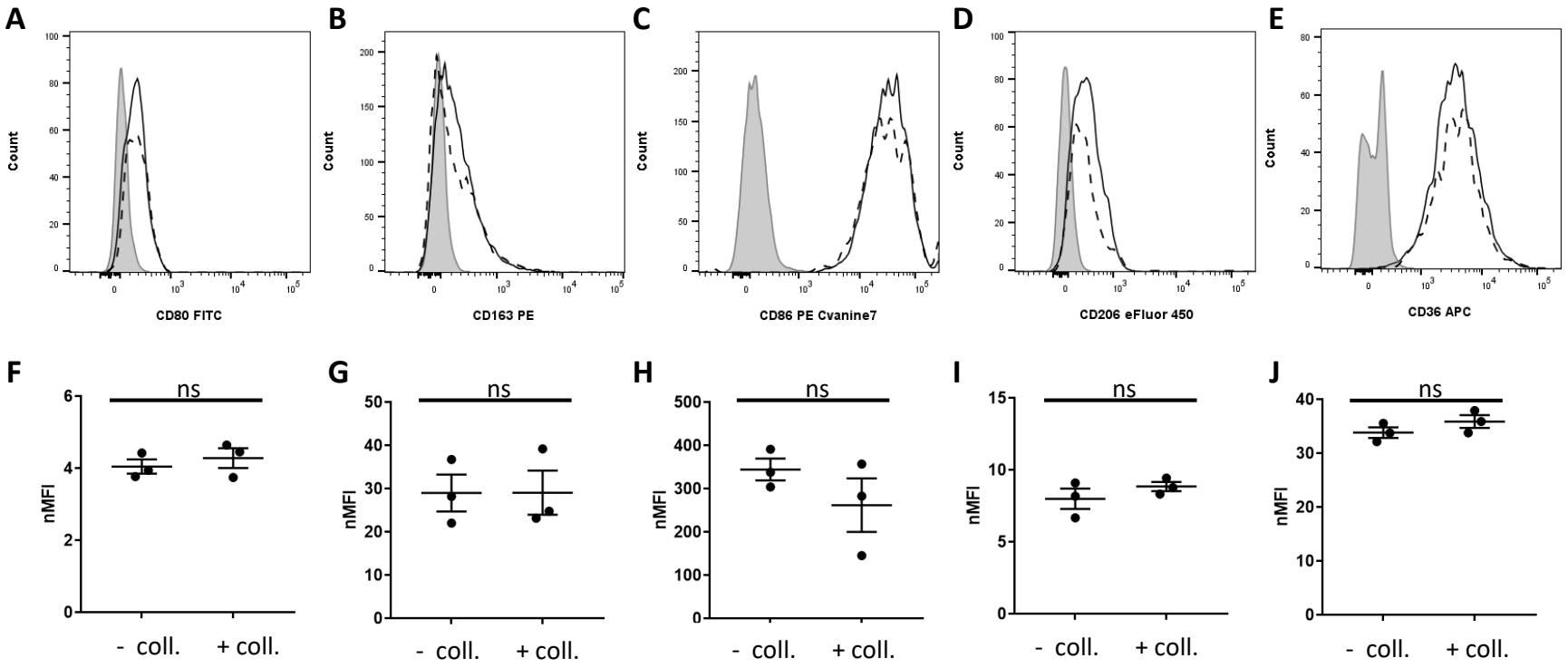

Figure 7.1. Disaggregation of collagen hydrogel using collagenase IV does not affect the expression of macrophage polarisation markers. Monocyte-derived macrophages (MDM) were adherently cultured for 7 days, retrieved using cell scraping and analysed using flow cytometry in the absence or presence of collagenase treatment. The differential expression of CD80 (**A** and **F**), CD163 (**B** and **G**), CD86 (**C** and **H**), CD206 (**D** and **I**) and CD36 (**E** and **J**) by macrophages cultured with (+ coll., dotted line) and without (- coll., solid line) collagenase IV treatment is compared as histograms (**A-E**) and column charts (**F-J**). Grey, filled histograms represent un-stimulated macrophages, error bars show standard error mean and significance was determined using an unpaired two-tailed T-test. Data are representative of three independent experiments (n=3).

Following treatment with collagenase IV, expression levels of CD36, CD80, CD86, CD163 and CD206 by MDM were similar to those of un-treated MDM; 26.6 ± 0.4 and 24.4 ± 1.9 for CD36, 4.0 ± 2.0 and 4.3 ± 0.27 for CD80, 344.1 ± 25.37 and 261.6 ± 62.0 for CD86, 29.0 ± 4.3 and 29.0 ± 5.1 for CD163, and 8.0 ± 0.7 and 8.8 ± 0.3 for CD206, in the absence or presence of collagenase treatment, respectively. An unpaired two-tailed T-test showed that MDM treated with collagenase IV displayed no significant difference in the expression of CD80 ($p=0.5251$), CD163 ($p=0.9941$), CD86 ($p=0.2855$), CD206 ($p=0.3325$) or CD36 ($p=0.2536$). Some cells were lost during the additional processing of samples treated with collagenase, resulting in reduced cell counts.

7.2.2 Use of additional controls

In chapter 6, a polychromatic flow cytometry panel was developed to enable analysis of polarisation status of MDM cultured within the tissue-engineered model of the oral mucosa presented in Chapter 5. In order for this panel to be used to analyse the changes in expression of key macrophage polarisation markers, CD36, CD80, CD86, CD163 and CD206, in response to MDM culture with NOK, FNB6 or H357 keratinocytes. However, additional controls may be required to accurately interpret results.

Monocyte-derived macrophages appear to change in morphology and expression of CD14 and CD45 in response to co-culture with normal oral keratinocytes, FNB6 and H357 cells

After 14 days of culture at ALI, hydrogels were disaggregated using collagenase IV, samples were processed into a single cell suspension using a cell strainer and stained using the multi-colour flow cytometry panel developed in chapter 6. Gates were set using FMO controls to measure percentages of cell expression and nMFI calculated (**Equation 2.1**). The FSC, SSC and expression of CD14 and CD45 was compared using flow cytometry (**Figure 7.2**).

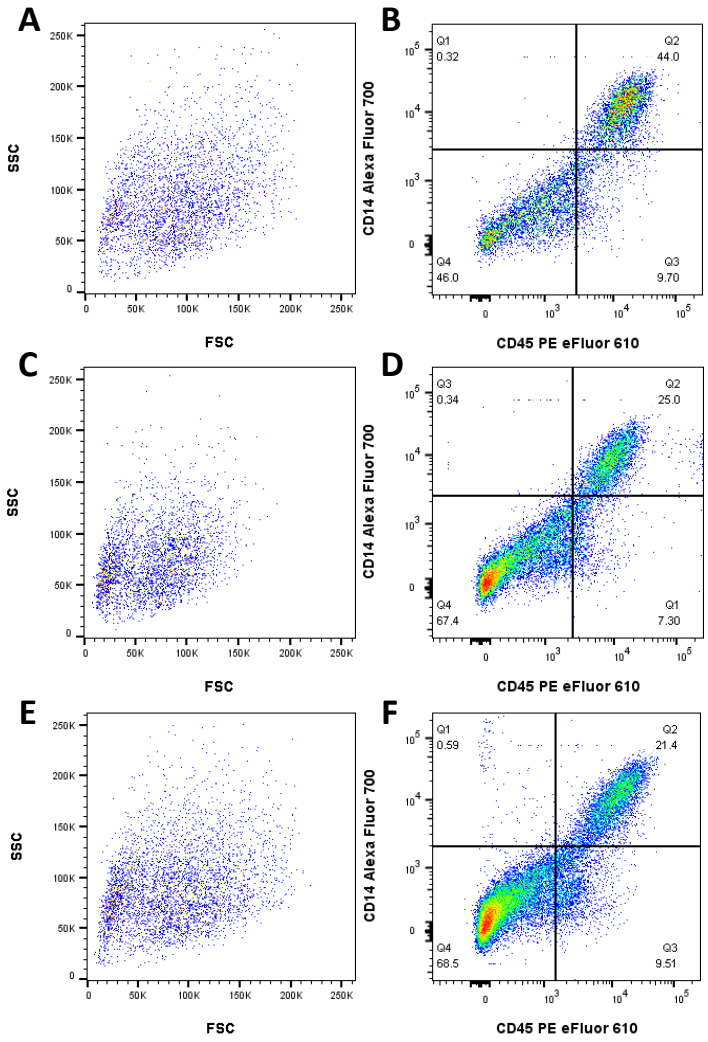

Figure 7.2. Monocyte-derived macrophages appear to undergo morphological changes and differentially express CD14 and CD45 within tissue-engineered oral mucosa containing normal oral keratinocytes, immortalised FNB6 keratinocytes or oral squamous cell carcinoma cell line, H357. Monocyte-derived macrophages (MDM) following 7 days of adherent culture were retrieved using cell scraping and additionally cultured within tissue-engineered oral mucosa containing normal oral fibroblasts in addition to normal oral keratinocytes (NOK, **A-B**), immortalised FNB6 keratinocytes (**C-D**) or oral squamous cell carcinoma cell line, H357 (**E-F**) for 14 days at air-liquid interface. MDM showed differences in size and granularity (**A**, **C** and **E**) and expression of key macrophage markers, CD14 and CD45 (**B**, **D** and **F**), following co-culture with the different keratinocytes. Gates were set based on fluorescence-minus-one controls following dead cell exclusion. Data shown are for a single experiment (n=1).

Following culture of MDM within a tissue-engineered model of the oral mucosa in the presence of NOK, FNB6 and H357, changes in MDM size and granularity were observed. MDM cultured in the presence of NOK had the highest measured FSC and SSC at 87 360 and 84 544 respectively, and those cultured with FNB6 cells had the lowest values at 65 408 and 68 544 respectively. MDM cultured in the presence of H357 keratinocytes has FSC and SSC values of 79 552 and 82 816 respectively.

Monocyte-derived macrophages appear to express altered levels of background auto-fluorescence in response to co-culture with different cells

The background fluorescence of MDM was altered following co-culture with NOK, FNB6 and H357 cells. Therefore, the detection of $CD45^{PE\ eFluor\ 610}$ and $CD14^{Alexa\ Fluor\ 700}$ was affected. Consequently, gates were required based on individual FMO controls for each model type. In models containing NOK, 44.0 % of events were CD14+CD45+ compared to 25.0 % in models containing FNB6 cells and 21.4 % in models containing H357 cells. However, as the percentages of CD14-CD45- varied between samples, a ratio was also produced to determine the ratio of CD14+CD45+ events compared to CD14-CD45+ events by dividing CD14+CD45+ events by CD14-CD45+ events. This ratio was found to 4.5 for NOK, 3.4 for FNB6 and 2.3 for H357 containing models. This indicates an increased ratio of CD14+CD45+ MDM in NOK-containing models compared to both FNB6 and H357 containing models.

The viability of cells was >90 % in all cases. In order to visualise the differences in auto-fluorescence of MDM co-cultured with NOK, FNB6 and H357 cells, the fluorescence of unstained MDM retrieved from collagen hydrogels was compared in all channels of interest (**Figure 7.3**).

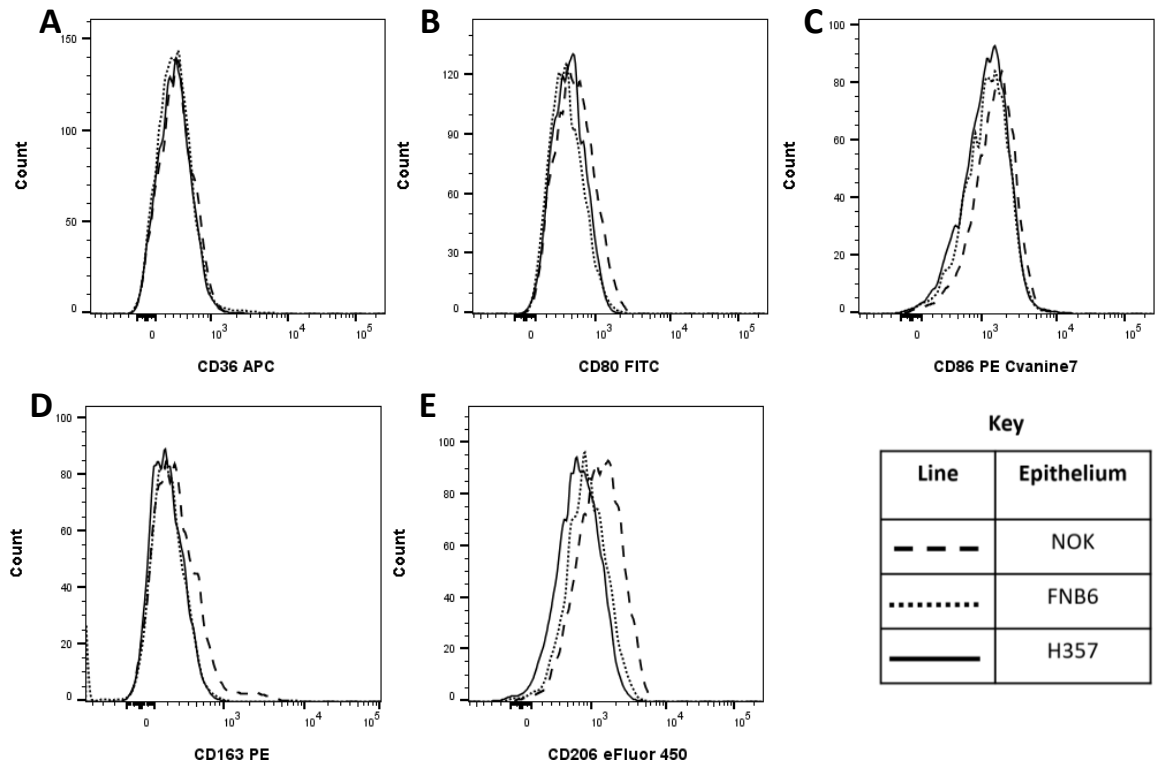

Figure 7.3. Background fluorescence of monocyte-derived macrophages appears to change in response to culture with normal oral keratinocytes, immortalised FNB6 keratinocytes and oral squamous cell carcinoma cell line, H357s. Monocyte-derived macrophages (MDM) cultured within tissue-engineered oral mucosa containing normal oral fibroblasts in addition to normal oral keratinocytes (NOK, dashed line), immortalised keratinocytes, FNB6 (dotted line) or oral squamous cell line, H357 (unbroken line) showed differences in background fluorescence of unstained samples at the wavelengths used to measure $CD36^{APC}$ (**A**), $CD80^{FITC}$ (**B**), $CD86^{PE\ Cyanine7}$ (**C**), $CD163^{PE}$ (**D**) and $CD206^{eFluor\ 450}$ (**E**). Data shown are for a single experiment (n=1).

In response to co-culture with NOK, FNB6 and H357 keratinocytes, in addition to changes in the expression of CD14 and CD45 and changes in FSC and SSC, the background fluorescence of MDM in FMO controls at wavelengths measuring the expression of key macrophages markers was also altered. The measured background MFI measured using a blue 530/30 laser (FITC) was 418 (FNB6), 540 (NOK), 460 (H357); for the blue 575/26 laser (PE) was 196 (FNB6), 253 (NOK), 188 (H357); for the blue 780/60 laser (PE Cyanine7) was 1201 (FNB6), 1467 (NOK), 1165 (H357); for the red 660/20 laser (APC) was 316 (FNB6), 340 (NOK), 318 (H357); and for the violet 450/50 laser (eFluor 450) was 866 (FNB6), 1253 (NOK), 702

(H357). MDM cultured with NOK expressed higher levels of background fluorescence at the same wavelength as FITC, PE, eFluor 450 and expressed a slightly higher MFI at the same wavelength as PE Cyanine 7 compared to those cultured with both FNB6 and H357. The background fluorescence of MDM at the same wavelength as APC remained unchanged.

7.3 The interaction of monocyte-derived macrophages with normal oral keratinocytes, FNB6 and H357 epithelia

Tissue-engineered oral mucosa models containing fibroblasts either in the presence or absence of MDM were cultured with an epithelium containing NOK, FNB6 or H357 cells. After 14 days of culture at ALI, models were formalin-fixed, paraffin-embedded and sections were stained with H&E (**Figure 7.4**).

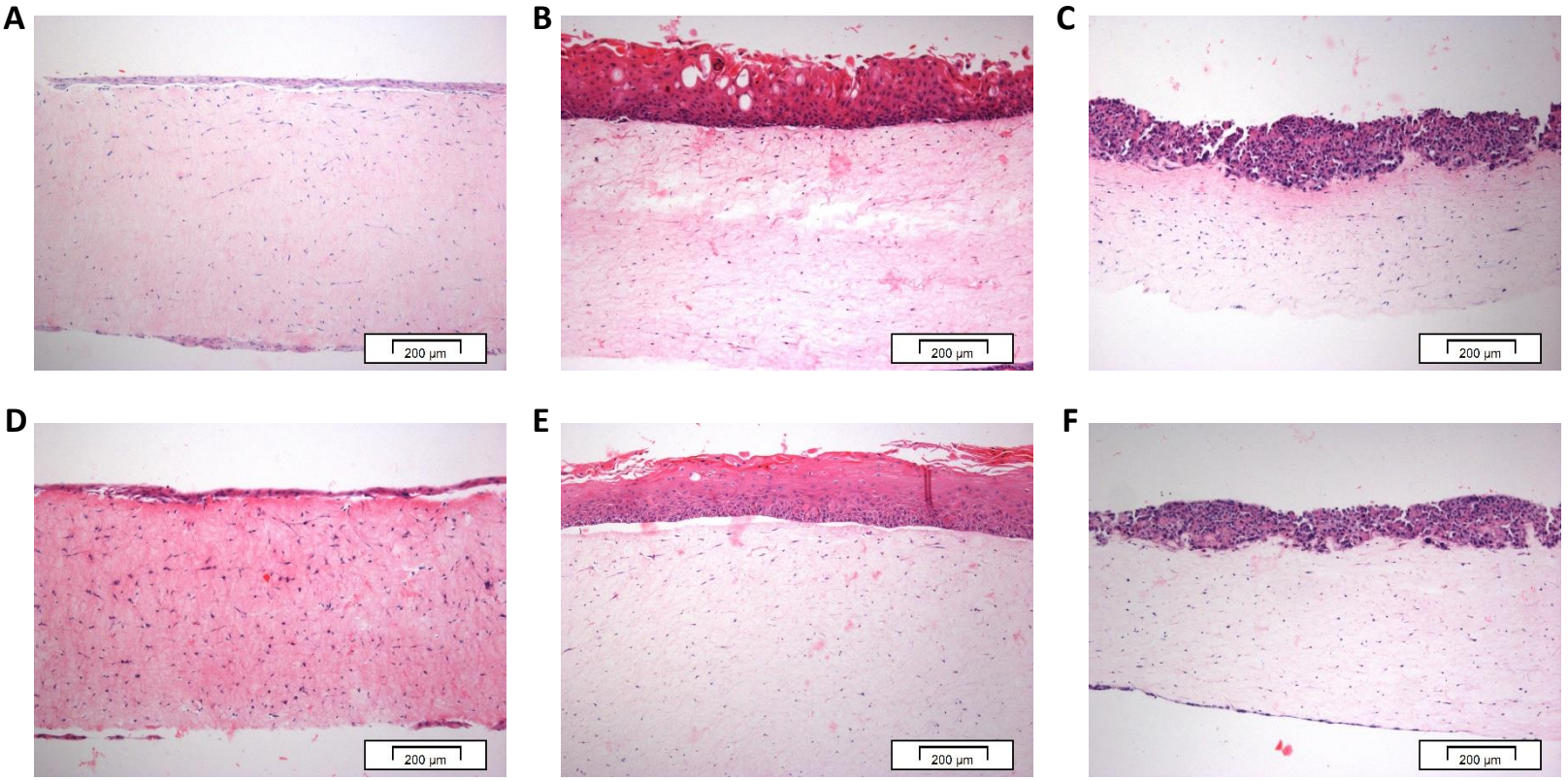

Figure 7.4. Histology of models containing normal oral keratinocytes, immortalised keratinocyte cell line, FNB6, or oral squamous cell carcinoma cell line, H357, in the absence or presence of monocyte-derived macrophages. Tissue engineered oral mucosa models containing normal oral fibroblasts (NOF) in addition to normal oral keratinocytes (NOK, **A** and **D**), immortalised keratinocytes, FNB6, (**B** and **E**) or oral squamous cell line, H357, (**C** and **F**) in the absence (**A-C**) or presence (**D-E**) of monocyte-derived macrophages (MDM) were cultured at air-liquid interface for 14 days. Models were formalin fixed, sectioned and stained with H&E. Data are representative of two independent experiments using NOK from different patients (n=2). Scale bars indicates 200 µm.

Models containing NOK demonstrated a thin epithelium compared to those containing FNB6 or H357 cells. In those models containing FNB6 cells, a thick, multi-layered epithelium could be observed with apical-basal polarity, forming a stratified epithelium. Whilst models containing an H357 epithelium were also several layers thick, no stratification was observed, instead the epithelium was disordered with evidence of some epithelial invasion into the connective tissue. Within the connective tissue, cells were evenly distributed and the ECM itself stained pink indicating matrix deposition by fibroblasts.

7.3.1 Monocyte-derived macrophages appear to express key macrophage markers at varying levels in response to co-culture with normal oral keratinocytes, FNB6 or H357 cells

Following the optimisation of controls required for the analysis of MDM cultured within a collagen hydrogel, the multi-colour flow cytometry panel developed in Chapter 6 was used to quantitatively measure differences in the expression of CD36, CD80, CD86, CD163 and CD206. Models containing MDM with either a NOK, FNB6 or H357 epithelium were cultured at ALI for 14 days. Models were disaggregated using collagenase IV, prepared into a single-cell suspension using a cell strainer and stained using the multi-colour flow cytometry panel developed in chapter 6. To analyse the differences in expression of the selected markers, gates to select CD14+ and CD45+ cells were set using FMO controls, and the MFI determined using separate FMO controls for each model type. The expression of CD36, CD80, CD86, CD163 and CD206 is presented as histograms **Figure 7.5** and summarised in bar charts displaying nMFI and % cells expressing each marker **Figure 7.6**.

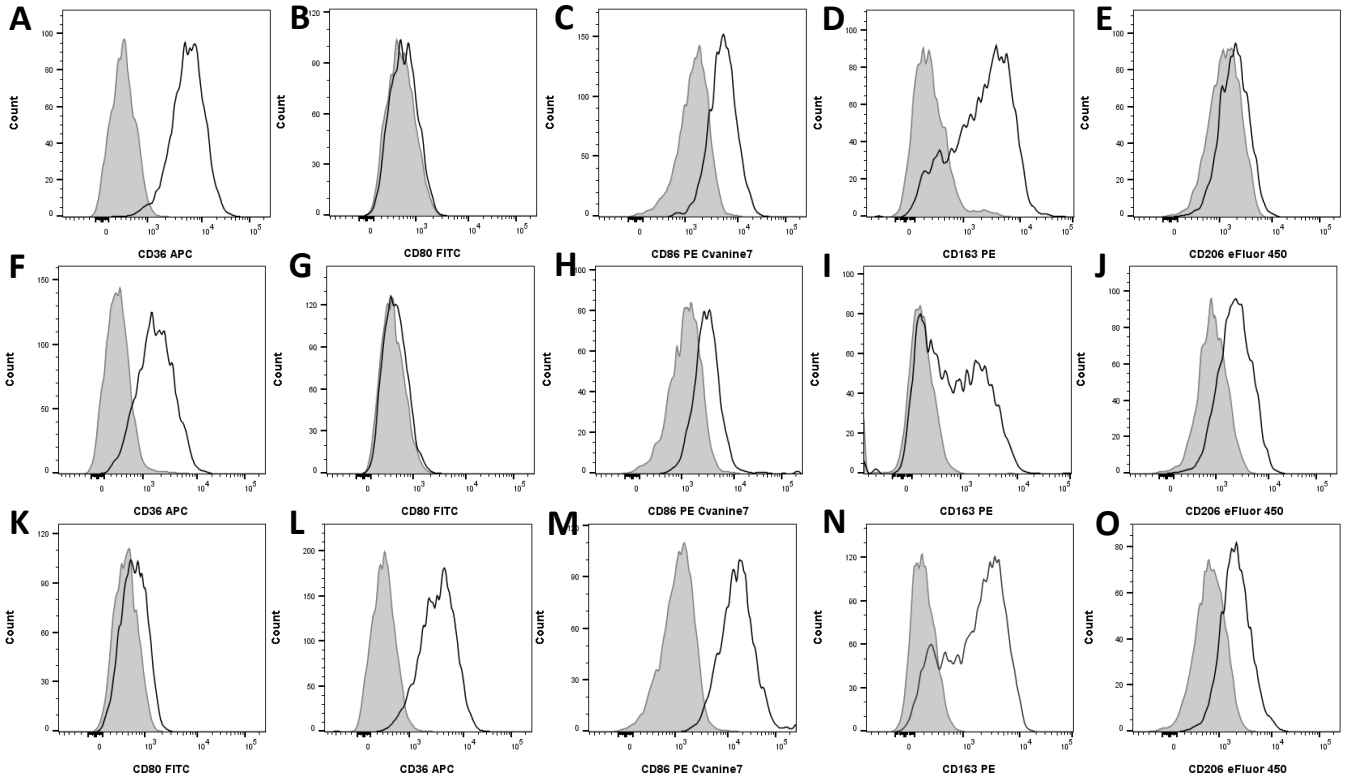

Figure 7.5. Differential expression of key markers by monocyte-derived macrophages in co-culture with normal oral keratinocytes, FNB6 and H357. Monocyte-derived macrophages (MDM) were cultured within tissue-engineered oral mucosa containing normal oral fibroblasts, in addition to normal oral keratinocytes (NOK), immortalised keratinocyte cell line, FNB6, and oral squamous cell line, H357. Following 14 days of culture at air-liquid interface, MDM were retrieved using collagenase and analysed using flow cytometry. CD14+CD45+ MDM were selected, following dead cell exclusion and the differential expression of CD36 (**A**, **F** and **K**), CD80 (**B**, **G** and **L**), CD86 (**C**, **H** and **M**), CD163 (**D**, **I** and **N**) and CD206 (**E**, **J** and **O**) in response to co-culture with normal oral keratinocytes (NOK, **A-E**), FNB6 (**F-J**) and H357 (**K-O**) was determined. Data shown are for a single experiment (n=1).

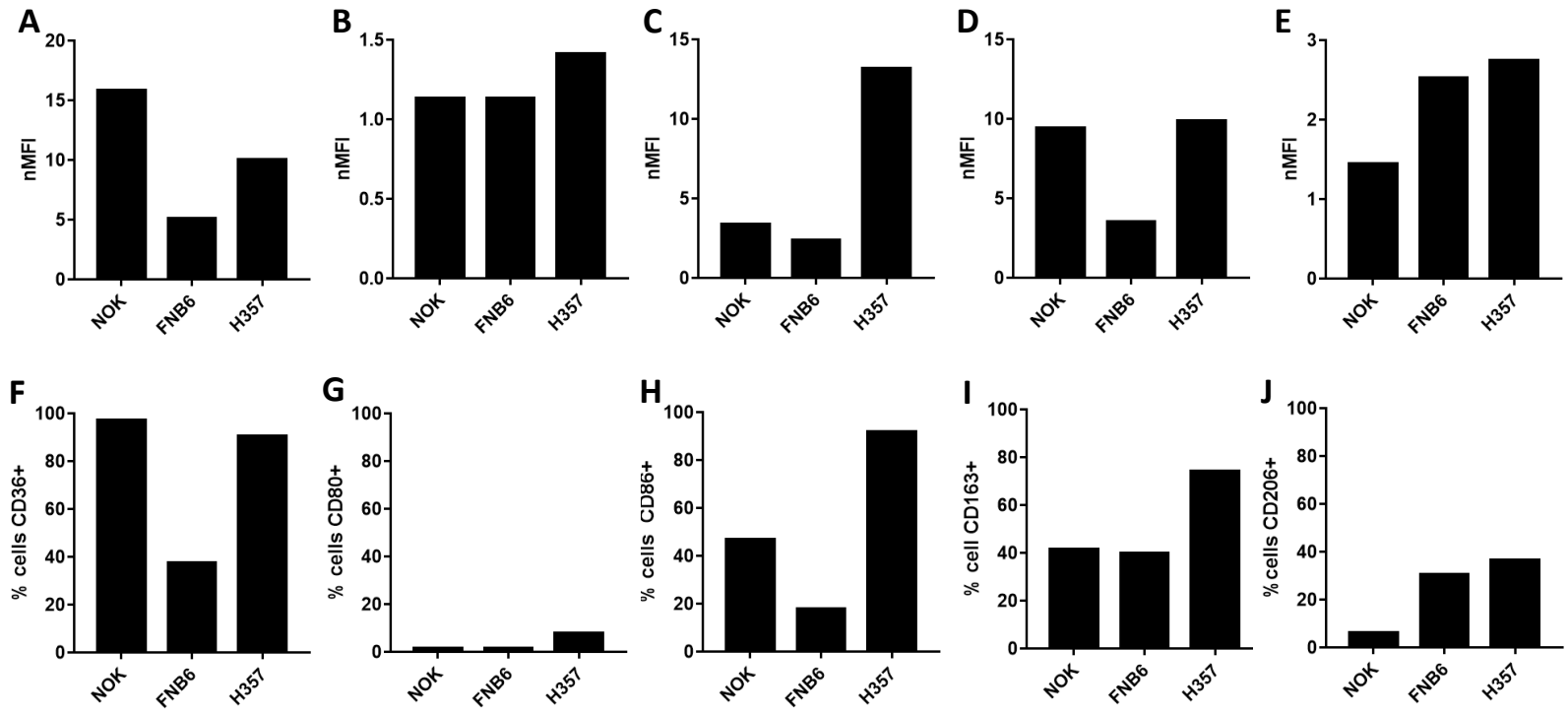

Figure 7.6. Protein expression of monocyte-derived macrophages isolated from engineered oral mucosa models containing normal oral keratinocyte, immortalized keratinocytes, FNB6, and oral squamous cell line, H357, epithelia. Monocyte-derived macrophages (MDM) were cultured within tissue-engineered oral mucosa containing normal oral fibroblasts, in addition to normal oral keratinocytes (NOK), immortalised keratinocyte cell line, FNB6, and oral squamous cell line, H357. Following 14 days of culture at air-liquid interface, MDM were retrieved using collagenase and analysed using flow cytometry. CD14+CD45+ MDM were selected, following dead cell exclusion and the differential expression of CD36 (**A** and **F**), CD80 (**B** and **G**), CD86 (**C** and **H**), CD163 (**D** and **I**) and CD206 (**E** and **J**) in response to co-culture with normal oral keratinocytes (NOK, **A-E**), FNB6 (**F-J**) and H357 (**K-O**) was determined as normalized median fluorescence intensity (nMFI) and percentage cell expressing the selected marker. Data are summarised from a single experiment (n=1).

Following co-culture of MDM with NOK, FNB6 and H357 keratinocytes, changes in the expression of key macrophage markers were observed. Models containing NOK contained a higher percentage of MDM expressing CD36 at 97.0 % compared to 37.3 % in FNB6 models and 90.4 % in H357 models. Similarly, the nMFI of CD36 expression was highest in NOK-containing models at 15.8 compared to 5.1 for FNB6 models and 10.0 for H357 models. Models containing H357 keratinocytes showed the highest percentage expression of CD80 with 7.6 % of cells expressing this antigen compared to 1.5 % in NOK models and 1.4 % in FNB6 models. This was reflected in nMFI data that showed the highest nMFI for H357 containing models at 1.4 compared to models containing NOK and FNB6 keratinocytes that both showed an nMFI of 1.1. Similarly, the highest percentage of CD86+ cells was found in models containing H357 cells as these made up 91.6 % of the cells compared to 46.8 % in NOK models and 17.8 % in FNB6 models. The nMFI for $CD86^{PE\ Cyanine7}$ was also highest in models containing H357 at 13.2 compared to 3.3 for NOK-containing models and 2.4 in FNB6-containing models. MDM cultured with H357 keratinocytes included the most CD163+ cells at 74.1 % compared to 41.5 % in NOK-containing models and 39.8 % in FNB6-containing models. Whilst the percentage expression of CD163 was much higher for H357 models, the nMFI of $CD163^{PE}$ measured for MDM cultured in the presence of NOK and H357 was very similar at 9.4 and 9.9 respectively, compared to 3.5 for MDM cultured with FNB6. The expression of CD206 increased from NOK to FNB6 to H357 models, with nMFI increasing from 1.4 to 2.5 to 2.7 respectively and the percentage of CD206+ cells increasing from 6.1 % to 30.4 % to 36.4 % respectively.

7.3.2 Contraction of tissue-engineered models containing monocyte-derived macrophages and either normal oral keratinocytes, FNB6 or H357 cells

Following 14 days of culture at ALI of models containing NOF with NOK, FNB6 or H357 keratinocytes in the presence or absence of MDM, the surface area of each model was measured to determine amount of contraction using ImageJ (**Figure 7.7**). This variation of a collagen contraction may provide an indication of the activation of fibroblasts within the co-culture.

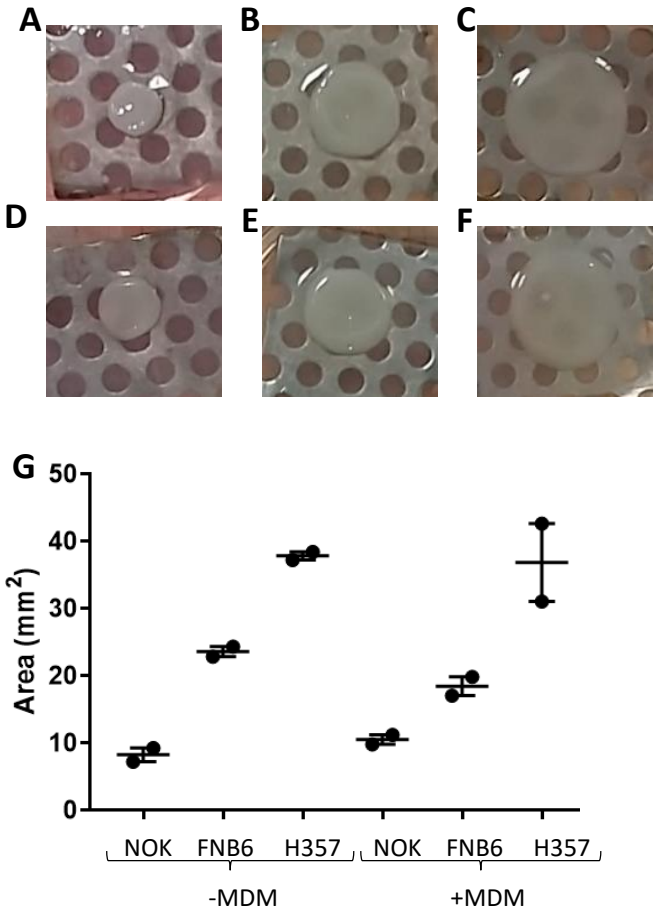

Figure 7.7. Contraction of hydrogels incorporating monocyte-derived macrophages, normal oral keratinocytes, immortalised keratinocytes, FNB6, and oral squamous cell line, H357. Monocyte-derived macrophages (MDM) were cultured within tissue-engineered oral mucosa containing normal oral fibroblasts, in addition to normal oral keratinocytes (NOK, **A** and **D**), immortalised keratinocyte cell line, FNB6 (**B** and **E**), and oral squamous cell line, H357 (**C** and **F**). Following 14 days of culture at air-liquid interface, hydrogels were analysed using a contraction assay. Images show contracted hydrogels (**A-F**) for models devoid of MDM (**A-C**) or containing MDM (**D-F**). Images are representative of two independent experiments, using different patient NOK, measured in duplicate (n=2). Column chart summarises the area of each model (**G**).

All models were set in a 24-well plate with surface area of 20.0 mm^2. Following culture for 14 days, models containing NOK had contracted the most, with the surface area decreasing to 8.2 mm^2 and 10.5 mm^2, in both the absence and presence of MDM, respectively. Models containing FNB6 cells were 23.6 mm^2 and 18.4 mm^2 after 14 days and models containing H357 keratinocytes were the largest at 37.8 mm^2 and 36.8 mm^2 in the absence and presence

of MDM respectively. The presence of MDM did not appear to affect the contraction of models.

7.3.3 The stiffness of tissue-engineered oral mucosa containing monocyte-derived macrophages, normal oral keratinocytes, FNB6 and H357 cells

Following culture of tissue-engineered models with NOF and NOK, FNB6 or H357 epithelium in the absence or presence of MDM, models were analysed using rheometry to determine whether changes in the epithelial cell type may be linked to matrix stiffness. Samples were analysed between parallel plates in a humidified environment and the elastic modulus at 0.1 Hz was measured to determine tissue stiffness (**Figure 7.8**).

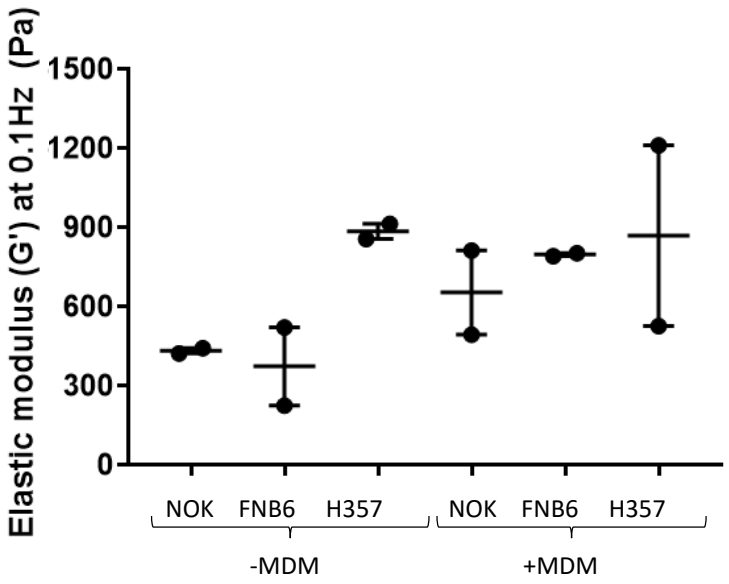

Figure 7.8. Differences in the stiffness of tissue-engineered oral mucosa containing normal oral keratinocytes, immortalised keratinocyte cell line, FNB6, and oral squamous cell line, H357. Monocyte-derived macrophages (MDM) were cultured within tissue-engineered oral mucosa containing normal oral fibroblasts, in addition to normal oral keratinocytes (NOK, **A** and **D**), immortalised keratinocyte cell line, FNB6 (**B** and **E**), and oral squamous cell line, H357 (**C** and **F**). Following 14 days of culture at air-liquid interface, hydrogels were analysed using rheometry. The elastic modulus (stiffness) of tissue-engineered oral mucosa containing NOK, FNB6 and H357 in the presence or absence of MDM was measured. Data are representative of two independent experiments (n=2).

Models containing H357 displayed a higher elastic modulus at 884 Pa and 868 Pa in the absence and presence of MDM respectively compared to models containing both NOK and H357. In the absence of MDM, models containing FNB6 displayed the lowest elastic modulus at 373 Pa compared to 432 Pa for models containing NOK. However, in the presence of MDM, models containing NOK displayed the smallest elastic modulus at 653 Pa compared to 797 Pa for models containing FNB6 keratinocytes. Additionally, all models containing MDM appeared to display an increase in stiffness compared to their MDM-free equivalents.

7.4 The interaction of polarised monocyte-derived macrophages on models containing an FNB6 epithelium

A previously published model of human skin SCC showed an increase in the invasion of epithelial cells in response to polarised macrophages (Linde *et al.,* 2012). Polarised MDM, added to tissue-engineered models containing FNB6 cells, were cultured in the presence of additional polarising cytokines as previously described (Linde *et al.,* 2012).

Initial experiments to incorporate polarised macrophages into the 3D tissue-engineered model of oral mucosa developed in this work, involved the polarising of MDM in 2D using polarising cytokines described in **Table 2.3**. The addition of these cytokines was maintained once models containing FNB6 cells and polarised MDM were established. The data presented here is very preliminary, as appropriate FMO controls could not be performed due to a lack of MDM. Following 14 days of culture, separate tissue-engineered models were analysed using histology (**Figure 7.9**), flow cytometry (**Figure 7.10** and **Figure 7.12**), rheometry (**Figure 7.14**), and a contraction assay (**Figure 7.15**).

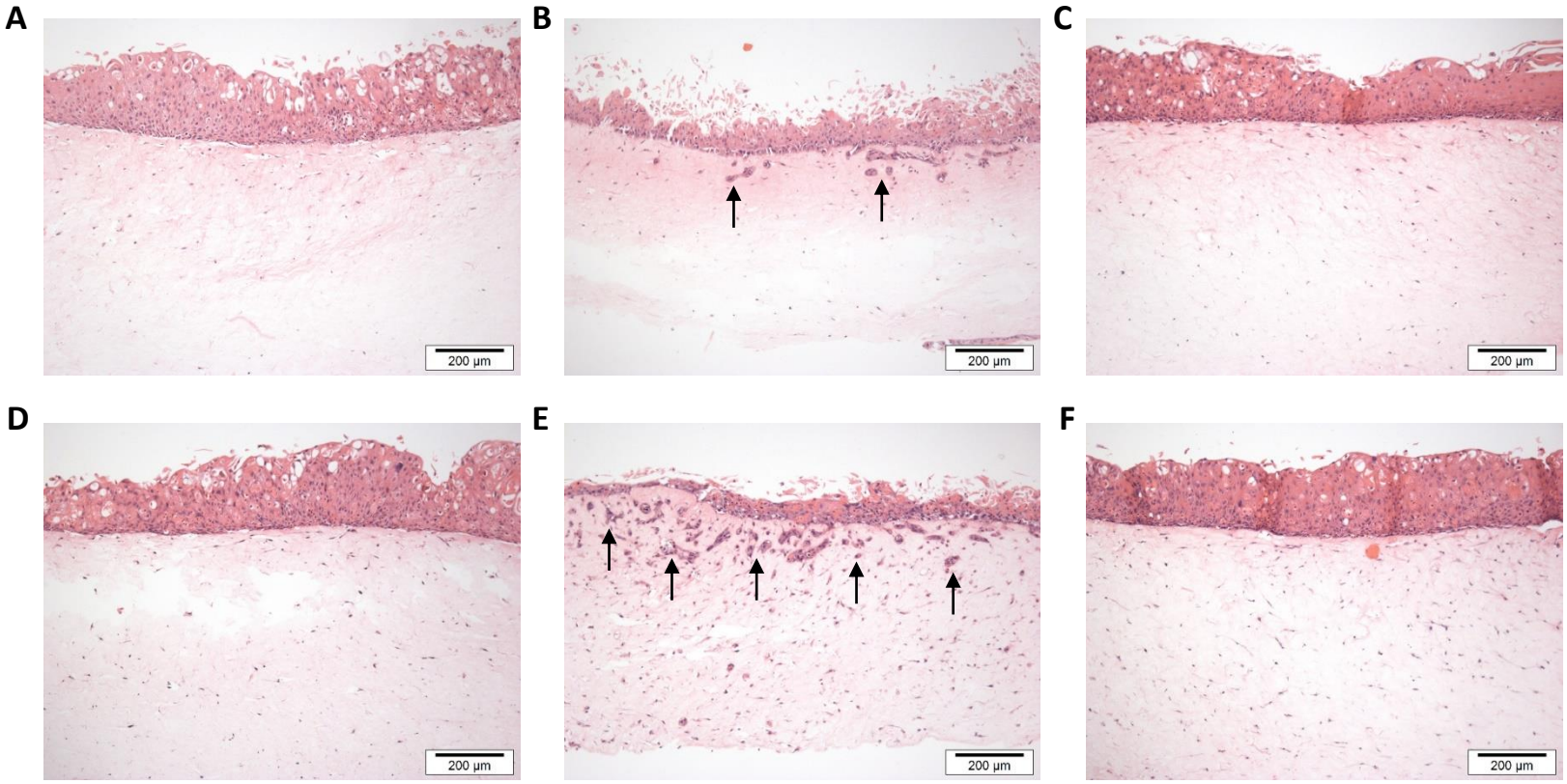

Figure 7.9. Invasion of immortalised FNB6 cell line into tissue engineered models containing polarised monocyte-derived macrophages. Tissue engineered oral mucosa containing immortalised keratinocyte cell line, FNB6, and normal oral fibroblasts, in the absence (**A-C**) or presence (**D-E**) of monocyte-derived macrophages (MDM) were cultured in the absence (**A** and **D**) or presence of M1 cytokines (**B** and **E**) or M2 cytokines (**C** and **F**) at air-liquid interface. Following 14 days of culture, models were formalin fixed, sectioned and stained with H&E. Data are representative of a single experiment (n=1). Arrows indicate areas of epithelial invasion and scale bars indicate 200 µm.

Histological analysis of tissue-engineered models of the oral mucosa containing polarised MDM co-cultured with an FNB6 epithelium indicates that the presence of GM-CSF, IFNγ and LPS induces higher levels of invasion (arrows) compared to the incorporation of both M0 and M2-polarised macrophages. Interestingly, the M1 cocktail of cytokines promotes epithelial invasion in the absence of MDM, but is noticeably more prominent in the presence of MDM.

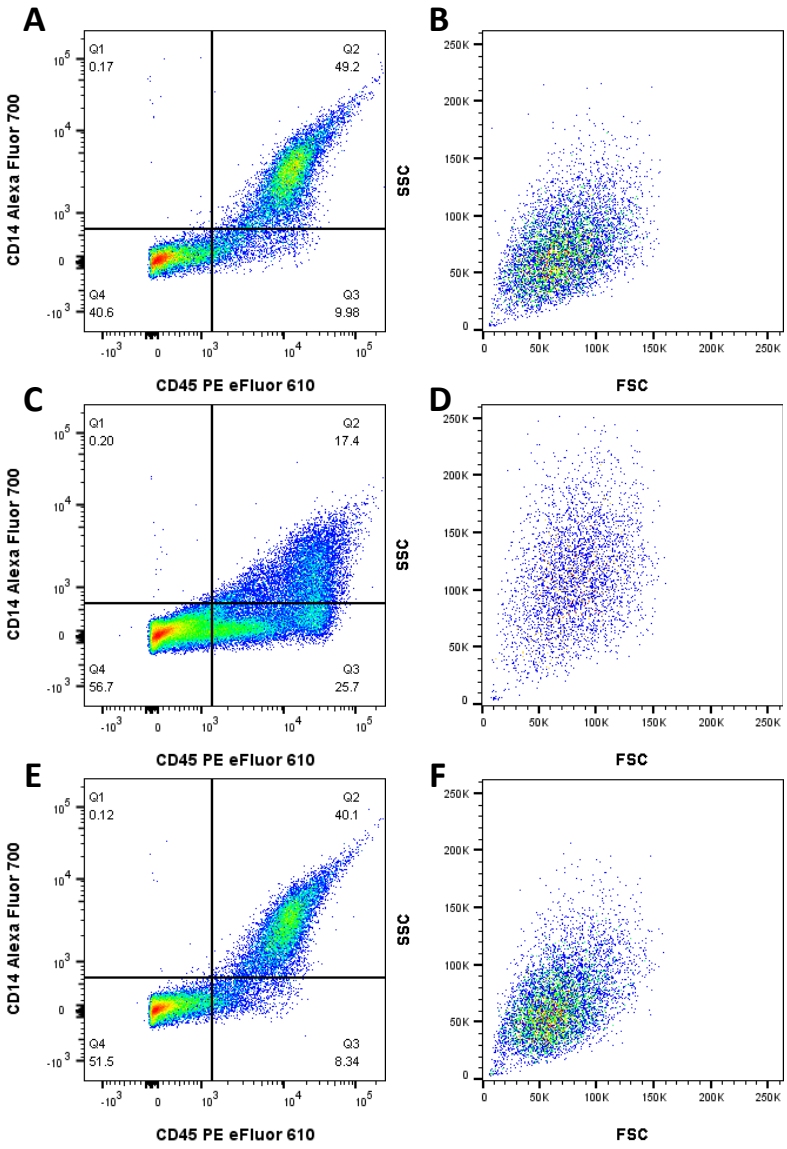

Figure 7.10. Monocyte-derived macrophages change in morphology and expression of CD14 and CD45 in response to M1 or M2 polarisation when cultured within tissue-engineered oral mucosa models containing immortalised keratinocyte cell line, FNB6. Tissue engineered oral mucosa containing immortalised keratinocyte cell line, FNB6, and normal oral fibroblasts, in addition to monocyte-derived macrophages (MDM) were cultured in the absence (**A**-**B**) or presence of M1 cytokines (**C**-**D**) or M2 cytokines (**E**-**F**) at air-liquid interface. Following 14 days of culture, MDM were retrieved using collagenase IV and analysed using flow cytometry. MDM showed differences in CD14 and CD45 expression (**A**, **C** and **E**) and changes in size (FSC) and granularity (SSC, **B**, **D** and **F**) in response to polarisation cytokines. Data shown are for a single experiment (n=1) and gates were based on unstained samples in the absence of fluorescence-minus-one controls.

The use of the multi-colour flow cytometry panel developed in Chapter 6 enabled polarised MDM to be selected using CD14 and CD45 and separated from FNB6 and NOF for analysis. In models containing M0 and M2 MDM, higher percentages of CD14+CD45+ cells were selected (49.2 % and 40.1 % respectively) compared to 17.4 % in models containing M1 MDM. Of these CD14+CD45+ events, differences were observed in the FSC and SSC. In models containing M0 MDM, FSC was 68352 and SSC was 66560. In models containing M1 MDM, FSC was 80320 and SSC was 109312. In models containing M2 MDM, FSC was 63360 and SSC was 61312. This could be visualised in dot plots which showed that M1 MDM isolated from the model were larger and more granular than those from M0 and M2 polarised MDM models.

Due to the reduced percentage of CD14+CD45+ events in M1 polarised MDM, the expression of markers was also assessed for CD45+ events (**Figure 7.11**).

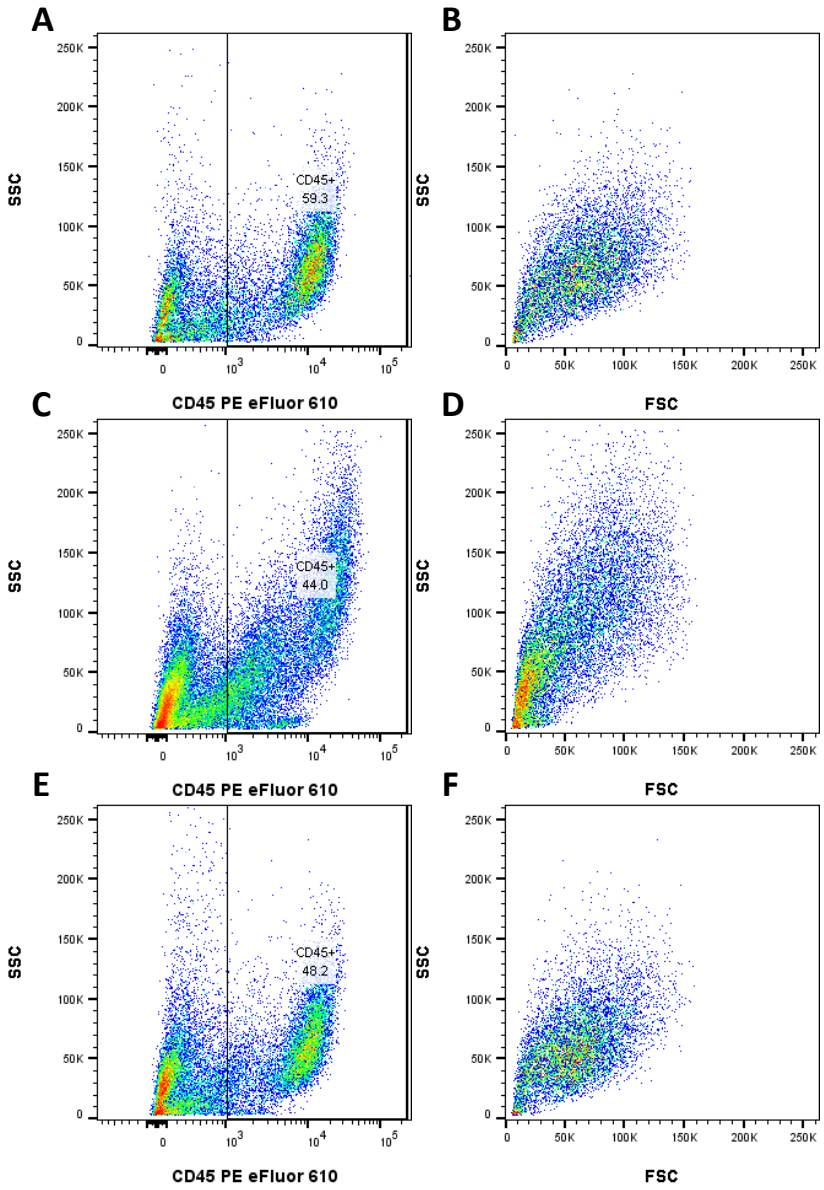

Figure 7.11. CD45+ monocyte-derived macrophages change in morphology and expression of CD14 and CD45 of monocyte-derived macrophages polarised in 3D culture models containing immortalised keratinocyte cell line, FNB6. Tissue engineered oral mucosa containing immortalised keratinocyte cell line, FNB6, and normal oral fibroblasts, in addition to monocyte-derived macrophages (MDM) were cultured in the absence (**A**-**B**) or presence of M1 cytokines (**C**-**D**) or M2 cytokines (**E**-**F**) at air-liquid interface. Following 14 days of culture, MDM were retrieved using collagenase IV and analysed using flow cytometry. MDM showed differences in CD45 expression (**A**, **C** and **E**) and changes in size (FSC) and granularity (SSC, **B**, **D** and **F**) in response to polarisation cytokines. Data shown are for a single experiment (n=1) and gates were based on unstained samples in the absence of fluorescence-minus-one controls.

Due to the reduced percentage of CD14+CD45+ events in M1 polarised MDM, the expression of macrophages polarisation markers was also assessed for CD45+ events. In models containing M0 MDM, FSC was 61376 and SSC was 61696. In models containing M1 MDM, FSC was 41280 and SSC was 68992. In models containing M2 MDM, FSC was 57172 and SSC was 57536. This could be visualised in dot plots which showed that M1 MDM isolated from the model were more granular than those from M0 and M2 polarised MDM models. This is comparable to data analysed from CD14+CD45+ events, and from MDM cultured in 2D.

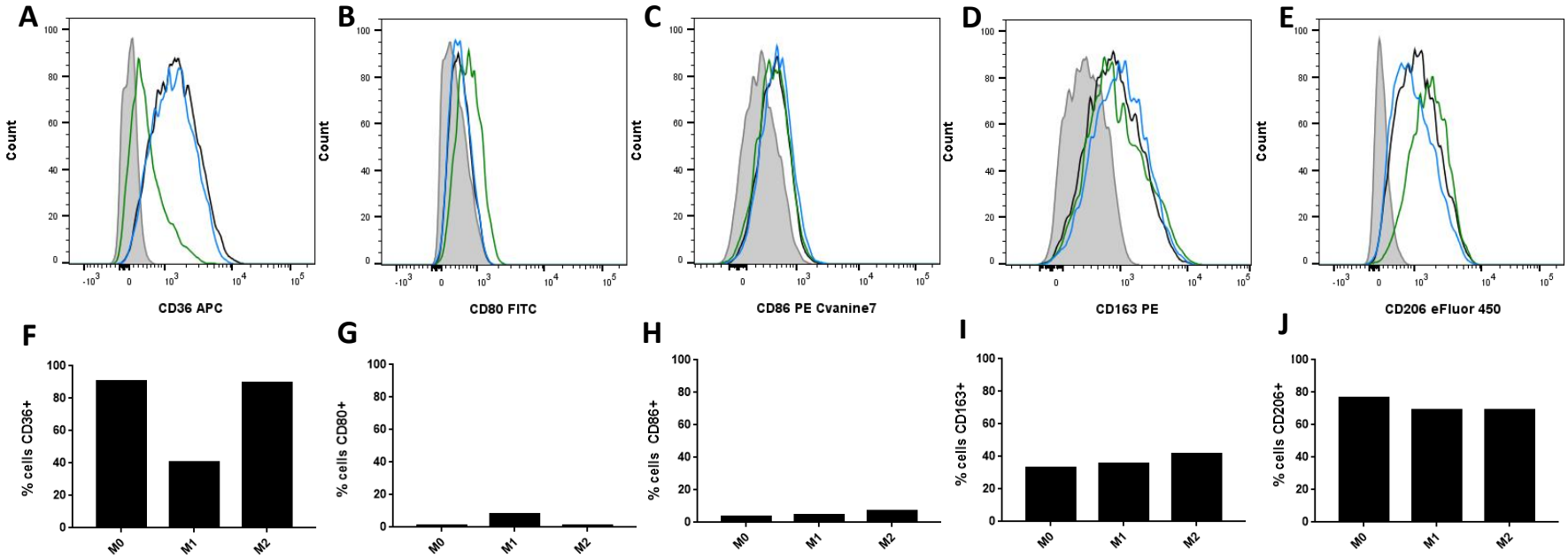

Figure 7.12. The differential expression of macrophage markers by CD14+CD45+ monocyte-derived macrophages within oral mucosa models containing immortalised keratinocyte cell line, FNB6, in response to polarisation cytokines. Tissue engineered oral mucosa containing immortalised keratinocyte cell line, FNB6, and normal oral fibroblasts, in addition to monocyte-derived macrophages (MDM) were cultured in the absence (M0, black line) or presence of M1 cytokines (green line) or M2 cytokines (blue line) at air-liquid interface. Following 14 days of culture, MDM were retrieved from the collagen hydrogels using collagenase IV and their expression of CD36 (**A** and **F**), CD80 (**B** and **G**), CD86 (**C** and **H**), CD163 (**D** and **I**) and CD206 (**E** and **J**) was measured using flow cytometry. Samples were compared to an unstained sample (grey, filled histogram) and median fluorescence measured (**A-E**). Gates to determine percentage expression (**F-J**) were set compared to an unstained sample in the absence of fluorescence-minus-one controls. Data are representative of a single experiment measured (n=1).

Using multi-colour flow cytometry, the expression of CD36, CD80, CD86, CD163 and CD206 could be measured on CD14+CD45+ events retrieved from models containing FNB6 cells and polarised MDM. The nMFI of CD36 was very similar in M0 and M2 MDM at 1394 and 1330, respectively, compared to 421 for M1 MDM. A similar pattern was observed in the percentage of cells expressing CD36 which was measured as 90.3 %, 40.3 % and 89.4 % respectively for M0, M1 and M2 MDM. M1 MDM displayed the highest expression of CD80 with an nMFI of 748 compared to 516 and 513 for M0 and M2 MDM. A similar pattern was also observed for the percentage of cells expressing CD80, which was 0.8 % for M0, 8.0 % for M1 and 0.8 % for M2 MDM. The nMFI for CD86 expression in M0, M1 and M2 MDM respectively was 460, 441 and 503. The percentage of cells expressing CD86 was 3.6 %, 4.4 % and 7.0 % respectively for M0, M1 and M2 MDM. The highest percentage of CD163+ cells were identified in M2 MDM-containing models with 41.5 % identified compared to 32.8 % in M0 MDM and 35.6 % in M1 MDM models. The nMFI representing CD163 expression was similar between M0 and M2 MDM at 1394 and 1330 respectively, compared to 421 in models containing M1 MDM. The expression of CD206 was very similar in all 3 culture conditions, with nMFI measured as 1101, 1600 and 914 for M0, M1 and M2 MDM respectively. The percentage of cells expressing CD206 was 76.4 %, 92.3 % and 68.8 % for M0, M1 and M2 respectively.

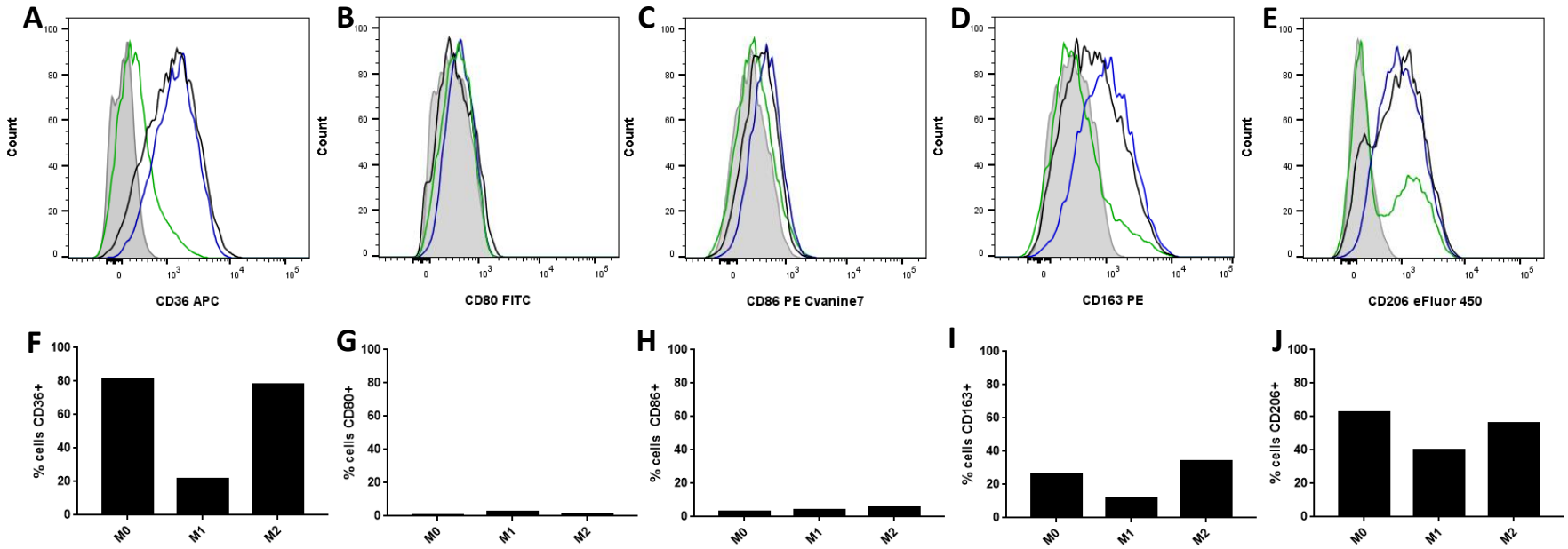

Figure 7.13. The differential expression of macrophage markers by CD45+ monocyte-derived macrophages within oral mucosa models containing immortalised keratinocyte cell line, FNB6, in response to polarisation cytokines. Tissue engineered oral mucosa containing immortalised keratinocyte cell line, FNB6, and normal oral fibroblasts, in addition to monocyte-derived macrophages (MDM) were cultured in the absence (M0, black line) or presence of M1 cytokines (green line) or M2 cytokines (blue line) at air-liquid interface. Following 14 days of culture, MDM were retrieved from the collagen hydrogels using collagenase IV and their expression of CD36 (**A** and **F**), CD80 (**B** and **G**), CD86 (**C** and **H**), CD163 (**D** and **I**) and CD206 (**E** and **J**) was measured using flow cytometry. Samples were compared to an unstained sample (grey, filled histogram) and median fluorescence measured (**A-E**). Gates to determine percentage expression (**F-J**) were set compared to an unstained sample in the absence of fluorescence-minus-one controls. Data are representative of a single experiment measured (n=1).

The expression of CD36, CD80, CD86, CD163 and CD206 was also measured on CD45+ MDM retrieved from models containing FNB6 cells and polarised MDM. The nMFI of CD36 was 9.9, 2.2 and 9.3 for M0, M1 and M2 MDM respectively. The nMFI of CD80 was 1.2, 1.1 and 1.2 for M0, M1 and M2 MDM respectively. The nMFI of CD86 was 1.5, 1.1 and 4.2 for M0, M1 and M2 MDM respectively. The nMFI of CD163 was 1.0, 1.1 and 2.3 for M0, M1 and M2 MDM respectively. The nMFI of CD206 was 5.8, 2.0 and 4.8 respectively for M0, M1 and M2 MDM respectively.

In addition, 81.0 %, 21.3 %, 78.2 % of MDM were CD36+ in M0, M1 and M2 MDM respectively. For CD80, 0.7 %, 2.5 % and 1.0 % of events were CD80+ for M0, M1 and M2 MDM respectively. Of the 45 + event, 2.9 %, 4.2 % and 5.7 % were CD86+ in M0, M1 and M2 stimulated MDM respectively. For CD163, 26.2 %, 11.4 % and 34.0 % were CD163+ in M0, M1 and M2 stimulated samples respectively. Lastly, 62.6 %, 39.8 % and 55.9 % of events were CD206+ in M0, M1, and M2 stimulated MDM respectively. Whilst the expression patterns for CD36, CD80 and CD86 were similar in CD14+CD45+ and CD45+ events, the expression patterns for CD163 and CD206 varied slightly.

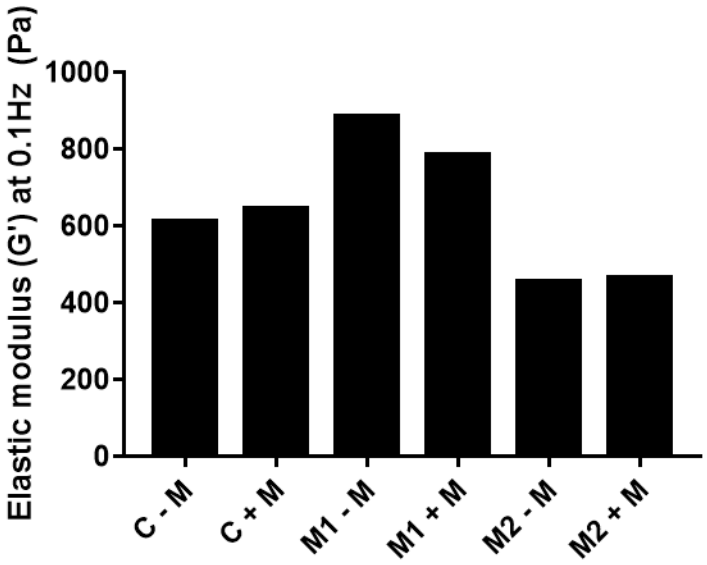

Figure 7.14. Hydrogel stiffness may be linked to macrophage polarisation. Tissue engineered oral mucosa containing immortalised keratinocyte cell line, FNB6, and normal oral fibroblasts, in the absence (-) or presence (+) of monocyte-derived macrophages (MDM) were cultured in the absence (C = control) or presence of M1 cytokines or M2 cytokines at air-liquid interface. Following 14 days of culture, collagen hydrogels were analysed using rheometry and the elastic modulus (stiffness) measured. Data are representative of a single experiment measured in duplicate (n=1).

The addition of M2-polarised macrophages appeared to have very little effect on the stiffness of the engineered tissue compared to the inclusion of un-stimulated macrophages. However, the addition of M1-stimulated macrophages and the addition of M1-polarising cytokines resulted in an increase in the stiffness of tissues both containing and devoid of macrophages.

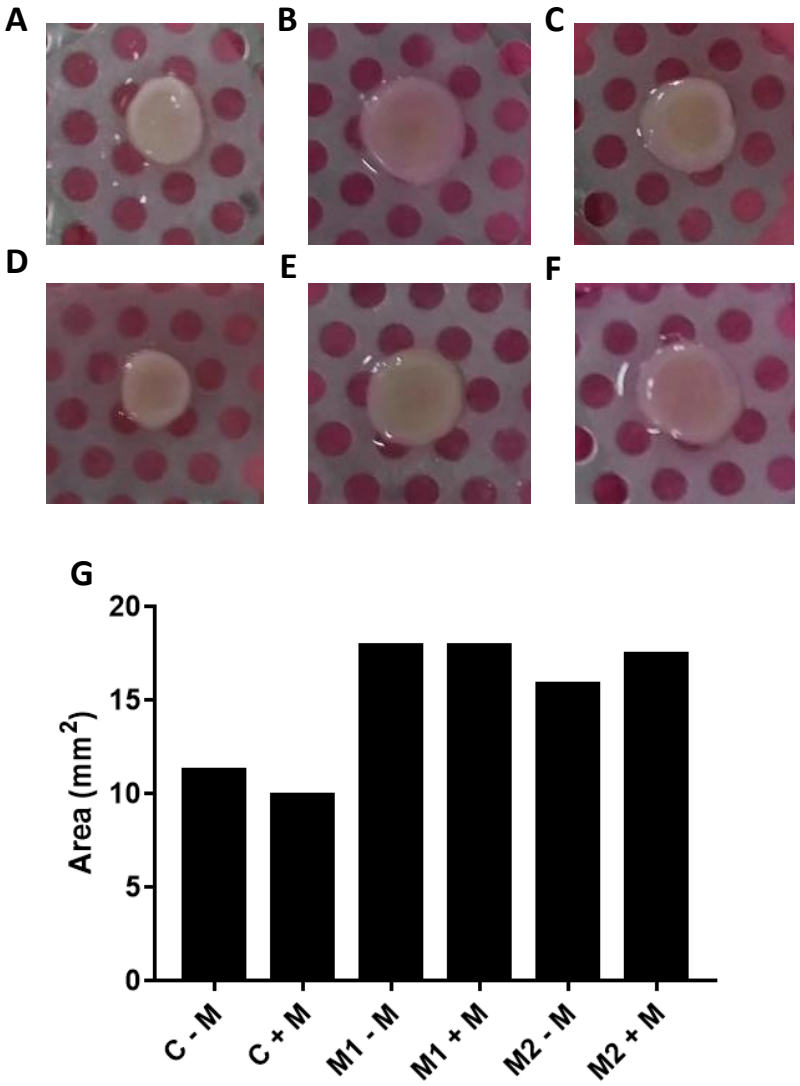

Figure 7.15. **Contraction of tissue-engineered oral mucosa model containing FNB6 and polarised monocyte-derived macrophages.** Tissue engineered oral mucosa containing immortalised keratinocyte cell line, FNB6, and normal oral fibroblasts, in the absence (-) or presence (+) of monocyte-derived macrophages (MDM) were cultured in the absence (C = control) or presence of M1 cytokines or M2 cytokines at air-liquid interface. Following 14 days of culture, collagen hydrogels were analysed using a contraction assay. Data are representative of a single experiment measured in duplicate (n=1). Images show models cultured alone (**A** and **D**) or with M1-stimulation (**B** and **E**) or M2-stimulation (**C** and **F**) either in the absence (**A-C**) or presence (**D-F**) of monocyte-derived macrophages (MDM). Images are representative of a single experiment, measured in duplicate (n=1). Column chart summarises the area of each model (**G**).

All models were set in a 24-well plate with surface area measuring 20 mm^2. During 14 days of culture, models containing un-stimulated MDM (M0) contracted the most, with surface area decreasing to 12.07 mm^2 and 10.00 mm^2 in models devoid or containing MDM, respectively. Models containing M1 polarised MDM were measured as 19.57 mm^2 and 18.69 mm^2 in the absence or presence of MDM respectively, and those models containing M2 polarised MDM were measured as 16.47 mm^2 and 17.05 mm^2 in the absence or presence of MDM respectively.

7.5 Discussion

Whilst much of the work described in this chapter is very preliminary, it demonstrates that the tissue-engineered model of the oral mucosa containing MDM developed in chapter 5 may be analysed using the multi-colour flow cytometry panel developed in chapter 6.

Effects of collagenase treatment on macrophage marker expression

Collagenases cleave helical regions of collagens at specific sites and were first prepared for research use in 1953 (Mandl *et al.,* 1953). Collagenase IV is often used in the disaggregation of human tissue and has been shown to offer improved disaggregation compared to other collagenases (Crabbe *et al.,* 1997). In particular, collagenase IV has a low tryptic value compared to other collagenases and therefore is more suited for use on cells analysed by flow cytometry as damage to membrane receptors is limited. Previous data has shown that collagenase type I decreased the expression of various surface markers on lymphocytes analysed using flow cytometry (Abuzakouk *et al.,* 1996). Therefore, the expression of the markers selected for analysis on 3D-cultured MDM was compared with and without additional treatment with collagenase IV. No significant difference in the expression of these antigens was observed, suggesting that disaggregation of tissue-engineered models could be achieved using collagenase IV without affecting marker expression.

7.5.1 Oral mucosa models containing monocyte-derived macrophages in the presence of normal oral keratinocytes, FNB6 and H357

During cancer progression, invasion of the epithelium into the connective tissue is characteristic of malignant transformation. Here, epithelial cells breach the basement membrane and begin to form clusters within the connective tissue (Bradley *et al.,* 2010). Preliminary data in chapter 5 showed an increase in the invasion of H357 cells into the connective tissue of models containing THP-1 monocytes, which was not observed in their absence, but was also demonstrated in models containing FNB6 cells. Therefore, it was hypothesised that macrophages may promote epithelial invasion.

In this chapter, models containing NOK, FNB6 and H357 cells were cultured for 14 days in the presence or absence of MDM and invasion analysed using histology. Contrary to the hypothesis, none of these models showed signs of epithelial invasion. No other models containing MDM comparing invasion in response to different epithelia could be found, although differences in epithelial invasion of models containing polarised macrophages are discussed below (**Page 234**).

A novel multi-colour flow cytometry panel was developed to analyse the expression of a range of macrophage polarisation markers on cells cultured within a 3D tissue-engineered model containing epithelial cells and fibroblasts. Previously, it has not been possible to quantitatively measure the expression of CD14, CD36, CD45, CD80, CD86, CD163 and CD206 simultaneously, or from macrophages cultured in 3D. Although preliminary, this data showed differences in the expression of these markers. Most importantly, the percentage of macrophages expressing CD163 increased from 41.5 % in NOK models and 39.8 % in FNB6 models to 74.1 % in H357 models. This is in line with previously published literature which shows an increase in the expression of CD163 in invasive oral cancers (Fujita *et al.,* 2014; Mori *et al.,* 2011; Weber *et al.,* 2014; Wehrhan *et al.,* 2014). The emerging use of CD163 for immunostaining of oral cancer biopsies to determine diagnosis and prognosis demonstrates the importance of this flow cytometry panel to quantitatively measure the changes in level of expression and the percentages of cells expressing this key marker.

Additionally, immunohistochemical analysis of OSCC specimens rarely detected CD80+ cells in lower grade specimens, and even less in higher grades of tumour (Mori *et al.,* 2011). The ability of this panel to detect even small numbers of cells in a tissue-engineered sample will provide a greater understanding of the phenotypes of macrophages found residing within tissues.

Collagen hydrogels are widely used to analyse the contraction of fibroblasts, particularly to understand wound healing processes. During wound healing, inflammation and proliferation of cells is followed by tissue remodelling, and wound closure which requires tissue deposition, epithelialisation and contraction (Bagul *et al.,* 2015). Many parallels can be drawn between the wound healing and tumour microenvironments, particularly due to the activation of fibroblasts to myofibroblasts, matrix remodelling, angiogenesis and the release of TGFβ (Kalluri and Zeisberg, 2006). Myofibroblasts display a highly contractile phenotype, which can be induced by TGFβ (Grinnell, 1994). In the tumour microenvironment, TGFβ is released by cancer cells, which activates fibroblasts to adopt a contractile phenotype and release further TGFβ to form a positive feedback loop (Comito *et al.,* 2014; Kobayashi *et al.,* 2005). In addition, any changes in the ECM can also activate fibroblasts to adopt a more contractile phenotype (Comito *et al.,* 2014).

Contraction assays relate the activation of fibroblasts with contraction of a collagen hydrogel. Typically, a collagen hydrogel containing the cells of interest is set within a culture well, and released once set to float in culture. Over the culture period, the hydrogel may contract and the surface area can be measured to compare between different conditions (Ngo *et al.,* 2006). Measuring the surface area of models following 14 days of culture may provide an insight into the activation status of fibroblasts residing within the models.

Results in Chapter 5 showed that models containing THP-1 monocytes appeared highly contracted, with a markedly smaller surface area compared to models devoid of THP-1 cells. Therefore, it was hypothesised that immune cells may induce activation of fibroblasts to a myofibroblast phenotype. The overexpression of TGFβ is often observed in OSCC and is correlated with poor survival rates (White *et al.,* 2010). Therefore, it was hypothesised that

models containing H357 cells, which release more TGFβ than normal cells, would promote activation of fibroblasts to myofibroblasts resulting in increased contraction of the model compared to those containing NOK and FNB6 cells. In addition, models containing MDM may experience increased contraction due to cell crosstalk. To test this hypothesis, the contraction of models containing NOK, FNB6 and H357 either in the absence or presence of MDM was measured.

The preliminary results described in this chapter demonstrate that models containing NOK contracted more than those containing either FNB6 or H357 cells as a decrease in surface area was measured. In addition, the absence or presence of MDM did not appear to result in noticeable difference in contraction. Previously published data has shown that M2 macrophages activate fibroblasts to a CAF or myofibroblast phenotype which is linked with poor prognosis in prostate cancer (Comito *et al.,* 2014). Whilst data in this chapter showed an increase CD163+ MDM considered to be M2 macrophages in models containing H357 cells, the contraction associated with fibroblast activation was not observed in these models.

Tissue stiffness varies in response to normal development and disease and can vary significantly between tissues of different types (Handorf *et al.,* 2015). The stiffness of the oral mucosa can vary dramatically between different sites of the oral cavity, and between patients (Chen *et al.,* 2015). During the development of cancer, abnormal matrix deposition and the degradation of the ECM by MMPs results in an increase in matrix stiffness, which can be one of the first indicators of the presence of a tumour, such as in breast cancer, (Boyd *et al.,* 2014). The contraction of myofibroblasts in cancer tissue is responsible for the increase in stiffness of these malignancies (Bagul *et al.,* 2015). In addition to data measuring the contraction of tissue-engineered models, comparisons in tissue stiffness may provide further insight into the activation of fibroblasts. Here, a frequency sweep was performed using a rheometer to measure the elastic modulus of models containing NOK, FNB6 or H357 cells in the presence or absence of MDM.

Preliminary data showed that models containing H357 cells displayed a higher elastic modulus, indicative of an increased tissue stiffness, compared to models containing NOK or FNB6 cells. Data also showed that stiffness may be increased in models containing MDM compared to those devoid of MDM. Whilst previously published literature has measured the elastic modulus of a breast cancer cell line cultured within a 3D alginate hydrogel using AFM (Cavo *et al.,* 2016) no studies could be found that analysed the stiffness of tissue-engineered models of the oral mucosa.

7.5.2 **FNB6 models containing polarised monocyte-derived macrophages**

In the work published by Linde *et al.,* models treated with M-CSF and IL-4 showed increased tumour cell invasion and spontaneous polarisation of macrophages to an M2 phenotype was observed after 21 days of culture (Linde *et al.,* 2012). However, in this work, alternative polarising cytokines were used to those presented in this thesis, primarily, GM-CSF was not used. In an alternative study, GM-CSF was shown to enhance invasion of a colon adenocarcinoma cell line by increasing the prevalence of MMPs, especially MMPs 2, 9 and 26, present in the collagen hydrogel (Gutschalk *et al.,* 2013). Blockade of GM-CSF signalling by neutralising antibodies reduced the invasion observed (Gutschalk *et al.,* 2013). Additionally, models of skin SCC found that IL-6 promotion of invasion was GM-CSF-dependent and the use of GM-CSF neutralising antibodies drastically reduced the invasion of HaCat-ras A-5 cells (Lederle *et al.,* 2011). This published study also found that IL-6 induced the release of MCP-1 by fibroblasts and keratinocytes which correlated with an increase in MMP2, which resulted in activation of fibroblasts and promotion of invasion.

The use of HSC-3 tongue carcinoma cells within a 3D co-culture with polarised PMA-treated THP-1 cells showed an increase in the invasion of cells in response to M2 polarisation which was not observed following M1 polarisation (Pirila *et al.,* 2015). In this study, macrophages migrated towards carcinoma cells and could be found preferentially at the tumour border in patient biopsies (Weber *et al.,* 2014). Additional experiments may use anti-CD68 antibodies to detect the location of macrophages within the engineered tissue using

immunhistochemistry. Additionally, the release of MMPs could be investigated using gelatin zymography.

7.6 Conclusion

The work presented in this chapter has optimised the use of the multi-colour flow cytometry panel on the tissue engineered model of the oral mucosa developed in chapter 5. It also begins to combine the use of this model with analysis using the multi-colour flow cytometry panel developed in chapter 6. The aim of combining these two novel tools is to gain an understanding of the role that macrophages may play in oral cancer progression. The preliminary data displayed in chapter 7 shows that the expression of key macrophage markers, including CD163, are altered in response to co-culture with different epithelial cells. Previously, it has not been possible to rapidly isolate macrophages from a 3D culture environment and analyse their protein expression using multi-colour flow cytometry to measure the expression of key macrophage markers on the same cells. Whilst the combination of flow cytometry, rheometry and histology provide a useful insight into the molecular interactions between keratinocytes, fibroblasts and macrophages in the engineered tumour microenvironment, the use of additional analyses such as gene expression and gelatin zymography, as well as a more detailed immunohistochemical analyses could provide valuable information regarding the activation status of the cells present. In particular, IHC using anti-CD163 antibodies may enable comparison between the tissue-engineered model presented here and previously published studies using primary patient material.

In conclusion, preliminary data has shown that there is an increase in the percentage of cells expressing CD163 in response to co-culture with H357 cells. Further repeats of this work are required to confirm results. Further investigation could determine whether this is also true for other OSCC cell lines, and dysplastic cell lines.

8 Chapter 8: Conclusions and Future Work

8.1 Conclusions

In summary, this thesis has described the development of a 3D tissue engineered model of the oral mucosa which contains not only viable macrophages, but macrophages which respond to stimulation with LPS by secreting a pro-inflammatory cytokine, IL-6. This model has been characterised using immunohistochemistry and compared to published literature describing patient samples of the oral mucosa. In addition, a multi-colour flow cytometry panel has been developed which can quantitatively analyse the expression of CD36, CD80, CD86, CD163 and CD206 on CD14+CD45+ macrophages cultured in 3D. This thesis concludes with the optimisation and preliminary use of the multi-colour flow cytometry panel to identify CD14+CD45+ macrophages from keratinocytes and fibroblasts present in the 3D co-culture. Therefore, the data presented in this thesis provides tools necessary to improve understanding of the role macrophages play in oral cancer progression.

The interactions of the different cells of the tumour microenvironment are complex and variable. Whilst two novel tools for the analysis of the role macrophages play in oral cancer progression are presented in this thesis, further experiments would provide further insight in to the details of the mechanisms involved.

8.2 Future work

The fully optimised 3D tissue-engineered model of the oral mucosa and multi-colour flow cytometry panel specifically designed for use on this model, could be used to address a huge variety of questions. In addition to the preliminary experiments described in chapter 7 that require further investigation, the following section describes possible future work.

8.2.1 Comparison of tissue resident macrophages in healthy and malignant tissue to those in engineered oral mucosa

The ability to quantitatively analyse the expression of macrophage polarisation markers on macrophages isolated from primary patient tissues could have real value in improving

understanding of the role macrophages play in oral cancer progression. In particular, the methods developed in this thesis provide rapid isolation of macrophages from 3D tissue to preserve the expression of selected markers.

Methods for the isolation of macrophages from primary tissues were preliminarily investigated. In addition to providing us with a deeper understanding of the molecular biology of macrophage residing within oral cancer tissues, this would enable the model developed in this thesis to be compared and validated against primary tissue.

Methods were developed according to the previously published protocols (Donnenberg and Donnenberg, 2011; Fletcher *et al.,* 2011; Misharin *et al.,* 2013);). Primary oral biopsies were collected from healthy volunteers (09/H1308/66) or obtained during surgical procedures with written, informed consent (13/NS/0120, STH17021) and stored in transport media overnight at 4°C. The following day, the tissue sample was dissected into pieces 2-4 mm in size. An enzyme mix containing 0.5 % collagenase A (Sigma Aldrich, Dorset, UK) and 0.1 mg/mL DNAse (Sigma Aldrich, Dorset UK) was prepared in DMEM and tissue disaggregation was initiated using a gentleMACS C tube (Miltenyi, Cologne, Germany). A 40 µm cell strainer was used to separate larger pieces from the single cell suspension and FACS Lyse (BD Biosciences, Oxford, UK). The resulting cell suspension was stained using the 8-colour multi-colour flow cytometry panel presented in this thesis.

Unfortunately, no cells could be identified during flow cytometry analysis and the lack of availability of primary patient tissue prevented this work from being repeated. In order for the flow cytometry panel to successfully identify macrophage within the mixture of cells present in an oral cancer biopsy, further dump channels may be required to be added to the panel, such as for the elimination of dendritic cells which may be CD14+CD45+, and the elimination of fibroblasts and keratinocytes as previously described. For the elimination of dendritic cells, not present in the co-culture model developed in this thesis, CD208 may be used (Allaoui *et al.,* 2016).

With increased availability of both normal and malignant primary tissue, the validation of the tissue-engineered model presented here could be achieved.

8.2.2 **Towards an animal-free tissue-engineered model of the oral mucosa**

Whilst 3D tissue-engineered models offer benefits to *in vivo* experiments due to reduced costs, increased simplicity and reproducibility, the model presented here is not entirely animal-free. Rat tail collagen was used to generate the collagen hydrogel, and although rat tails were discarded from other research studies, alternative forms of collagen are available that are animal-free. For example, plant-derived human collagen can be produced in the tobacco plant using recombinant human collagen type I. This collagen is homogenic, well-organised, mechanically strong, and provides an excellent model of the ECM (Shoseyov *et al.,* 2013). A tissue-engineered model of the skin has been developed using plant-derived human collagen which includes PMA-treated THP-1 cells (Willard *et al.,* 2013).

Alternatively, MAPTrix (Amsbio, Oxon, UK) is a commercially available animal-free ECM which combines synthetic ECM peptides within mussel adhesive protein. MAPTrix HyGel™ (Amsbio, Oxon, UK) is specifically designed for use in 3D culture and can easily be adapted to alter elasticity and pore size. Despite the availability of MAPTrix containing a huge variety of ECM proteins, such as collagen, fibronetctin, laminin, vitronectin and cadherin, no published examples of use of this matrix could be found. As well as a reducing the use of animal components, both of these matrices offer improved batch-to-batch reproducibility, and most importantly, reduced immunogenicity.

Perhaps the most biologically relevant, animal-free matrix may be achieved by using a fibroblast-derived matrix which has previously been shown to accurately represent *in vivo* dermal architecture (Berning *et al.,* 2015). Whilst this matrix contains native proteoglycans and glycoproteins, the long culture periods and numbers of cells required to generate this fibroblast-derived matrix may be limiting for some applications.

9 Chapter 9: References

Abbott, A. (2003). Cell culture: Biology's new dimension. Nature *424*, 870-872.

Abuzakouk, M., Feighery, C., and Ofarrelly, C. (1996). Collagenase and dispase enzymes disrupt lymphocyte surface molecules. Journal of Immunological Methods *194*, 211-216.

Ackerman, L.V., and McGavran, M.H. (1958). Proliferating benign and malignant epithelial lesions of the oral cavity. Journal of Oral Surgery *16*, 400-413.

Ahn, G.O., Tseng, D., Liao, C.-H., Dorie, M.J., Czechowicz, A., and Brown, J.M. (2010). Inhibition of Mac-1 (CD11b/CD18) enhances tumor response to radiation by reducing myeloid cell recruitment. Proceedings of the National Academy of Sciences of the United States of America *107*, 8363-8368.

Ahrens, W., Pohlabeln, H., Foraita, R., Nelis, M., Lagiou, P., Lagiou, A., Bouchardy, C., Slamova, A., Schejbalova, M., Merletti, F., Richiardi, L., Kjaerheim, K., Agudo, A., Castellsague, X., Macfarlane, T.V., Macfarlane, G.J., Lee, Y.A., Talamini, R., Barzan, L., Canova, C., Simonato, L., Thomson, P., McKinney, P.A., McMahon, A.D., Znaor, A., Healy, C.M., McCartan, B.E., Metspalu, A., Marron, M., Hashibe, M., Conway, D.I., Brennan, P. (2014). Oral health, dental care and mouthwash associated with upper aerodigestive tract cancer risk in Europe: The ARCAGE study. Oral Oncology *50*, 616-625.

Aljitawi, O.S., Li, D., Xiao, Y., Zhang, D., Ramachandran, K., Stehno-Bittel, L., Van Veldhuizen, P., Lin, T.L., Kambhampati, S., and Garimella, R. (2014). A novel three-dimensional stromal-based model for *in vitro* chemotherapy sensitivity testing of leukemia cells. Leukemia & Lymphoma *55*, 378-391.

Allaoui, R., Bergenfelz, C., Mohlin, S., Hagerling, C., Salari, K., Werb, Z., Anderson, R.L., Ethier, S.P., Jirstrom, K., Pahlman, S., *et al.,* (2016). Cancer-associated fibroblast-secreted CXCL16 attracts monocytes to promote stroma activation in triple-negative breast cancers. Nature Communications *7*.

Allison, P., Franco, E., Black, M., and Feine, J. (1998). The role of professional diagnostic delays in the prognosis of upper aerodigestive tract carcinoma. Oral Oncology *34*, 147-153.

Alon, R., Cahalon, L., Hershkoviz, R., Elbaz, D., Reizis, B., Wallach, D., Akiyama, S.K., Yamada, K.M., and Lider, O. (1994). TNF-alpha binds to the N-terminal domain of fibronectin and augments the beta(1)-integrin-mediated adhesion of CD4+ T-lymphocytes to the glycoprotein. Journal of Immunology *152*, 1304-1313.

Alvarez, D.F., Helm, K., DeGregori, J., Roederer, M., and Majka, S. (2010). Publishing flow cytometry data. American Journal of Physiology-Lung Cellular and Molecular Physiology *298*, L127-L130.

Ambarus, C.A., Krausz, S., van Eijk, M., Hamann, J., Radstake, T.R.D.J., Reedquist, K.A., Tak, P.P., and Baeten, D.L.P. (2012). Systematic validation of specific phenotypic markers for *in vitro* polarized human macrophages. Journal of Immunological Methods *375*, 196-206.

Andersen, M.N., Al-Karradi, S.N.H., Kragstrup, T.W., and Hokland, M. (2016). Elimination of erroneous results in flow cytometry caused by antibody binding to Fc receptors on human monocytes and macrophages. Cytometry Part A *89A*, 1001-1009.

Anneroth, G., Batsakis, J., and Luna, M. (1987). Review of the literature and a recommended system of malignancy grading in oral squamous-cell carcinomas. Scandinavian Journal of Dental Research *95*, 229-249.

AntalSzalmas, P., VanStrijp, J.A.G., Weersink, A.J.L., Verhoef, J., and VanKessel, K.P.M. (1997). Quantitation of surface CD14 on human monocytes and neutrophils. Journal of Leukocyte Biology *61*, 721-728.

Argiris, A., Karamouzis, M.V., Raben, D., and Ferris, R.L. (2008). Head and neck cancer. Lancet *371*, 1695-1709.

Arnaoutova, I., and Kleinman, H.K. (2010). *In vitro* angiogenesis: endothelial cell tube formation on gelled basement membrane extract. Nature Protocols *5*, 628-635.

Asou, H., Eguchi, M., Suzukawa, K., Morishita, K., Tanaka, K., Date, M., Hamamoto, K., and Kamada, N. (1996). Establishment of a myeloid leukaemia cell line (Kasumi-4) with t(9;22;11)(q34;q11;q13), inv(3)(q21q26) and the EVI1 gene activation from a patient with chronic myelogenous leukaemia in blast crisis. British Journal of Haematology *93*, 68-74.

Auffray, C., Sieweke, M.H., and Geissmann, F. (2009). Blood monocytes: development, heterogeneity, and relationship with dendritic cells. Annual Review of Immunology *27*, 669-692.

Bach, J.-P., Rinn, B., Meyer, B., Dodel, R., and Bacher, M. (2008). Role of MIF in Inflammation and Tumorigenesis. Oncology *75*, 127-133.

Bagan, J., Sarrion, G., and Jimenez, Y. (2010). Oral cancer: Clinical features. Oral Oncology *46*, 414-417.

Bagul, N., Ganjre, A., Goryawala, S.N., Kathariya, R., and Dusane, S. (2015). Dynamic role of myofibroblasts in oral lesions. World Journal of Clinical Oncology *6*, 264-271.

Bagul, N., Roy, S., Ganjre, A., Kathariya, R., Meher, A., and Singh, P. (2016). Quantitative assessment of tumor associated macrophages in head and neck squamous cell carcinoma using CD68 marker: An Immunohistochemical Study. Journal of clinical and diagnostic research : JCDR *10*, ZC81-84.

Bagwell, C.B., and Adams, E.G. (1993). Fluorescence spectral overlap compensation for any number of flow-cytometry parameters. Annals of the New York Academy of Sciences *677*, 167-184.

Balasundaram, P., Singh, M.K., Dinda, A.K., Thakar, A., and Yadav, R. (2014). Study of beta-catenin, E-cadherin and vimentin in oral squamous cell carcinoma with and without lymph node metastases. Diagnostic Pathology *9*.

Balermpas, P., Roedel, F., Liberz, R., Oppermann, J., Wagenblast, J., Ghanaati, S., Harter, P.N., Mittelbronn, M., Weiss, C., Roedel, C., Fokas,E. (2014). Head and neck cancer relapse after chemoradiotherapy correlates with CD163+macrophages in primary tumour and CD11b+myeloid cells in recurrences. British Journal of Cancer *111*, 1509-1518.

Balkwill, F. (2006). TNF-alpha in promotion and progression of cancer. Cancer and Metastasis Reviews *25*, 409-416.

Balkwill, F., Charles, K.A., and Mantovani, A. (2005). Smoldering and polarized inflammation in the initiation and promotion of malignant disease. Cancer Cell *7*, 211-217.

Bao, K., Belibasakis, G.N., Selevsek, N., Grossmann, J., and Bostanci, N. (2015a). Proteomic profiling of host-biofilm interactions in an oral infection model resembling the periodontal pocket. Scientific Reports *5*.

Bao, K., Papadimitropoulos, A., Akguel, B., Belibasakis, G.N., and Bostanci, N. (2015b). Establishment of an oral infection model resembling the periodontal pocket in a perfusion bioreactor system. Virulence *6*, 265-273.

Baral, R., Patnaik, S., and Das, B.R. (1998). Co-overexpression of p53 and c-myc proteins linked with advanced stages of betel- and tobacco-related oral squamous cell carcinomas from eastern India. European Journal of Oral Sciences *106*, 907-913.

Batista, U., Garvas, M., Nemec, M., Schara, M., Veranic, P., and Koklic, T. (2010). Effects of different detachment procedures on viability, nitroxide reduction kinetics and plasma membrane heterogeneity of V-79 cells. Cell Biology International *34*, 663-668.

Beatty, G.L., Chiorean, E.G., Fishman, M.P., Saboury, B., Teitelbaum, U.R., Sun, W., Huhn, R.D., Song, W., Li, D., Sharp, L.L., Torigian, D.A., O'Dwyer, P.J., Vonderheide, R.H. (2011). CD40 agonists alter tumor stroma and show efficacy against pancreatic carcinoma in mice and humans. Science *331*, 1612-1616.

Bechetoille, N., Vachon, H., Gaydon, A., Boher, A., Fontaine, T., Schaeffer, E., Decossas, M., Andre-Frei, V., and Mueller, C.G. (2011). A new organotypic model containing dermal-type macrophages. Experimental Dermatology *20*, 1035-1037.

Bektas-Kayhan, K., Unur, M., Boy-Metin, Z., and Cakmakoglu, B. (2012). MCP-1 and CCR2 gene variants in oral squamous cell carcinoma. Oral Diseases *18*, 55-59.

Berggren, P., Kumar, R., Sakano, S., Hemminki, L., Wada, T., Steineck, G., Adolfsson, J., Larsson, P., Norming, U., Wijkstrom, H., Hemminki, K. (2003). Detecting homozygous deletions in the CDKN2Ap16INK4 alpha ARF(p14ARF) gene in urinary bladder cancer using real-time quantitative PCR. Clinical Cancer Research *9*, 235-242.

Berning, M., Pratzel-Wunder, S., Bickenbach, J.R., and Boukamp, P. (2015). Three-dimensional *in vitro* skin and skin cancer models based on human fibroblast-derived matrix. Tissue Engineering Part C-Methods *21*, 958-970.

Berthod, F., Symes, J., Tremblay, N., Medin, J.A., and Auger, F.A. (2012). Spontaneous fibroblast-derived pericyte recruitment in a human tissue-engineered angiogenesis model *in vitro*. Journal of Cellular Physiology *227*, 2130-2137.

Billinton, N., Knight, A.W., (2001). Techniques for distinguishing GFP from endogenous autofluorescence. Analytical Biochemistry *291*, 175-197.

Bingle, L., Brown, N.J., and Lewis, C.E. (2002). The role of tumour-associated macrophages in tumour progression: implications for new anticancer therapies. Journal of Pathology *196*, 254-265.

Biswas, S.K., and Mantovani, A. (2010). Macrophage plasticity and interaction with lymphocyte subsets: cancer as a paradigm. Nature Immunology *11*, 889-896.

Blot, W.J., McLaughlin, J.K., Winn, D.M., Austin, D.F., Greenberg, R.S., Prestonmartin, S., Bernstein, L., Schoenberg, J.B., Stemhagen, A., and Fraumeni, J.F. (1988). Smoking and drinking in relation to oral and pharyngeal cancer. Cancer Research *48*, 3282-3287.

Boas, D.S.V., Takiya, C.M., Gurgel, C.A.S., Cabral, M.G., and Santos, J.N.d. (2013). Tumor-infiltrating macrophage and microvessel density in oral squamous cell carcinoma. Brazilian Dental Journal *24*, 194-199.

Bonapace, L., Coissieux, M.-M., Wyckoff, J., Mertz, K.D., Varga, Z., Junt, T., and Bentires-Alj, M. (2014). Cessation of CCL2 inhibition accelerates breast cancer metastasis by promoting angiogenesis. Nature *515*.

Bosque, F., Belkaid, Y., Briend, E., Hevin, B., Lebastard, M., Soussi, N., and Milon, G. (1997). The biology of macrophages. Pathologie Biologie *45*, 103-109.

Bottaro, D.P., Rubin, J.S., Faletto, D.L., Chan, A.M.L., Kmiecik, T.E., Vandewoude, G.F., and Aaronson, S.A. (1991). Identification of the hepatocyte growth-factor receptor as the c-met protooncogene product. Science *251*, 802-804.

Boyd, N.F., Li, Q., Melnichouk, O., Huszti, E., Martin, L.J., Gunasekara, A., Mawdsley, G., Yaffe, M.J., and Minkin, S. (2014). Evidence that breast tissue stiffness is associated with risk of breast cancer. Plos One *9*.

Boyle, J.O., Hakim, J., Koch, W., Vanderriet, P., Hruban, R.H., Roa, R.A., Correo, R., Eby, Y.J., Ruppert, J.M., and Sidransky, D. (1993). The incidence of p53 mutations increases with progression of head and neck cancer. Cancer Research *53*, 4477-4480.

Bradley, G., Odell, E.W., Raphael, S., Ho, J., Le, L.W., Benchimol, S., and Kamel-Reid, S. (2010). Abnormal DNA content in oral epithelial dysplasia is associated with increased risk of progression to carcinoma. British Journal of Cancer *103*, 1432-1442.

Brandizzi, D., Gandolfo, M., Velazco, M.L., Cabrini, R.L., and Lanfranchi, H.E. (2008). Clinical features and evolution of oral cancer: A study of 274 cases in Buenos Aires, Argentina. Medicina Oral Patologia Oral Y Cirugia Bucal *13*, E544-E548.

Broders, A.C. (1927). Carcinoma of the mouth types and degrees of malignancy. American Journal of Roentgenology and Radium Therapy *17*, 90-93.

Brusevold, I.J., Husvik, C., Schreurs, O., Schenck, K., Bryne, M., and Soland, T.M. (2010). Induction of invasion in an organotypic oral cancer model by CoCl2, a hypoxia mimetic. European Journal of Oral Sciences *118*, 168-176.

Buccisano, F., Rossi, F.M., Venditti, A., Del Poeta, G., Cox, M.C., Abbruzzese, E., Rupolo, M., Berretta, M., Degan, M., Russo, S., Tamburini, A., Maurillo, L., Del Principe, M.I., Postorino, M., Amadori, S., Gattei, V. (2004). CD90/Thy-1 is preferentially expressed on blast cells of high risk acute myeloid leukaemias. British Journal of Haematology *125*, 203-212.

Bundscherer, A., Malsy, M., Lange, R., Hofmann, P., Metterlein, T., Graf, B.M., and Gruber, M. (2013). Cell harvesting method influences results of apoptosis analysis by annexin V staining. Anticancer Research *33*, 3201-3204.

Burke, B., Sumner, S., Maitland, N., and Lewis, C.E. (2002). Macrophages in gene therapy: cellular delivery vehicles and *in vivo* targets. Journal of Leukocyte Biology *72*, 417-428.

Bye, F.J., Bullock, A.J., Singh, R., Sefat, F., Roman, S., and MacNeil, S. (2014). Development of a basement membrane substitute incorporated into an electrospun scaffold for 3D skin tissue engineering. Journal of Biomaterials and Tissue Engineering *4*, 686-692.

Caamano, J., Zhang, S.Y., Rosvold, E.A., Bauer, B., and Kleinszanto, A.J.P. (1993). P53 alterations in human squamous-cell carcinomas and carcinoma cell-lines. American Journal of Pathology *142*, 1131-1139.

Cabelguenne, A., Blons, H., de Waziers, I., Carnot, F., Houllier, A.M., Soussi, T., Brasnu, D., Beaune, P., Luccourreye, O., and Laurent-Puig, P. (2000). p53 alterations predict tumor response to neoadjuvant chemotherapy in head and neck squamous cell carcinoma: A prospective series. Journal of Clinical Oncology *18*, 1465-1473.

Candia, J., Somarriva, C., Fonseca, D., Parada, F., Briceno, J., Fernandez, A. (2016). TGF-β alterations in oral squamous cells carcinoma. Journal of Oral Research *5*, 207-214.

Canovic, E.P., Qing, B., Mijailovic, A.S., Jagielska, A., Whitfield, M.J., Kelly, E., Turner, D., Sahin, M., and Van Vliet, K.J. (2016). Characterizing multiscale mechanical properties of brain tissue using atomic force microscopy, impact indentation, and rheometry. Journal of Visualized Experiments : JoVE, *115*.

Cao, H., Dan, Z., He, X., Zhang, Z., Yu, H., Yin, Q., and Li, Y. (2016). Liposomes coated with isolated macrophage membrane can target lung metastasis of breast cancer. Acs Nano *10*, 7738-7748.

Carmeliet, P. (2005). VEGF as a key mediator of angiogenesis in cancer. Oncology *69*, 4-10.

Cassol, E., Cassetta, L., Rizzi, C., Alfano, M., and Poli, G. (2009). M1 and M2a Polarization of Human Monocyte-Derived Macrophages Inhibits HIV-1 Replication by Distinct Mechanisms. Journal of Immunology *182*, 6237-6246.

Cavo, M., Fato, M., Penuela, L., Beltrame, F., Raiteri, R., and Scaglione, S. (2016). Microenvironment complexity and matrix stiffness regulate breast cancer cell activity in a 3D *in vitro* model. Scientific Reports *6*.

Chan, L.Y., Yim, E.K.F., and Choo, A.B.H. (2013). Normalized median fluorescence: an alternative flow cytometry analysis method for tracking human embryonic stem cell states during differentiation. Tissue Engineering Part C-Methods *19*, 156-165.

Chang, M.Y., Chan, C.K., Braun, K.R., Green, P.S., O'Brien, K.D., Chait, A., Day, A.J., and Wight, T.N. (2012). Monocyte-to-macrophage differentiation synthesis and secretion of a complex extracellular matrix. Journal of Biological Chemistry *287*, 14122-14135.

Chanput, W., Mes, J.J., Savelkoul, H.F.J., and Wichers, H.J. (2013). Characterization of polarized THP-1 macrophages and polarizing ability of LPS and food compounds. Food & Function *4*, 266-276.

Chavez-Galan, L., Olleros, M.L., Vesin, D., and Garcia, I. (2015). Much more than M1 and M2 macrophages, there are also CD169(+) and TCR+ macrophages. Frontiers in Immunology *6*.

Chen, J., Ahmad, R., Li, W., Swain, M., and Li, Q. (2015). Biomechanics of oral mucosa. Journal of the Royal Society Interface *12*.

Chen, Y.K., Huang, H.C., Lin, L.M., and Lin, C.C. (1999). Primary oral squamous cell carcinoma: an analysis of 703 cases in southern Taiwan. Oral Oncology *35*, 173-179.

Cheng, H., Clarkson, P.W., Gao, D., Pacheco, M., Wang, Y., and Nielsen, T.O. (2010). Therapeutic antibodies targeting CSF1 impede macrophage recruitment in a xenograft model of tenosynovial giant cell tumor. Sarcoma, 174528-Article No.: 174528.

Chitra, S., Nalini, G., Lokeswari, T.S. (2014). Comparison of differentiation to macrophages in isolated monocytes from human peripheral blood and THP1 cells. Sri Ramachandra Journal of Medicine *7*, 1-6.

Chiu, K.-C., Lee, C.-H., Liu, S.-Y., Yeh, C.-T., Huang, R.-Y., Yuh, D.-Y., Cheng, J.-C., Chou, Y.-T., and Shieh, Y.-S. (2014). Protumoral effect of macrophage through Axl activation on mucoepidermoid carcinoma. Journal of Oral Pathology & Medicine *43*, 538-544.

Cho, K.W., Morris, D.L., and Lumeng, C.N. (2014). Flow cytometry analyses of adipose tissue macrophages. Methods of Adipose Tissue Biology, Pt A *537*, 297-314.

Choi, S., and Myers, J.N. (2008). Molecular pathogenesis of oral squamous cell carcinoma: Implications for therapy. Journal of Dental Research *87*, 14-32.

Chorro, L., Sarde, A., Li, M., Woollard, K.J., Chambon, P., Malissen, B., Kissenpfennig, A., Barbaroux, J.P., Groves, R., Geissmann, F. (2009). Langerhans cell (LC) proliferation

mediates neonatal development, homeostasis, and inflammation-associated expansion of the epidermal LC network. The Journal of Experimental Medicine *206*, 3089-3100.

Choudhari, S.K., Chaudhary, M., Gadbail, A.R., Sharma, A., and Tekade, S. (2014). Oxidative and antioxidative mechanisms in oral cancer and precancer: A review. Oral Oncology *50*, 10-18.

Christensen, A., Kristensen, E., Therkildsen, M.H., Specht, L., Reibel, J., and Homoe, P. (2013). Ten-year retrospective study of head and neck carcinoma *in situ*: incidence, treatment, and clinical outcome. Oral Surgery Oral Medicine Oral Pathology Oral Radiology *116*, 174-178.

Chuang, J.-Y., Yang, W.-H., Chen, H.-T., Huang, C.-Y., Tan, T.-W., Lin, Y.-T., Hsu, C.-J., Fong, Y.-C., and Tang, C.-H. (2009). CCL5/CCR5 axis promotes the motility of human oral cancer cells. Journal of Cellular Physiology *220*, 418-426.

Chung, E., Choi, H., Lim, J.E., and Son, Y. (2014). Development of skin inflammation test model by co-culture of reconstituted 3D skin and RAW264.7 cells. Tissue Engineering and Regenerative Medicine *11*, 87-92.

Coffelt, S.B., Chen, Y.-Y., Muthana, M., Welford, A.F., Tal, A.O., Scholz, A., Plate, K.H., Reiss, Y., Murdoch, C., De Palma, M., Lewis, C.E. (2011). Angiopoietin 2 stimulates TIE2-expressing monocytes to suppress T cell activation and to promote regulatory T cell expansion. Journal of Immunology *186*, 4183-4190.

Coleman, R., Cook, R., Hirsh, V., Major, P., and Lipton, A. (2011). Zoledronic acid use in cancer patients more than just supportive care? Cancer *117*, 11-23.

Colley, H.E., Hearnden, V., Jones, A.V., Weinreb, P.H., Violette, S.M., MacNeil, S., Thornhill, M.H., and Murdoch, C. (2011). Development of tissue-engineered models of oral dysplasia and early invasive oral squamous cell carcinoma. British Journal of Cancer *105*, 1582-1592.

Collins, S.J. (1987). The HL-60 promyelocytic leukemia-cell line - proliferation, differentiation, and cellular oncogene expression. Blood *70*, 1233-1244.

Comito, G., Giannoni, E., Segura, C.P., Barcellos-de-Souza, P., Raspollini, M.R., Baroni, G., Lanciotti, M., Serni, S., and Chiarugi, P. (2014). Cancer-associated fibroblasts and M2-polarized macrophages synergize during prostate carcinoma progression. Oncogene *33*, 2423-2431.

Cook, M.M., Futrega, K., Osiecki, M., Kabiri, M., Kul, B., Rice, A., Atkinson, K., Brooke, G., and Doran, M. (2012). Micromarrows-three-dimensional coculture of hematopoietic stem cells and mesenchymal stromal cells. Tissue Engineering Part C-Methods *18*, 319-328.

Costa, N.L., Valadares, M.C., Chaves Souza, P.P., Mendonca, E.F., Oliveira, J.C., Silva, T.A., and Batista, A.C. (2013). Tumor-associated macrophages and the profile of inflammatory cytokines in oral squamous cell carcinoma. Oral Oncology *49*, 216-223.

Costea, D.E., Loro, L.L., Dimba, E.A.O., Vintermyr, O.K., and Johannessen, A.C. (2003). Crucial effects of fibroblasts and keratinocyte growth factor on morphogenesis of

reconstituted human oral epithelium. Journal of Investigative Dermatology *121*, 1479-1486.

Coussens, L.M., and Werb, Z. (2002). Inflammation and cancer. Nature *420*, 860-867.

Crabbe, E., Verheyen, G., Tournaye, H., and VanSteirteghem, A. (1997). The use of enzymatic procedures to recover testicular germ cells. Human Reproduction *12*, 1682-1687.

Cukierman, E., Pankov, R., Stevens, D.R., and Yamada, K.M. (2001). Taking cell-matrix adhesions to the third dimension. Science *294*, 1708-1712.

Cumming, G., Fidler, F., and Vaux, D.L. (2007). Error bars in experimental biology. Journal of Cell Biology *177*, 7-11.

Curat, C.A., Miranville, A., Sengenes, C., Diehl, M., Tonus, C., Busse, R., and Bouloumie, A. (2004). From blood monocytes to adipose tissue-resident macrophages - Induction of diapedesis by human mature adipocytes. Diabetes *53*, 1285-1292.

Dai, T., Song. Y., Ma, H., Feng, H. (2007). Studies on the expression of MMP-9 and significance of a macrophage assay in oral squamous cell carcinoma. Chinese Journal of Clinical Oncology *4*, 333-337.

Daigneault, M., Preston, J.A., Marriott, H.M., Whyte, M.K.B., and Dockrell, D.H. (2010). The Identification of Markers of Macrophage Differentiation in PMA-Stimulated THP-1 Cells and Monocyte-Derived Macrophages. Plos One *5*.

Dale, D.C. (2002). Colony-stimulating factors for the management of neutropenia in cancer patients. Drugs *62*, 1-15.

Davies, L.C., Jenkins, S.J., Allen, J.E., Taylor, P.R. (2013). Tissue-resident macrophages. Nature Immunology *14*, 986-995.

Davies, L.C., Taylor, P.R. (2015). Tissue-resident macrophages: then and now. Immunology *144*, 541-548.

Davis, M.J., Tsang, T.M., Qiu, Y., Dayrit, J.K., Freij, J.B., Huffnagle, G.B., and Olszewski, M.A. (2013). Macrophage M1/M2 Polarization Dynamically Adapts to Changes in Cytokine Microenvironments in Cryptococcus neoformans Infection. Mbio *4*.

De Palma, M., Mazzieri, R., Politi, L.S., Pucci, F., Zonari, E., Sitia, G., Mazzoleni, S., Moi, D., Venneri, M.A., Indraccolo, S.*, et al.,* (2008). Tumor-targeted interferon-alpha delivery by Tie2-expressing monocytes inhibits tumor growth and metastasis. Cancer Cell *14*, 299-311.

DeCicco-Skinner, K.L., Henry, G.H., Cataisson, C., Tabib, T., Gwilliam, J.C., Watson, N.J., Bullwinkle, E.M., Falkenburg, L., O'Neill, R.C., Morin, A.*, et al.,* (2014). Endothelial cell tube formation assay for the *in vitro* study of angiogenesis. Jove-Journal of Visualized Experiments.

DesRochers, T.M., Holmes, L., O'Donnell, L., Mattingly, C., Shuford, S., O'Rourke, M.A., Rippon, M.B., Edenfield, W.J., Gevaert, M.R., Orr, D.E., Crosswell, H.E. (2015). Macrophage

incorporation into a 3D perfusion tri-culture model of human breast cancer. Journal for ImmunoTherapy of Cancer *3*, 401.

Deszo, E.L., Brake, D.K., Cengel, K.A., Kelley, K.W., and Freund, G.G. (2001). CD45 negatively regulates monocytic cell differentiation by inhibiting phorbol 12-myristate 13-acetate-dependent activation and tyrosine phosphorylation of protein kinase C delta. Journal of Biological Chemistry *276*, 10212-10217.

Dongari-Bagtzoglou, A., and Kashleva, H. (2006). Development of a highly reproducible three-dimensional organotypic model of the oral mucosa. Nature Protocols *1*, 2012-2018.

Donnenberg, V.S., Donnenberg A.D. (2011). Flow Cytometry on disaggregated solid tissues. International Drug Discovery, 1-3.

Duque, G.A., and Descoteaux, A. (2014). Macrophage cytokines: involvement in immunity and infectious diseases. Frontiers in Immunology *5*, 1-12.

Ehsan, S.M., Welch-Reardon, K.M., Waterman, M.L., Hughes, C.C.W., and George, S.C. (2014). A three-dimensional *in vitro* model of tumor cell intravasation. Integrative Biology *6*, 603-610.

El-Rouby, D.H. (2010). Association of macrophages with angiogenesis in oral verrucous and squamous cell carcinomas. Journal of Oral Pathology & Medicine *39*, 559-564.

Eligini, S., Crisci, M., Bono, E., Songia, P., Tremoli, E., Colombo, G.I., and Colli, S. (2013). Human monocyte-derived macrophages spontaneously differentiated *in vitro* show distinct phenotypes. Journal of Cellular Physiology *228*, 1464-1472.

Erbel, C., Rupp, G., Helmes, C.M., Tyka, M., Linden, F., Doesch, A.O., Katus, H.A., and Gleissner, C.A. (2013). An *in vitro* model to study heterogeneity of human macrophage differentiation and polarization. Jove-Journal of Visualized Experiments, *76*.

Espinosa, I., Carnicer, M.J., Catasus, L., Canet, B., D'Angelo, E., Zannoni, G.F., and Prat, J. (2010). Myometrial invasion and lymph node metastasis in endometrioid carcinomas: Tumor-associated macrophages, microvessel density, and HIF1A have a crucial role. American Journal of Surgical Pathology *34*, 1708-1714.

Essa, A.A.M., Yamazaki, M., Maruyama, S., Abe, T., Babkair, H., Raghib, A.M., Megahed, E.M.E., Cheng, J., and Sakui, T. (2016). Tumour-associated macrophages are recruited and differentiated in the neoplastic stroma of oral squamous cell carcinoma. Pathology *48*, 219-227.

Feller, L., Altini, M., Khammissa, R.A.G., Chandran, R., Bouckaert, M., and Lemmer, J. (2013). Oral mucosal immunity. Oral Surgery Oral Medicine Oral Pathology Oral Radiology *116*, 576-583.

Fennema, E., Rivron, N., Rouwkema, J., van Blitterswijk, C., and de Boer, J. (2013). Spheroid culture as a tool for creating 3D complex tissues. Trends in Biotechnology *31*, 108-115.

Fenton, M.J., and Golenbock, D.T. (1998). LPS-binding proteins and receptors. Journal of Leukocyte Biology *64*, 25-32.

Fischer, A.H., Jacobson, K.A., Rose, J., and Zeller, R. (2008). Hematoxylin and eosin staining of tissue and cell sections. CSH protocols *2008*, pdb.prot4986-pdb.prot4986.

Fleetwood, A.J., Dinh, H., Cook, A.D., Hertzog, P.J., and Hamilton, J.A. (2009). GM-CSF- and M-CSF-dependent macrophage phenotypes display differential dependence on Type I interferon signaling. Journal of Leukocyte Biology *86*, 411-421.

Fletcher, A.L., Malhotra, D., Acton, S.E., Lukacs-Kornek, V., Bellemare-Pelletier, A., Curry, M., Armant, M., and Turley, S.J. (2011). Reproducible isolation of lymph node stromal cells reveals site-dependent differences in fibroblastic reticular cells. Frontiers in Immunology *2*.

Forastiere, A.A., Trotti, A., Pfister, D.G., and Grandis, J.R. (2006). Head and neck cancer: Recent advances and new standards of care. Journal of Clinical Oncology *24*, 2603-2605.

Forssell, J., Oberg, A., Henriksson, M.L., Stenling, R., Jung, A., and Palmqvist, R. (2007). High macrophage infiltration along the tumor front correlates with improved survival in colon cancer. Clinical Cancer Research *13*, 1472-1479.

Foulkes, M. (2013). Oral cancer: risk factors, treatment and nursing care. Nursing standard (Royal College of Nursing (Great Britain) : 1987) *28*, 49-57.

Franca, C.M., Batista, A.C., Borra, R.C., Ventiades-Flores, J.A., Mendona, E.F., Deana, A.M., Mesquita-Ferrari, R.A., Caly, D.d.N., Rode, S.d.M., and Faria, M.R. (2013). Macrophage migration inhibitory factor and oral cancer. Journal of Oral Pathology & Medicine *42*, 368-373.

Franklin, R.A., Liao, W., Sarkar, A., Kim, M.V., Bivona, M.R., Liu, K., Pamer, E.G., Li M.O. (2014). The cellular and molecular origin of tumour-associated macrophages. Science *344*, 921-925.

Fraser, A.R., Cook, G., Franklin, I.M., Templeton, J.G., Campbell, M., Holyoake, T.L., and Campbell, J.D.M. (2006). Immature monocytes from G-CSF-mobilized peripheral blood stem cell collections carry surface-bound IL-10 and have the potential to modulate alloreactivity. Journal of Leukocyte Biology *80*, 862-869.

Freudenthal, P.S., and Steinman, R.M. (1990). The distinct surface of human blood dendritic cells, as observed after an improved isolation method. Proceedings of the National Academy of Sciences of the United States of America *87*, 7698-7702.

Fujii, N., Shomori, K., Shiomi, T., Nakabayashi, M., Takeda, C., Ryoke, K., and Ito, H. (2012). Cancer-associated fibroblasts and CD163-positive macrophages in oral squamous cell carcinoma: their clinicopathological and prognostic significance. Journal of Oral Pathology & Medicine *41*, 444-451.

Fujita, Y., Okamoto, M., Goda, H., Tano, T., Nakashiro, K.-i., Sugita, A., Fujita, T., Koido, S., Homma, S., Kawakami, Y., Hamakawa, H. (2014). Prognostic significance of interleukin-8

and CD163-positive cell-infiltration in tumor tissues in patients with oral squamous cell carcinoma. Plos One *9*.

Funk, G.F., Karnell, L.H., Robinson, R.A., Zhen, W.N.K., Trask, D.K., and Hoffman, H.T. (2002). Presentation, treatment, and outcome of oral cavity cancer: A national cancer data base report. Head and Neck-Journal for the Sciences and Specialties of the Head and Neck *24*, 165-180.

Gaballah, K., Costea, D.E., Hills, A., Gollin, S.M., Harrison, P., and Partridge, M. (2008). Tissue engineering of oral dysplasia. Journal of Pathology *215*, 280-289.

Gautier, E.L., Shay, T., Miller, J., Greter, M., Jakubzick, C., Ivanov, S., Helft, J., Chow, A., Elpek, K.G., Gordonov, S., Mazloom, A.R., Ma'ayan, A., Chua, W.J., Hansen, T.H., Turley, S.J., Merad, M., Randolph, G.J. (2012). Gene-expression profiles and transcriptional regulatory pathways that underlie the identity and diversity of mouse tissue macrophages. Nature Immunology *13*, 1118-1128.

Gedye, C.A., Hussain, A., Paterson, J., Smrke, A., Saini, H., Sirskyj, D., Pereira, K., Lobo, N., Stewart, J., Go, C., Ho, J., Medrano, M., Hyatt, E., Yuan, J., Lauriault, S., Kondratyev, M., van den Beuken, T., Jewett, M., Dirks, P., Guidos, C.J., Danska, J., Wang, J.,Wouters, B., Neel, B., Rottapel, R., Ailles, L.E. (2014). Cell surface profiling using high-throughput flow cytometry: A platform for biomarker discovery and analysis of cellular heterogeneity. Plos One *9*.

Geetha, K.M., Leeky, M., Narayan, T.V., Sadhana, S., and Saleha, J. (2015). Grading of oral epithelial dysplasia: Points to ponder. Journal of Oral and Maxillofacial Pathology : JOMFP *19*, 198-204.

Geissmann, F. (2010). Development of monocytes, macrophages, and dendritic cells (vol 327, pg 656, 2010). Science *330*, 1318-1318.

Georgoudaki, A.-M., Prokopec, K.E., Boura, V.F., Hellqvist, E., Sohn, S., Ostling, J., Dahan, R., Harris, R.A., Rantalainen, M., Klevebring, D., Sund, M., Brage, S.E., Fuxe, J., Rolny, C., Li, F.B., Ravetch, J.V., Karlsson, M.C.I. (2016). Reprogramming tumor-associated macrophages by antibody targeting inhibits cancer progression and metastasis. Cell Reports *15*, 2000-2011.

Ginhoux, F., and Jung, S. (2014). Monocytes and macrophages: developmental pathways and tissue homeostasis. Nature Reviews Immunology *14*, 392-404.

Goerdt, S., and Orfanos, C.E. (1999). Other functions, other genes: Alternative activation of antigen-presenting cells. Immunity *10*, 137-142.

Gokcinar-Yagci, B., Uckan-Cetinkaya, D., and Celebi-Saltik, B. (2015). Pericytes: properties, functions and applications in tissue engineering. Stem Cell Reviews and Reports *11*, 549-559.

Gong, D., Shi, W., Yi, S.-j., Chen, H., Groffen, J., and Heisterkamp, N. (2012). TGF beta signaling plays a critical role in promoting alternative macrophage activation. BMC Immunology *13*.

Graversen, J.H., and Moestrup, S.K. (2015). Drug trafficking into macrophages via the endocytotic receptor CD163. Membranes *5*, 228-252.

Griffin, J.D., Ritz, J., Nadler, L.M., and Schlossman, S.F. (1981). Expression of myeloid differentiation antigens on normal and malignant myeloid cells. Journal of Clinical Investigation *68*, 932-941.

Griffon, D.J., Sedighi, M.R., Schaeffer, D.V., Eurell, J.A., and Johnson, A.L. (2006). Chitosan scaffolds: Interconnective pore size and cartilage engineering. Acta Biomaterialia *2*, 313-320.

Grimshaw, M.J., Wilson, J.L., and Balkwill, F.R. (2002). Endothelin-2 is a macrophage chemoattractant: implications for macrophage distribution in tumors. European Journal of Immunology *32*, 2393-2400.

Grinnell, F. (1994). Fibroblasts, myofibroblasts, and wound contraction. Journal of Cell Biology *124*, 401-404.

Guilliams, M., Bruhns, P., Saeys, Y., Hammad, H., and Lambrecht, B.N. (2014). The function of Fc gamma receptors in dendritic cells and macrophages. Nature Reviews Immunology *14*, 94-108.

Guillot-Delost, M., Le Gouvello, S., Mesel-Lemoine, M., Cherai, M., Baillou, C., Simon, A., Levy, Y., Weiss, L., Louafi, S., Chaput, N., Berrehar, F., Kerbrat, S., Klatzmann, D., Lemoine, F.M. (2012). Human CD90 identifies Th17/Tc17 T cell subsets that are depleted in HIV-infected patients. Journal of Immunology *188*, 981-991.

Gupta, P.C., Sinor, P.N., Bhonsle, R.B., Pawar, V.S., and Mehta, H.C. (1998). Oral submucous fibrosis in India: A new epidemic? National Medical Journal of India *11*, 113-116.

Gutschalk, C.M., Herold-Mende, C.C., Fusenig, N.E., and Mueller, M.M. (2006). Granulocyte colony-stimulating factor and granulocyte-macrophage colony-stimulating factor promote malignant growth of cells from head and neck squamous cell carcinomas *in vivo*. Cancer Research *66*, 8026-8036.

Gutschalk, C.M., Yanamandra, A.K., Linde, N., Meides, A., Depner, S., and Mueller, M.M. (2013). GM-CSF enhances tumor invasion by elevated MMP-2,-9, and-26 expression. Cancer Medicine *2*, 117-129.

Hagemann, T., Wilson, J., Kulbe, H., Li, N.F.F., Leinster, D.A., Charles, K., Klemm, F., Pukrop, T., Binder, C., and Balkwill, F.R. (2005). Macrophages induce invasiveness of epithelial cancer cells via NF-kappa B and JNK. Journal of Immunology *175*, 1197-1205.

Han, J., Zhen, J., Van Du, N., Go, G., Choi, Y., Ko, S.Y., Park, J.-O., and Park, S. (2016). Hybrid-actuating macrophage-based microrobots for active cancer therapy. Scientific Reports *6*.

Handorf, A.M., Zhou, Y., Halanski, M.A., and Li, W.-J. (2015). Tissue stiffness dictates development, homeostasis, and disease progression. Organogenesis *11*, 1-15.

Hao, N.-B., Lu, M.-H., Fan, Y.-H., Cao, Y.-L., Zhang, Z.-R., and Yang, S.-M. (2012). Macrophages in tumor microenvironments and the progression of tumors. Clinical & Developmental Immunology.

Harris, J.A., Jain, S., Ren, Q.H., Zarineh, A., Liu, C., and Ibrahim, S. (2012). CD163 versus CD68 in tumor associated macrophages of classical hodgkin lymphoma. Diagnostic Pathology *7*.

Hasina, R., Matsumoto, K., Matsumoto-Taniura, N., Kato, I., Sakuda, M., and Nakamura, T. (1999). Autocrine and paracrine motility factors and their involvement in invasiveness in a human oral carcinoma cell line. British Journal of Cancer *80*, 1708-1717.

Hasina, R., Whipple, M.E., Martin, L.E., Kuo, W.P., Ohno-Machado, L., and Lingen, M.W. (2008). Angiogenic heterogeneity in head and neck squamous cell carcinoma: biological and therapeutic implications. Laboratory Investigation *88*, 342-353.

Hauptmann, S., Zwadloklarwasser, G., Jansen, M., Klosterhalfen, B., and Kirkpatrick, C.J. (1993). Macrophages and multicellular tumor spheroids in coculture - a 3-dimensional model to study tumor-host interactions - evidence for macrophage-mediated tumor-cell proliferation and migration. American Journal of Pathology *143*, 1406-1415.

Haw, R.T.Y., Tong, C.K., Yew, A., Lee, H.C., Phillips, J.B., and Vidyadaran, S. (2014). A three-dimensional collagen construct to model lipopolysaccharide-induced activation of BV2 microglia. Journal of Neuroinflammation *11*.

He, K.F., Zhang, L., Huang, C.F., Ma, S.R., Wang, Y.F., Wang, W.M., Zhao, Z.L., Liu, B., Zhao, Y.F., Zhang, W.F., Sun, Z.J. (2014). CD163+ tumor-associated macrophages correlated with poor prognosis and cancer stem cells in oral squamous cell carcinoma. Biomed Research International.

Hearnden, V., Lomas, H., MacNeil, S., Thornhill, M., Murdoch, C., Lewis, A., Madsen, J., Blanazs, A., Armes, S.P., and Battaglia, G. (2009). Diffusion studies of nanometer polymersomes across tissue engineered human oral mucosa. Pharmaceutical Research *26*, 1718-1728.

Helal, D.S., Wahba, O.M. (2016). Immunohistochemical study of CD68, CD3 and Bcl-2 and their role in progression and prognosis of head and neck squamous cell carcinoma. Archives in Cancer Research *4*, 1.

Heldin, C.-H., Vanlandewijck, M., and Moustakas, A. (2012). Regulation of EMT by TGF beta in cancer. Febs Letters *586*, 1959-1970.

Herrero, R., Castellsague, X., Pawlita, M., Lissowska, J., Kee, F., Balaram, P., Rajkumar, T., Sridhar, H., Rose, B., Pintos, J., Fernandez, L., Idris, A., Sanchez, M.J., Nieto, A., Talamini, R., Tavani, A., Bosch, F.X., Reidel, U., Snijders, P.J.F., Meijer, C.J.L.M., Vsicidi, R., Munoz, N., Franceschi, S. (2003). Human papillomavirus and oral cancer: The international agency for research on cancer multicenter study. Journal of the National Cancer Institute *95*, 1772-1783.

Herzenberg, L.A., Tung, J., Moore, W.A., and Parks, D.R. (2006). Interpreting flow cytometry data: a guide for the perplexed. Nature Immunology *7*, 681-685.

Hicklin, D.J., and Ellis, L.M. (2005). Role of the vascular endothelial growth factor pathway in tumor growth and angiogenesis. Journal of Clinical Oncology *23*, 1011-1027.

Hirz, T., and Dumontet, C. (2016). Neutrophil isolation and analysis to determine their role in lymphoma cell sensitivity to therapeutic agents. Jove-Journal of Visualized Experiments.

Hofkens, W., Storm, G., van den Berg, W., and van Lent, P. (2011). Inhibition of M1 macrophage activation in favour of M2 differentiation by liposomal targeting of glucocorticoids to the synovial lining during experimental arthritis. Annals of the Rheumatic Diseases *70*, A40-A40.

Hsia, L.T., Ashley, N., Ouaret, D., Wang, L.M., Wilding, J., and Bodmer, W.F. (2016). Myofibroblasts are distinguished from activated skin fibroblasts by the expression of AOC3 and other associated markers. Proceedings of the National Academy of Sciences of the United States of America *113*, E2162-E2171.

Hu, H., Sun, L.C., Guo, C.G., Liu, Q., Zhou, Z., Peng, L., Pan, J., Yu, L., Lou, J.N., Yang, Z.H., Zhao, P., Ran, Y.L. (2009). Tumor cell-microenvironment interaction models coupled with clinical validation reveal CCL2 and SNCG as two predictors of colorectal cancer hepatic metastasis. Clinical Cancer Research *15*, 5485-5493.

Huang, S.C.C., Everts, B., Ivanova, Y., O'Sullivan, D., Nascimento, M., Smith, A.M., Beatty, W., Love-Gregory, L., Lam, W.Y., O'Neil, C.M., Yan, C., Du, H., Abumrad, N.A., Urban, J.F., Artyomov, M.N., Pearce, E.L., Pearce, E.J. (2014). Cell-intrinsic lysosomal lipolysis is essential for alternative activation of macrophages. Nature Immunology *15*, 846-855.

Hudson, J.D., Shoaibi, M.A., Maestro, R., Carnero, A., Hannon, G.J., and Beach, D.H. (1999). A proinflammatory cytokine inhibits p53 tumor suppressor activity. Journal of Experimental Medicine *190*, 1375-1382.

Iwasaki, A., and Medzhitov, R. (2004). Toll-like receptor control of the adaptive immune responses. Nature Immunology *5*, 987-995.

Jaguin, M., Houlbert, N., Fardel, O., and Lecureur, V. (2013). Polarization profiles of human M-CSF-generated macrophages and comparison of M1-markers in classically activated macrophages from GM-CSF and M-CSF origin. Cellular Immunology *281*, 51-61.

Jenkins, S.J., Ruckerl, D., Cook, P.C., Jones, L.H., Finkelman, F.D., van Rooijen, N., MacDonald, A.S., and Allen, J.E. (2011). Local macrophage proliferation, rather than recruitment from the blood, Is a signature of T(h)2 inflammation. Science *332*, 1284-1288.

Jersmann, H.P.A. (2005). Time to abandon dogma: CD14 is expressed by non-myeloid lineage cells. Immunology and Cell Biology *83*, 462-467.

Joshi, P., Dutta, S., Chaturvedi, P., and Nair, S. (2014). Head and neck cancers in developing countries. Rambam Maimonides Medical Journal *5*.

Kalluri, R., and Zeisberg, M. (2006). Fibroblasts in cancer. Nature Reviews Cancer *6*, 392-401.

Keeney, M., Gratama, J.W., Chin-Yee, I.H., and Sutherland, D.R. (1998). Isotype controls in the analysis of lymphocytes and CD34+ stem and progenitor cells by flow cytometry - Time to let go! Cytometry *34*, 280-283.

Kelley, J.L., Rozek, M.M., Suenram, C.A., and Schwartz, C.J. (1987). Activation of human-blood monocytes by adherence to tissue-culture plastic surfaces. Experimental and Molecular Pathology *46*, 266-278.

Kelly, C., Jefferies, C., and Cryan, S.-A. (2011). Targeted liposomal drug delivery to monocytes and macrophages. Journal of drug delivery *2011*.

Kim, S.-K., Park, S.-G., and Kim, K.-W. (2015). Expression of vascular endothelial growth factor in oral squamous cell carcinoma. Journal of the Korean Association of Oral and Maxillofacial Surgeons *41*, 11-18.

Kim, S.W., Park, Y.C., Kim, H.J., Cho, K.H., Chung, J.H., Kim, K.H., Eun, H.C., Lee, J.S., and Park, K.D. (2001). Effects of collagen IV and laminin on the reconstruction of human oral mucosa. Journal of Biomedical Materials Research *58*, 108-112.

Kimlin, L.C., Casagrande, G., and Virador, V.M. (2013). *In vitro* three-dimensional (3D) models in cancer research: An update. Molecular Carcinogenesis *52*, 167-182.

Klappacher, G.W., Lunyak, V.V., Sykes, D.B., Sawka-Verhelle, D., Sage, J., Brard, G., Ngo, S.D., Gangadharan, D., Jacks, T., Kamps, M.P., Rose, D.W., Rosenfeld, M.G., Glass, C.K. (2002). An induced Ets repressor complex regulates growth arrest during terminal macrophage differentiation. Cell *109*, 169-180.

Kobayashi, T., Liu, X.D., Kim, H.J., Kohyama, T., Wen, F.Q., Abe, S., Fang, Q.H., Zhu, Y.K., Spurzem, J.R., Bitterman, P., Rennars, S.I. (2005). TGF-beta 1 and serum both stimulate contraction but differentially affect apoptosis in 3D collagen gels. Respiratory Research *6*.

Koh, W., Stratman, A.N., Sacharidou, A., and Davis, G.E. (2008). *In vitro* three dimensional collagen matrix models of endothelial lumen formation during vasculogenesis and angiogenesis. Angiogenesis: *in Vitro* Systems *443*, 83-101.

Koontongkaew, S. (2013). The tumor microenvironment contribution to development, growth, invasion and metastasis of head and neck squamous cell carcinomas. Journal of Cancer *4*, 66-83.

Korc, M., and Friesel, R.E. (2009). The role of fibroblast growth factors in tumor growth. Current Cancer Drug Targets *9*, 639-651.

Kosten, I.J., Buskermolen, J.K., Spiekstra, S.W., de Gruijl, T.D., and Gibbs, S. (2015). Gingiva equivalents secrete negligible amounts of key chemokines involved in langerhans cell migration compared to skin equivalents. Journal of Immunology Research.

Kowal, K., Silver, R., Slawinska, E., Bielecki, M., Chyczewski, L., and Kowal-Bielecka, O. (2011). CD163 and its role in inflammation. Folia Histochemica Et Cytobiologica *49*, 365-374.

Koyama, E., Wu, C.S., Shimo, T., Iwamoto, M., Ohmori, T., Kurisu, K., Ookura, T., Bashir, M.M., Abrams, W.R., Tucker, T., Pacifici, M. (2001). Development of stratum intermedium and its role as a Sonic hedgehog-signaling structure during odontogenesis. Developmental Dynamics *222*, 178-191.

Kreutz, M., Andreesen, R. (1990). Induction of human monocyte to macrophage maturation *in vitro* by 1,25-dihydroxyvitamin D_3. Blood *76*, 2457-2461.

Kriegebaum, U., Mildenberger, M., Mueller-Richter, A., Klammert, U., Kuebler, A.C., and Reuther, T. (2012). Tissue engineering of human oral mucosa on different scaffolds: *in vitro* experiments as a basis for clinical applications. Oral Surgery Oral Medicine Oral Pathology Oral Radiology *114*, S190-S198.

Kukreja, I., Kapoor, P., Deshmukh, R., and Kulkarni, V. (2013). VEGF and CD 34: A correlation between tumor angiogenesis and microvessel density-an immunohistochemical study. Journal of Oral and Maxillofacial Pathology : JOMFP *17*, 367-373.

Kuper, H., Adami, H.O., and Trichopoulos, D. (2000). Infections as a major preventable cause of human cancer. Journal of Internal Medicine *248*, 171-183.

Lacombe, F., Durrieu, F., Briais, A., Dumain, P., Belloc, F., Bascans, E., Reiffers, J., Boisseau, M.R., and Bernard, P. (1997). Flow cytometry CD45 gating for immunophenotyping of acute myeloid leukemia. Leukemia *11*, 1878-1886.

Lamouille, S., Xu, J., and Derynck, R. (2014). Molecular mechanisms of epithelial-mesenchymal transition. Nature Reviews Molecular Cell Biology *15*, 178-196.

Lange, B., Valtieri, M., Santoli, D., Caracciolo, D., Mavilio, F., Gemperlein, I., Griffin, C., Emanuel, B., Finan, J., Nowell, P., Rovera, G. (1987). Growth-factor requirements of childhood acute-leukemia - establishment of GM-CSF dependent cell-lines. Blood *70*, 192-199.

Latkowski, J.A.M., Freedberg, I.M., and Blumenberg, M. (1995). Keratinocyte growth-factor and keratin gene-regulation. Journal of Dermatological Science *9*, 36-44.

Lavin, Y., Winter, D., Blecher-Gonen, R., David, E., Keren-Shaul, H., Merad, M., Jung, S., Amit, I. (2014). Tissue-resident macrophage enhancer landscapes are shaped by the local microenvironment. Cell *159*, 1312-26.

Lederle, W., Depner, S., Schnur, S., Obermueller, E., Catone, N., Just, A., Fusenig, N.E., and Mueller, M.M. (2011). IL-6 promotes malignant growth of skin SCCs by regulating a network of autocrine and paracrine cytokines. International Journal of Cancer *128*, 2803-2814.

Lee, C.-H., Liu, S.-Y., Chou, K.-C., Yeh, C.-T., Shiah, S.-G., Huang, R.-Y., Cheng, J.-C., Yen, C.-Y., and Shieh, Y.-S. (2014). Tumor-associated macrophages promote oral cancer progression through activation of the Axl signaling pathway. Annals of Surgical Oncology *21*, 1031-1037.

Lee, J., Cuddihy, M.J., and Kotov, N.A. (2008). Three-dimensional cell culture matrices: State of the art. Tissue Engineering Part B-Reviews *14*, 61-86.

Lee, J.A., Spidlen, J., Boyce, K., Cai, J., Crosbie, N., Dalphin, M., Furlong, J., Gasparetto, M., Goldberg, M., Goralczyk, E.M., Hyun, B., Jansen, K., Kollmann, T., Kong, M., Leif, R., McWeeney, S., Moloshok, T.D., Moore, W., Nolan, G., Nolan, J., Nikolich-Zugich, J., Parrish, D., Purcell, B., Qian, Y., Selvaraj, B., Smith, C., Tchuvatkina, O., Wertheimer, A., WilkinSon, P., Wilson, C., Wood, J., Zigon, R., Scheuermann, R.H., Brinkman, R.R. (2008). MIIFlowCyt: the minimum information about a flow cytometry experiment. Cytometry Part A *73A*, 926-930.

Leisten, I., Kramann, R., Ferreiraa, M.S.V., Bovi, M., Neuss, S., Ziegler, P., Wagner, W., Knuechel, R., and Schneider, R.K. (2012). 3D co-culture of hematopoietic stem and progenitor cells and mesenchymal stem cells in collagen scaffolds as a model of the hematopoietic niche. Biomaterials *33*, 1736-1747.

Leonard, F., Collnot, E.-M., and Lehr, C.-M. (2010). A three-dimensional coculture of enterocytes, monocytes and dendritic cells to model inflamed intestinal mucosa *in vitro*. Molecular Pharmaceutics *7*, 2103-2119.

Levi, F., Pasche, C., La Vecchia, C., Lucchini, F., Franceschi, S., and Monnier, P. (1998). Food groups and risk of oral and pharyngeal cancer. International Journal of Cancer *77*, 705-709.

Lewis, C.E., and Pollard, J.W. (2006). Distinct role of macrophages in different tumor microenvironments. Cancer Research *66*, 605-612.

Li, C.N., Shintani, S., Terakado, N., Nakashiro, K.I., and Hamakawa, H. (2002). Infiltration of tumor-associated macrophages in human oral squamous cell carcinoma. Oncology Reports *9*, 1219-1223.

Li, N., Wang, D., Sui, Z., Qi, X., Ji, L., Wang, X., and Yang, L. (2013). Development of an improved three-dimensional *in vitro* intestinal mucosa model for drug absorption evaluation. Tissue Engineering Part C-Methods *19*, 708-719.

Lilienblum, W., Dekant, W., Foth, H., Gebel, T., Hengstler, J.G., Kahl, R., Kramer, P.J., Schweinfurth, H., and Wollin, K.M. (2008). Alternative methods to safety studies in experimental animals: Role in the risk assessment of chemicals under the new European

Chemicals Legislation (REACH) (Reprinted from Archives of Toxicology, vol 82, pg 211-236, 2008). Toxicology *248*, 158-159.

Lin, S.M., Frevert, C.W., Kajikawa, O., Wurfel, M.M., Ballman, K., Mongovin, S., Wong, V.A., Selk, A., and Martin, T.R. (2004). Differential regulation of membrane CD14 expression and endotoxin-tolerance in alveolar macrophages. American Journal of Respiratory Cell and Molecular Biology *31*, 162-170.

Linde, N., Gutschalk, C.M., Hoffmann, C., Yilmaz, D., and Mueller, M.M. (2012). Integrating macrophages into organotypic co-cultures: A 3D *in vitro* model to study tumor-associated macrophages. Plos One *7*.

Liu, C.-Y., Lin, H.-H., Tang, M.-J., and Wang, Y.-K. (2015). Vimentin contributes to epithelial-mesenchymal transition cancer cell mechanics by mediating cytoskeletal organization and focal adhesion maturation. Oncotarget *6*, 15966-15983.

Liu, S.-Y., Chang, L.-C., Pan, L.-F., Hung, Y.-J., Lee, C.-H., and Shieh, Y.-S. (2008). Clinicopathologic significance of tumor cell-lined vessel and microenvironment in oral squamous cell carcinoma. Oral Oncology *44*, 277-285.

Liu, X.-q., Kiefl, R., Roskopf, C., Tian, F., and Huber, R.M. (2016). Interactions among lung cancer cells, fibroblasts, and macrophages in 3D co-cultures and the impact on MMP-1 and VEGF expression. Plos One *11*.

Lo Muzio, L., Santoro, A., Pieramici, T., Bufo, P., Di Alberti, L., Mazzotta, P., Mazzotta, A., Carinci, F., Rubini, C., and Lo Russo, L. (2010). Immunohistochemical expression of CD3, CD20, CD45, CD68 and Bcl-2 in oral squamous cell carcinoma. Analytical and Quantitative Cytology and Histology *32*, 70-77.

Lu, C.F., Huang, C.S., Tjiu, J.W., and Chiang, C.P. (2010). Infiltrating macrophage count: A significant predictor for the progression and prognosis of oral squamous cell carcinomas in Taiwan. Head and Neck-Journal for the Sciences and Specialties of the Head and Neck *32*, 18-25.

Ma, P.C., Maulik, G., Christensen, J., and Salgia, R. (2003). c-Met: Structure, functions and potential for therapeutic inhibition. Cancer and Metastasis Reviews *22*, 309-325.

MaasSzabowski, N., and Fusenig, N.E. (1996). Interleukin-1-induced growth factor expression in postmitotic and resting fibroblasts. Journal of Investigative Dermatology *107*, 849-855.

Maecker, H.T., McCoy, J.P., Jr., and Cons, F.H.I. (2010). A model for harmonizing flow cytometry in clinical trials. Nature Immunology *11*, 975-978.

Maecker, H.T., and Trotter, J. (2006). Flow cytometry controls, instrument setup, and the determination of positivity. Cytometry Part A *69A*, 1037-1042.

Maeda, H., and Akaike, T. (1998). Nitric oxide and oxygen radicals in infection, inflammation, and cancer. Biochemistry-Moscow *63*, 854-865.

Majchrzak, E., Szybiak, B., Wegner, A., Pienkowski, P., Pazdrowski, J., Luczewski, L., Sowka, M., Golusinski, P., Malicki, J., and Golusinski, W. (2014). Oral cavity and oropharyngeal squamous cell carcinoma in young adults: a review of the literature. Radiology and Oncology *48*, 1-10.

Mandl, I., Maclennan, J.D., and Howes, E.L. (1953). Isolation and characterization of proteinase and collagenase from *Cl-histolyticum*. Journal of Clinical Investigation *32*, 1323-1329.

Mantovani, A., and Allavena, P. (2015). The interaction of anticancer therapies with tumor-associated macrophages. Journal of Experimental Medicine *212*, 435-445.

Mantovani, A., Sica, A., and Locati, M. (2005). Macrophage polarization comes of age. Immunity *23*, 344-346.

Mantovani, A., Sica, A., Sozzani, S., Allavena, P., Vecchi, A., and Locati, M. (2004). The chemokine system in diverse forms of macrophage activation and polarization. Trends in Immunology *25*, 677-686.

Mantovani, A., Sozzani, S., Locati, M., Allavena, P., and Sica, A. (2002). Macrophage polarization: tumor-associated macrophages as a paradigm for polarized M2 mononuclear phagocytes. Trends in Immunology *23*, 549-555.

Martinez, F.O., and Gordon, S. (2014). The M1 and M2 paradigm of macrophage activation: time for reassessment. F1000prime reports *6*.

Martinez, F.O., Gordon, S., Locati, M., and Mantovani, A. (2006). Transcriptional profiling of the human monocyte-to-macrophage differentiation and polarization: New molecules and patterns of gene expression. Journal of Immunology *177*, 7303-7311.

Martinez, F.O., Sica, A., Mantovani, A., and Locati, M. (2008). Macrophage activation and polarization. Frontiers in Bioscience-Landmark *13*, 453-461.

Mason, B., Califano, J.P., Reinhart-King, C.A. (2011). Matrix stiffness: A regulator of cellular behavior and tissue formation. Engineering Biomaterials for Regenerative Medicine, 19-37.

Mazzoleni, G., Di Lorenzo, D., and Steimberg, N. (2009). Modelling tissues in 3D: the next future of pharmaco-toxicology and food research? Genes and Nutrition *4*, 13-22.

Medrek, C., Ponten, F., Jirstrom, K., and Leandersson, K. (2012). The presence of tumor associated macrophages in tumor stroma as a prognostic marker for breast cancer patients. BMC Cancer *12*.

Mendez, M.G., Kojima, S.-I., and Goldman, R.D. (2010). Vimentin induces changes in cell shape, motility, and adhesion during the epithelial to mesenchymal transition. Faseb Journal *24*, 1838-1851.

Merker, H.J. (1994). Morphology of the basement-membrane. Microscopy Research and Technique *28*, 95-124.

Merry, R., Belfield, L., McArdle, P., McLennan, A., Crean, S., and Foey, A. (2012). Oral health and pathology: a macrophage account. British Journal of Oral & Maxillofacial Surgery *50*, 2-7.

Mia, S., Warnecke, A., Zhang, X.M., Malmstrom, V., and Harris, R.A. (2014). An optimized protocol for human M2 macrophages using M-CSF and IL-4/IL-10/TGF-beta yields a dominant immunosuppressive phenotype. Scandinavian Journal of Immunology *79*, 305-314.

Miller, J.S., Stevens, K.R., Yang, M.T., Baker, B.M., Nguyen, D.-H.T., Cohen, D.M., Toro, E., Chen, A.A., Galie, P.A., Yu, X.*, et al.,* (2012). Rapid casting of patterned vascular networks for perfusable engineered three-dimensional tissues. Nature Materials *11*, 768-774.

Miller, M.A., Zheng, Y.-R., Suresh, G.W., Pfirschke, C., Zope, H., Engblom, C., Kohler, R.H., Iwamoto, Y., Yang, K.S., Askevold, B.*, et al.,* (2015). Tumour-associated macrophages act as a slow-release reservoir of nano-therapeutic Pt(IV) pro-drug. Nature Communications *6*.

Mills, C.D., Kincaid, K., Alt, J.M., Heilman, M.J., and Hill, A.M. (2000). M-1/M-2 macrophages and the Th1/Th2 paradigm. Journal of Immunology *164*, 6166-6173.

Mills, C.D., Lenz, L.L., and Harris, R.A. (2016). A Breakthrough: Macrophage-directed cancer immunotherapy. Cancer Research *76*, 513-516.

Misharin, A.V., Morales-Nebreda, L., Mutlu, G.M., Budinger, G.R.S., and Perlman, H. (2013). Flow cytometric analysis of macrophages and dendritic cell subsets in the mouse lung. American Journal of Respiratory Cell and Molecular Biology *49*, 503-510.

Mitchell, R.A. (2004). Mechanisms and effectors of MIF-dependent promotion of tumourigenesis. Cellular Signalling *16*, 13-19.

Mittal, N. (2012). Cell surface concentrations and concentration ranges for testing *in vitro* autocrine loops and small molecules. Plos One *7*.

Mittar, D., Paramban, R., McIntyre, C. (2011). Flow cytometry and high-content imaging to identify markers of monocyte-macrophage differentiation. Engineering Biomaterials for Regenerative Medicine, 19-37.

Mognetti, B., Di Carlo, F., and Berta, G.N. (2006). Animal models in oral cancer research. Oral Oncology *42*, 448-460.

Moharamzadeh, K., Brook, I.M., Van Noort, R., Scutt, A.M., Smith, K.G., and Thornhill, M.H. (2008). Development, optimization and characterization of a full-thickness tissue engineered human oral mucosal model for biological assessment of dental biomaterials. Journal of Materials Science-Materials in Medicine *19*, 1793-1801.

Moharamzadeh, K., Colley, H., Murdoch, C., Hearnden, V., Chai, W.L., Brook, I.M., Thornhill, M.H., and MacNeil, S. (2012). Tissue-engineered oral mucosa. Journal of Dental Research *91*, 642-650.

Moller, H., Fairley, L., Coupland, V., Okello, C., Green, M., Forman, D., Moller, B., and Bray, F. (2007). The future burden of cancer in England: incidence and numbers of new patients in 2020. British Journal of Cancer *96*, 1484-1488.

Morandi, A., Barbetti, V., Riverso, M., Dello Sbarba, P., and Rovida, E. (2011). The colony-stimulating factor-1 (CSF-1) receptor sustains ERK1/2 activation and proliferation in breast cancer cell lines. Plos One *6*.

Mori, K., Hiroi, M., Shimada, J., and Ohmori, Y. (2011). Infiltration of M2 tumor-associated macrophages in oral squamous cell carcinoma correlates with tumor malignancy. Cancers *3*, 3726-3739.

Mosser, D.M. (2003). The many faces of macrophage activation. Journal of Leukocyte Biology *73*, 209-212.

Mueller, M.M., and Fusenig, N.E. (2004). Friends or foes - Bipolar effects of the tumour stroma in cancer. Nature Reviews Cancer *4*, 839-849.

Muraille, E., Leo, O., and Moser, M. (2014). Th1/Th2 paradigm extended: macrophage polarization as an unappreciated pathogen-driven escape mechanism? Frontiers in Immunology *5*.

Murdoch, C., Muthana, M., Coffelt, S.B., and Lewis, C.E. (2008). The role of myeloid cells in the promotion of tumour angiogenesis. Nature Reviews Cancer *8*, 618-631.

Murray, P.J., Allen, J.E., Biswas, S.K., Fisher, E.A., Gilroy, D.W., Goerdt, S., Gordon, S., Hamilton, J.A., Ivashkiv, L.B., Lawrence, T.*, et al.,* (2014). Macrophage activation and polarization: Nomenclature and experimental guidelines. Immunity *41*, 14-20.

Murray, P.J., and Wynn, T.A. (2011). Obstacles and opportunities for understanding macrophage polarization. Journal of Leukocyte Biology *89*, 557-563.

Muthana, M., Giannoudis, A., Scott, S.D., Fang, H.-Y., Coffelt, S.B., Morrow, F.J., Murdoch, C., Burton, J., Cross, N., Burke, B.*,* Mistry, R., Hamdy, F., Brown, N.J., Georgopoulos, L., Hoskin, P., Essand, M., Lewis, C.E., Maitland, N.J. (2011). Use of macrophages to target therapeutic adenovirus to human prostate tumors. Cancer Research *71*, 1805-1815.

Muthana, M., Rodrigues, S., Chen, Y.-Y., Welford, A., Hughes, R., Tazzyman, S., Essand, M., Morrow, F., and Lewis, C.E. (2013). Macrophage delivery of an oncolytic virus abolishes tumor regrowth and metastasis after chemotherapy or irradiation. Cancer Research *73*, 490-495.

Mutin, M., George, F., Lesaule, G., Sampol, J. (1996). Re-evaluation of trypsin-EDTA for endothelial cell detachment before flow cytometry analysis. Journal of Endothelial Research *4*, 289-295.

Nagy, J.A., Chang, S.H., Dvorak, A.M., and Dvorak, H.F. (2009). Why are tumour blood vessels abnormal and why is it important to know? British Journal of Cancer *100*, 865-869.

Nayak, S., Goel, M.M., Makker, A., Bhatia, V., Chandra, S., Kumar, S., and Agarwal, S.P. (2015). Fibroblast growth factor (FGF-2) and its receptors FGFR-2 and FGFR-3 may be putative biomarkers of malignant transformation of potentially malignant oral lesions into oral squamous cell carcinoma. Plos One *10*.

Neu, C., Sedlag, A., Bayer, C., Foerster, S., Crauwels, P., Niess, J.-H., van Zandbergen, G., Frascaroli, G., and Riedel, C.U. (2013). CD14-Dependent Monocyte Isolation Enhances Phagocytosis of Listeria monocytogenes by Proinflammatory, GM-CSF-Derived Macrophages. Plos One *8*.

Neville, B.W., and Day, T.A. (2002). Oral cancer and precancerous lesions. Ca-a Cancer Journal for Clinicians *52*, 195-215.

Ngo, P., Ramalingam, P., Phillips, J.A., and Furuta, G.T. (2006). Collagen gel contraction assay. Cell-Cell Interactions: Methods and Protocols *341*, 103-109.

Nguyen, K.T., and West, J.L. (2002). Photopolymerizable hydrogels for tissue engineering applications. Biomaterials *23*, 4307-4314.

Ni, Y.H., Ding, L., Huang, X.F., Dong, Y.C., Hu, Q.G., and Hou, Y.Y. (2015). Microlocalization of CD68(+) tumor-associated macrophages in tumor stroma correlated with poor clinical outcomes in oral squamous cell carcinoma patients. Tumor Biology *36*, 5291-5298.

Niino, D., Komohara, Y., Murayama, T., Aoki, R., Kimura, Y., Hashikawa, K., Kiyasu, J., Takeuchi, M., Suefuji, N., Sugita, Y., Takeya, M., Ohshima, K. (2010). Ratio of M2 macrophage expression is closely associated with poor prognosis for Angioimmunoblastic T-cell lymphoma (AITL). Pathology International *60*, 278-283.

Njoroge, J.M., Mitchell, L.B., Centola, M., Kastner, D., Raffeld, M., and Miller, J.L. (2001). Characterization of viable autofluorescent macrophages among cultured peripheral blood mononuclear cells. Cytometry *44*, 38-44.

Noy, R., and Pollard, J.W. (2014). Tumor-associated macrophages: From mechanisms to therapy. Immunity *41*, 49-61.

Nurmenniemi, S., Sinikumpu, T., Alahuhta, I., Salo, S., Sutinen, M., Santala, M., Risteli, J., Nyberg, P., and Salo, T. (2009). A novel organotypic model mimics the tumor microenvironment. American Journal of Pathology *175*, 1281-1291.

Ohri, C.M., Shikotra, A., Green, R.H., Waller, D.A., and Bradding, P. (2011). The tissue microlocalisation and cellular expression of CD163, VEGF, HLA-DR, iNOS, and MRP 8/14 is correlated to clinical outcome in NSCLC. Plos One *6*.

Panni, R.Z., Linehan, D.C., and DeNardo, D.G. (2013). Targeting tumor-infiltrating macrophages to combat cancer. Immunotherapy *5*, 1075-1087.

Park, E.K., Jung, H.S., Yang, H.I., Yoo, M.C., Kim, C., and Kim, K.S. (2007). Optimized THP-1 differentiation is required for the detection of responses to weak stimuli. Inflammation Research *56*, 45-50.

Paszek, M.J., Zahir, N., Johnson, K.R., Lakins, J.N., Rozenberg, G.I., Gefen, A., Reinhart-King, C.A., Margulies, S.S., Dembo, M., Boettiger, D., Hammer, D.A., Weaver, V.M. (2005). Tensional homeostasis and the malignant phenotype. Cancer Cell *8*, 241-254.

Patel, B.P., Shah, P.M., Rawal, U.M., Desai, A.A., Shah, S.V., Rawal, R.M., and Patel, P.S. (2005). Activation of MMP-2 and MMP-9 in patients with oral squamous cell carcinoma. Journal of Surgical Oncology *90*, 81-88.

Patel, B.P., Shah, S.V., Shukla, S.N., Shah, P.M., and Patel, P.S. (2007). Clinical significance of MMP-2 and MMP-9 in patients with oral cancer. Head and Neck-Journal for the Sciences and Specialties of the Head and Neck *29*, 564-572.

Petersen, P.E. (2008). World Health Organization global policy for improvement of oral health - World Health Assembly 2007. International Dental Journal *58*, 115-121.

Petti, S. (2009). Lifestyle risk factors for oral cancer. Oral Oncology *45*, 340-350.

Pidone Ribeiro, F.A., Noguti, J., Fujiyama Oshima, C.T., and Ribeiro, D.A. (2014). Effective targeting of the epidermal growth factor receptor (EGFR) for treating oral cancer: A promising approach. Anticancer Research *34*, 1547-1552.

Pietrzyk-Nivau, A., Poirault-Chassac, S., Gandrille, S., Derkaoui, S.-M., Kauskot, A., Letourneur, D., Le Visage, C., and Baruch, D. (2015). Three-dimensional environment sustains hematopoietic stem cell differentiation into platelet-producing megakaryocytes. Plos One *10*.

Pirila, E., Vayrynen, O., Sundquist, E., Pakkila, K., Nyberg, P., Nurmenniemi, S., Paakkonen, V., Pesonen, P., Dayan, D., Vered, M., Uhlin-Hansen, L., Salo, T. (2015). Macrophages modulate migration and invasion of human tongue squamous cell carcinoma. Plos One *10*.

Pollard, J.W. (2004). Tumour-educated macrophages promote tumour progression and metastasis. Nature Reviews Cancer *4*, 71-78.

Porcheray, F., Viaud, S., Rimaniol, A.C., Leone, C., Samah, B., Dereuddre-Bosquet, N., Dormont, D., and Gras, G. (2005). Macrophage activation switching: an asset for the resolution of inflammation. Clinical and Experimental Immunology *142*, 481-489.

Poussin, C., Foti, M., Carpentier, J.L., and Pugin, J. (1998). CD14-dependent endotoxin internalization via a macropinocytic pathway. Journal of Biological Chemistry *273*, 20285-20291.

Prime, S.S., Nixon, S.V.R., Crane, I.J., Stone, A., Matthews, J.B., Maitland, N.J., Remnant, L., Powell, S.K., Game, S.M., and Scully, C. (1990). The behavior of human oral squamous-cell carcinoma in cell-culture. Journal of Pathology *160*, 259-269.

Qian, B., Deng, Y., Im, J.H., Muschel, R.J., Zou, Y., Li, J., Lang, R.A., and Pollard, J.W. (2009). A distinct macrophage population mediates metastatic breast cancer cell extravasation, establishment and growth. Plos One *4*.

Qian, B.-Z., Li, J., Zhang, H., Kitamura, T., Zhang, J., Campion, L.R., Kaiser, E.A., Snyder, L.A., and Pollard, J.W. (2011). CCL2 recruits inflammatory monocytes to facilitate breast-tumour metastasis. Nature *475*, 222-U129.

Qian, B.-Z., and Pollard, J.W. (2010). Macrophage diversity enhances tumor progression and metastasis. Cell *141*, 39-51.

Qin, Z. (2012). The use of THP-1 cells as a model for mimicking the function and regulation of monocytes and macrophages in the vasculature. Atherosclerosis *221*, 2-11.

Quan, J., Elhousiny, M., Johnson, N.W., and Gao, J. (2013). Transforming growth factor-beta 1 treatment of oral cancer induces epithelial-mesenchymal transition and promotes bone invasion via enhanced activity of osteoclasts. Clinical & Experimental Metastasis *30*, 659-670.

Quatromoni, J.G., and Eruslanov, E. (2012). Tumor-associated macrophages: function, phenotype, and link to prognosis in human lung cancer. American Journal of Translational Research *4*, 376-389.

Radoi, L., and Luce, D. (2013). A review of risk factors for oral cavity cancer: the importance of a standardized case definition. Community Dentistry and Oral Epidemiology *41*.

Rajan, N., Habermehl, J., Cote, M.-F., Doillon, C.J., and Mantovani, D. (2006). Preparation of ready-to-use, storable and reconstituted type I collagen from rat tail tendon for tissue engineering applications. Nature Protocols *1*, 2753-2758.

Ramanujan, S., Pluen, A., McKee, T.D., Brown, E.B., Boucher, Y., and Jain, R.K. (2002). Diffusion and convection in collagen gels: Implications for transport in the tumor interstitium. Biophysical Journal *83*, 1650-1660.

Rao, L., He, Z., Meng, Q.-F., Zhou, Z., Bu, L.-L., Guo, S.-S., Liu, W., and Zhao, X.-Z. (2016). Effective cancer targeting and imaging using macrophage membrane-camouflaged upconversion nanoparticles. Journal of Biomedical Materials Research Part A.

Rehli, M., Krause, S.W., and Andreesen, R. (2000). The membrane-bound ectopeptidase CPM as a marker of macrophage maturation *in vitro* and *in vivo*. Cellular Peptidases in Immune Functions and Diseases 2 *477*, 205-216.

Rehli, M., Krause, S.W., Kreutz, M., and Andreesen, R. (1995). Carboxypeptidase-M is identical to the Max.1 antigen and its expression is associated with monocyte to macrophage differentiation. Journal of Biological Chemistry *270*, 15644-15649.

Reid, B.C., Winn, D.M., Morse, D.E., and Pendrys, D.G. (2000). Head and neck *in situ* carcinoma: incidence, trends, and survival. Oral Oncology *36*, 414-420.

Rheinwald, J.G., and Green, H. (1975). Serial cultivation of strains of human epidermal keratinocytes - formation of keratinizing colonies from single cells. Cell *6*, 331-344.

Roach, T., Slater, S., Koval, M., White, L., McFarland, E.C., Okumura, M., Thomas, M., and Brown, E. (1997). CD45 regulates Src family member kinase activity associated with macrophage integrin-mediated adhesion. Current Biology *7*, 408-417.

Roederer, M. (2001). Spectral compensation for flow cytometry: Visualization artifacts, limitations, and caveats. Cytometry *45*, 194-205.

Rogers, T.L., and Holen, I. (2011). Tumour macrophages as potential targets of bisphosphonates. Journal of Translational Medicine *9*.

Rosas, M., Gordon, S., and Taylor, P.R. (2007). Characterisation of the expression and function of the GM-CSF receptor alpha-chain in mice. European Journal of Immunology *37*, 2518-2528.

Rosso, M., Heine, H., Meusch, U., Quandt, D., Klein, C., Sweet, M.J., and Hauschildt, S. (2011). LPS-induced cytokine production in human monocytes and macrophages. Critical Reviews in Immunology *31*, 379-446.

Roszer, T. (2015). Understanding the mysterious M2 macrophage through activation markers and effector mechanisms. Mediators of Inflammation.

Saman, D.M. (2012). A review of the epidemiology of oral and pharyngeal carcinoma: update. Head & Neck Oncology *4*.

Sanderson, R.D., Fitch, J.M., Linsenmayer, T.R., and Mayne, R. (1986). Fibroblasts promote the formation of a continuous basal lamina during myogenesis *in vitro*. Journal of Cell Biology *102*, 740-747.

Sanford, D.E., Belt, B.A., Panni, R.Z., Mayer, A., Deshpande, A.D., Carpenter, D., Mitchem, J.B., Plambeck-Suess, S.M., Worley, L.A., Goetz, B.D., Wang-Gillam, D., Eberlein, T.J., Denardo, D.G., Goedegebuure, S.P., Linehan, D.C. (2013). Inflammatory monocyte mobilization decreases patient survival in pancreatic cancer: A role for targeting the CCL2/CCR2 axis. Clinical Cancer Research *19*, 3404-3415.

Sargeran, K., Murtomaa, H., Safavi, S.M.R., Vehkalahti, M.M., and Teronen, O. (2008). Survival after diagnosis of cancer of the oral cavity. British Journal of Oral & Maxillofacial Surgery *46*, 187-191.

Sawant, S.S., Vaidya, M.M., Chaukar, D.A., Alam, H., Dmello, C., Gangadaran, P., Kannan, S., Kane, S., Dange, P.P., Dey, N., Ranganathan, K., D'Cruz, A.K. (2014). Clinical significance of aberrant vimentin expression in oral premalignant lesions and carcinomas. Oral Diseases *20*, 453-465.

Schimek, K., Busek, M., Brincker, S., Groth, B., Hoffmann, S., Lauster, R., Lindner, G., Lorenz, A., Menzel, U., Sonntag, F., Walles, H., Marx, U., Horland, R. (2013). Integrating biological vasculature into a multi-organ-chip microsystem. Lab on a Chip *13*, 3588-3598.

Schneider, C.A., Rasband, W.S., and Eliceiri, K.W. (2012). NIH image to imageJ: 25 years of image analysis. Nature Methods *9*, 671-675.

Schneider, M.R., and Wolf, E. (2009). The epidermal growth factor receptor ligands at a glance. Journal of Cellular Physiology *218*, 460-466.

Schroeder, H.E. (1981). Differentiation of human oral stratified epithelia. Differentiation of human oral stratified epithelia Xi+306p S Karger: Basel, Switzerland; New York, NY, USA Illus, XI+306P-XI+306P.

Schwende, H., Fitzke, E., Ambs, P., and Dieter, P. (1996). Differences in the state of differentiation of THP-1 cells induced by phorbol ester and 1,25-dihydroxyvitamin D-3. Journal of Leukocyte Biology *59*, 555-561.

Scott, S.E., Grunfeld, E.A., and McGurk, M. (2006). Patient's delay in oral cancer: a systematic review. Community Dentistry and Oral Epidemiology *34*, 337-343.

Scully, C., and Bagan, J. (2009a). Oral squamous cell carcinoma overview. Oral Oncology *45*, 301-308.

Scully, C., and Bagan, J.V. (2009b). Oral squamous cell carcinoma: overview of current understanding of aetiopathogenesis and clinical implications. Oral Diseases *15*, 388-399.

Shafer, W.G., and Waldron, C.A. (1975). Erythroplakia of oral cavity. Cancer *36*, 1021-1028.

Shapiro, H., Lutaty, A., and Ariel, A. (2011). Macrophages, meta-inflammation, and immuno-metabolism. The Scientific World Journal *11*, 2509-2529.

Sharon, Y., Alon, L., Glanz, S., Servais, C., Erez, N. (2013). Isolation of normal and cancer-associated fibroblasts from fresh tissues by Fluorescence Activated Cell Sorting (FACS). Journal of visualized experiments *71*.

Sheel, M., and Engwerda, C.R. (2012). The diverse roles of monocytes in inflammation caused by protozoan parasitic diseases. Trends in Parasitology *28*, 408-416.

Shi, C., and Pamer, E.G. (2011). Monocyte recruitment during infection and inflammation. Nature Reviews Immunology *11*, 762-774.

Shoseyov, O., Posen, Y., and Grynspan, F. (2013). Human recombinant type I collagen produced in plants. Tissue Engineering Part A *19*, 1527-1533.

Silva, T.A., Leite Ribeiro, F.L., De Oliveira-Neto, H.H., Watanabe, S., Goncalves Alencar, R.D.C., Fukada, S.Y., Cunha, F.Q., Leles, C.R., Mendonca, E.F., and Batista, A.C. (2007). Dual role of CCL3/CCR1 in oral squamous cell carcinoma: Implications in tumor metastasis and local host defense. Oncology Reports *18*, 1107-1113.

Silverman, S., and Gorsky, M. (1997). Proliferative verrucous leukoplakia - A follow-up study of 54 cases. Oral Surgery Oral Medicine Oral Pathology Oral Radiology and Endodontics *84*, 154-157.

Smith, H.A., and Kang, Y. (2013). The metastasis-promoting roles of tumor-associated immune cells. Journal of Molecular Medicine-Jmm *91*, 411-429.

Smith, M.P., Young, H., Hurlstone, A., Wellbrock, C. (2015). Differentiation of THP1 cells into macrophages for transwell co-culture assay with melanoma cells. Bio-protocol *5*, 21.

Smola, H., Stark, H.J., Thiekotter, G., Mirancea, N., Krieg, T., and Fusenig, N.E. (1998). Dynamics of basement membrane formation by keratinocyte-fibroblast interactions in organotypic skin culture. Experimental Cell Research *239*, 399-410.

Squier, C.A., and Kremer, M.J. (2001). Biology of oral mucosa and esophagus. Journal of the National Cancer Institute Monographs, 7-15.

Sridevi, U., Jain, A., Nagalaxmi, V., Kumar, U.V., and Goyal, S. (2015). Expression of E-cadherin in normal oral mucosa, in oral precancerous lesions and in oral carcinomas. European Journal of Dentistry *9*, 364-372.

St-Pierre, J., and Ostergaard, H.L. (2013). A role for the protein tyrosine phosphatase CD45 in macrophage adhesion through the regulation of paxillin degradation. Plos One *8*.

Stein, M., Keshav, S., Harris, N., and Gordon, S. (1992). Interleukin-4 potently enhances murine macrophage mannose receptor activity - a marker of alternative immunological macrophage activation. Journal of Experimental Medicine *176*, 287-292.

Steinman, R.M., and Idoyaga, J. (2010). Features of the dendritic cell lineage. Immunological Reviews *234*, 5-17.

Sugimoto, C., Fujieda, S., Sunaga, H., Noda, I., Tanaka, N., Kimura, Y., Saito, H., and Matsukawa, S. (2001). Granulocyte colony-stimulating factor (G-CSF)-mediated signaling regulates type IV collagenase activity in head and neck cancer cells. International Journal of Cancer *93*, 42-46.

Sundstrom, C., and Nilsson, K. (1976). establishment and characterization of a human histiocytic lymphoma cell line (U-937). International Journal of Cancer *17*, 565-577.

Susewind, J. (2015). A cell line-based co-culture model of the inflamed intestinal mucosa and its application for safety and efficacy testing of nanomaterials. Published dissertation found at http://d-nb.info/1074404564/34 on 31/07/2016.

Sutherland, R., Carlsson, J., Durand, R., and Yuhas, J. (1981). Spheroids in cancer-research. Cancer Research *41*, 2980-2984.

Tarique, A.A., Logan, J., Thomas, E., Holt, P.G., Sly, P.D., and Fantino, E. (2015). Phenotypic, functional, and plasticity features of classical and alternatively activated human macrophages. American Journal of Respiratory Cell and Molecular Biology *53*, 676-688.

Terry, R.L., and Miller, S.D. (2014). Molecular control of monocyte development. Cellular Immunology *291*, 16-21.

Thomas, L., Moore, E.J., McGree, M.E., Olsen, K.D., Kasperbauer, J.L., Erickson, L.A., and Schembri-Wismayer, D.J. (2012). Prognostic features, human papillomavirus status, and epidermal growth factor receptor expression in oral squamous cell carcinoma in young adults. American Journal of Otolaryngology *33*, 650-656.

Thorley, A.J., Ford, P.A., Giembycz, M.A., Goldstraw, P., Young, A., and Tetley, T.D. (2007). Differential regulation of cytokine release and leukocyte migration by lipopolysaccharide-

stimulated primary human lung alveolar type II epithelial cells and macrophages. Journal of Immunology *178*, 463-473.

Tourovskaia, A., Fauver, M., Kramer, G., Simonson, S., and Neumann, T. (2014). Tissue-engineered microenvironment systems for modeling human vasculature. Experimental Biology and Medicine *239*, 1264-1271.

Traore, K., Trush, M.A., George, M., Spannhake, E.W., Anderson, W., and Asseffa, A. (2005). Signal transduction of phorbol 12-myristate 13-acetate (PMA)-induced growth inhibition of human monocytic leukemia THP-1 cells is reactive oxygen dependent. Leukemia Research *29*, 863-879.

Tschachojan, V., Schroer, H., Averbeck, N., and Mueller-Klieser, W. (2014). Carbon ions and X-rays induce pro-inflammatory effects in 3D oral mucosa models with and without PBMCs. Oncology Reports *32*, 1820-1828.

Tsuchiya, S., Yamabe, M., Yamaguchi, Y., Kobayashi, Y., Konno, T., and Tada, K. (1980). Establishment and characterization of a human acute monocytic leukemia-cell line (THP-1). International Journal of Cancer *26*, 171-176.

Tung, J.W., Heydari, K., Tirouvanziam, R., Parks, D.R., and Herzenberg, L.A. (2007). Modern flow cytometry: A practical approach. Clinics in Laboratory Medicine *27*.

Uchino, T., Shimizu, K., Yamashita, K., Kojima, H., Takezawa, T., Akiyama, T., and Ikarashi, Y. (2013). Development of skin sensitization test method utilizing THP-1 cells cultured on a collagen vitrigel membrane chamber. Toxicology Letters *221*, S135-S135.

Uchino, T., Takezawa, T., and Ikarashi, Y. (2009). Reconstruction of three-dimensional human skin model composed of dendritic cells, keratinocytes and fibroblasts utilizing a handy scaffold of collagen vitrigel membrane. Toxicology *in Vitro 23*, 333-337.

van den Bogaard, E.H., Tjabringa, G.S., Joosten, I., Vonk-Bergers, M., van Rijssen, E., Tijssen, H.J., Erkens, M., Schalkwijk, J., and Koenen, H.J.P.M. (2014). Crosstalk between Keratinocytes and T Cells in a 3D Microenvironment: A Model to Study Inflammatory Skin Diseases. Journal of Investigative Dermatology *134*, 719-727.

Vanderriet, P., Nawroz, H., Hruban, R.H., Corio, R., Tokino, K., Koch, W., and Sidransky, D. (1994). Frequent loss of chromosome 9p21-22 early in head and neck-cancer progression. Cancer Research *54*, 1156-1158.

Vasselon, T., Hailman, E., Thieringer, R., and Detmers, P.A. (1999). Internalization of monomeric lipopolysaccharide occurs after transfer out of cell surface CD14. Journal of Experimental Medicine *190*, 509-521.

Viney, M.E., Bullock, A.J., Day, M.J., and MacNeil, S. (2009). Co-culture of intestinal epithelial and stromal cells in 3D collagen-based environments. Regenerative Medicine *4*, 397-406.

Virchow, R. Cellular Pathology as Based Upon Physiological and Pathological Histology. Philadelphia: J.B. Lippincott; 1863.

Vogel, D.Y.S., Vereyken, E.J.F., Glim, J.E., Heijnen, P., Moeton, M., van der Valk, P., Amor, S., Teunissen, C.E., van Horssen, J., and Dijkstra, C.D. (2013). Macrophages in inflammatory multiple sclerosis lesions have an intermediate activation status. Journal of Neuroinflammation *10*.

Vogt, G., and Nathan, C. (2011). *In vitro* differentiation of human macrophages with enhanced antimycobacterial activity. Journal of Clinical Investigation *121*, 3889-3901.

Warnakulasuriya, S. (2009). Global epidemiology of oral and oropharyngeal cancer. Oral Oncology *45*, 309-316.

Warnakulasuriya, S. (2010). Living with oral cancer: Epidemiology with particular reference to prevalence and life-style changes that influence survival. Oral Oncology *46*, 407-410.

Weber, M., Buettner-Herold, M., Hyckel, P., Moebius, P., Distel, L., Ries, J., Amann, K., Neukam, F.W., and Wehrhan, F. (2014). Small oral squamous cell carcinomas with nodal lymphogenic metastasis show increased infiltration of M2 polarized macrophages - An immunohistochemical analysis. Journal of Cranio-Maxillofacial Surgery *42*, 1087-1094.

Weber, M., Iliopoulos, C., Moebius, P., Buettner-Herold, M., Amann, K., Ries, J., Preidl, R., Neukam, F.W., and Wehrhan, F. (2016). Prognostic significance of macrophage polarization in early stage oral squamous cell carcinomas. Oral Oncology *52*, 75-84.

Wehrhan, F., Buettner-Herold, M., Hyckel, P., Moebius, P., Preidl, R., Distel, L., Ries, J., Amann, K., Schmitt, C., Neukam, F.W., Weber, M. (2014). Increased malignancy of oral squamous cell carcinomas (oscc) is associated with macrophage polarization in regional lymph nodes - an immunohistochemical study. BMC Cancer *14*.

White, R.A., Malkoski, S.P., and Wang, X.J. (2010). TGF beta signaling in head and neck squamous cell carcinoma. Oncogene *29*, 5437-5446.

Whitmore, S.E., and Lamont, R.J. (2014). Oral bacteria and cancer. Plos Pathogens *10*.

Willard, J.J., Drexler, J.W., Das, A., Roy, S., Shilo, S., Shoseyov, O., and Powell, H.M. (2013). Plant-Derived Human Collagen Scaffolds for Skin Tissue Engineering. Tissue Engineering Part A *19*, 1507-1518.

Wiseman, M. (2008). The second World Cancer Research Fund/American Institute for Cancer Research expert report. Food, nutrition, physical activity, and the prevention of cancer: A global perspective. Proceedings of the Nutrition Society *67*, 253-256.

Wrigley, B.J., Lip, G.Y.H., and Shantsila, E. (2011). The role of monocytes and inflammation in the pathophysiology of heart failure. European Journal of Heart Failure *13*, 1161-1171.

Wyckoff, J., Wang, W.G., Lin, E.Y., Wang, Y.R., Pixley, F., Stanley, E.R., Graf, T., Pollard, J.W., Segall, J., and Condeelis, J. (2004). A paracrine loop between tumor cells and macrophages is required for tumor cell migration in mammary tumors. Cancer Research *64*, 7022-7029.

Xia, H.H.X., Yang, Y., Chu, K.M., Gu, Q., Zhang, Y.Y., He, H., Wong, W.M., Leung, S.Y., Yuen, S.T., Yuen, M.F., Chan, A.O.O., Wong, B.C.Y. (2009). Serum macrophage migration-

inhibitory factor as a diagnostic and prognostic biomarker for gastric cancer. Cancer *115*, 5441-5449.

Xu, J., Lamouille, S., and Derynck, R. (2009). TGF-beta-induced epithelial to mesenchymal transition. Cell Research *19*, 156-172.

Yang, J., Zhang, L., Yu, C., Yang, X.-F., and Wang, H. (2014a). Monocyte and macrophage differentiation: circulation inflammatory monocyte as biomarker for inflammatory diseases. Biomarker research *2*, 1-1.

Yang, S.F., Leong, K.F., Du, Z.H., and Chua, C.K. (2001). The design of scaffolds for use in tissue engineering. Part 1. Traditional factors. Tissue Engineering *7*, 679-689.

Yang, Y., Qin, J., Lan, L., Li, N., Wang, C., He, P., Liu, F., Ni, H., and Wang, Y. (2014b). M-CSF cooperating with NF kappa B induces macrophage transformation from M1 to M2 by upregulating c-Jun. Cancer Biology & Therapy *15*, 99-107.

Zhang, B., Shan, H., Li, D., Li, Z.R., Zhu, K.S., Jiang, Z.B., and Huang, M.S. (2012). Different methods of detaching adherent cells significantly affect the detection of TRAIL receptors. Tumori *98*, 800-803.

Zhang, Y., Choksi, S., Chen, K., Pobezinskaya, Y., Linnoila, I., and Liu, Z.G. (2013). ROS play a critical role in the differentiation of alternatively activated macrophages and the occurrence of tumor-associated macrophages. Cell Research *23*, 898-914.

Zhou, J., and Chng, W.-J. (2014). Identification and targeting leukemia stem cells: The path to the cure for acute myeloid leukemia. World journal of stem cells *6*, 473-484.

Zieglerheitbrock, H.W.L., Schraut, W., Wendelgass, P., Strobel, M., Sternsdorf, T., Weber, C., Aepfelbacher, M., Ehlers, M., Schutt, C., and Haas, J.G. (1994). Distinct patterns of differentiation-induced in the monocytic cell-line Mono-Mac-6. Journal of Leukocyte Biology *55*, 73-80.

Zieglerheitbrock, H.W.L., Thiel, E., Futterer, A., Herzog, V., Wirtz, A., and Riethmuller, G. (1988). Establishment of a human cell-line (Mono Mac-6) with characteristics of mature monocytes. International Journal of Cancer *41*, 456-461.

Zieglerheitbrock, H.W.L., and Ulevitch, R.J. (1993). CD14 - cell-surface receptor and differentiation marker. Immunology Today *14*, 121-125.

Zilfou, J.T., and Lowe, S.W. (2009). Tumor suppressive functions of p53. Cold Spring Harbor Perspectives in Biology *1*.

10 Chapter 10: Appendix

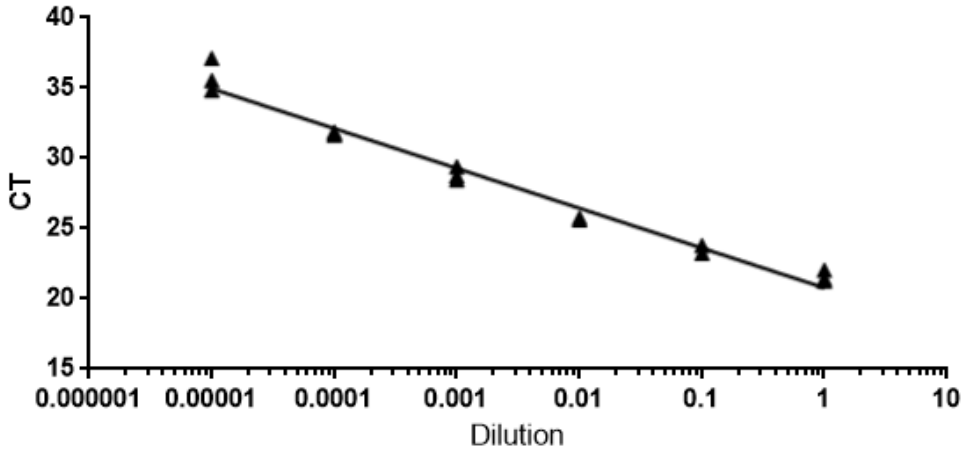

Appendix Figure 1. Melt curve for primers targeted to carboxypeptidase M gene. M = -2.835.

Primer efficiency (E) was calculated using the following equation:

$$E = 10^{(-1/-2.835)} = 2.253$$

Primer percentage efficiency (% E) was calculated using the following equation:

$$\% E = (2.253-1) \times 100\% = 125.26\ \%$$